NASA CR 73908 FZA -439 - 1
1 NOV. 1968

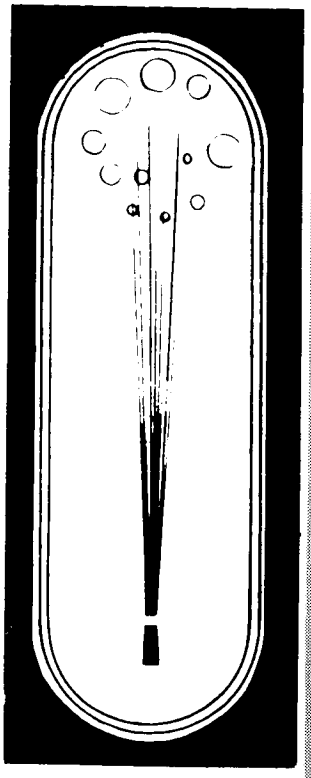

A STUDY OF CRYOGENIC PROPELLANT MIXING TECHNIQUES

Final Report

(July 1967 - September 1968)

Volume I - Mixer Design and Experimental Investigations

GENERAL DYNAMICS
Fort Worth Division

GENERAL DYNAMICS
Fort Worth Division

FZA-439-1
1 November 1968

A STUDY OF CRYOGENIC PROPELLANT MIXING TECHNIQUES

FINAL REPORT

(July 1967 - September 1968)

Volume I : Mixer Design and
Experimental Investigations

L. J. Poth, Jr.
J. R. Van Hook
D. M. Wheeler
C. R. Kee, Jr.

Prepared for the
George C. Marshall Space Flight Center
National Aeronautics and Space Administration
Huntsville, Alabama

under

Contract No. NAS-8-20330

Approved by:

L. J. Poth, Jr.
Senior Aerothermodynamics Engineer

Approved by:

R. A. Stevens
Aerothermodynamics Group Engineer

GENERAL DYNAMICS
Fort Worth Division

F O R E W O R D

This document is Volume I of the annual report on NASA Contract NAS8-20330, "A Study of Cryogenic Propellant Stratification Reduction Techniques." The study was performed by the Fort Worth Division of General Dynamics Corporation for the George C. Marshall Space Flight Center of the National Aeronautics and Space Administration. The program was conducted under the technical direction of Mr. T. W. Winstead of the MSFC Propulsion and Vehicle Engineering Laboratory. His assistance in the performance of this study is gratefully acknowledged.

The final report consists of two volumes:

Volume I. Mixer Design and Experimental Investigations

Volume II. Experimental Data

Volume I contains a presentation of the mixer design and experimental investigations, together with a summary of the important findings of the study. Volume II contains a presentation of the experimental data utilized in the study.

TABLE OF CONTENTS

T A B L E O F C O N T E N T S (Cont'd)

T A B L E O F C O N T E N T S (Cont'd)

TABLE OF CONTENTS (Cont'd)

L I S T O F F I G U R E S

L I S T O F F I G U R E S (Cont'd)

L I S T O F F I G U R E S (Cont'd)

L I S T O F F I G U R E S (Cont'd)

L I S T O F F I G U R E S (Cont'd)

L I S T O F F I G U R E S (Cont'd)

L I S T O F T A B L E S

L I S T O F T A B L E S (Cont'd)

S U M M A R Y

The design of present and future spacecraft utilizing cryogens requires that adequate prediction and control of the propellant thermodynamic state be achieved. In this study, the technology required for the prediction of the departure of the cryogen from equilibrium conditions (thermal stratification) and the means by which equilibrium conditions can be achieved (mixing) was developed and a mixer design procedure evolved.

The study consisted of an analytical and experimental investigation of methods of prediction and control of the cryogenic propellant thermodynamic state. The axial jet mixer concept was the primary mixer system considered in this study phase. This system had earlier (Ref. 1) been found to offer the best performance of the concepts evaluated.

An intensive experimental investigation using small scale tanks with water as the test fluid was conducted in order to simulate mixing and ullage breakup in large scale cryogenic tanks. The mixing tests were conducted in both pressurized and non-pressurized tanks. The non-pressurized tests enabled mixing and jet motion to be observed visually and provided insight into the basic mechanisms of mixing. These tests were intended to verify the analytical predictions and provide data for correlating the dimensionless parameters obtained from the

analytical predictions. These results amplified and expanded previous test data. The test data correlations presented in Section 5 indicated that mixing occurs somewhat faster than predicted analytically. The delay in mixing due to buoyancy is relatively small for conditions simulating low-g environments. This condition may be ignored in designing mixers for low-g conditions. Results of the pressurized tests indicate that substantial reductions in the ullage pressure are obtained during mixing. This pressure decay was, in general, somewhat slower than the temperature decay. Further investigation of this phenomenon is needed.

A series of tests utilizing a miniature test apparatus to simulate low-g conditions were also conducted. The small size of the test tank used in these tests enabled low Bond numbers to be obtained and produced the corresponding curved liquid/vapor interface found in cryogenic tanks for a low-g environment. The results of these tests are shown in Tables 4-1 and 4-2. These tests indicated that ullage breakup could be obtained at Reynolds numbers much less than would occur in a large scale cryogenic tank under low-g conditions.

A mixer design requirements investigation was conducted for a mixer system for use in a Nuclear Flight Module vehicle for a manned Mars mission. The significant design parameters

applied in this study were

1. Tank size and geometry
2. Tank acceleration
3. Mission time
4. Cryogenic storage mode
5. Propellant heating rates

These parameters were defined for each of the tanks considered and are summarized in Table 2-1. These parameters were utilized in predicting stratification development by means of several analytical models. Stratification predictions based on thermal conduction and ullage heating models were used to provide upper and lower limits of stratification development. This is shown in Figure 2-3.

Design criteria were developed for an axial flow mixer. The recommendation was made that a mixer be placed in both ends of the tank. This was done for several reasons:

1. Stagnant regions were observed experimentally near the mixer, while the most active mixing occurred at the regions furthest from the mixer.
2. Mixers at opposite ends of the tank assure proper mixing during special ullage conditions.

The special ullage conditions were reflected in two criteria used in the investigation

1. Ullage encapsulation of the mixer
2. Ullage breakup by the mixer.

The number of duty cycles was evaluated based on non-vented storage mode in which the stratification development time varied during the mission. The mixing time during each duty cycle and the sequence of mixer operation were determined by using upper and lower limits on the mixing time. These limits were based on the motion of the jet and tank fluid during mixing.

The nozzle outlet diameter of the mixer unit was sized to satisfy the requirements of mixing time and ullage de-encapsulation of the mixer as well as the pump flow characteristics. The nozzle should be as large as possible for a given fluid power since the product of the fluid power and the nozzle diameter establishes the mixing time. This product is 0.15 watt-ft for a minimum size conventional axial pump design. Unless there are criteria to be satisfied (such as ullage breakup), the use of this minimum size pump provides essentially the same results at lower cost (in terms of weight) than larger systems.

Conventional (state-of-the-art) vane axial pumps were considered (even though not of optimum design) since these systems will provide adequate results without extensive

development. Two types of motors were considered to drive the pumps; an ac and a brushless dc motor. The brushless dc motor has a higher efficiency than the ac motor. Using the same input power, the fluid power-outlet diameter can be doubled by the use of a brushless dc motor driven pump. This product establishes the mixing time and other associated mixing criteria such as those associated with ullage de-encapsulation, vapor removal from the tank wall, and ullage breakup by a liquid jet. As a result of the higher efficiency, a mixer driven by a brushless dc motor will have a lower weight penalty than a comparable mixer system driven by an ac motor. An additional advantage of the brushless dc motor driven mixer results from its torque-speed characteristics. These characteristics allow the motor to speed up if vapor is ingested by the pump. The increased vapor momentum then obtained will serve to dispel vapor formations in the vicinity of the mixer. An ac motor driven unit does not have this ability and would allow the mixing performance to degrade to an unacceptable level. The major disadvantage of the brushless dc motor is its requirement for additional development work.

The mixer design criteria developed in this study were applied to selection of mixer units for a manned Mars vehicle. The design data developed are shown in Tables 3-1 through 3-15.

The mixer design drawings are given, with the selected location of the mixer, venting system propellant feedlines, etc., indicated. The requirements of a mixer control subsystem and operational sequence are also defined.

SECTION 1

INTRODUCTION

The design of present and future spacecraft requires that adequate prediction and control of the propellant thermodynamic state be achieved. In this study, the technology required for the prediction of the departure of the cryogenic propellant from equilibrium conditions (thermal stratification) and the means by which equilibrium conditions can be achieved (mixing) is developed and applied to typical spacecraft conditions.

The principal effort in this study has been expended to develop analytical methods to predict and control the thermodynamic state of cryogens stored under low gravity conditions. The experimental study was conducted to verify and supplement the analytical investigations. Many of the results of the analytical investigations have been reported in Reference 1. Further analytical results are reported in References 2 through 4 and are summarized in this report. A variety of mixing concepts to implement the control of the propellant thermodynamic state were investigated in the first phase of the study and reported in Reference 1. Two mixer concepts were selected for a more detailed analytical

and experimental investigation. The design of the two mixer concepts, or destratification subsystems, selected were applied to typical spacecraft and mission conditions. The example tanks considered approximated the size of (1) a "Project Thermo" tank, (2) an S-IVB tank and (3) a typical nuclear flight module tank. A large portion of this phase of the study was experimental in nature. The results of the experimental and analytical investigations were applied by performing a mixer design study for the three stages of a manned Mars space vehicle. In addition, the sequence of mixer operation and the corresponding mixer control system requirements have been defined.

1.1 STUDY OBJECTIVES

The objectives of this study were (1) to determine the extent to which a cryogenic propellant stored in a low-g environment for a long period of time will depart from themodynamic equilibrium, (2) to determine, in those cases in which stratification is found to be severe, the feasibility of utilizing mechanical mixing techniques to achieve the desired controlled thermodynamic state, and to apply the criteria developed to the design of a mixer system.

In order to determine the severity of thermal stratification existing, simplified analyses were developed and utilized in conjunction with available analyses to predict the performance of mixers in order to provide adequate information as to the design requirements for mixer subsystems for applicable spacecraft.

The objectives of the experimental investigation were:

1. To observe mixing phenomena visually in order to obtain insight into the basic mechanism of mixing,

2. To verify, in some cases, the analytical investigations performed, and

3. To correlate the dimensionless parameters obtained from the analytical investigations.

1.2 BACKGROUND

The propellant thermodynamic conditions which require adequate prediction and control include tank pressure, quality of the propellant, and temperature and ullage spacial distributions. The relation between the tank pressure and propellant temperature distribution is very significant to the cryogenic tank design criteria. This is true since thermal stratification of liquid hydrogen propellants may typically cause the tank pressure to rise an order of magnitude faster than it would under uniform temperature or mixed conditions. Consequently, thermal stratification results in an increased mass penalty associated with propellant storage due to an increased tank mass or boiloff mass. In addition, thermal stratification may have a significant effect on the performance of the propellant utilization systems (pump and propellant feed systems) during propellant outflow.

For these reasons, the prediction and control of the degree of the departure of the propellant from thermodynamic equilibrium has been the subject of numerous investigations (References 5 through 30). Most of these studies of the prediction of

thermal stratification were concerned principally with high-gravity storage and propellant draining conditions. A limited number of investigations have been conducted to determine means of controlling thermal nonequilibrium or stratification conditions.

These studies include the effect of baffles on stratification (Refs. 5 and 6) and stratification reduction by means of a helium bubble pump (Ref. 7). It was found in these studies that baffles had very little effect on stratification and that the use of a helium bubble pump during venting conditions appeared to mix the tank contents; however, increased evaporation resulted from the concentration gradients produced by the injection of pure helium. The bubble-pump technique has only limited applications to the mixing or destratification of a closed cryogenic propellant tank.

There are, in general, at least four thermodynamic storage modes for long periods of time which require that thermal nonequilibrium or stratification be adequately controlled in order to minimize the mass penalty for storage. These storage modes utilize the following systems:

- Non-vented storage systems
- Vented systems (nominally some form of "zero-gravity system)
- Partial recondensation systems
- Refrigeration systems

A destratification or mixer subsystem to implement thermodynamic control of the cryogen is associated with each of the above thermal control or conditioning systems and is required as an integral part of the system concepts.

More recent studies have been conducted to develop "zero-gravity" vent systems whose operation depends upon the effective utilization of a mixer (Refs. 8 and 9). The satisfactory operation of these vent systems utilizing a mixer subsystem have been demonstrated under ground conditions in cryogenic propellant tanks.

Stratification nominally develops because the conduction of heat from the tank wall to the bulk fluid is the principal mode of energy transfer in the absence of gravity. The prediction of stratification by either of three models used to characterize three different phenomena results in an appreciable stratification for typical vehicle conditions. In fact, these three analytical models (conduction alone, free

convection with ullage heating, and ullage heating alone) predict a very similar stratification development for a "locked-up" tank. Hence, it is anticipated that the use of mixers to assure cryogenic propellant thermodynamic control will be required for non-vented storage. Other considerations, as discussed in Subsection 2.1, indicate that a mixer is required for the other modes of storage (vented system, partial recondensation system, and refrigeration system).

The experimental investigation is discussed in Section 4.0. The correlation of the results of the experimental investigation and a corresponding comparison of the experimental results with analytical prediction are described in Section 5.0. A summary of the design criteria formulated from the analytical and experimental studies is described in Section 3.0.

The results of the application of the mixer design criteria to typical space while condition (3 stages of a manned Mars vehicle) are given in Section 3.0. The conclusions and recommendations derived from the study are presented in Sections 6 and 7.

SECTION 2

MIXER DESIGN REQUIREMENTS

A realistic mixer subsystem design must take into account a considerable amount of vehicle-mission information formulated in terms of characteristic flight, fluid and thermodynamic parameters. From these basic vehicle-mission related parameters, the fluid thermodynamic behavior manifested in terms of thermal stratification determines the tank pressure history.

Once the basic mission-vehicle-parameters are established, thermal stratification should be evaluated. Simplified models which represent the dominent mode of energy transfer should be utilized in the preliminary design phase. For the typical vehicle-mission conditions considered in this study various types of thermal conduction and ullage heating models (see Reference 1) are suitable. A comparison of the stratification predictions of various simplified models with a numerical solution of the Navier Stokes Equations is made in Reference 1 . It was concluded that ullage heating models and thermal conduction models compare favorably, especially at early phases of stratification. The early

phase of stratification development is of particular significance when mixers are utilized. Pressure buildup in the tank due to stratification development will cause the mixer to be operated before fully developed free convection can occur.

In addition to the stratification prediction described in Reference 1 an investigation was conducted in which the results of the Lockheed Asymmetric Propellant Heating program was compared with the ullage heating model described in Reference 1. The Lockheed Asymmetric Propellant Heating program was used to predict the pressure history for a typical nuclear module under an acceleration of 10^{-7} g. The heating rate was assumed to be 1000 Btu/hr with a portion of the heating considered to be ullage heating. The results compared very favorably with the ullage heating model.

After the assessment of stratification, the number of mixer duty cycles required is determined. In addition, criteria for selection of the mixer size, flow rate, power level, location of mixers and operational sequence is established. These are discussed in more detail in the following subsections.

2.1 REFERENCE VEHICLES AND MISSIONS

Reference space vehicles and missions were considered in order to establish the sensitivity of the mixer design requirements to vehicle mission. Some of the significant parameters are

1. Tank size and geometry
2. Tank acceleration
3. Mission time
4. Cryogenic storage mode
5. Propellant heating rates

Typical examples of vehicle/mission parameters were selected for the following stage cryogenic tanks

- S-IVB
- Project Thermo
- S-IVC
- NFM (Nuclear Flight Module)

The mixer design criteria were developed in Reference 1 and applied to the S-IVB, Project Thermo, S-IVC and NFM. In this phase of study the mixer design criteria were applied in particular to the NFM vehicle for a manned Mars mission.

The nuclear powered manned Mars vehicle has been used as a representative vehicle for illustrating the design of a mixing sub-system. This vehicle is shown in Figures 2-1 and 2-2 . The pertinent vehicle mission parameters are shown in Table 2-1. These results are taken from References 32 and 33. This vehicle consists of three sizes of propellant tanks. Mixer units are incorporated in each tank.

A manned Mars vehicle has been chosen because

1. It represents typical long term storage conditions and
2. The required data was readily available.

The storage mode for the earth escape stage and the Mars braking stage is nonvented. The Mars escape stage includes both nonvent and vented storage mode. The propellant is initially stored at the triple point. A solar shield is assumed to be deployed during the earth to Mars transfer stage and consequently the heat input during this leg of the mission is essentially zero (significant heating occurs only for a short period of time during midcourse correction).

Tank acceleration in earth orbit is assumed to be due to atmospheric drag. The tank acceleration due to attitude

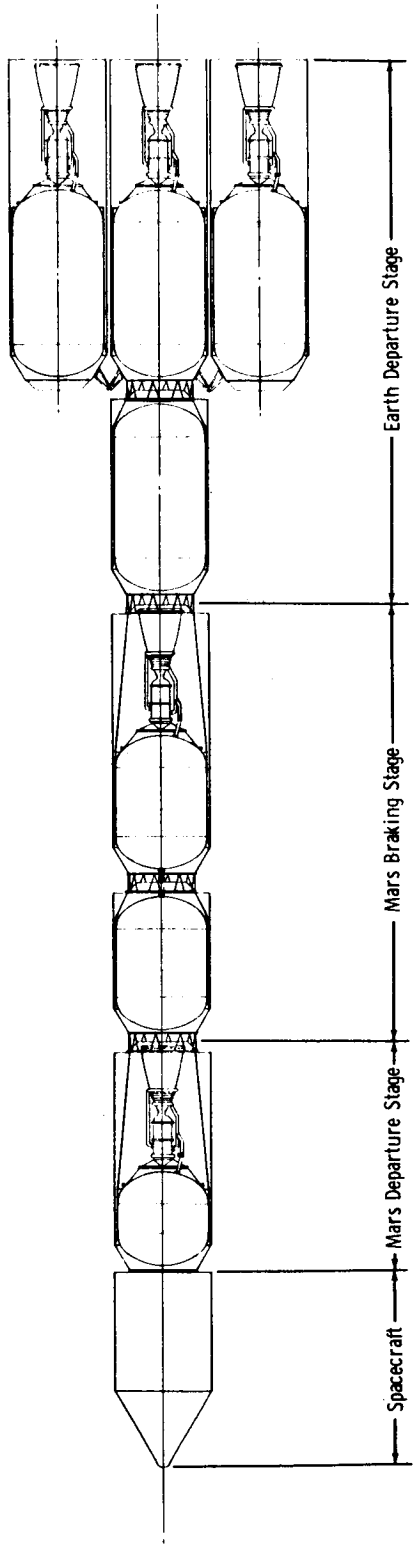

Figure 2-1 Conjunction - Class Mars Vehicle

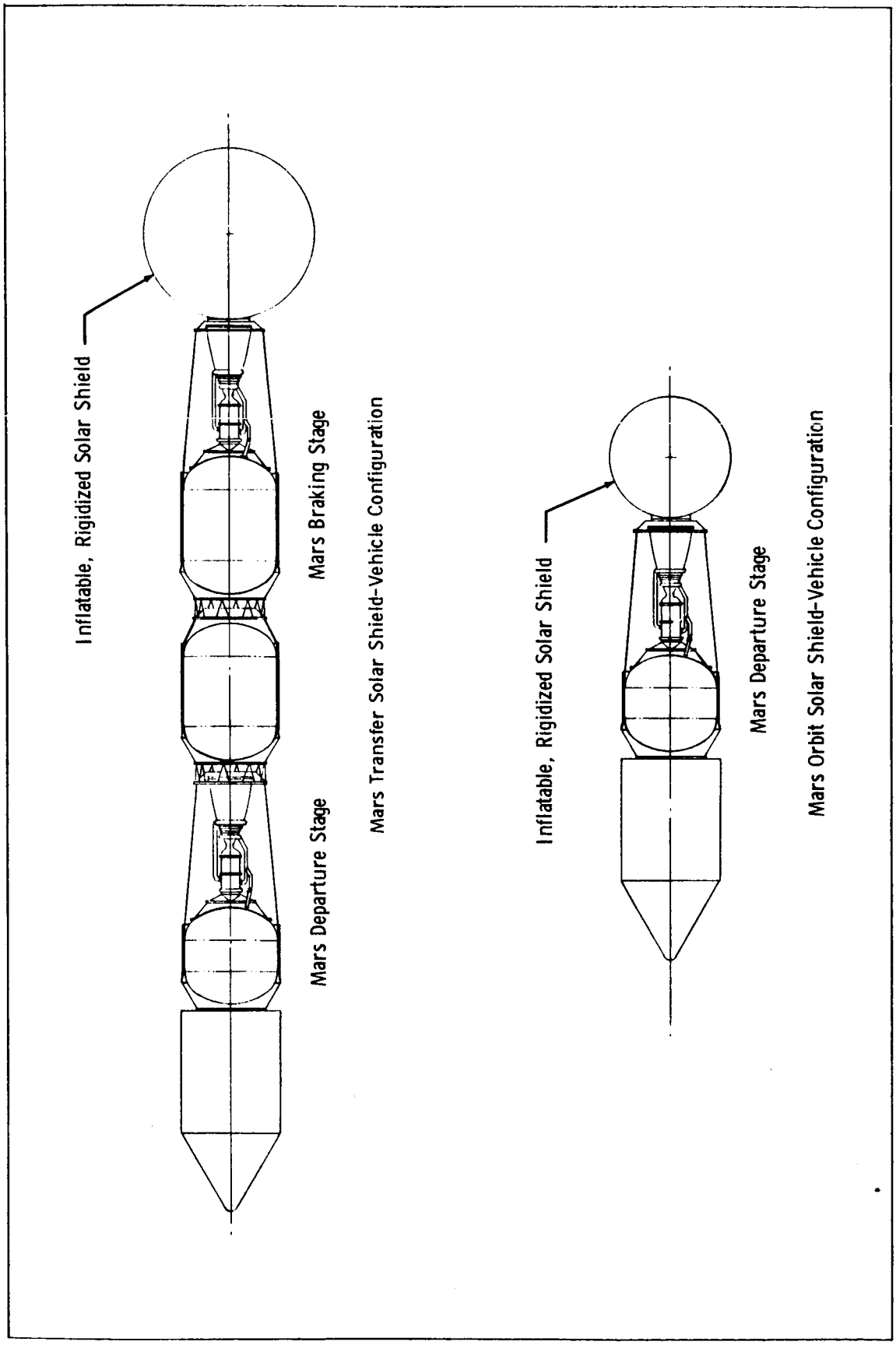

Figure 2-2 Mars Transfer and Mars Orbit Solar Shield-Vehicle Configuration

Table 2-1

VEHICLE MISSION PARAMETERS

	Earth Escape Stage	Mars Braking Stage		Earth Escape		
	Earth Orbit	Earth Orbit	Earth to Mars	Earth Orbit	Earth to Mars	Mars Orbit
Time, days	180	120	210	60	210	510
Tank Diameter, ft	32	32	32	32	32	32
Tank Length, ft	72.45	53.82	53.82	27.27	27.27	27.27
Tank Volume, ft^3	52207	37222	37227	15870	15870	15870
Tank Area, ft^2	7620.3	5747.2	5747.2	3078.2	3078.2	3078.2
Propellant Mass (Initial), lbs	219539	156540	156540	66713	66713	66713
Initial Temperature, ^oR	24.85	24.85	36.48	24.85	32.2	32.2
Final Temperature, ^oR	36.48	36.48	36.48	32.2	32.2	37.2
Initial Pressure, Psia	1.02	1.02	14.7	1.02	7.0	7.0
Final Pressure, psia	14.7	14.7	14.7	7.0	7.0	14.7
Initial Density, lb_m/ft^3	4.808*	4.808*	4.425	4.808*	4.557	4.557
Final Density, lb_m/ft^3	4.425	4.425	4.425	4.557	4.557	4.425
ΔT, NPSP, ^oR	1.9	1.9	1.9	1.9	1.9	1.9

*Triple point in initial Earth orbit

Table 2-1 (Cont'd)

	Earth Escape Stage	Mars Braking Stage		Earth Escape Stage		
	Earth Orbit	Earth Orbit	Earth to Mars	Earth Orbit	Earth to Mars	Mars Orbit
Initial Void Fraction	.125	.125	.05	.125	-.07	.07
Final Void Fraction	.05	.05	.05	.07	-.07	.152
Firings Per Stage	1	1	1	1	1	1
Number of Tanks Per Stage	4	2	2	1	1	1
Heating, Btu/hr	1128	1208	-	620	0	248
Q/A_t, Btu/hr ft^2	.148	.210	-	.2014	0	.0805
Nonvent Time, days	180	120	210	60	210	279
Vent Time, days	0	0	0	0	0	231
Max Acc, a/g	10^{-5}	10^{-5}		10^{-5}		10^{-8}
ΔIMIEO (Mass fixed)	1.802	3.132	3.132	4.504	4.504	4.504
Boiloff, lb_m	0	0	0	0	0	7198.9
Bulkhead Length, ft	11.3	11.3	11.3	11.3	11.3	11.3
Orbital Altitude, n.mi.	262	262		262		3238

control is not presently known. In any event, a tank acceleration level less than 10^{-5} g does not adversely affect the mixer requirements. Under this acceleration level, buoyancy effects on jet mixing and the effect of acceleration on ullage breakup can usually be neglected. In such cases the severity of the mixer design requirements tend to increase with decreasing acceleration due to increased stratification, lack of vapor removal from heat shorts and vapor encapsulation of the mixer. Hence, when buoyancy is not important and ullage breakup is desired the mixer is designed for a very low acceleration (10^{-8} or less).

2.1.1 Tank Size and Geometry

The dimensions and geometry of the propellant tank affects a number of parameters which are used to determine mixer design and performance. Two major items affected are mixing time and the stratification development rate. For example, the magnitude of the jet momentum required to ensure mixing at the tank end furthest from the mixer is a function of the tank dimensions. In addition, the time required for all of the tank contents to mix and the required jet outlet diameter are influenced by tank dimensions. The development of free convection in the tank is dependent on the tank size. The free

convection phenomena influences stratification development rates and, hence, the duty cycle of the mixer.

It is also expected that mixing system weight and power requirements will increase as the tank dimensions increase. These quantities are also dependent on the geometry since the tank bulkhead shape assumed in an analysis can also affect the predicted weight and power requirements. The mixing requirements, in terms of power and weight, tend to reach a maximum at L/D_t of about 1.5 for tanks of the same volume with hemispheric or elliptical ends. The mixing requirements do not vary with L/D_t (for L/D_t less than about 1.5) for flat end tanks. The reason that the mixing requirements tend to decrease for L/D_t greater than 1.5 is due to the area of the jet flow region up the central portion of the tank, which increases bulk fluid motion (see bulk motion equation which includes the effect of the jet area or bulk fluid motion in Appendix B).

Implied within analyses shown in Appendix B is the finding that mixing will take place faster in a tank with hemispheric or elliptical ends than for a tank with flat ends. Experiments performed in this study have shown that agitation caused by the jet mixer is considerably more vigorous at the end opposite to that in which the mixer is located. A stagnation region forms next to an axial jet mixer, resulting in little or no flow in

the vicinity of the mixer. The flow is so slight near the mixer that it is difficult to remove bubbles from heat shorts and sweep away stratified layers that form at the tank bottom during non-mixing periods. This can be alleviated by counter directed mixers operated alternately or by utilizing combined axial and radial jets.

2.1.2 Tank Acceleration

Tank acceleration can have a marked effect on mixer design and performance. In a large tank, under orbital conditions, it is not uncommon to have a Bond number somewhere greater than 1. This is due to deceleration from atmospheric drag in low orbit and centrifugal acceleration in higher orbit due to velocity orientations produced by the attitude control system.

Sloshing due to acceleration perturbation of the spacecraft attitude control system can have an effect on stratification development rates, especially for a single-ullage condition. The influence of tank acceleration on free convection can be established by using a criterion such that the Grashof or modified Grashof number is much greater than 1. This criterion indicates that free convection will occur in most spacecraft applications. In fact, turbulent-flow free convection is possible in longer vehicles, even with the use of high-performance insulation.

For a given heat input and tank size, local boiling along the tank sidewall (especially at heat penetration locations) tends to increase as acceleration decreases due to lack of free convection currents. In addition, the required momentum to be produced by the mixer to disrupt a single ullage is influenced by the acceleration. It has been shown (Ref. 1) that ullage disruption enhances destratification. (There are, of course, mass penalties for ullage disruption associated with ullage settlement before engine firing unless a propellant utilization system is available that can handle small amounts of two-phase flow.)

Under high tank acceleration levels buoyancy forces tend to retard development of a jet sufficient to penetrate a stratified layer. In addition, bubbles if sufficiently large, will migrate in a direction opposite to the acceleration, coalesce, and settle at one end of the tank during mixer non-operation. If the acceleration is sufficiently large, or if the mixer does not have the ability to break the bubbles into small size, the propellant may remain in a more or less settled condition even during mixer operations. It is also possible for tank accelerations to cause bubble encapsulation of the mixer, thereby reducing the mixing efficiency. This situation can be circumvented by placing mixers at each end of the tank.

2.1.3 Mission Time

The principal effect of mission time is to influence the size, weight, and type of power supply. On long-term missions, a nuclear power supply may be available and the penalty attributable to power consumption is a function of the power level and essentially independent of the mission time. Hence, the duty cycle does not affect the system weight, except for increased boiloff as a result of propellant heating due to the mixing. The weight of conventional power supplies (batteries, fuel cells) are dependent upon mission time, duty cycle, and power level required.

2.1.4 Cryogenic Storage Mode

The mode of storage and the initial propellant thermodynamic condition affect the mixer concept design and integration into an overall thermodynamic control or conditioning system. The common modes of long-term storage are

1. Nonvented
2. Vented
3. Partial recondensation
4. Refrigeration

The use of slush or, to a lesser degree, a "subcooled" condition permits the cryogen to be stored a long period of time without venting. Under nonvent storage, stratification can typically cause the tank pressure to rise as much as 10 times faster than it would rise under equilibrium conditions (mixed) for the same heat input. If the tank is to be vented at 15 psia, 22 Btu/lb can be absorbed if the initial condition is triple-point liquid. If 50% slush conditions are utilized as initial conditions, 35 Btu/lb can be absorbed. The boiloff savings are 12% ($C_L \Delta T/h_{fg} = 0.12$) of the storage mass for nonvented triple-point storage and 18% of the original storage mass for an initial slush condition. For a nuclear powered Mars stopover vehicle, the weight saving (ΔIMIEO) due to nonvented storage can be as much as 153,000 pounds (12%) for 1,258,000 pounds of propellant initially stored at the triple point. If a destratification device were not utilized during the nonvented storage period, the weight savings of the boiloff due to subcooled storage would be only 15,000 pounds before venting would be required (assuming that the tank pressure rises 10 times faster than it would under thermally mixed conditions).

The use of the mixer subsystem in conjunction with a "zero gravity" vent system is necessary for the proper operation of the vent device. When venting is necessary, the combined zero-gravity vent system results in a substantial decrease in the mass penalty required for venting when compared with the use of an ullage thruster for venting.

Studies (Ref. 32) have indicated that a partial recondensation system is in most instances considerably superior to pure vent systems as a mode of propellant storage when combined nonvented-vented systems are required. (Venting is required because of either the magnitude of the heat input or the nonavailability of "subcooled" or triple-point initial propellant conditions.) Nominal partial recondensation systems (Ref. 34), however, require the availability of vapor input to the system. Under low-g conditions the availability of vapor at the inlet to the recondensation system cannot be achieved without a considerable mass penalty if conventional settling methods are utilized. In order to achieve a combined, efficient partial recondensation system, a zero-gravity vent system will be needed to provide vapor to a typical recondensation system such as described in Reference 34 . The partial recondensation

system's flow and other thermodynamic-condition requirements have to match with zero-gravity and mixer-subsystem requirements to obtain a feasible optimum thermal control or conditioning system.

It can be seen that, for the two most efficient methods of storage (nonvented and the use of a partial recondensation system), a mixer subsystem and the mixing technology to control the thermodynamic equilibrium condition in a cryogenic propellant tank are required. The exact nature of the hardware requirements for the mixer subsystem is dependent upon the selected mode of propellant storage. The overall mixing technology to determine the requirements for such a subsystem can be established somewhat independently of the mode of storage. Hence, the major emphasis in this study is in the development of mixing technology rather than in the direction of the development of hardware items, since most items are readily available (unless miniaturization is required).

The use of a mixer in conjunction with nonvented storage can provide information as to the magnitude of the heating during a mission, in order to obtain up-to-date evaluation of the space vehicle's thermal protection system performance.

2.1.5 Propellant Heating Rates

Tank heating rates influence the following subsystem design parameters:

1. Mixer flow rate, hence power requirements.
2. Initial stratification and/or stratification development time before mixer is operated, and residual stratification during duty cycle.
3. Boiling at sidewalls (methods are needed either to suppress boiling or to remove vapor to prevent all the ullage from collecting at the tank walls).

The mixer flow rate for continuously operating destratification systems was shown in Reference 1 to be proportional to the heating rate. This is due to stratification developing faster and becoming more severe with an increase in heating rate. Therefore, in order to obtain a given residual stratification level the flow rate must be increased with increasing heat input.

The flow rate or power requirement for an intermittently operating mixer system was shown in Reference 1 to have no direct relationship with the heating rate. However, an increased heating rate does reduce the stratification development time. This results in an increase in the number of duty cycles required by an intermittently operating system.

Under very low-g conditions, boiling is more likely to occur at the tank side wall (especially at heat shorts) as

the heating rate is increased. For a nonvented tank, the total vapor volume remains essentially constant (actually decreases for small void fractions). Condensation occurs at subcooled regions if vapor is available, and continues to occur until all of the vapor is in the vicinity of the heat inputs. For periods of time during which the mixer is not operated, the principal mode of energy transfer is reduced to thermal conduction alone - increasing the rate of stratification development. Removing vapor from the wall or suppressing its formation enhances destratification. As a result, criteria have been developed which, when used, determine the system flow rate required to suppress or remove bubbles from the heated surface (Ref. 1).

2.2 THERMAL STRATIFICATION

The tank pressure rise during nonvent storage when the mixers are not operated determines the number of duty cycles for mixing. Thermal stratification development, or the departure of the propellant (liquid) from a uniform temperature, in turn determines the tank pressure rise. Under a gravity field sufficient to maintain a settled propellant, stratified layers develops normal to the gravity vector. In this case, there are many models (Ref. 1) which can be used to predict the tank pressure rise, as shown in the sketch below:

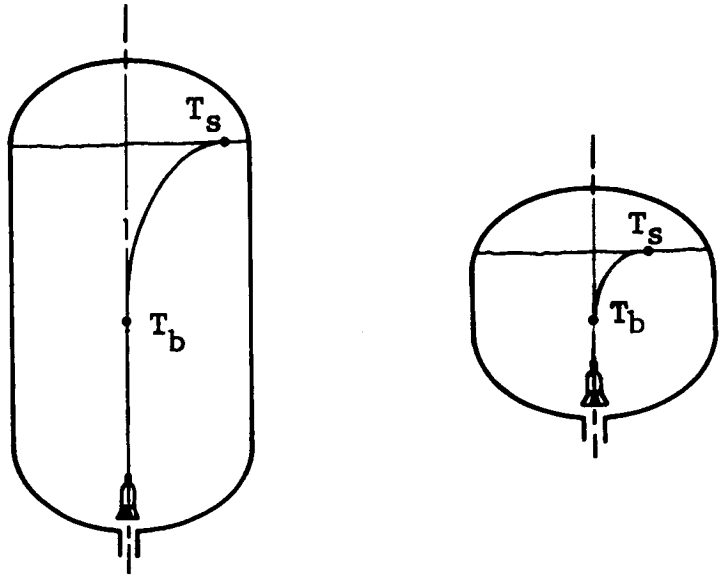

Under very low gravity conditions, stratification may take place in numerous ways, depending upon the ullage configuration, and location, shown below

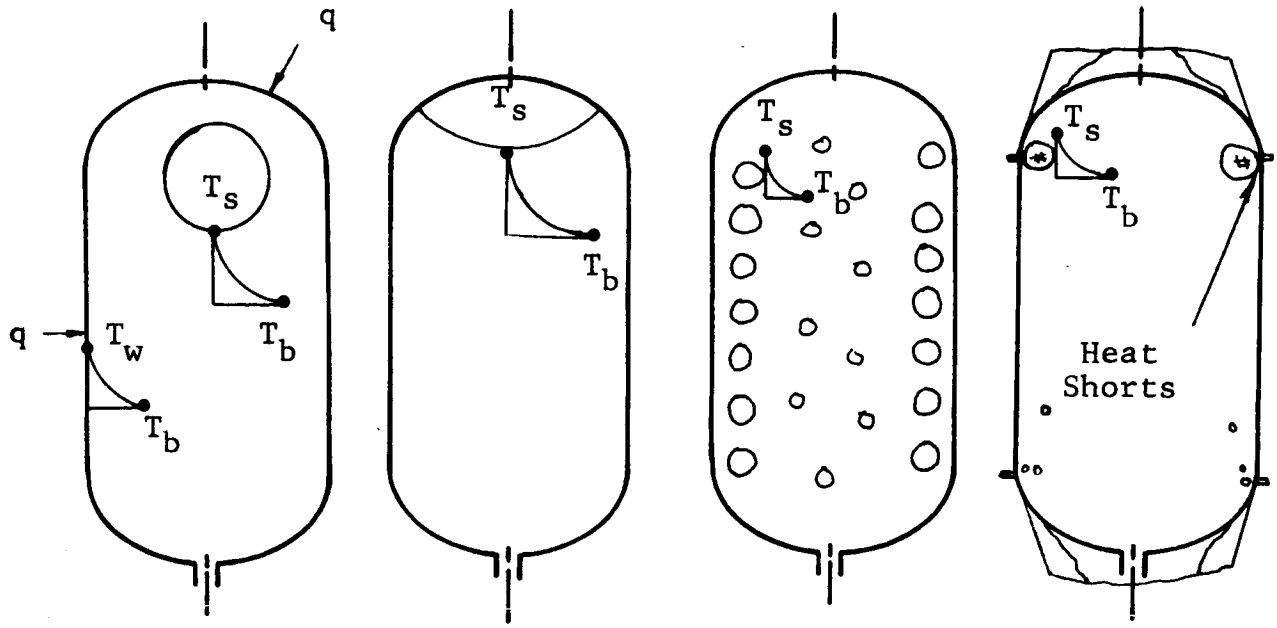

Under these very low gravity conditions the conventional models are in most instances not applicable to predicting stratification. Because of the reduction in free convection flow and the length of time required to establish free convection flow, thermal conduction and vapor heating models are applicable especially in attempting to establish upper limits of stratification development. Boiling along the sidewall and especially at heat shorts needs to be taken into account. These ullage heating and conduction models are discussed in Reference 1. Figure 2-3 shows the predictions made from these models. The shaded area of this figure represents the range of stratification prediction.

Under low gravity conditions the energy exchange between bubbles in the tank become important when boiling occurs.

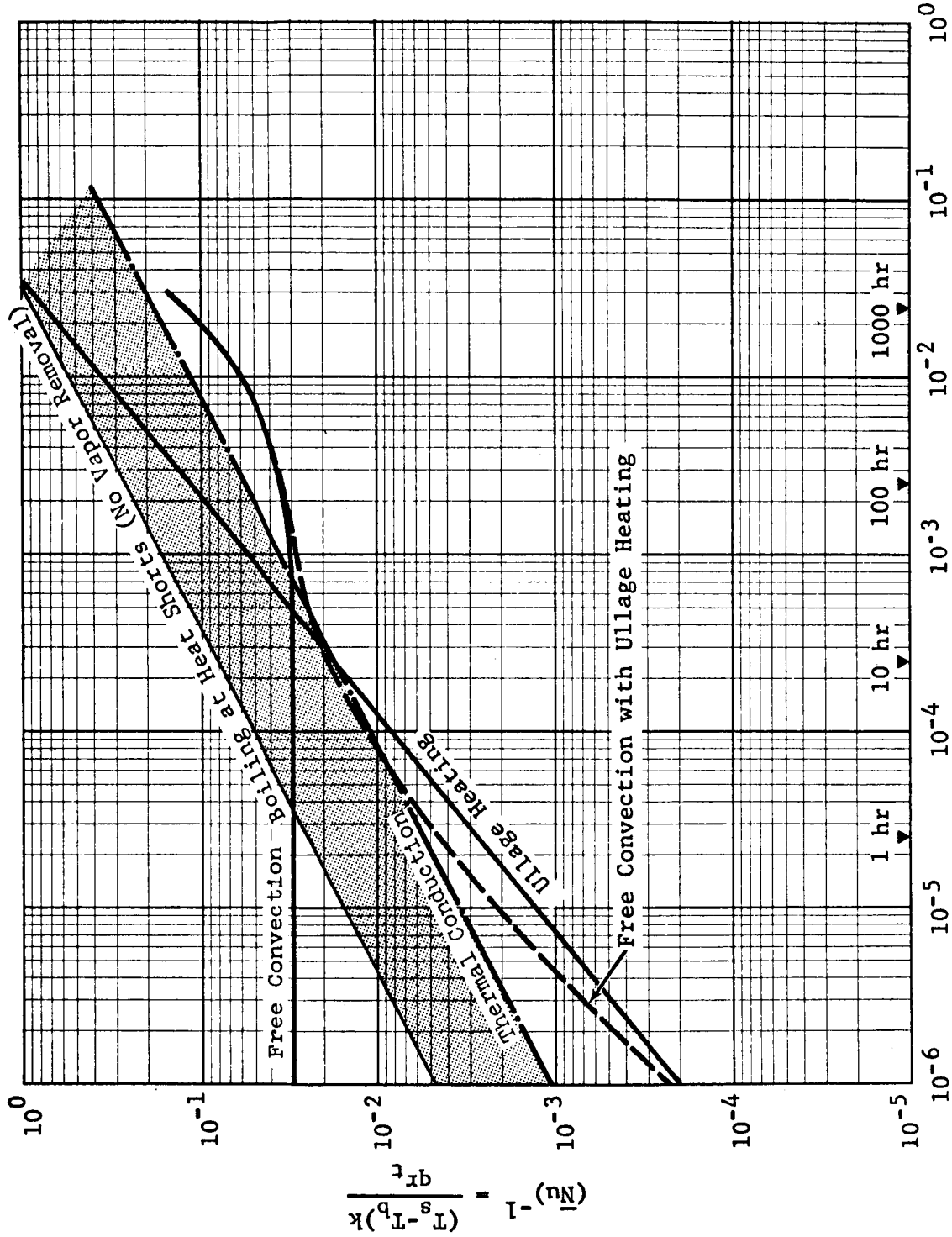

Figure 2-3 Comparison of Simplified Stratification Models for Typical Nuclear Flight Module Conditions

The major thermal resistance to heat transfer under boiling and condensation conditions is thermal conduction in the vicinity of the bubbles. In establishing the rate of pressure rise, thermal conduction, ullage heating and free convection models yield similar predictions. The thermal conduction models do, however, tend to yield an upper bound on the stratification development. The conduction models are used to predicting the pressure rise, from which the number of duty cycles are calculated. In these models, the temperature stratification develops as the square root of the time.

The relation can be expressed as

$$T_s - T_b = C_s (\theta)^{\frac{1}{2}}$$

where T_s is the liquid/vapor interface temperature, T_b is the bulk fluid temperature, C_s is a constant and θ is the time. The constant C_s is defined for conduction models as

$$C_s = 1.1\ q\sqrt{\alpha}\ /K$$

where q is the heat flux to the interface, α is the thermal diffusivity and K is the liquid thermal conductivity. The heat flux calculated is based on the total heating and the surface area of the tank wall or of the bubble interface surface. This is shown in the shaded region of Figure 2-3.

The results of the use of a thermal conduction model are shown in Table 3-3 for the selected manned Mars vehicle. In addition, an equilibrium constant, C_e is given. The constant, C_e is defined as

$$C_e = (T_f - T_i + \Delta T_{np})/\theta_t$$

where T_f is the final fluid temperature before engine firing, ΔT_{np} is related to the difference between the tank design pressure and the final pressure before pressurization and engine firing. T_i is the initial propellant temperature at the start of the mission (from earth orbit), and θ_t is the storage time.

2.3 DESIGN CRITERIA

2.3.1 Mixer Concepts

During the study numerous mixing concepts were evaluated. The most promising concepts were:

1. Paddle wheel and unshrouded propeller concept
2. Ducted-flow concept
3. Wall heat exchanger concept
4. Radial and axial jet concepts.

The concept selected in Reference 1 was axial or radial jet flow produced by an axial flow pump. The axial jet was utilized in the design study since experimental data indicated that this concept provided a superior mixing performance compared with the radial jet.

The design criteria for the axial jet mixer are developed in the following subsections. These criteria, which were used for sizing the axial jet, insure that the two basic requirements for proper mixing are met. These requirements are

1. Removal of energy from near the wall and depositing it in the bulk fluid, and
2. Mixing of the bulk fluid.

Space vehicle applications may exist in which one of the rejected concepts might perform better than the axial flow jet. However, for large space vehicles (the primary application of this study) the axial jet is superior. The following paragraphs detail some of the disadvantages of the other concepts when compared with the axial jet.

For the purpose of bulk fluid mixing, a simple propeller is the most effective of the concepts as evidenced by the results of many studies of mixing and agitation of tank contents conducted in the field of chemical engineering. The principal objective to an unshrouded propeller for agitation of space vehicle tank contents is that fluid rotation or swirl is produced during mixing. To avoid fluid rotation, either vertical baffles are needed or the propeller axis should be offset from the centerline of the tank. The dynamic forces produced by using either vertical baffles or a nonsymmetric flow pattern in the tank must be offset by increased attitude control system requirements. However, a shrouded propeller utilizing stationary flow straightening vanes is more efficient (from a hydraulic standpoint) than a propeller. In addition, fluid rotation is eliminated. Weightwise, the shrouded and unshrouded propellers are comparable.

The heat exchanger or flow distribution concepts have some advantages due to the fact that energy from the tank wall can be immediately intercepted (provided that continuous pump operation is feasible). The added installation complications and weight of the heat exchanger concepts makes them less attractive than the axial flow mixer.

The weight and complexity of a flow distribution system for a large space vehicle far exceeds that of two or more small axial flow pump-mixers fitted with appropriate outlet nozzles. In comparison, the axial flow pumps can be conveniently installed at each end of the tanks and all associated equipment is located in two small regions of the tank and outside the tank.

2.3.2 Nonvented Duty Cycle Evaluation

It is desired to evaluate the number of duty cycles required for a nonvented storage mode in which the stratification development time is not constant but varies during the course of a mission. As an example, if the propellant is originally stored at triple point conditions, operation of the mixer is not required until the tank pressure has reached the selected tank vent or design pressure. Typically, this pressure is around 20 psia. Thus, for a long period of time during the initial phase of a mission, the mixer operation will not be required (depending upon the rate at which stratification develops). As the mission time increases, the mixer operation will be required between shorter periods of stratification development. The sketch shown below represents a typical liquid/vapor interface temperature and equilibrium temperature history.

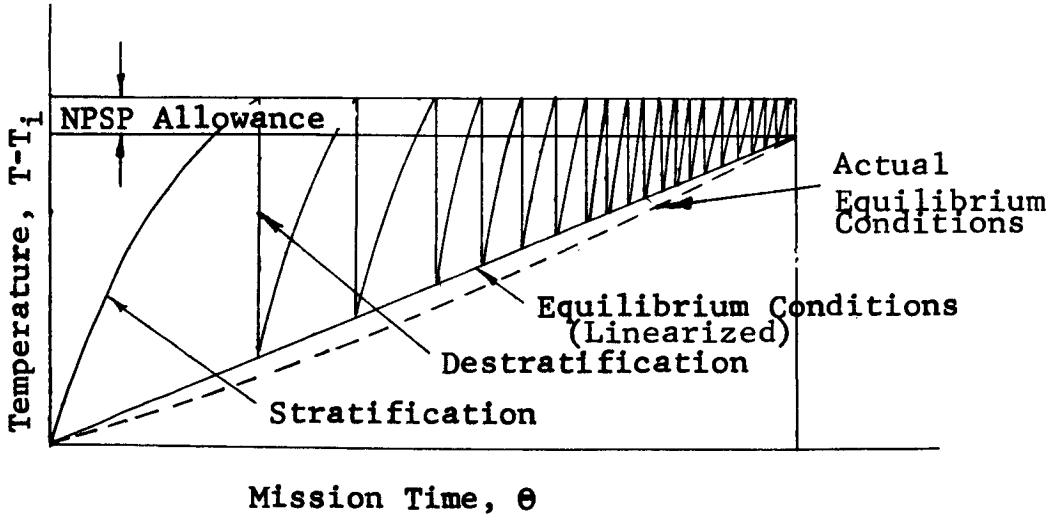

The equilibrium temperature rise was approximated as a linear function of time for a constant heating phase of a mission

$$T_e - T_i = \Delta T_e = C_e \Theta$$

where

T_e is the mixed temperature

T_i is the initial temperature

Θ is the mission leg time

C_e is an equilibrium constant

If a conduction model is used for stratification

$$T_s - T_i = C_s \Theta^{\frac{1}{2}}$$

where

T_s is the maximum tank liquid/vapor interface temperature, and

C_s is a stratification coefficient defined in Subsection 2.2 .

Normally, the mixing time can be neglected since it will typically contribute only a small portion of the total storage time. The approximate analysis shows an infinite number of duty cycles would be approached as the equilibrium thermodynamic condition approached the tank vent or design pressure. In order to obtain a finite number of duty cycles, the temperature drop due to mixing during the final duty cycle is set

equal to the temperature decay, ΔT_f. In a typical case the final temperature destratification is equivalent to the $1.9^{\circ}R$ corresponding to 5 psia or the NPSP.

The number of duty cycles will be calculated for the typical NFM conditions based on the above sequences. The sequence utilizing NPSP allowances will result in a small number of duty cycles.

The ratio, f, of the destratification temperature drop to temperature rise before the mixer is operated is

$$f = \frac{\Delta T_s - \Delta T_e}{\Delta T_s}$$

Since $\Delta T_e = C_e\theta$ and $\Delta T_s = C_s\theta^{\frac{1}{2}}$

$$f = 1 - \frac{C_e\theta^{\frac{1}{2}}}{C_s}$$

The temperature drop during the first duty cycle is

$$\Delta T_1 = f_1 \Delta T_{s_1}$$

and the temperature drop during subsequent cycles is

$$\Delta T_2 = f_2 \Delta T_{s_2}$$

$$\Delta T_3 = f_3 \Delta T_{s_3}$$

$$\Delta T_4 = f_4 \Delta T_{s_4}, \text{ etc.}$$

where

$$f_1 = 1 - \frac{C_e}{C_s} (\theta_1)^{\frac{1}{2}}$$

$$f_2 = 1 - \frac{C_e}{C_s} (\Theta_2)^{\frac{1}{2}}$$

$$f_3 = 1 - \frac{C_e}{C_s} (\Theta_3)^{\frac{1}{2}}$$

Also

$$\Delta T_1 = \Delta T_{s_2}$$

$$\Delta T_2 = \Delta T_{s_3}, \text{ etc.}$$

The final temperature drop, ΔT_f is

$$\Delta T_f = (f_1 \ f_2 \ f_3 \ f_4 \ f_5 \ . \ . \ f_f) \ \Delta T_{s_1}$$

For the final decay in stratification, ΔT_f;

$$\Delta T_f = \Delta T_{NPSP}$$

The stratification development times, $\Theta_1^{\frac{1}{2}}$, $\Theta_2^{\frac{1}{2}}$, $\Theta_3^{\frac{1}{2}}$, are then calculated in **order** to determine f_1, f_2, f_3,

$$\Theta_1^{\frac{1}{2}} = \frac{\Delta T_{s_1}}{C_s}$$

and

$$f_1 = 1 - \frac{C_e}{C_s^2} \Delta T_{s_1}$$

also

$$\Theta_1^{\frac{1}{2}} = \frac{\Delta T_{s_1}}{C_s} \left(1 - \frac{C_e}{C_s^2} \Delta T_{s_1}\right)$$

Finally for

$$\overline{f}_1 = \frac{C_e}{C_s^2} \Delta T_{s_1} f_1$$

$$f_2 = 1 - \overline{f}_1$$

$$f_3 = 1 - \overline{f}_1 f_2$$

$$f_4 = 1 - \overline{f}_1 f_2 f_3$$

$$f_5 = 1 - \overline{f}_1 f_2 f_3 f_4$$

The final decay in stratification, ΔT_f,

$$\Delta T_f = \Delta T_{s_1} (f_1 f_2 f_3 f_4 \ldots f_f)$$

Using the previous equation, the number of duty cycles can be determined for any mission phase.

The results for a dimensionless decay in stratification (destratification) are obtained from the equation

$$\frac{\Delta T_f}{\Delta T_{s_1}} = f_1 f_2 f_3 f_4 \ldots\ldots f_n$$

The number of duty cycles is $n_d = n$. Because of the tedious calculations required, the above equations were evaluated by use of a computer. The results of the calculations for a manned Mars vehicle are shown in Table 3-4 of Subsection 3-2 .

2.3.3 Mixing Time

The mixing time is the total time the mixers are required to operate during each duty cycle. From a design point of view it is desirable to place an upper and lower limit on the anticipated length of time a mixer is to be operated.

The absolute lower limit on mixing time can be obtained based on the time required for the jet to develop and traverse the length of the tank. It does not appear that the mixing time could be less than this because there is very little motion in the tank (based upon experimental observation) until the jet has traversed the length of the tank. The jet motion mixing time is written in terms of a dimensionless time

$$\frac{V_o D_o \theta_j}{D_t^2}$$

where θ_j is the time required for the jet to traverse the length of the tank, V_o is the outlet velocity, D_o is the outlet diameter, and D_t is the tank diameter. It should be pointed out that the dimensionless time defined above is consistent with dimensionless time associated with mixing in general. The motion of the bulk fluid as fluid particles move from one end of the tank to the other is based on the same group of variables. The dimensionless time for jet fluid particle to traverse the length of the tank is derived in Appendix A and

is given by

$$\frac{V_o D_o \theta_j}{D_t^2} = 0.152\left(\frac{Z_b}{D_t}\right)^2$$

where Z_b is the liquid height above the nozzle and is assumed to be the tank length for low g conditions.

In order to estimate a lower limit on the dimensionless mixing time $\left((V_o D_o \theta)/D_t^2\right)$, the time required for the jet to traverse the tank is added to that time required for a particle to travel from the top of the tank to the junction of the upper bulkhead and the cylindrical tank section as shown below

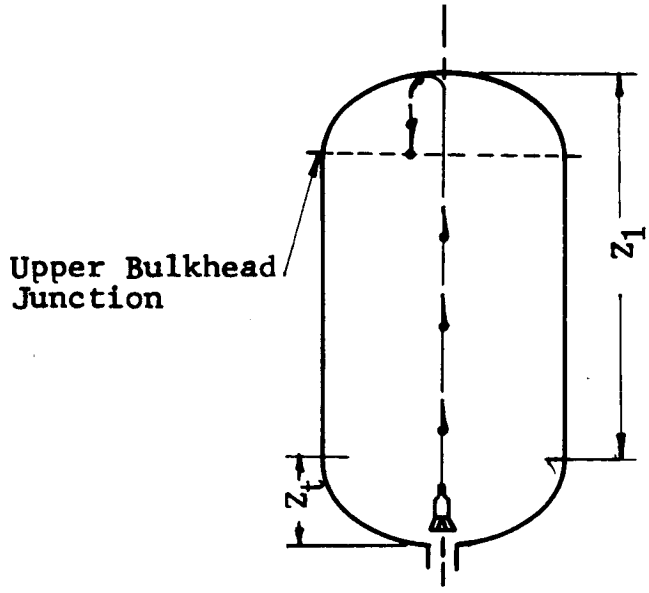

In order to calculate the bulk fluid motion of the particle after the jet has reached the top of the upper bulkhead, the bulkhead is assumed to be a straight cylindrical section. The equations for bulk fluid motion in a straight tank section given in Appendix B are then applicable. The bulk motion equation is (assuming that the

nozzle is at the same level as the bottom bulkhead)

$$\frac{V_o D_o \theta_B}{D_t^2} = 2.193 \ln \left(\frac{Z_1 + Z_t}{Z_1} \right)$$

where Z_1 is distance from the junction of the lower bulkhead to the top of the tank, Z_t is the bulkhead height (assuming similar bulkheads on each end of the tank), and θ_B is the time for the bulk flow to move from the top of the tank to the junction of the upper bulkhead and the cylindrical tank section.

The lower limit of the estimate of the mixing time is then

$$\frac{V_o D_o \theta_M}{D_t^2} = 2 \frac{V_o D_o}{D_t^2} (\theta_j + \theta_B)$$

where θ_M is the mixing time for each duty cycle. The factor of 2 accounts for operating each mixer for one-half of the total mixer time.

A mixer, as mentioned before, is located on each end of the tank to satisfy the ullage encapsulation criterion for a bubble Bond number greater than 1.0 and to implement mixing in the vicinity of each mixer.

Two mixers, one located on each end of the tank, are considered in order to satisfy the ullage encapsulation criterion for a bubble Bond number greater than about 1.0 and to

implement mixing in the vicinity of each mixer. When the bubble Bond number is greater than about 1.0 vapor formations are not expected to occur simultaneously in both tank ends (Ref. 35), thus leaving one mixer available for mixing. Mixers in both ends are necessary since the ullage position will be determined by the acceleration vector. More complete mixing is obtained using a mixer in each end since the most efficient mixing occurs furthest from the mixer.

In the experimental program, it was obvious that the most efficient mixing was achieved at the tank end opposite to that end at which the mixer was located. Also, a stagnation region occurred in the vicinity of the mixer because there was little or no fluid entrainment near the mixer. The mass flow of bulk fluid was very small in the vicinity of the operating mixer, whereas bulk fluid motion orders of magnitude greater than the mixer flow rate was observed in the tank region away from the mixer. The mathematical expression for the bulk fluid flow rate ratio which characterizes this phenomena is

$$\frac{\dot{M}_Z}{\dot{M}_O} = 0.456 \frac{Z}{D_O}$$

where Z is the distance above the nozzle, $\dot{M}_Z$ is the bulk fluid flow rate and $\dot{M}_O$ is the outlet flow rate. Typically,

Z/D_o is from 200 to 300, indicating a large bulk flow rate at the end of the tank opposite to which the mixer is located.

The second mixer was assumed to be activated (by use of a timer) after a time interval determined by an estimate of a maximum mixing time based upon the time for the jet to reach the top of the tank plus the time for a particle of fluid to move from the top of the tank to the lower bulkhead. The dimensionless mixing time in this case is

$$V_o D_o \theta_m / D_t^2 = 0.152(Z_b/D_t)^2 + 2.193 \ln (1.0 + Z_1/Z_2)$$

2.3.4 Minimum Fluid Power

Current axial pump designs limit the smallest conventional liquid hydrogen pumps to a fluid power in the vicinity of 1 watt. The corresponding pump-motor efficiency is in the vicinity of from 10 to 15%. Below a fluid power of 1 watt, the overall pump-motor efficiency and reliability begin to drop off sharply. A pump blade diameter of about 2 inches is typical for this design.

The fluid power-outlet nozzle diameter product establishes the mixing time and other associated mixing criteria such as those associated with ullage de-encapsulation, vapor removal from the tank wall, and ullage breakup by a liquid jet. The fluid power-outlet diameter product for a minimum size conventional design is on the order of 0.15 watt-ft. This number represents a good starting point for a minimum weight conventional pump-motor design if there are no overriding criteria such as an ullage breakup criterion, etc. When these criteria do not need to be satisfied, total mixer weight is needlessly increased as fluid power is increased. The conclusion is that gentle agitation of the fluid results eventually in essentially the same mixing at a lower cost in weight than more vigorous mixing.

The conventional pump design referenced is powered by a.c. electric motors. For the same input power (7 to 10 watts),

the fluid power-outlet diameter can be doubled by the use of a "brushless" d.c. motor driven pump.

D.C. motor efficiencies quoted for liquid hydrogen are estimated (Ref. 9) since there was no data available on a liquid hydrogen compatible brushless d.c. motor. The high efficiency of the brushless d.c. motor is not only the result of small d.c. motor characteristics (which have characteristic higher efficiencies than a.c. motor) but also due to the elimination of friction losses of the internal brushes. In addition, brush wear and the associated problems with reliability are minimized, assuming external commutation can be reliably demonstrated.

In most instances, the minimum size utilizing conventional designs will result in a very modest total system weight (say from 20 to 50 pounds). There are, however, severe cases in which either stratification is expected to develop rapidly or the length of mission is such that it is desirable to seek ways to reduce the overall weight. If low power is desired, a weight reduction will result if the size of the mixer unit is increased out of proportion to conventional size-power characteristics. For example, a tradeoff of the mixer weight and weight associated with mixer power (boiloff and power supply weight) may indicate that a 4 to 6-inch diameter mixer is needed with a fluid power of one watt. In

such cases, development work would be required for such an "out of proportion" mixer unit. The unit would have an unconventionally low speed, requiring either a larger electric motor (a.c.) or a low frequency power source or both. From a weight standpoint, the proper proportion of boiloff and power supply weight to mixer weight is approximately 6 to 1. Whether or not a conventional mixer unit satisfies this weight tradeoff trend is dependent solely upon the total length of time the unit is operated.

2.3.5 Ullage Location and Distribution

The ullage location and distribution under high gravity conditions is adequately controlled by buoyancy forces on the vapor and is, of course, quite predictable. For this case, the mixer should be located at the end opposite to which the vapor tends to accumulate, as shown below.

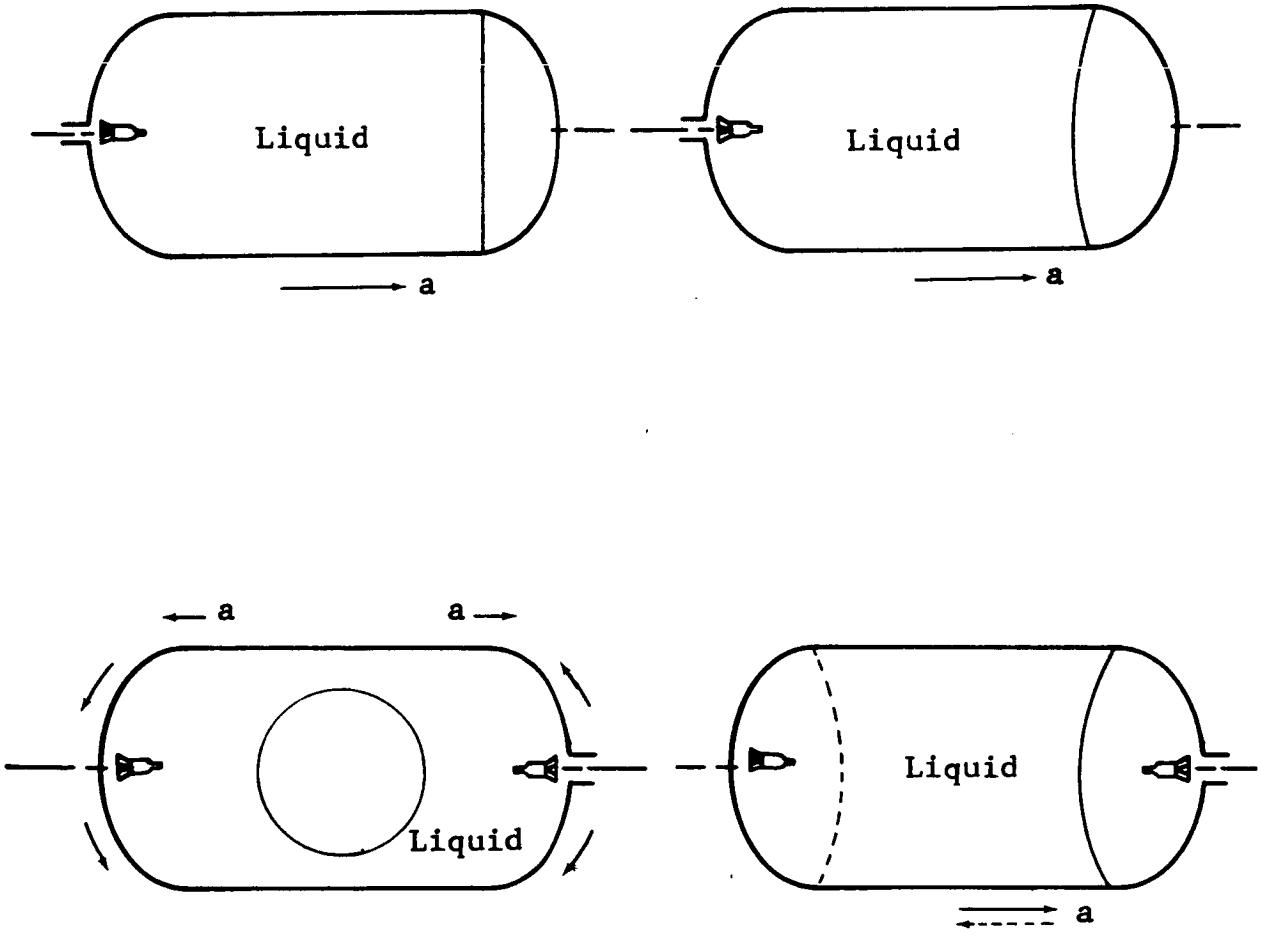

The four sketches are for various acceleration levels. If the tank acceleration tends to vary from time to time in the axial direction, a mixer should be located in each end of the tank, and the operation of each mixer cycled (one unit operated for a specified period of time and then the other operated). Mixers in each end of the tank should also be utilized when acceleration due to tank rotation is present, especially if there are shifts in the center of gravity during the mission. Special ullage conditions which must also be considered are discussed below.

Ullage Encapsulation of Mixers

During nonvent storage modes, special consideration must be given to situations in which the ullage is distributed in such a manner that sizable vapor formations occur in the vicinity of each mixer simultaneously. If vapor surrounds the mixer and the vane-axial pump output of jet momentum is not sufficient to remove the vapor formation, general tank mixing cannot be assured. (A similiar situation is present under a one g condition in which a mixer is placed in the vapor space). In this case, the vapor circulates in a region confined by the liquid-vapor interface and does not mix the liquid.

Under low g conditions, a small vane-axial pump should be capable of speeding up when vapor is ingested to promote

disintegration of the vapor deposit and general liquid mixing. From ullage stability considerations, (Ref. 35), the vapor formations are not expected at each end of the tank simultaneously if the absolute value of the bubble Bond number is greater than about 1.0. Ullage configurations for bubble Bond numbers greater than 0.85, less than -0.85 and between 0.85 and -0.85 are shown below (these Bond numbers are based on the bubble radius).

ABSOLUTE VALUE OF BOND NUMBER
REATER THAN ONE

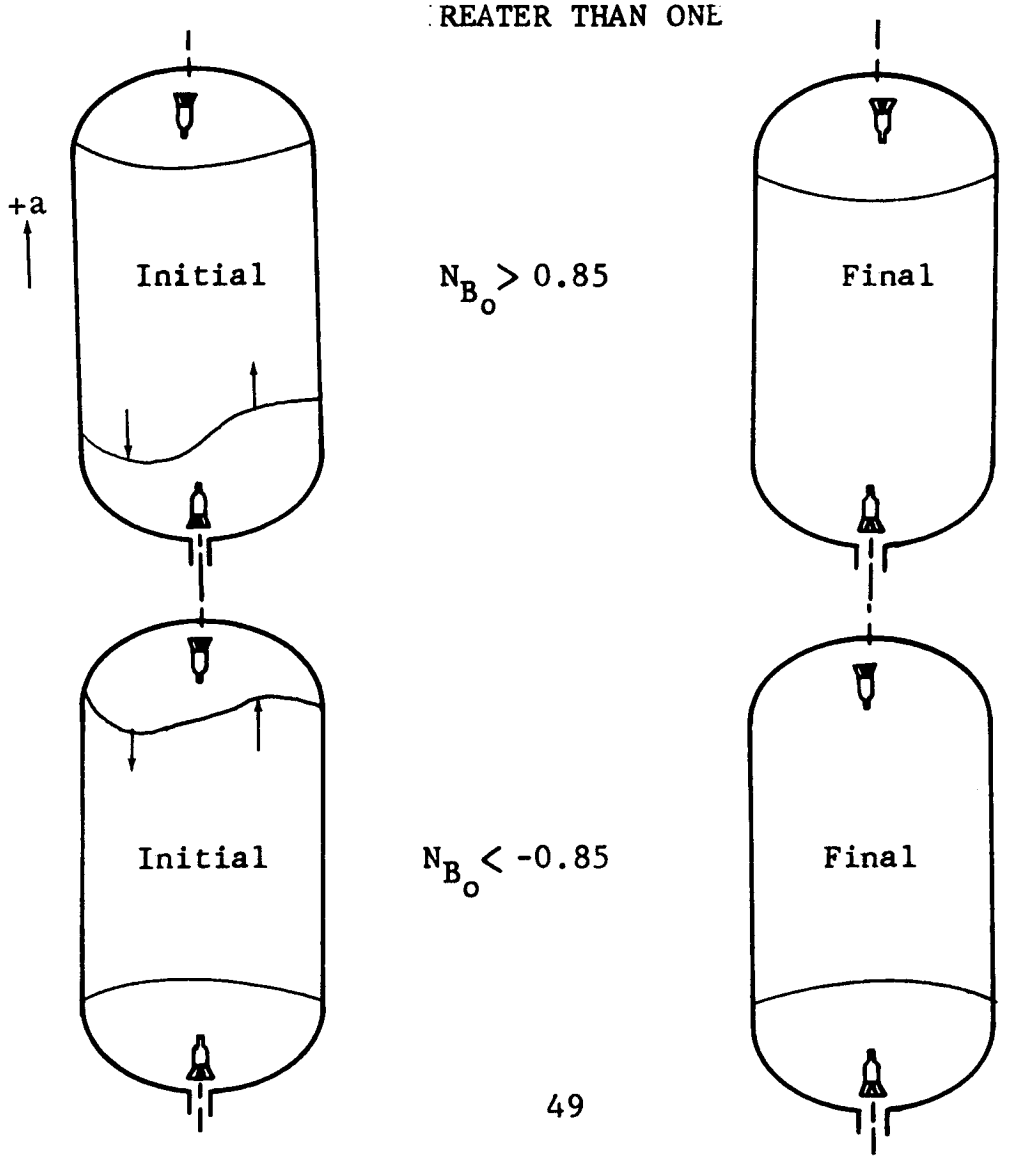

ABSOLUTE VALUE OF THE BOND
NUMBER LESS THAN 0.85

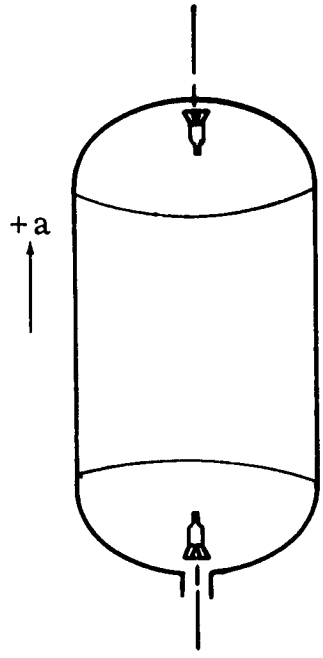

$$-0.85 < N_{B_o} < 0.85$$

In the case of the absolute value of the bubble Bond number greater than 1.0, the vapor formation will detach from the end of the tank and migrate toward the opposite end leaving one mixer free of large vapor formation.

The above criterion is considered an important conclusion as it shows that if mixers are placed at each end of the tank, significant ullage encapsulation of both mixers will not occur simultaneously if the absolute value of the bubble Bond number is greater than unity.

This criterion simplifies the equation for ullage encapsulation when mixers are located at each end of the tank by requiring that the mixer jet momentum be only sufficiently large to overcome the surface tension forces which tend to keep the vapor formation attached to the wall in the vicinity of the mixer. Any bubble buoyancy forces due to acceleration tend to assist in removing vapor formation from one of the mixer units.

It is then postulated that if one unit is essentially free from "large bubbles" ("large bubbles" are more precisely defined by the mathematical equations describing ullage encapsulation conditions given in Appendix G), allowing the unit to produce liquid circulation sufficient to break up the vapor formation at the other end of the tank.

In summary, the mixer design criteria to overcome ullage encapsulation during nonvent storage mode are not dependent upon tank acceleration if mixers are located on each end of the tank. As a result, it has been concluded that mixers utilized during nonvented storage modes should be installed at each end of the propellant tank.

Ullage Breakup

The ullage encapsulation criterion previously mentioned is applicable when vapor is in the vicinity of the mixer unit. As discussed, the ullage encapsulation and the phenomena of

vapor formation at heat shorts influence the mixer design. On the other hand, breakup of vapor not surrounding the operating mixer does not influence the mixer design.

When liquid surrounds the mixer unit and the vapor is located at the other end of the tank, two ullage break-up criteria are derived beginning on page 165 of Reference 1. These two criteria are based on

1. Weber number and
2. Froude number.

It was shown that for vane-axial mixers of practical size ($P_oD_o > 0.01$) the Weber number criterion is satisfied and has no influence on mixer selection. For a tank Bond number greater than 10, the Froude number criteria is applicable. By use of mixers at each end of the tank, the Froude number criterion need not be satisfied for higher tank Bond numbers, just as it is not satisfied in many one-g mixing tests even though adequate mixing is accomplished.

In terms of the outlet diameter-fluid power product, the Weber number criterion is

$$P_oD_o \geq 0.0179\ \rho \left(\sigma\ g_c Z_b/\rho\right)^{3/2}$$

where σ is the surface tension, and Z_b is the liquid depth above the nozzle, and ρ is the liquid density. The Froude number criterion (for L/D = 2.0) is

$$P_o D_o \geq 0.826 \quad (a/g_o)^{3/2} \quad (D_t)^{4.5}$$

Vapor Formation at Heat Shorts

The applicability of the ullage de-encapsulation criteria is dependent upon the location and distribution vapor bubbles in the propellant tank. The heat transfer rates to the propellant at the heat shorts for the manned Mars vehicle examined in this study indicate that boiling will occur at the heat shorts. As a result, vapor formations away from the heated areas will collapse as vapor is formed at the heat shorts. Eventually, all of the vapor will be located at the heated area provided that the vapor is not removed by buoyancy effects on the bubbles. For this reason the mixers should not be located in the vicinity of a major heat short (tank and engine supports).

It is not expected that the ullage de-encapsulation criterion need be satisfied when considerable boiling takes place at the heat shorts because if the buoyancy forces are not sufficient to remove bubbles from the heat shorts then the vapor will be removed from the mixer by condensation and will form at the heat shorts. On the other hand, if the vapor is removed from the heat shorts by the buoyancy effect,

vapor located at one of the mixers will also be removed (when mixers are placed on each end of the tank). A sketch of the two situations is shown below

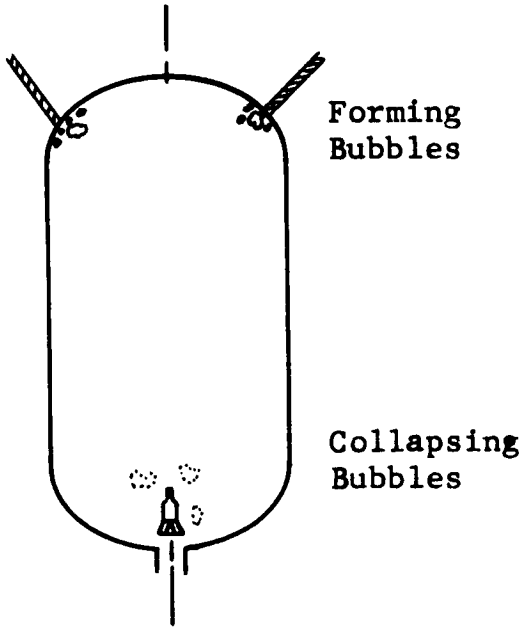

Vapor Not Removed
From Heat Short

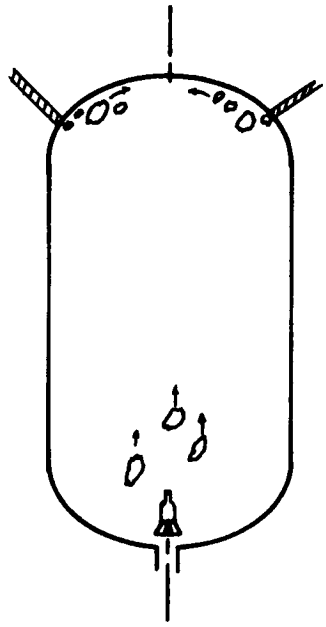

Vapor Removed
From Heat Short
(Vapor also removed
from vicinity of
mixer)

2.3.6 Outlet Diameter

The nozzle outlet diameter of a mixer should be sized to satisfy the mixing time and ullage de-encapsulation requirements (normally specified in terms of the fluid power-outlet diameter product) and to match the pump flow characteristics. A typical mixer with a nozzle attachment and support structure is shown below.

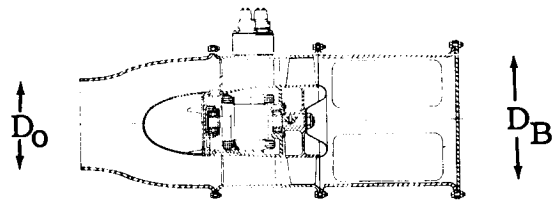

For a given fluid power, the nozzle outlet should be chosen to be as large as is practical. The nozzle configuration should be as near as is practical to a **cylindrical** shape. The nozzle outlet diameter, D_o, is related to the pump blade diameter, D_B, and the pump characteristics (specific speed, N_S, and head coefficient, ψ, by the following relation

$$D_o = \frac{D_B \, N_S \, \psi^{\frac{1}{2}}}{5933.3}$$

where N_s = (n, rpm) x (G, gpm)$^{1/2}$/(H,ft)$^{3/4}$

and $\psi = (H,ft)(g,ft/sec^2)/(\Omega, rad/sec)^2(r_B, ft)^2$

For a given vane-axial pump, in which N_s and D_B are known, the outlet diameter, D_o, can be calculated. As discussed in Appendix I an approximate relationship exists between N_S and ψ for conventional pump design. Using this relationship, the outlet diameter is approximately equal to the blade diameter when $N_S = 30,000$ and $\psi = 0.04$. The nozzle configuration, in this case, is essentially a straight cylindrical tube. At a lower specific speed, the nozzle section becomes convergent.

Conventional vane-axial pump designs have a blade diameter of from 2 to 4 inches at pump speeds above 1000 and below 10,000 rpm. The fluid power output for pump blade diameters in this range varies from a minimum of about 1.0 watt upwards to 100 watts.

For cases in which the mixer unit is not required to operate for an extended period of time (i.e., below 500 hours), the weight penalty associated with mixing large cryogenic tanks is usually less than 50 pounds per tank when a low power unit is utilized. For mixers operating over long periods of time a more unconventional design is required in that the pump blade diameter can be considerably larger than 2 to 4 inches. The larger blade size results from a tradeoff of the pump weight and power supply plus boiloff weight versus outlet diameter. The outlet diameter should be such that the boiloff and power supply weight is 6 to 7 times the weight

of the pump plus supports. The summary of equations used in the outlet diameter tradeoff is given in Appendix J.

When adhering to conventional pump design, the tradeoff diameter cannot in general be selected since pump characteristics N_S, ψ , and D_B, cannot be matched to the outlet diameter. The approach suggested in selecting an outlet diameter is to first try to utilize a conventional design. If the resulting weights are small, and the weight ratio (power supply plus boiloff weight divided by pump weight) is less than 10 a conventional design should be used, otherwise an unconventional pump design may be desired to minimize penalties.

2.3.7 Mixer Reliability

The reliability of the vane axial pump determines the total number of units required in each propellant tank. For nonvented storage modes of a manned Mars vehicle, one unit is utilized at each end of each tank and the total operating time for each unit is on the order of a few hundred hours. The mean time before failure (MTBF) of a typical vane axial pump is on the order of 10^5 hours. The reliability of the mixer is

$$R = e^{-\frac{\theta_o}{MTBF}}$$

where θ_o is the total mixer operating time. For a total operating time of 500 hours and a mean time before failure of 100,000 hours the mixer reliability is .995.

The component reliability of the mixer can, of course, be increased by installing two mixer units at each end of the tank. The units are operated in parallel such that the units at each end operate simultaneously and the reliability is

$$R = 1 - \left(1 - e^{-\frac{\theta_o}{MTBF}}\right)^2$$

The combined component reliability is increased to .99997.

2.3.8 Effect of Baffles and Other Obstructions

If it is assumed that boiling at the wall will take place between baffles then vapor formations trapped by the baffles could very possibly degrade mixing performance, since mixing in the vicinity of a large portion of the liquid-vapor interface is essential for effective mixing. On the other hand, typical propellant storage conditions under low gravity conditions result in boiling only at the heat shorts (since boiling in the vicinity of high heat inputs will suppress boiling along the tank sidewalls). Baffles should be located away from heat shorts, if possible.

2.3.9 Electric Motor Selection

The selection of the type of electric motor (a.c. or d.c.) to drive the axial flow pump is dependent upon:

1. Current state-of-the-art
2. Pump vapor removal requirements (ullage de-encapsulation)
3. Simplicity and reliability
4. Weight consideration
5. Electric motor efficiency

The a.c. motor driven pump operation has been adequately demonstrated in liquid hydrogen, by Pesco Products of Bedford, Ohio and other pump manufacturers. This type of motor is well within the existing state of the art. A mixing system utilizing such a system could be built without further pump-motor development effort.

The squirrel cage a.c. motor design is used and is simple and reliable. Although the basic unit weight of the a.c. pump motor is less than that of a comparable brushless d.c. pump motor, the potential d.c. electric motor efficiency is considerably superior to that which is obtainable with the a.c. pump motor (see Appendix K). Whether the d.c. pump motor design will achieve the efficiency potential must be determined in the appropriate development program.

As a result of the higher efficiency of the brushless d.c. motor, the mixer unit having a comparable mixing ability will result in a small weight penalty primarily because of decreased boiloff (due to mixing) and power supply weight.

An important advantage of the more complex d.c. motor driven unit is due to the torque-speed characteristics which results in a considerable speed up of the unit when vapor is ingested. The increased vapor momentum produced by the mixer will serve to dispel vapor formations in the vicinity of the mixer unit. The vapor formation, if allowed to persist, will degrade mixing performance to an unacceptable level.

A typical a.c. motor driven pump does not have the required torque speed characteristic to permit the mixer to dispel vapor formation. If an a.c. motor driven pump is to be used, extensive modifications of conventional a.c. squirrel cage motors will be required. Pertinent discussion of the vapor encapsulation is presented in another part of this section. Results of an analysis which substantiates this conclusion are given in Appendix L. Hence a d.c. motor-pump should be used unless other dominant phenomena are present in mixing situations which preclude the possibility of vapor encapsulation of both mixers (if one is installed at each end of the tank) during nonvent mixing operation.

It should be pointed out that venting by use of a thermodynamic separator would alleviate vapor encapsulation of a mixer if a vent mode was appropriate. However, when a nonvent mode of storage is called for, as in the cases using propellant "subcooling" to reduce boiloff, arbitrary venting (as the ullage encapsulation situation arises) cannot generally be tolerated.

If mixers are installed at both ends of the tank, there are at least two situations in which ullage encapsulation of a mixer during the nonvent mode of storage will not occur. These situations are:

1. Tank acceleration sufficient to maintain the large vapor formations at one end of the tank. (Absoluce value of the Bond number, N_{B_o}, greater than 10.0).
2. Sufficient tank wall vapor formation due to boiling at heat shorts under low acceleration conditions ($|N_{B_o}| < 1.0$) such that the movement of bubbles away from the heat shorts does not occur between mixing cycles.

The second condition exists for manned Mars missions for which the tank pressure rise is sufficiently severe to require mixings at short intervals of time. The bubbles

which form at the heat shorts thus are not allowed to grow large enough to be removed by slight buoyancy effects.

Page intentionally left blank

SECTION 3

MIXER DESIGN STUDY RESULTS

The mixer design criteria given in Section 2 of this report were applied to the case of a manned Mars vehicle. Mixer units were selected for the three different sizes of tanks of this vehicle. The mixer design drawings are given, with the selected location of the mixer, venting system propellant feed lines, etc. indicated. The requirements of a mixer control subsystem are also defined along with the suggested mixer operational sequence.

The design data developed or used in the selected designs are shown in tables and appropriately discussed. The designs were based on conventional (state-of-the-art) vane-axial pump size and power output (except in areas in which a d.c. motor is used). The vane-axial pump was always of conventional design.

A tradeoff analysis was conducted to obtain information which was used in the selection of the mixer nozzle outlet diameter. The mixer weight plus structural support weight were formulated as a function of the mixer nozzle outlet diameter for a required P_oD_o (for ullage encapsulation, or other criteria) or minimum power level. The mathematical expressions in the tradeoff were solved by use of the

computer procedure described in Section 4, Volume II of Reference 1. The results were the jet momentum in terms of the product of the jet nozzle outlet diameter and the jet velocity (V_oD_o).

As pointed out in Subsection 2.3.6, the outlet diameter obtained on the basis of a weight tradeoff is basically dependent upon the total operating time of a mixer. The conventional vane-axial pump design may not be suited for an optimum design. However, unless the weight penalty for a conventional vane axial pump design is excessive, a conventional design should be used due to the cost of developing unconventional vane axial pumps.

The number of mixer duty cycles was estimated on the basis of the time for the tank pressure to rise from an initial mixed condition to very near tank design pressure. A thermal stratification analyses served as the basis for determing the tank pressure rise. The pressure rise is implicitly determined in terms of stratification coefficients. The stratification and equilibrium coefficients were then used to determine the number of duty cycles. Mixing time coefficients were calculated based on correlations of jet motion, bulk fluid motion and temperature decay obtained by analytical and experimental methods.

A fuel cell power supply was selected and the weights attributed to mixing were obtained as a function of total mixer operating time. The weights of the mixer including boiloff and power supply (excluding mixer support, electrical wiring, feed throughs, etc.) were obtained for a.c. and brushless d.c. motor driven pumps for a minimum fluid power level. In addition, weights are given for a brushless d.c. motor driven pump system which includes the criterion to satisfy ullage de-encapsulation of the mixer. In addition, the power supply plus boiloff weight was also formulated in terms of the outlet diameter.

The differences in the mixer subsystem weight were converted into an initial mass in earth orbit (ΔIMIEO). These weight differences were interpreted in terms of a cost savings for a single vehicle by using a specific cost of one thousand dollars per pound of weight in Earth orbit.

The methods used and the results are discussed and shown in detail in the following subsections.

3.1 STRATIFICATION

As discussed in Subsection 2.2, the stratification prediction was based on a thermal-conduction-boiling model at the heat shorts. For the reference manned Mars vehicle, the summary of the heat shorts are given in Table 3-1. The top main tank support and the engine mount heat shorts contribute significantly to the heating. The tank supports, etc., were considered to be the base of a fin (tank wall) as shown below

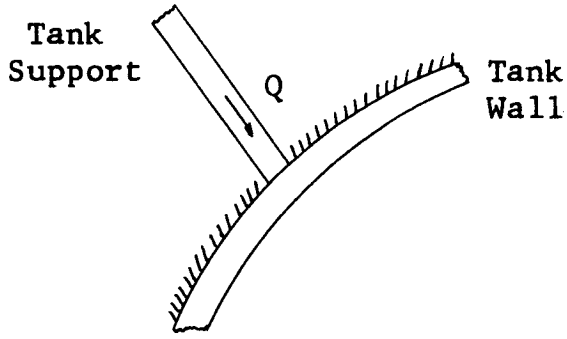

The tank wall "fin" was assumed to be insulated on one side. A simplified analysis was conducted in which the following were assumed

1. A constant heat transfer coefficient was assumed between the tank wall and the fluid, and
2. A transient heat transfer coefficient (based on thermal conduction within the propellant).

A resulting temperature difference between the tank wall and the fluid was obtained from this analysis. Because

Table 3-1

SUMMARY OF HEAT SHORTS FOR MANNED MARS VEHICLE

	EARTH ESCAPE STAGE	MARS BRAKING STAGE		MARS ESCAPE STAGE		
	EARTH ORBIT	EARTH ORBIT	EARTH TO MARS	EARTH ORBIT	EARTH TO MARS	MARS ORBIT
Top Tank Support	282.0	219.3	---	205.8	---	82.6
Bottom Tank Support	59.5	53.0	---	65.6	---	
Others	230.9	205.2	---	253.9	---	101.9
Engine Feed Line	37.2	33.0	---	41.2	---	16.5
Fill & Drain Line	10.9	9.6	---	11.9	---	4.8
Engine Support	168.4	149.5	---	185.0	---	74.3
Vent Line	5.0	4.5	---	5.6	---	2.2
Pressurization Line	9.2	8.0	---	10.1	---	4.0
Total, Btu/Hr	572.7	477.4	---	525.3	---	210.8

of the highly concentrated heat flux the temperature difference between the base of the fin and the fluid was found to be above 1.0° F in all cases except for an initial transient (which consisted of a time interval of less than an hour).

The significant point to be made, however, is that the heating in the vicinity of tank supports, etc. is severe enough to dominate the stratification process and heating along the tank wall is of such less magnitude that boiling along the tank wall away from heat short will be suppressed.

When the mixers are not operated, it may be postulated that free convection and bubble motion away from the heat short will be the primary mode of energy transfer. However, free convection is not expected to be initiated because of the low Rayleigh number (less than 1700) for the combined heating rate-acceleration conditions. Bubble removal by bouyancy forces is not expected if the bubble Bond number is less than 1.0. For the acceleration condition postulated ($a/g_o \approx 10^{-8}$) the bubble Bond number is considerably less than one. As a result, thermal conduction has been postulated as the major resistance to heat transfer, with evaporation taking place at the heat short and condensation (collapse of bubbles) occurring at vapor locations away from the concentrated heating areas. The thermal conduction

resistance is then proportional to the bubble interfacial areas.

The single bubble diameter and corresponding interfacial area are given in Table 3-2 and are based on the tank void fraction. The tanks are nonvented (except for the Mars orbit phase of the Mars escape stage) and the void fraction decreases as heating takes place. The minimum and maximum single bubble diameters are shown (minimum occurs at the end of a mission phase). In addition, a comparison was made of single bubble and one-tenth single-bubble-diameter area (interfacial area when the tank contains 1000 bubbles whose diameters are one-tenth that of the single bubble diameter) and tank area. The one-tenth-single-bubble-diameter area is given for comparison only and is not used in calculations. The interfacial area is increased by a factor of ten when the bubble diameter is decreased by a factor of ten. This indicates the desirable effect obtained by breaking up large bubbles.

Thermal stratification and equilibrium coefficients are given in Table 3-3 for the heat flux from a single bubble in liquid hydrogen (maximum stratification) and the heating of liquid hydrogen through the tank wall (minimum

Table 3-2

CHARACTERISTIC BUBBLE PARAMETERS

	EARTH ESCAPE STAGE	MARS BRAKING STAGE		MARS ESCAPE STAGE		
	EARTH ORBIT	EARTH ORBIT	EARTH TO MARS	EARTH ORBIT	EARTH TO MARS	MARS ORBIT
Maximum Bubble Diameter, D_{b1}, Ft	23.18	20.70	15.26	15.60	12.85	12.85
Minimum Bubble Diameter, D_{b1}, Ft	17.08	15.26	15.26	12.85	12.85	16.64
Maximum Single Bubble Area, Ft^2	1688.	1346.	732.	765.	519.	519.
Minimum Single Bubble Area, Ft^2	916.	732.	732.	519.	519.	879.
Maximum Total Bubble Area ($D_b = 0.1D_{b1}$), Ft^2	16880	13460	7320	7650	5190	5190
Minimum Total Bubble Area ($D_b = 0.1D_{b1}$), Ft^2	9160	7320	7320	5190	5190	8790
Tank Area, Ft^2	7620	5747	5747	3078	3078	3078

Table 3-3

THERMAL STRATIFICATION AND THERMODYNAMIC EQUILIBRIUM COEFFICIENTS

	EARTH ESCAPE STAGE	MARS BRAKING STAGE		MARS ESCAPE STAGE		
	EARTH ORBIT	EARTH ORBIT	EARTH TO MARS	EARTH ORBIT	EARTH TO MARS	MARS ORBIT
Minimum heat flux to liquid hydrogen due to heat shorts for a single bubble, Btu/hr-ft^2	0.34	0.35		0.27		0.41
Maximum heat flux to liquid hydrogen due to heat shorts for a single bubble, Btu/hr-ft^2	0.625	0.65		1.01		0.24
Maximum short stratification coefficient, C_s, $(1.1q\sqrt{\alpha}/k)$, $^oR/(hr)^{1/2}$	0.833	0.866		1.34		0.32
Minimum heat short stratification coefficient, C_s, $^oR/(hr)^{1/2}$	0.453	0.466		0.36		0.55
Stratification Coefficient based on total heating at tank wall, $^oR/(hr)^{1/2}$	0.1973	0.28		0.269		0.107
Temperature difference during first stratification period, ΔT_{si}, ^oR	13.53	13.53		14.25		6.9
Equilibrium temperature rise coefficient, C_e, $^oR/hr$	0.00269	0.00404		0.0051		0.000747
Maximum $C_e \Delta T_{si}/C_s^2$	0.9445	0.697		1.0		0.45
Minimum $C_e \Delta T_{si}/C_s^2$	0.05245	0.0729		0.0405		0.05033

stratification). The coefficients are defined in Subsection 2.2 and were used to calculate the number of duty cycles required for each phase of the mission.

3.2 DUTY CYCLE EVALUATION FOR NONVENTED STORAGE

The number of duty cycles were evaluated for the characteristic stratification and equilibrium coefficients for nonvented storage. The results are tabulated in Table 3-4. The maximum and minimum number of duty cycles were based on the "heat short" stratification and stratification due to wall heating respectively. The maximum and minimum times between mixer operations for the maximum number of duty cycles are also tabulated.

The results of the prediction of the number of duty cycles are applicable to the nonvent portion of the mission (which includes the total mission time for the Earth escape stage, Mars braking stage and all but the last 231 days of the Mars escape stage). The vent system is required to function in the Mars escape stage for the last 231 days of the Mars orbit phase of the mission. The mixer units envisioned are not considered as components of the vent system due to the larger pressure drop (heat exchanger) requirements of the vent system.

Table 3-4

NUMBER OF DUTY CYCLES AND STRATIFICATION DEVELOPMENT TIMES

	EARTH ESCAPE STAGE	MARS BRAKING STAGE		MARS ESCAPE STAGE		
	EARTH ORBIT	EARTH ORBIT	EARTH TO MARS	EARTH ORBIT	EARTH TO MARS	MARS ORBIT
Maximum number of duty cycles, N_D	115	83	---	26	---	52
Minimum number of duty cycles, N_D	3	9	---	3	---	8
First stratification development time for maximum number of duty cycles, hours	264	244.0	---	113.0	---	466.5
Last stratification development time for maximum number of duty cycles, hours	5.2	4.8	---	27.0	---	35.0

3.3 MIXING TIME

The parameters associated with the calculations of mixing time and the resulting mixing time coefficients, C_M, are tabulated in Table 3-5. The mixing time coefficient as discussed in Subsection 2.3.3 is defined as

$$C_M = V_o D_o \theta_M / D_t^2$$

where θ_M is the mixing time. The mixing times for each stage are tabulated in Table 3-6 for two cases (excluding and including the ullage de-encapsulation criterion) For the case in which the ullage de-encapsulation criterion was applied, the estimated time to remove a large bubble from the vicinity of the mixer was included in the maximum operating time of the mixer.

Table 3-5

MIXING TIME COEFFICIENTS

	Earth Escape Stage	Mars Braking Stage		Mars Escape Stage		
	Earth Orbit	Earth Orbit	Earth to Mars	Earth Orbit	Earth to Mars	Earth Orbit
Tank Length, ft	72.45	53.82	53.82	27.27	27.27	27.27
Bulkhead Length, ft	11.3	11.3	11.3	11.3	11.3	11.3
Mixing Length to Top Bulkhead, ft	11.3	11.3	11.3	11.3	11.3	11.3
Distance From Bottom of Tank to Nozzle Outlet, ft	2.5	2.5	2.5	2.5	2.5	2.5
Mixing Length to Bottom Bulkhead, ft	61.15	42.52	42.52	15.97	15.97	15.97
Tank Length/Tank Diameter	2.264	1.68	1.68	0.85	0.85	0.85
Dimensionless Time for Jet to Traverse Tank, $V_o D_o \theta_j / D_t^2$	0.78	0.43	0.43	0.11	0.11	0.11
Dimensionless Time for Bulk Fluid Particles to Move to Top Bulkhead Junction, $V_o D_o \theta_B / D_t^2$	0.3864	0.545	0.545	1.34	1.34	1.34
Dimensionless Time for Bulk Fluid Particles to Move From Top of Tank to Lower Bulkhead Junction, $V_o D_o \theta_B / D_t^2$	4.55	3.87	3.87	2.27	2.27	2.27
Maximum $V_o D_o (\theta_j + \theta_B) / D_t^2$	5.33	4.30	4.30	2.35	2.38	2.38
Minimum $V_o D_o (\theta_j + \theta_B) / D^2$	1.17	0.98	0.98	1.45	1.45	1.45
Maximum $V_o D_o (\theta m) / D_t^2$	10.66	8.60	8.60	5.76	5.76	5.76
Minimum $V_o D_o (\theta m) / D_t^2$	2.33	1.95	1.95	2.90	2.90	2.90
$V_o D_o \theta_e / D_t^2$	8.6	6.88	6.88	3.77	3.77	9.38

Table 3-6

MIXING TIME WITH AND WITHOUT ULLAGE ENCAPSULATION CRITERIA

	Earth Escape Stage	Mars Braking Stage		Mars Escape Stage		
	Earth Orbit	Earth Orbit	Earth to Mars	Earth Orbit	Earth to Mars	Mars Orbit
Excluding Ullage Encapsulation Criteria						
Maximum Time for Mixing, hours	2.3	1.86	1.86	1.25	1.25	1.25
Minimum Time for Mixing, hours	0.5	0.42	0.42	0.626	0.626	0.626
Maximum Total Operating Time, hours	264.5	153.6	0	32.5	0	65.0
Minimum Total Operating Time, hours	1.5	3.78	0	1.26	0	5.0
Including Ullage Encapsulation Criteria						
Time to Remove Bubble, hours	1.62	1.298	1.298	0.71	0.71	0.826
Maximum Time for Mixing, hours	2.03	1.632	1.632	1.097	1.097	1.097
Minimum Time for Mixing, hours	0.44	0.37	0.37	0.55	0.55	0.55
Maximum Total Operating Time, hours	420.0	243.0	0	47.0	0	100.0
Minimum Total Operating Time, hours	1.3	3.3	0	1.1	0	4.4

3.4 POWER SUPPLY WEIGHT COEFFICIENT

The power supply and boiloff weight were determined from the coefficients tabulated in Table 3-7. The fuel cell weight was calculated from two coefficients, since the weight is a function of both the power level and the product of the power level and operating time. The boiloff is solely a function of the product of the power level and total mixer operating time. An dc-ac inverter coefficient is also shown since for ac motor driven pumps, a dc-ac inverter is required. The silver zinc battery coefficient is shown for comparison purposes. If a silver zinc battery power supply is used, the weights attributable to mixing are approximately twice the weight (including boiloff) for a fuel-cell powered system.

Table 3-7

POWER SUPPLY WEIGHT COEFFICIENTS

	POWER LEVEL-OPERATING TIME COEFFICIENT, POUNDS/WATT-HR	POWER LEVEL COEFFICIENT POUNDS/WATT
Fuel Cell	0.00135	0.15
Boiloff	0.0175	---
Silver Zinc Battery	0.014	---
Inverter (50% efficient)	---	0.024

3.5 PUMP-MOTOR CHARACTERISTICS

The pertinent parameters required to define the mixer design are summarized in Table 3-8. The two basic cases are shown; including and excluding the criterion for ullage de-encapsulation. Both a.c. and d.c. motor driven pumps are shown for the case in which the ullage de-encapsulation criteria is not applicable.

In the case in which ullage de-encapsulation is applicable, an a.c. motor system is not considered due to the difficulty in matching vapor and liquid flow conditions through the pump. A conventional a.c. motor does not have the speed characteristics necessary to satisfy required vapor flow rates without utilizing excessive power when liquid is pumped.

In the case not requiring ullage de-encapsulation, the fluid power level was selected on the basis of a practical minimum level of one watt. The corresponding blade diameter of the pump was selected on the basis of conventional pump size and taking into account the optimum diameter obtained by a tradeoff analysis.

The specific speed of the pump was selected so that the outlet diameter was equal to the pump blade diameter in order to obtain a maximum jet performance for a given

Table 3-8
PUMP MOTOR CHARACTERISTICS

	Ullage Encapsulation Criterion Not Applicable		Ullage Encapsulation Criterion Applicable	
	A.C. MOTOR	D.C. MOTOR	D.C. MOTOR	
Fluid Power, Watts	1.0	1.0	1.5	1.5
Outlet Velocity, Ft/Sec.	7.9	7.9	9.0	9.0
Pump Head, Feet of LH_2	0.97	0.97	1.27	1.27
Flow Rate, gpm	77.4	77.4	88.6	88.6
Specific Speed,	30,000	30,000	30,000	30,000
Head Coefficient	0.04	0.04	0.04	0.04
Pump Blade Diameter, inches	2.0	2.0	2.0	2.0
Outlet Diameter, inches	2.0	2.0	2.0	2.0
Fluid Power x outlet Diameter, watt-ft	0.167	0.167	0.25	0.25
Pump Speed, rpm	3200	3200	13,500	3,600
Hydraulic Efficiency, %	60	60.	60.	60.
Torque, inch-ounce	0.7	0.7	0.16	0.6
Fan Weight, lbs.	0.3	0.3	0.3	0.3
Electric Motor Weight, lbs.	0.15	1.2	1.4	1.4
Mixer Unit Weight, lbs.	0.45	1.5	1.7	1.7
Electric Motor Efficiency, %	23	62	69	31
Overall Pump-Motor Efficiency, %	14	37	41	19
Power Input to Electric Motor, Watts	7.14	2.7	3.62	8.1

Table 3-8 (Cont'd)

	Ullage Encapsulation Criterion Not Applicable		Ullage Encapsulation Criterion Applicable	
	AC MOTOR	DC MOTOR	DC MOTOR	
Inverter Weight, lbs.	0.34			
Power Output From Power Supply, Watts	14.3	2.7	3.62	8.1
Power Supply Fixed Weight, lbs.		0.6	1.22	1.22
Number of Mixers Per Tank Operating Simultaneously	1.0	1.0	1.0	1.0
Number of Mixers Per Tank	2	2	2	2
Mixer Weight Per Tank (Excluding Support Structure), lbs.	0.9	3.0	3.4	3.4

pump blade diameter and fluid power. The nozzle in this case, has a cylindrical shape.

One mixer was located at each end of the tank and the operation of both mixers cycled such that neither mixer operates simultaneously. A typical mixer design is shown in Figure 3-1. Mixer system installations are shown in Figures 3-2 through 3-4.

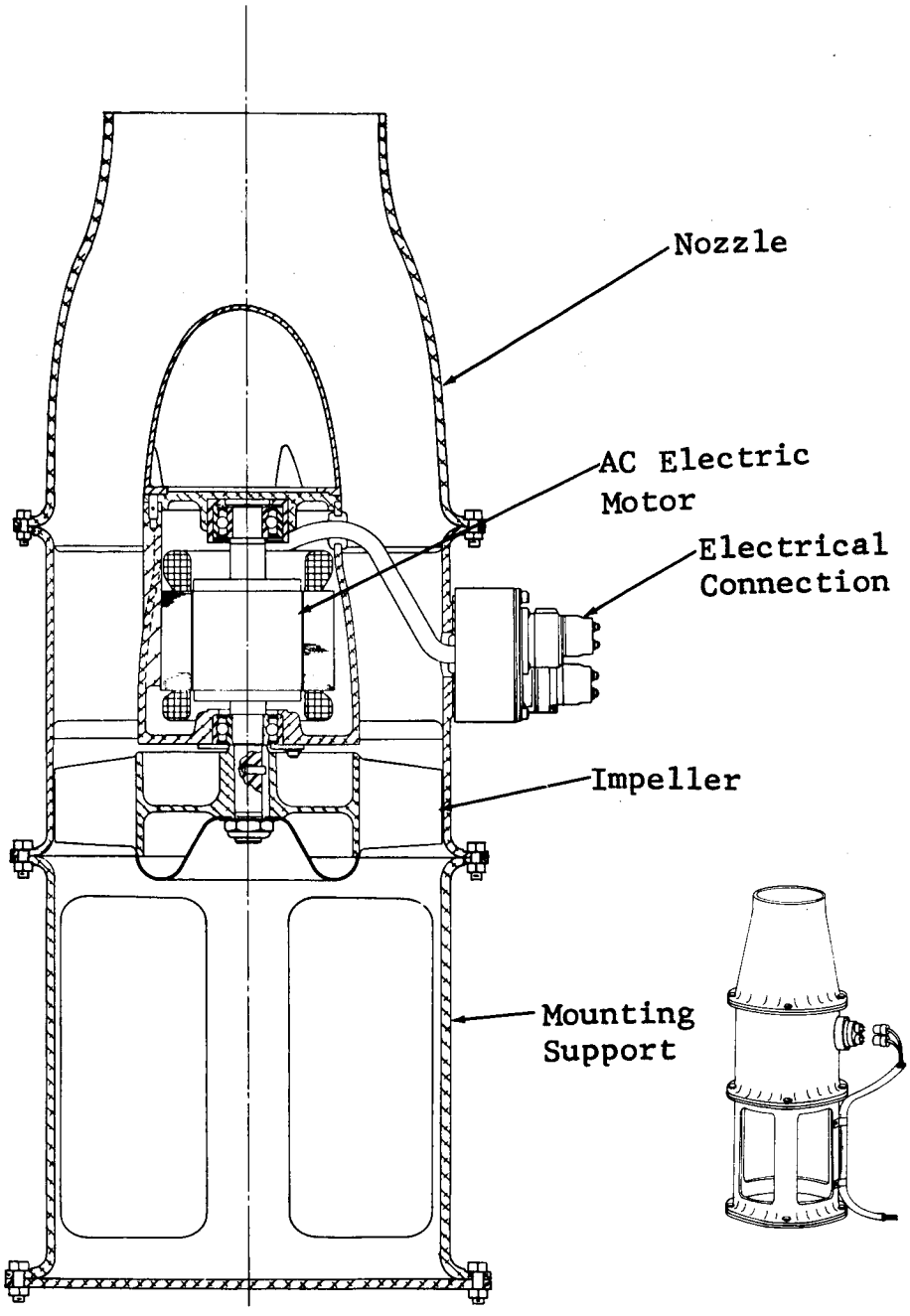

Figure 3-1 Vane Axial Pump, Nozzle, and Mounting Supports

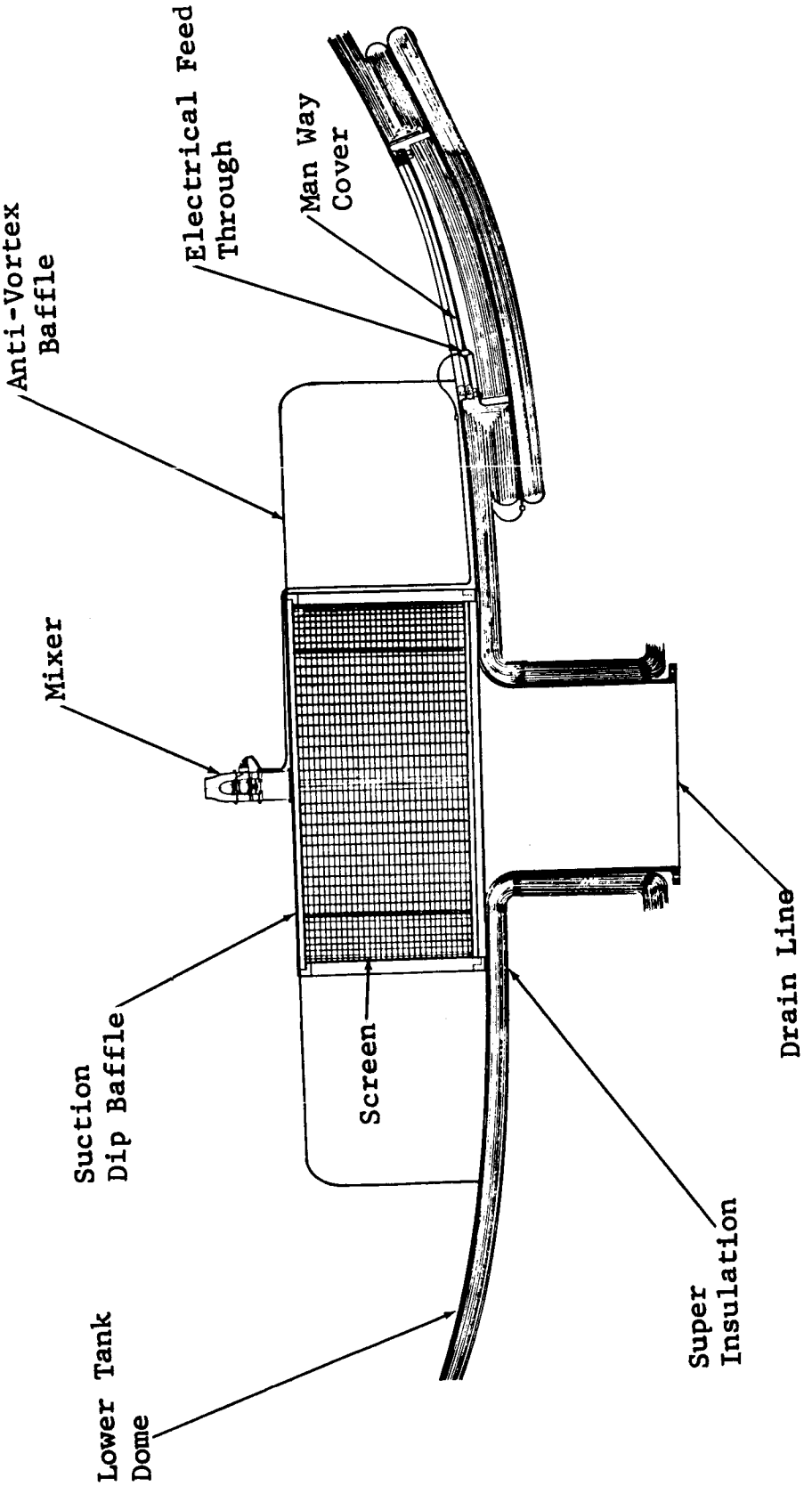

Figure 3-2 Mixer Installation on Aft Bulkhead of Tank

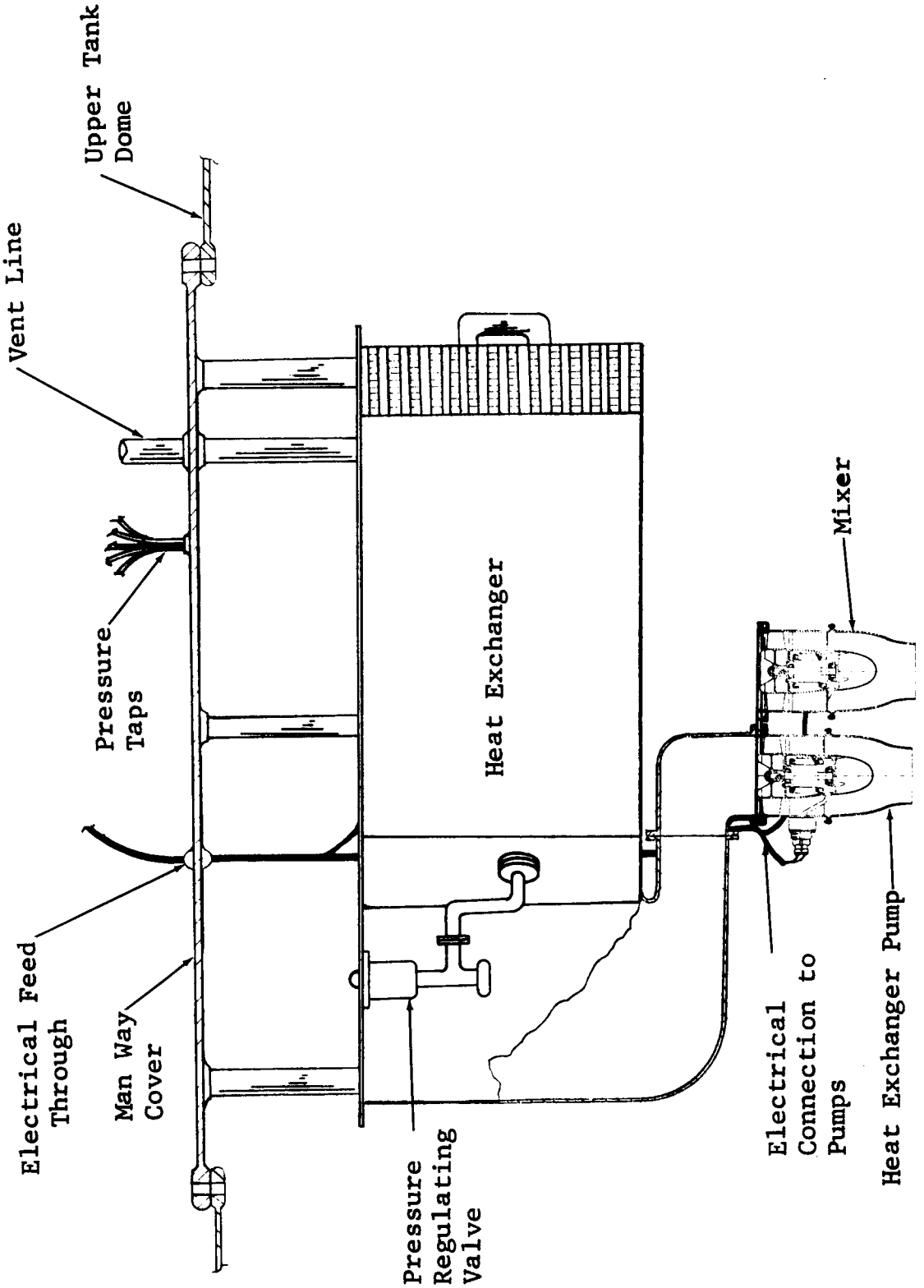

Figure 3-3 Mixer and Vent System Installation on Forward Bulkhead

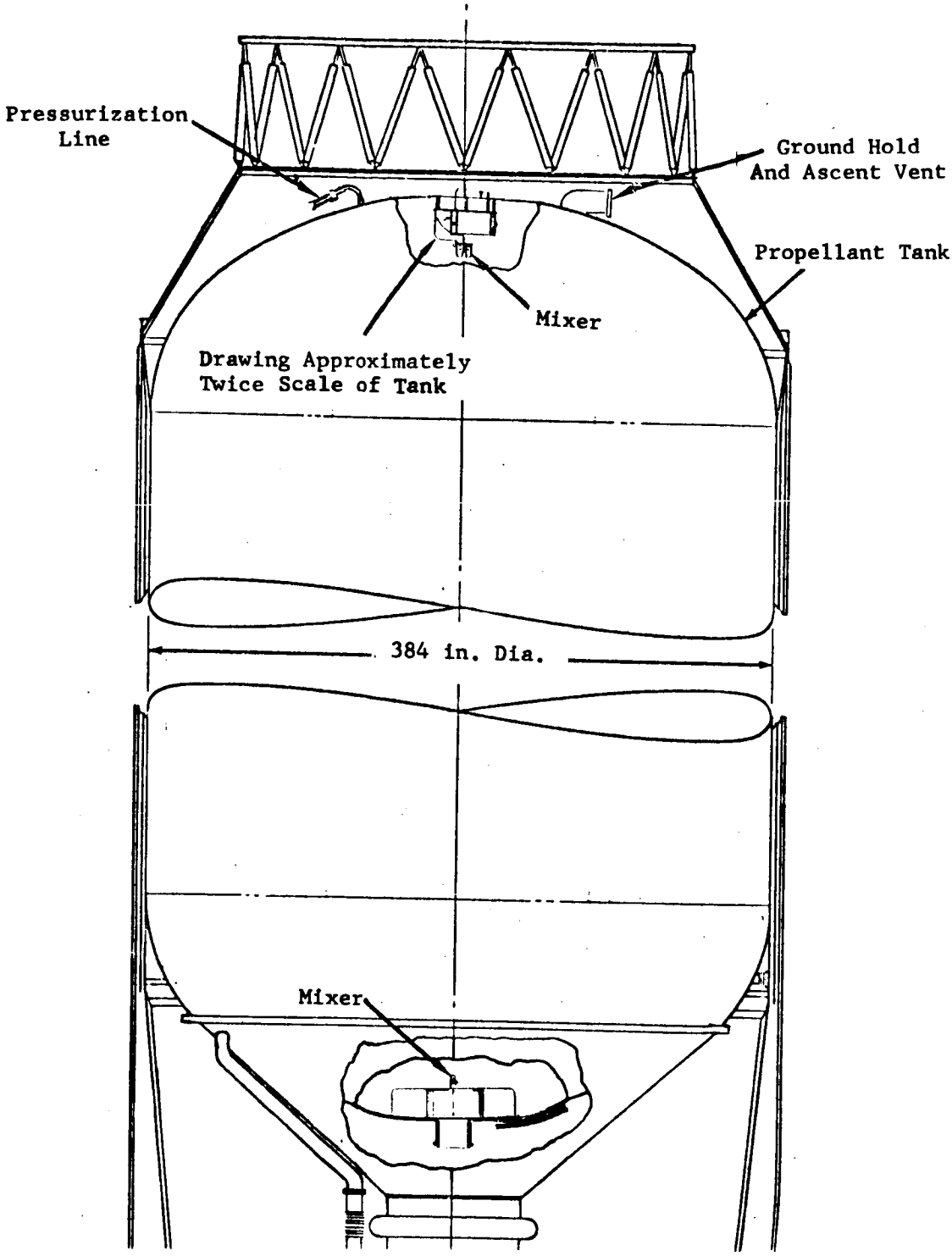

Figure 3-4 Mixer Installation in Nuclear Flight Module

3.6 MIXER WEIGHT SUMMARY

The weight summaries of the mixer system (excluding structural supports, electrical wiring, feed throughs, etc.) are tabulated in Table 3-9 through 3-14 for the case of a fuel cell as the power source. Maximum and minimum weights are given corresponding to the maximum and minimum number of duty cycles and mixing time. The weights are converted to an initial mass in Earth orbit (ΔIMIEO) for consistent comparison since one additional pound of weight in the Earth escape stage requires approximately two pounds of weight initially (additional propellant, etc.) in Earth orbit, and one pound of additional weight in the Mars escape stage requires over four pounds of weight initially in Earth orbit. The boiloff, which constitutes part of the weight penalty, was assumed to be a fixed weight associated with the tank. If boiloff occurs before final stage burnout, the estimated weight of the boiloff is conservative.

Table 3-9

MAXIMUM WEIGHT SUMMARY
FOR A.C. MOTOR DRIVEN PUMP
(EXCLUDING STRUCTURAL SUPPORT AND OTHER FIXED WEIGHT)

	EARTH ESCAPE STAGE	MARS BRAKING STAGE		MARS ESCAPE STAGE		
	EARTH ORBIT	EARTH ORBIT	EARTH TO MARS	EARTH ORBIT	EARTH TO MARS	MARS ORBIT
Fuel Cell Weight/lbs.	6.18	4.04		1.7		1.25
Boiloff Weight, lbs	33.0	19.2		4.1		8.1
Inverter Weight, lbs.	0.34	0.34		0.34		0.34
Total Pump Weight, lbs.	0.9	0.9		0.9		
Weight Per Tank, lbs.	40.42	24.48		16.37		
Weight per Stage, lbs.	161.68	49.96		16.37		
Δ IMIEO per Stage/lbs.	291.3	153.		73.73		
Total Δ IMIEO, lbs.			518			

Table 3-10

MINIMUM WEIGHT SUMMARY FOR A.C. MOTOR DRIVEN PUMP
(EXCLUDING STRUCTURAL SUPPORTS AND OTHER FIXED WEIGHT)

	EARTH ESCAPE STAGE	MARS BRAKING STAGE		MARS ESCAPE STAGE		
	EARTH ORBIT	EARTH ORBIT	EARTH TO MARS	EARTH ORBIT	EARTH TO MARS	MARS ORBIT
Fuel Cell Weight, lbs.	1.1	1.14		1.09		1.17
Boiloff Weight, lbs.	0.19	0.47		0.157		0.625
Inverter Weight, lbs.	0.34	0.34		0.34		
Total Pump Weight, lbs.	0.9	0.9		0.9		
Weight Per Tank, lbs.	2.53	2.85			4.28	
Weight Per Stage, lbs.	10.12	5.7			4.28	
Δ IMIEO Per Stage, lbs.	18.23	17.85			19.28	
Total Δ IMIEO, lbs.			53.36			

Table 3-11

MAXIMUM WEIGHT SUMMARY
FOR BRUSHLESS D.C. MOTOR DRIVEN PUMP
(EXCLUDING STRUCTURAL SUPPORT AND OTHER FIXED WEIGHT)

	EARTH ESCAPE STAGE	MARS BRAKING STAGE		MARS ESCAPE STAGE		
	EARTH ORBIT	EARTH ORBIT	EARTH TO MARS	EARTH ORBIT	EARTH TO MARS	MARS ORBIT
Fuel Cell Weight, lbs.	2.03	1.43		0.776		0.35
Boiloff Weight, lbs.	12.5	7.26		1.54		3.07
Total Pump Weight, lbs.	3.0	3.0		3.0		
Weight Per Tank, lbs.	17.53	11.69			8.74	
Weight Per Stage, lbs.	70.12	23.38			8.74	
Δ IMIEO Per Stage/lbs	126.4	73.23			39.4	
Total Δ IMIEO, lbs.			239			

Table 3-12

MINIMUM WEIGHT SUMMARY
FOR BRUSHLESS D.C. MOTOR DRIVEN PUMP
(EXCLUDING STRUCTURAL SUPPORT AND OTHER FIXED WEIGHT)

	EARTH ESCAPE STAGE	MARS BRAKING STAGE		MARS ESCAPE STAGE		
	EARTH ORBIT	EARTH ORBIT	EARTH TO MARS	EARTH ORBIT	EARTH TO MARS	MARS ORBIT
Fuel Cell Weight, lbs.	0.608	0.62		0.606		0.027
Boiloff Weight, lbs.	0.077	0.178		0.06		0.236
Total Pump Weight, lbs.	3.0	3.0		3.0		
Weight Per Tank, lbs.	3.695	3.80			3.93	
Weight Per Stage, lbs.	14.74	7.6			3.93	
Δ IMIEO Per Stage/lbs.	26.56	23.79			17.70	
Total Δ IMIEO, lbs.			68			

Table 3-13

MAXIMUM WEIGHT SUMMARY
(EXCLUDING STRUCTURAL SUPPORTS, ETC)
FOR BRUSHLESS D.C. MOTOR DRIVEN PUMP
INCLUDING ULLAGE ENCAPSULATION CRITERION

	EARTH ESCAPE STAGE	MARS BRAKING STAGE		MARS ESCAPE STAGE		
	EARTH ORBIT	EARTH ORBIT	EARTH TO MARS	EARTH ORBIT	EARTH TO MARS	MARS ORBIT
Fuel Cell Weight, lbs.	5.8	3.81		1.73		1.09
Boiloff Weight, lbs.	59.5	34.4		6.7		14.2
Pump Weight, lbs.	3.4	3.4		3.4		
Weight Per Tank, lbs.	69	42			27	
Weight Per Stage, lbs.	276	84			27	
Δ Imieo Per Stage, lbs.	497	263			122	
Total Δ Imieo, lbs.			848			

Table 3-14

MINIMUM WEIGHT SUMMARY
FOR BRUSHLESS D.C. MOTOR DRIVEN PUMP
INCLUDING ULLAGE ENCAPSULATION CRITERION
(EXCLUDING STRUCTURAL SUPPORTS, ETC.)

	EARTH ESCAPE STAGE	MARS BRAKING STAGE		MARS ESCAPE STAGE		
	EARTH ORBIT	EARTH ORBIT	EARTH TO MARS	EARTH ORBIT	EARTH TO MARS	MARS ORBIT
Fuel Cell Weight, lbs.	1.23	1.26		1.23		1.27
Boiloff Weight, lbs.	0.21	0.54		0.18		0.71
Pump Weight, lbs.	3.4	3.4		3.4		
Weight Per Tank, lbs.	4.84	5.2		4.77		1.84
Weight Per Stage, lbs.	19.4	10.4			6.61	
Δ IMIEO Per Stage, lbs.	35.0	20.8			29.8	
Total Δ IMIEO, lbs.			85.57			

3.7 COST SAVINGS

The differential in costs of placing the various mixer subsystems and their corresponding weight in Earth orbit assists in the justification of the mixer subsystem selected and the corresponding costs of the development of unconventional systems. The maximum and minimum costs for placing three conventional mixer systems in Earth orbit are shown in Table 3-15. These systems are ac or dc motor driven pumps for the cases including the ullage encapsulation criterion and the case of a dc motor driven pump not considering the ullage encapsulation criterion. The data shown in Table 3-15 are based on a cost of one thousand dollars per pound of weight in Earth orbit. These data may be interpreted as the relative cost estimate for a conventional miser system for this specific vehicle.

The cost differential between the maximum and minimum values shown in Table 3-15 are based on the assumed difference in prediction of stratification development (maximum and minimum stratification coefficients are given in Table 3-3) and mixing time (mixing time coefficients are given in Table 3-5). The cost differential can be interpreted as an anticipated overdesign required for the uncertainty in stratification development and mixing time. As an example, the cost

Table 3-15

EFFECTIVE COST OF
INCREASE IN NFM MIXER SYSTEM MASS IN EARTH
ORBIT (EXCLUDING FIXED WEIGHTS)

	Maximum Cost Dollars	Minimum Cost Dollars
A.C. Motor Driven Pump Not Including Ullage Encapsulation Criterion	518,000	53,000
D.C. Motor Driven Pump Not Including Ullage Encapsulation Criterion	239,000	68,000
D.C. Motor Driven Pump Including Ullage Encapsulation Criterion	848,000	86,000

differential for an ac motor driven pump is estimated as $465,000 per Mars vehicle. For three Mars vehicles, the cost differential is about $1,400,000. These cost differentials can be utilized as the basis of the cost effectiveness of refining stratification and mixing prediction techniques by performing additional analytical and experimental studies.

In a similar manner, there is approximately $800,000 (for three Mars vehicles) difference between the ac and dc motor driven pumps which may be utilized to determine the cost effectiveness of developing the dc motor driven pump (if further refinements in stratification and mixing time predictions are not made).

A comparison of the cost differential between the dc motor with and without the applicability of the ullage encapsulation criteria results in a cost differential of about $1,800,000. This differential is indicative of the cost effectiveness of further investigation (analytical and experimental) to establish the validity of the ullage encapsulation criterion.

Comparison of these costs with the development and orbital costs of unconventional systems provides a basis for a decision to develop an unconventional system. The decision to develop the unconventional system must also

require some estimate of the improvement in performance over the conventional systems described in this section.

3.8 MIXER OPERATIONAL SEQUENCE

The mixer operational control requirements are derived from the operational sequence of the mixer. The type of operational sequence required results from the selected propellant storage mode. For the Earth escape and Mars braking stage, the cryogenic propellant is stored in a nonvented mode. Venting is anticipated only during ground hold, launch and helium vapor "blowdown" initially in Earth orbit. Venting during ground hold, etc. is carried out by use of a conventional vent system in which the propellant is settled.

An emergency vent system utilizing a thermodynamic separator is envisioned for both the Earth escape and Mars braking stages. The emergency vent system operates automatically when the tank pressure approaches the tank design pressure (slightly above the pressurization level during engine firing) and continues to operate until the tank pressure drops an amount specified by a practical vent band (1.0 to 2.0 psi). Mixers are located on both the forward and aft tank bulkheads. The emergency vent system is located on the forward bulkhead.

The mixers in the Earth escape and Mars braking stages are activated at a pressure corresponding to the pressure level produced by the pressurization system (a pressure above

the propellant saturation pressure before pressurization by an amount corresponding to the initial NPSP).

Four tank pressure levels are of interest in the description of the mixer operating sequence. The four pressure levels are shown below

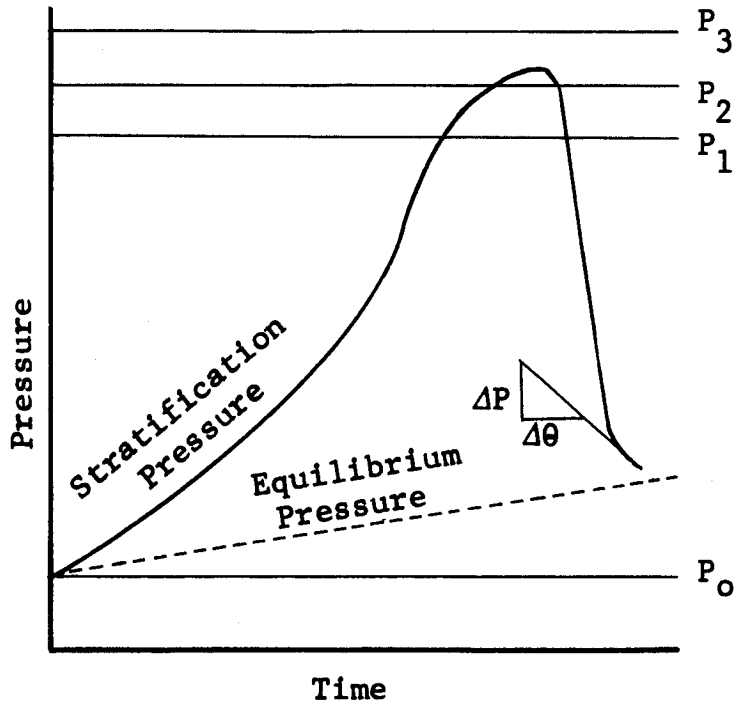

The storage begins at an initial saturation (mixed) pressure, P_o, which in the Mars manned vehicle corresponds to the triple point pressure.

The final mixed saturation pressure of the liquid before engine firing is P_1. P_2 is the pressure to which the tank is pressurized during engine firing. Pump initial NPSP

requirements are satisfied by the difference between P_2 and P_1. P_3 is a maximum allowable pressure.

The mixing cycle is initiated at the pressurization pressure P_2. Mixer I is operated and after a specified period of time Mixer II is operated. The mixer locations are shown below

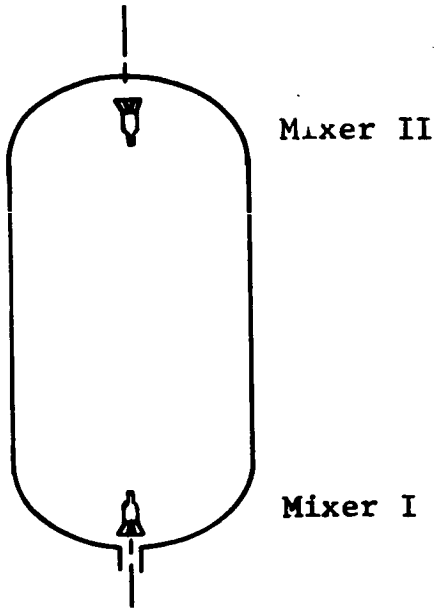

The mixing cycle (activated by $P_t > P_2$) is as follows

1. Mixer I is activated by a pressure switch when $P_t > P_2$
2. Mixer I is deactivated either
   a) At θ_{min} by a timer (Timer I (θ_{min})) which overrides the $(\Delta P/\Delta\theta)_d$ switch if $\Delta P/\Delta\theta < (\Delta P/\Delta\theta)_d$ for $\theta \leq \theta_{min}$, where $(\Delta P/\Delta\theta)_d$ is the selected tank pressure decay rate (the pressure decay rate switch deactivates the mixers if the pressure decay rate, $\Delta P/\Delta\theta$, is less than $(\Delta P/\Delta\theta)_d$ at $\theta > \theta_{min}$).

b) When $\Delta P/\Delta\theta = (\Delta P/\Delta\theta)_d$ by a pressure transducer if $\Delta P/\Delta\theta > (\Delta P/\Delta\theta)_d$ at θ_{min} and $\Delta P/\Delta\theta < (\Delta P/\Delta\theta)_d$ at θ_{max}, or

c) By a timer (Timer I, θ_{max}) where $\Delta P/\Delta\theta > (\Delta P/\Delta\theta)_d$ in the time interval $\theta_{min} < \theta < \theta_{max}$.

d) By an onboard computer system.

3. Mixer II is activated by Timer II at a time equal to θ_{max} after Mixer I was activated.

4. Mixer II is deactivated in the same manner as Mixer I is deactivated.

The time, θ_{min}, is the minimum anticipated length of the mixing time and θ_{max} is the maximum length of the mixing time, as is given in Table 3-6.

Two sequences of possible Mixer I and II operation are shown in Figures 3-5 and 3-6 for

1. A rapid destratification in which $\Delta P/\Delta\theta < (\Delta P/\Delta\theta)_d$ when θ_{min} is reached and the mixers are deactivated by the θ_{min} timers.

2. A destratification time in which $\Delta P/\Delta\theta > (\Delta P/\Delta\theta)_d$ at θ_{min} and $\Delta P/\Delta\theta = (\Delta P/\Delta\theta)_d$ in the time interval $\theta_{min} < \theta < \theta_{max}$, and the mixers are deactivated at $\Delta P/\Delta\theta = (\Delta P/\Delta\theta)_d$

The rate of pressure decay $\Delta P/\Delta\theta$ is sensed either mechanically by use of a small storage chamber and an orifice or electronically.

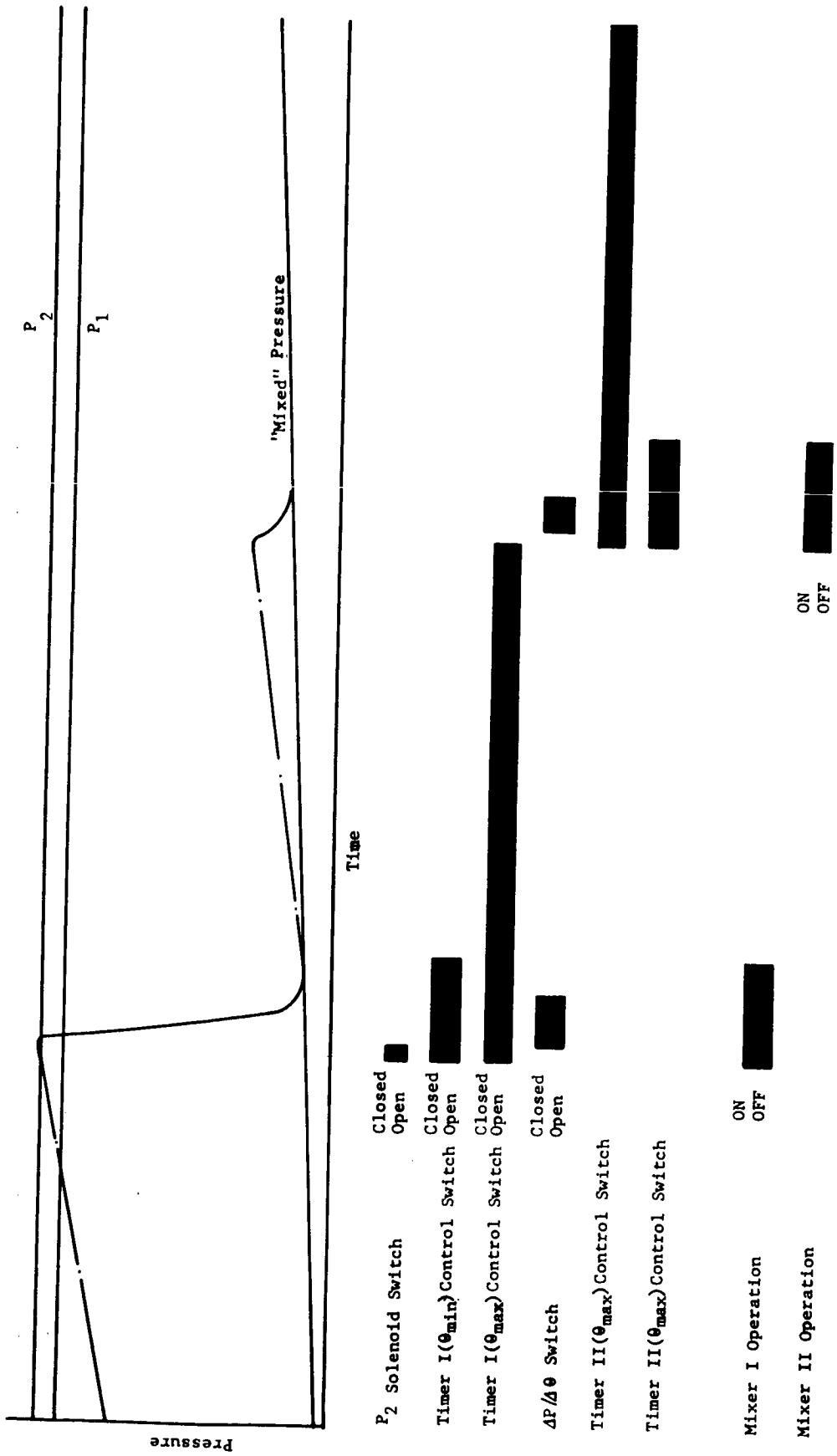

Figure 3-5 Operational Sequence in Which The Timer I(θ_{min}) and Timer II(θ_{min}) Deactivates The Mixer

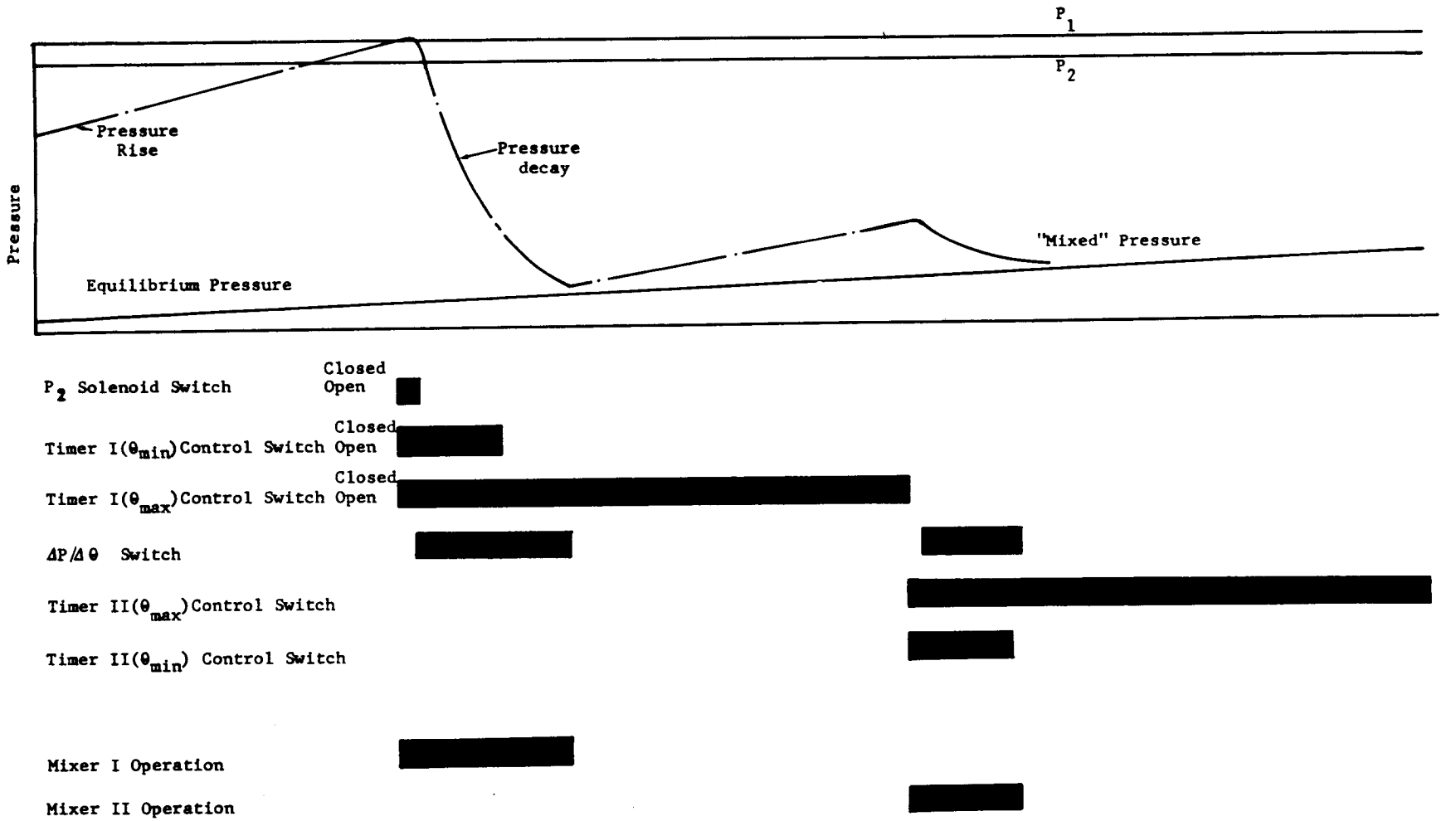

Figure 3-6 Operational Sequence In Which Pressure Decay Rate Switch Deactivates The Mixer

There are at least two other modes of operation of the mixers once the pressure P_2 is reached. These two are

1. The Mixer I can be activated at P_2 and deactivated at P_1. When P_2 is reached again Mixer II can be activated and deactivated at P_1 (A timer can be also used to activate Mixer II) as shown below.

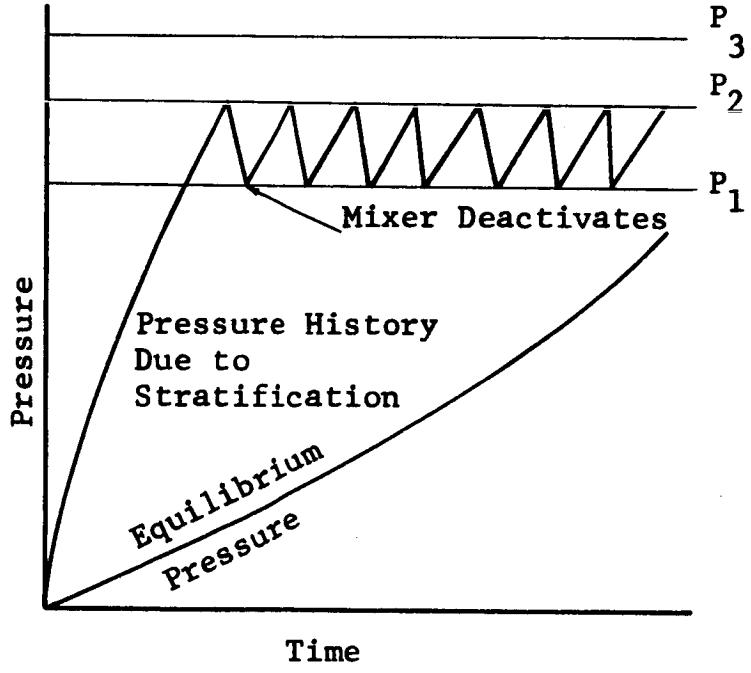

2. A programmed tank pressure history can be used to deactivate both mixers as shown below.

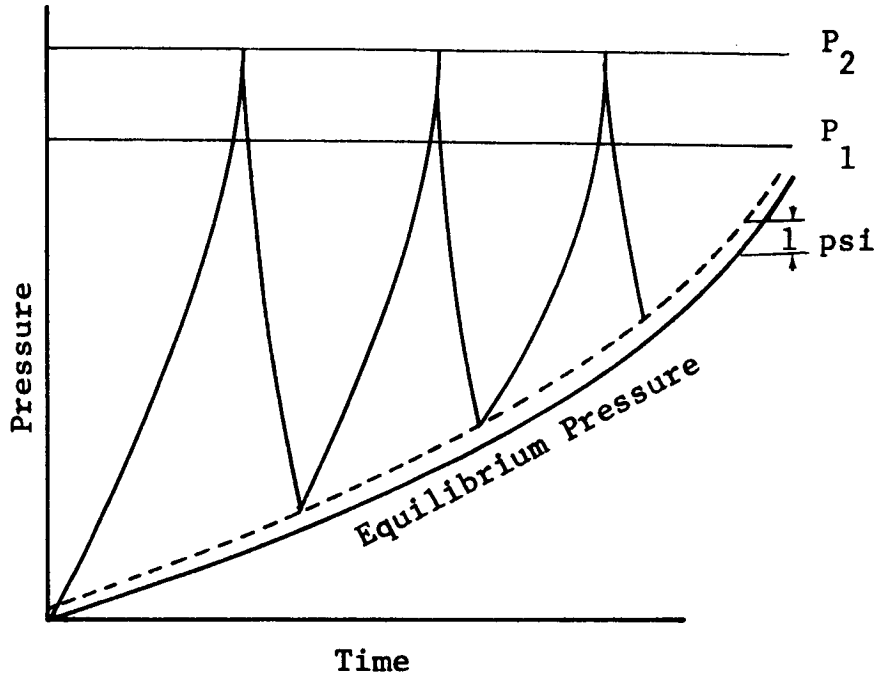

The programmed tank pressure history can be set to be one psi higher than the anticipated non-vent pressure history of the tank.

SECTION 4

EXPERIMENTAL INVESTIGATIONS

The experimental phase of the program has provided data on mixing, ullage breakup and liquid/vapor flow characteristics. The experimental mixing investigations were conducted under both pressurized and nonpressurized conditions and primarily considered axial jet mixing concepts which previous experimental results indicated to be superior to radial jet mixing. In addition, a test was conducted using a jet directed at a 60^{o} angle from the horizontal in order to evaluate the effectiveness of this concept. The experimental investigations considering ullage breakup and liquid/vapor flow characteristics were conducted in a miniature tank using an axial jet. These tests were designed to simulate low gravity tank interface conditions. The experimental data has been used to compare analytical predictions and to develop mixer design parameters.

4.1 EXPERIMENTAL TEST OBJECTIVES

The objective of the experimental tests was to perform mixing and ullage breakup investigations with water to supplement and expand previous testing in support of the development and verification of analytical techniques for predicting the performance of mixing devices and to provide design information. This was done in three test phases. The first phase involved open tank or non-pressurized mixing and the second phase involved closed tank or pressurized mixing. The third phase utilized a miniature non-pressurized tank. The miniature tank test considered ullage breakup and liquid/vapor flow characteristics due to the axial jet mixing when the liquid/vapor interface was curved. The ullage, in this case, consisted of air.

4.1.1 Test Data Requirements

Test data requirements were much the same as reported in Reference 1 except that interest was entirely on mixing rather than partially on stratification and draining. Also, additional detail and continuity in the data were sought. For example, dye movements in the open tank were recorded continuously by motion picture rather than by

slides and closed tank ullage pressures were recorded on continuous trace strip charts. Test variables for the open and closed tank tests requiring experimental data for verification of their effect on mixing were liquid level, ullage heating, and a jet directed at a 60^{o} angle from the horizontal in addition to the nozzle diameters and heater combinations used in previous tests. The miniature test variables were water level, flow rates and tank diameter.

The open tank tests were designed to yield data on both the jet motion and bulk fluid motion during mixing as well as temperature data. The closed tank tests were intended to yield data on temperature and pressure histories during mixing. The miniature tests were intended to determine the mixing jet flow rate required to break up the ullage into small bubbles whose diameter is at least on order of magnitude smaller than the tank diameter. (The analytical study had indicated that it is desirable to break the ullage into a number of small bubbles to reduce the possibility of ullage encapsulation of the mixers and to reduce the rate of pressure rise when the mixers are not operated). The data from the experimental testing were analyzed to yield mixing times, mixing performance, transient pressure and temperature effects, and data on ullage breakup during mixing.

4.1.2 Experimental/Analytical Data Comparison

The experimental and analytical comparisons that can be made to determine the validity of analytical predictions are principally those described in Reference 1. In addition, the ullage pressure history provides a comparison with liquid surface temperature since it is a function of saturation temperature. The pressure decay is an indication of mixing. The ullage breakup data showed the ability to breakup the ullage and avoid ullage encapsulation of a mixer.

The comparison of experimental data with analytical predictions in some cases can be made without further analysis, however, for the most part some analysis is required. The jet motion and bulk fluid motion, as revealed by dye movements during mixing, required analysis of experimental data first. The comparison of the bulk fluid motion with experimental pressure and temperature decay also requires analysis of the data. The ullage breakup data is not compared directly with an analytical prediction, instead it confirms the possibility of breaking up the ullage. In some cases, the interpretation of the data is a matter of judgement. This is particularly true in determining temperature differences and dye position during mixing.

4.2 TEST FACILITY DESIGN CONSIDERATION

Verification of analytical predictions and determining design information for large scale mixing systems from small scale experimental results require that careful consideration be given to geometrical similarity and the conservation equations. These considerations were used in the original design of the test systems.

4.2.1 Geometrical Similarity

Geometrical similarity requires that the configuration of the test tank and the full scale tank for which a mixer system is to be designed be as similar in shape as possible. The original test system was designed to simulate a cylindrical tank with a hemispherical top and a hemispherical concave tank bottom. An additional convex hemispherical bottom was also utilized in this test series. The closed tank tests utilized the hemispherical top and the convex bottom. The open tank tests did not use the hemispherical top, but did utilize both bottom bulkhead configurations. As before, the most significant variation between the open and closed test tanks and an actual space application was

the existance of a flat liquid/vapor interface rather than a curved interface as would be found in an operational tank in a low-g environment. The miniature test considered this curved interface.

4.2.2 Conservation Equations

The original design of the test system utilized dimensionless parameters obtained from the conservation equations in order to insure that the test results would adequately simulate heating conditions and acceleration levels of typical vehicles and missions (S-IVC Orbital and Manned Interplanetary). The analysis showed that, with water as the test fluid, the experimental tanks used in this study would provide valid data.

4.3 EXPERIMENTAL EQUIPMENT

4.3.1 Summary

The experimental testing was conducted using three separate test systems. The open and closed tank systems were essentially the same as those described in Reference 1 except for modifications and additions found to be desirable during the first test series and those changes necessary to expand test conditions. In order to avoid repetition of the information reported in Reference 1, this report will describe only the modifications and additions to the original test apparatus. For more detailed information see Reference 1. The miniature test system was an entirely new design.

The major additions to the open tank system consisted of the following components:

- Convex bottom bulkhead
- An axial nozzle designed to direct a jet in the shape of a hollow cone at a 60^{o} angle from the horizontal
- An 0.032 inch diameter axial jet orifice
- Digital acquisition of test data.

These open tank test system additions and other modifications are described in detail in Subsection 4.3.2.

The major additions to the closed tank consisted of the following items:

- Convex bottom bulkhead
- An 0.032 inch diameter axial jet orifice
- Vacuum pump

These closed tank test system additions and other modifications are described in detail in Subsection 4.3.3.

The miniature test system was very simple and consisted of the following three basic components:

- Two interchangeable glass tubes (13 and 6 mm in diameter) with approximately hemispherical tops. These tubes served as the test tanks.
- Two interchangeable orifices 0.0356 and 0.0216 mm in diameter which served as the axial jet mixer nozzles.
- The associated plumbing lines carrying water to and from the test tanks.

Due to the simplicity of design of this test apparatus and the importance of it on the data, the system will be described along with the experimental data in Subsection 4.5.3.

4.3.2 Open Tank Experimental Equipment

4.3.2.1 Open Tank Test System

The test system for the open tank tests were essentially the same as used in previous tests. The system consisted of the following components:

- A 12-in.-O.D. by 24-in.-high lucite cylinder installed on a stainless steel concave or convex bulkhead tank bottom.
- A nozzle assembly installed on the tank bottom
- A pump and flow loop installed beneath the tank bottom
- Sidewall, top, and bottom heaters, all internal to the tank. Instrumentation for measurement and recording of liquid temperatures and pressure drop across the nozzle.
- Power supplies and controls for electrical heater excitation.

A number of modifications and additions were made to the open tank system in order to expand test conditions and to facilitate data acquisition. The additions and modifications are described below. Figure 4-1 shows a simplified sketch of the open tank test system with a concave bottom bulkhead. Figure 4-2 is a photograph of an actual test setup with a convex bottom bulkhead.

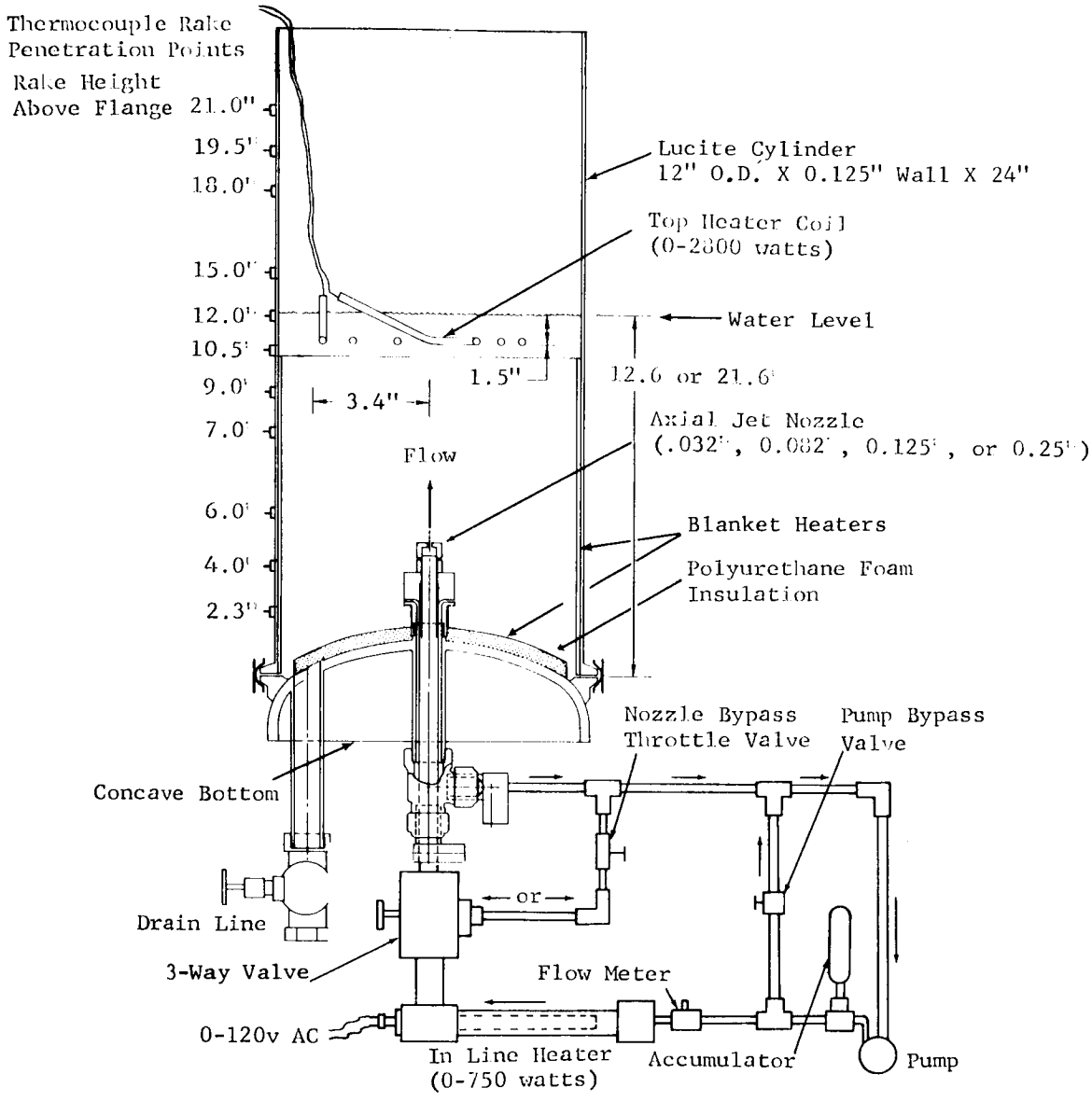

Figure 4-1 Schematic of Open-Tank Test System With Concave Bottom Bulkhead

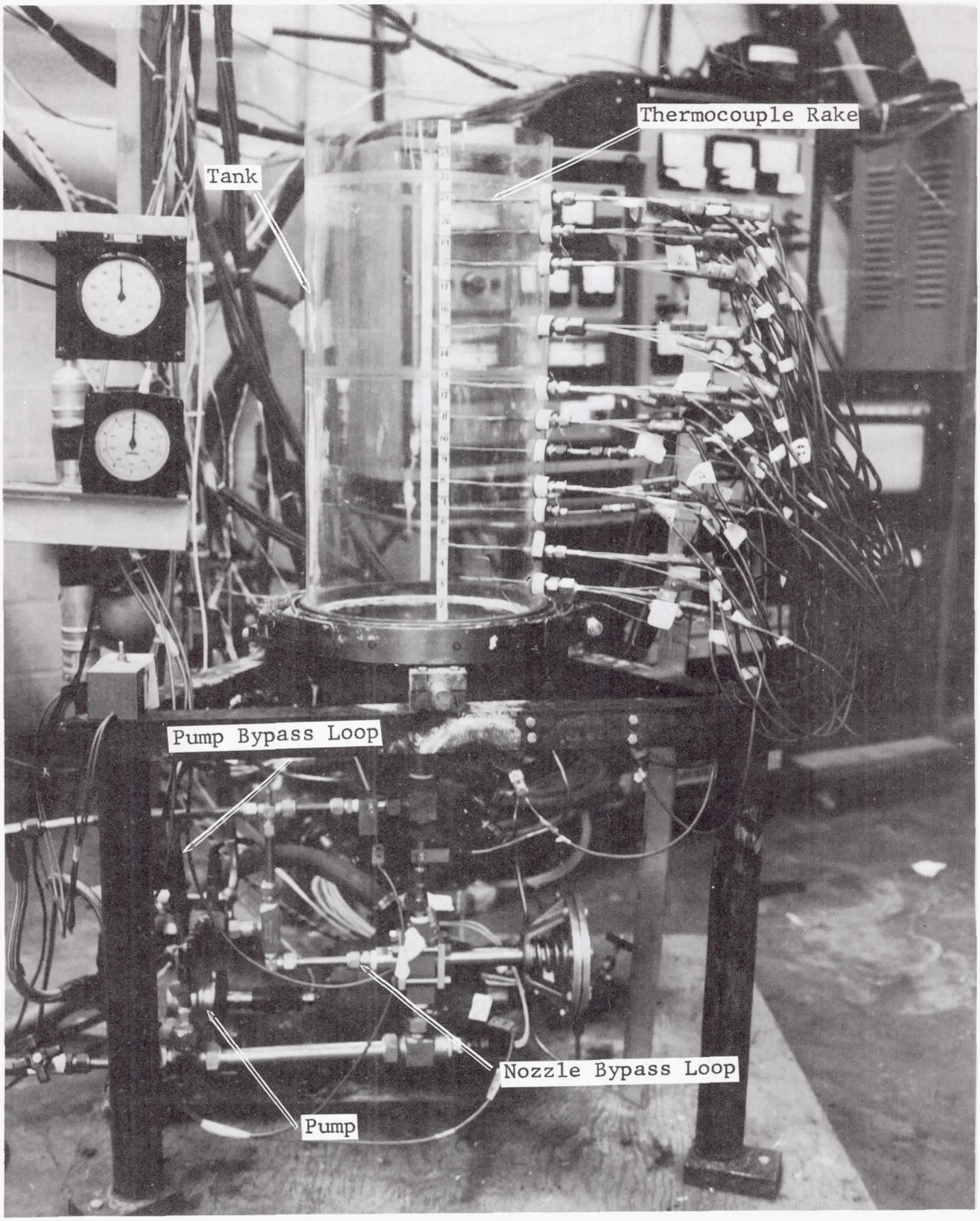

Figure 4-2 Photograph of the Open Tank Test System

Test Tank Additions and Modifications

In addition to the concave bottom bulkhead used in previous tests, a convex bottom bulkhead was also used in the open tank tests. The convex bulkhead is a reverse of the concave bulkhead. Figure 4.3-6 in Reference 1 shows details of this bulkhead. This additional bottom bulkhead was used in order to obtain information on the effect of the geometry change on mixing.

Heater Modifications

The size of the sidewall heater was increased to have a total height above the bottom flange of the tank of 21.6 inches. This was done in order to perform sidewall heating tests at higher water levels.

The bottom heater used on the convex bulkhead was of the same type used previously on the concave bulkhead. The installation procedures were also similar.

Pump and Flow Loop Modifications

The general arrangement of the pump flow loop was as shown in Figure 4-1. The pump was a Tuthill Model 100W positive-displacement, vane-type pump. Capacity was 95 gphr at 1725 rpm. The maximum discharge pressure was 100 psi. The pump was driven by a reversible, 1/2 hp variable speed

d.c. motor, with output speed remotely adjustable from 0 to 1800 rpm. An integral tachometer-generator circuit provided speed regulation to ± 1% of setpoint.

The pump flow loop contained two bypasses for use in controlling flow rates and pump loop temperatures. The pump bypass loop was used to accommodate the pump to some of the lower nozzle flow rates. The nozzle bypass loop was used prior to turning the jet on to recirculate fluid in the pump flow loop past an inline heater in order to warm the fluid to approximately the same temperature as the tank fluid.

The inline heater was an electrical cartridge type with a rating of 0-750 watts. This heater was also used to make up for heat losses from the pump flow loop during tests.

The pump flow loop also contained an accumulator which served to dampen pump discharge pressure pulsations. An in-line filter unit was an integral part of the accumulator.

Flow measurements were obtained by two redundant methods. A Flow Technology turbine meter located downstream from the pump provided one means of measuring the flow. This meter had two ranges; 0.01-0.1 gpm and 0.1-1.0 gpm. In addition,

a Statham Instruments differential pressure transducer, Model PM-280TC, was used to measure the pressure drop across the nozzle inlet and outlet. The pressure drop could then be used to obtain a flow rate. This transducer had a 0-±100 psi range.

Nozzle Assembly Modifications

The nozzle assembly used in earlier tests was redesigned to reduce its mass and height in order to provide a more realistic mixer model. The redesigned assembly is detailed in Figure 4-3. It consists of a flanged sleeve and a threaded collar which, together, form the slit for the radial jet; and interchangeable caps with 0.032-, 0.082-, 0.125-, and 0.25- inch diameter orifices for the axial jets. The parts were all of aluminum, type 6061-T-6.

An additional nozzle assembly designed to direct flow at a 60° angle from the horizontal was also manufactured. This assembly is shown in Figure 4-4. It consists of a sleeve with a flared flange directed outward at a 60° angle and a threaded collar in the shape of a truncated 60° cone which, together, form the slit for the 60° jet; a threaded lock ring or nut; and 3 centering screws. The slit width

Nozzle Material: 6061-T6, Aluminum

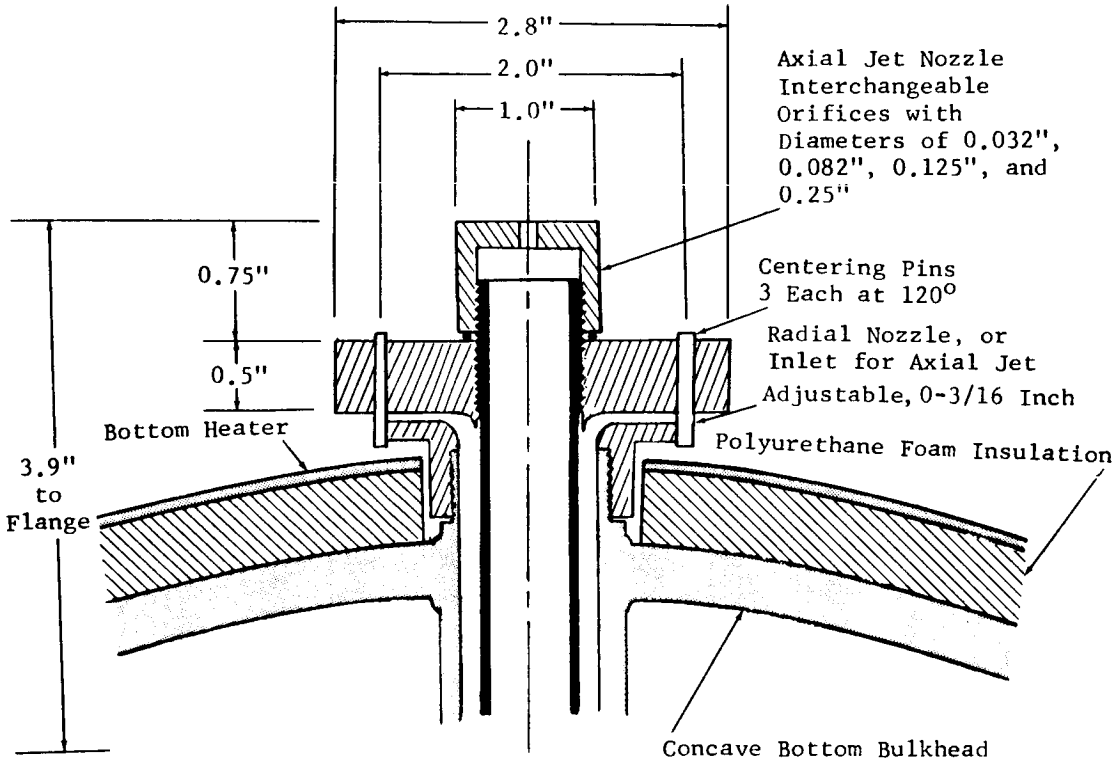

Figure 4-3 Schematic of Axial Jet Nozzle Assembly

Nozzle Material: 6061-T6, Aluminum

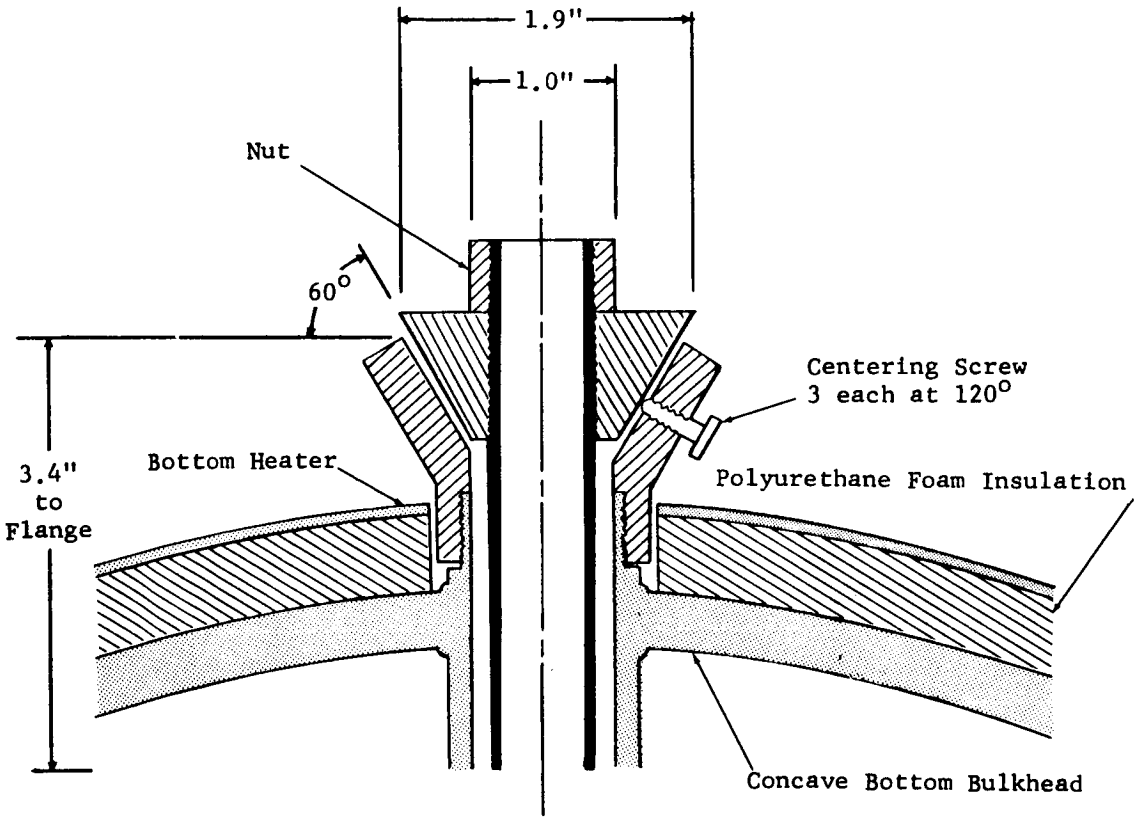

Figure 4-4 Schematic of 60° Jet Nozzle Assembly

can be varied with different positions of the centering screws. All parts, except for the centering screws, are made from 6061-T6 aluminum.

4.3.2.2 Open Tank Control System

The control system for the heater power and pump motor were essentially the same as used in earlier tests. Additional controls were added to allow remote draining and filling of the test tank. Controls for the pump loop heater were also added to maintain the nozzle inlet and outlet temperatures within a preset temperature difference and account for heat transfer from the pump loop.

4.3.2.3 Instrumentation System and Components

Measurements made during the open-tank tests included water and bottom heater temperatures, pump flow rates, drain flow rates, nozzle pressure drop, and heater power. The instrumentation system is described in Reference 1 except for the following changes.

Temperature Measurement

Temperatures were sensed with copper-constantan thermocouples. The thermocouples were installed in rakes which

penetrated the sidewall of the test tank rather than a single rake extending downward from the surface. Figure 4-2 shows the rakes in place. Figure 4-5 shows the thermocouple locations for the concave bulkhead tank and Figure 4-6 shows the locations for the convex bulkhead tank.

Flow Measurement

Flow measurements were made directly with the turbine meter and indirectly with the pressure transducers described in the description of the pump flow loop (Subsection 4.2.2.1).

Data Recording

Temperature data was recorded on both strip charts and in digital form on punched paper tape by use of a Dymec Model 2010D-1716 data system. This was similar to the system described for the closed tank tests in Reference 1. Power inputs to the heaters were recorded periodically on log sheets during each run. Punched tape data was reduced to printed form using General Dynamics Computer Procedure RPO.

Photography:

Sixteen millimeter color movies were made to record dye motion in the tank for later study. A clock was also photographed to provide timing data during the film. Tank lighting

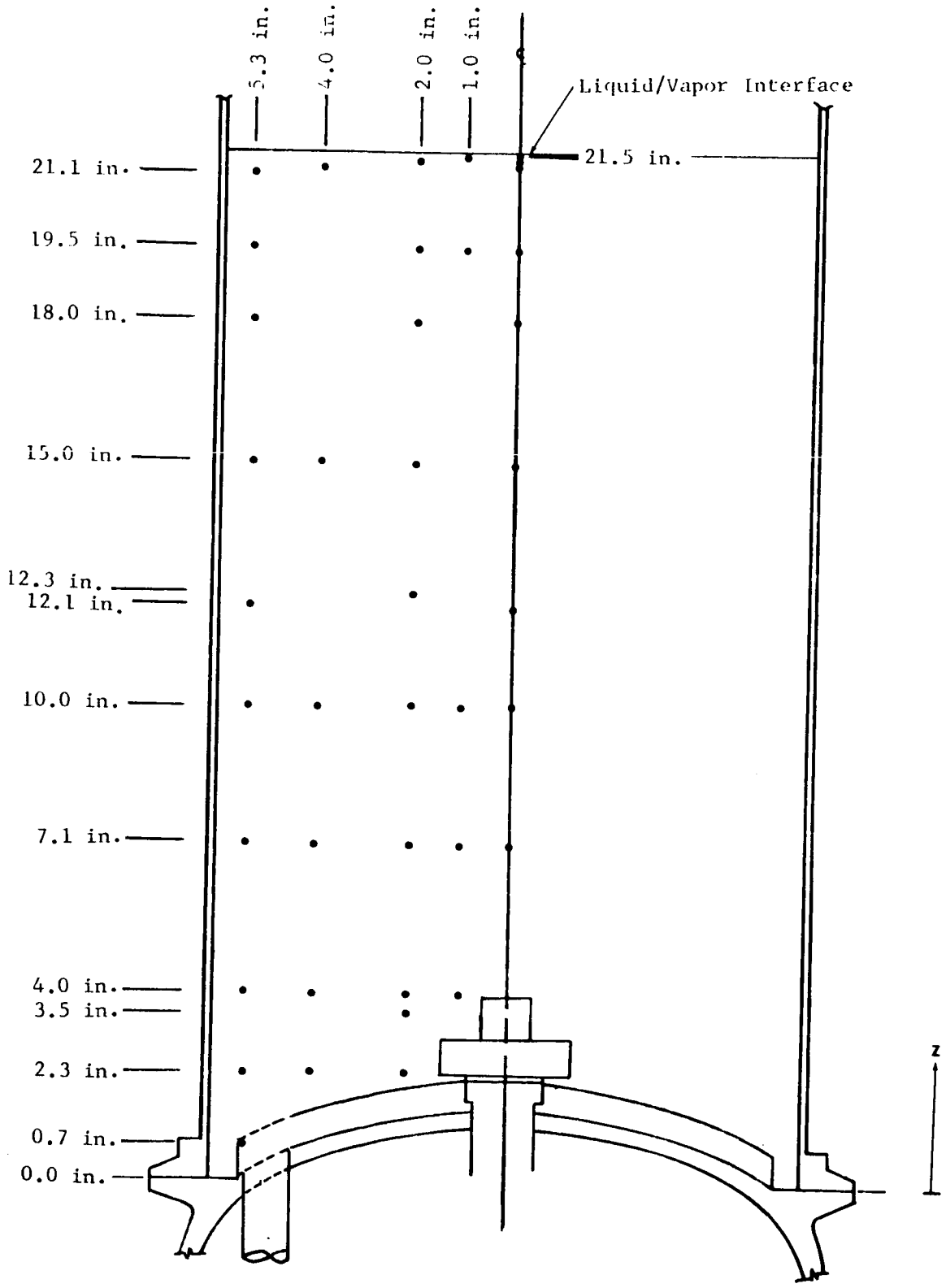

Figure 4-5 Schematic of Concave Bulkhead Thermocouple Rake Assembly For Open Tank Tests

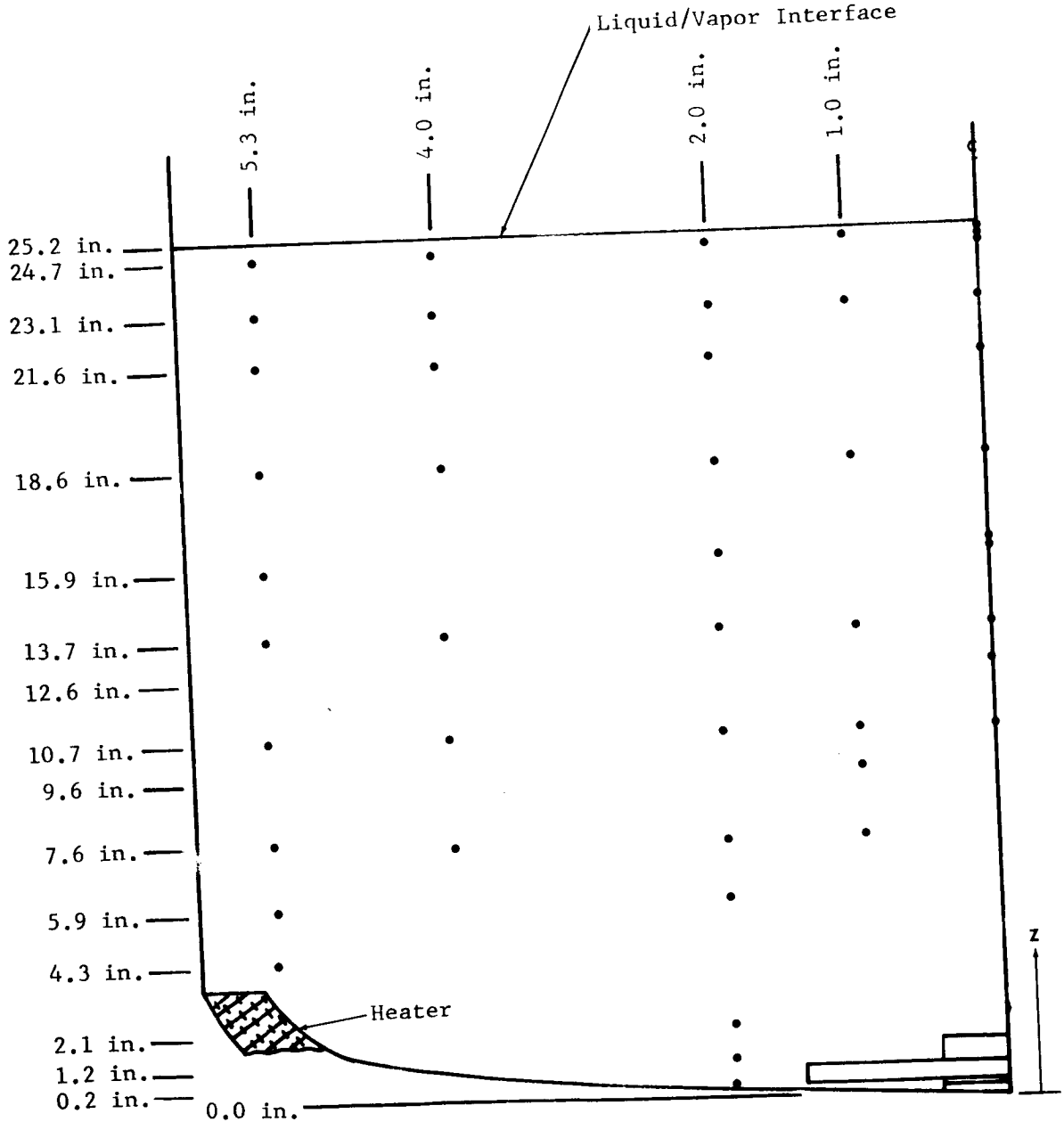

Figure 4-6 Schematic of Convex Bulkhead Thermocouple Rake Assembly For Closed Tank Tests

was provided by flood lights placed around the tank for non-side wall heating runs. During sidewall heating tests the same lighting procedure described in Reference 1 was used.

4.3.3 Closed Tank Experimental Equipment

4.3.3.1 Closed Tank Test System

The closed tank test system is basically the same as used in previous tests. Figure 4-7 shows a simplified schematic of the system and Figure 4-8 shows a photograph of the system. The system components consist of those described in detail in Reference 1 and additions or modifications described as follows:

Test Tank Modification

The basic test tank remained the same except for use of a convex bottom bulkhead. This was the same bulkhead used in the open tank tests.

The temperature sensor rake feed-through assembly which had passed through a flange in the tank top was eliminated and replaced by rake penetrations through the tank sidewall at each axial position where temperatures were measured. This was done in order to eliminate the heat short from the ullage to the outside environment. This also reduced the mass and volume of the sensor sheaths.

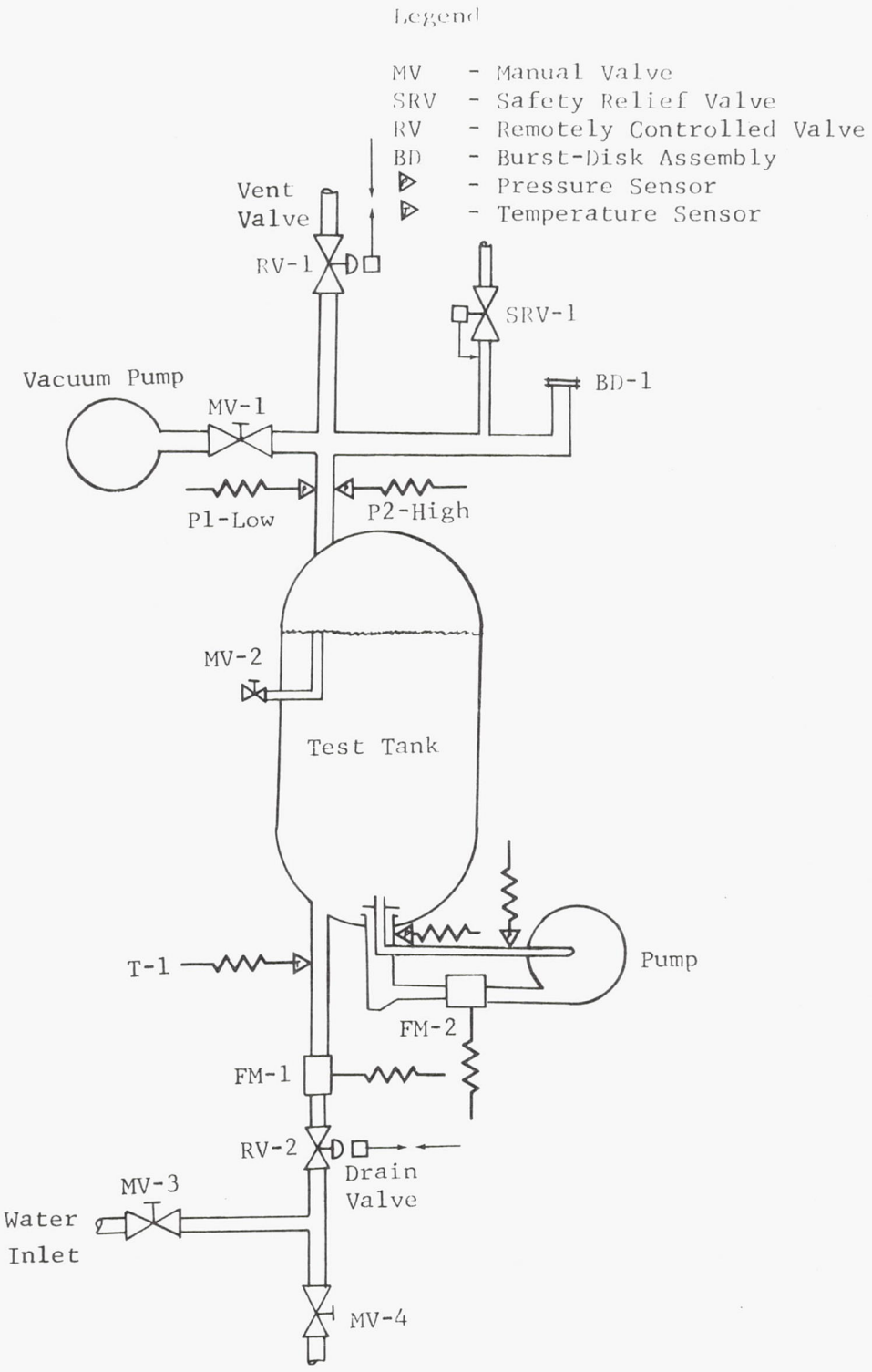

Figure 4-7 Schematic of the Closed Tank Test System

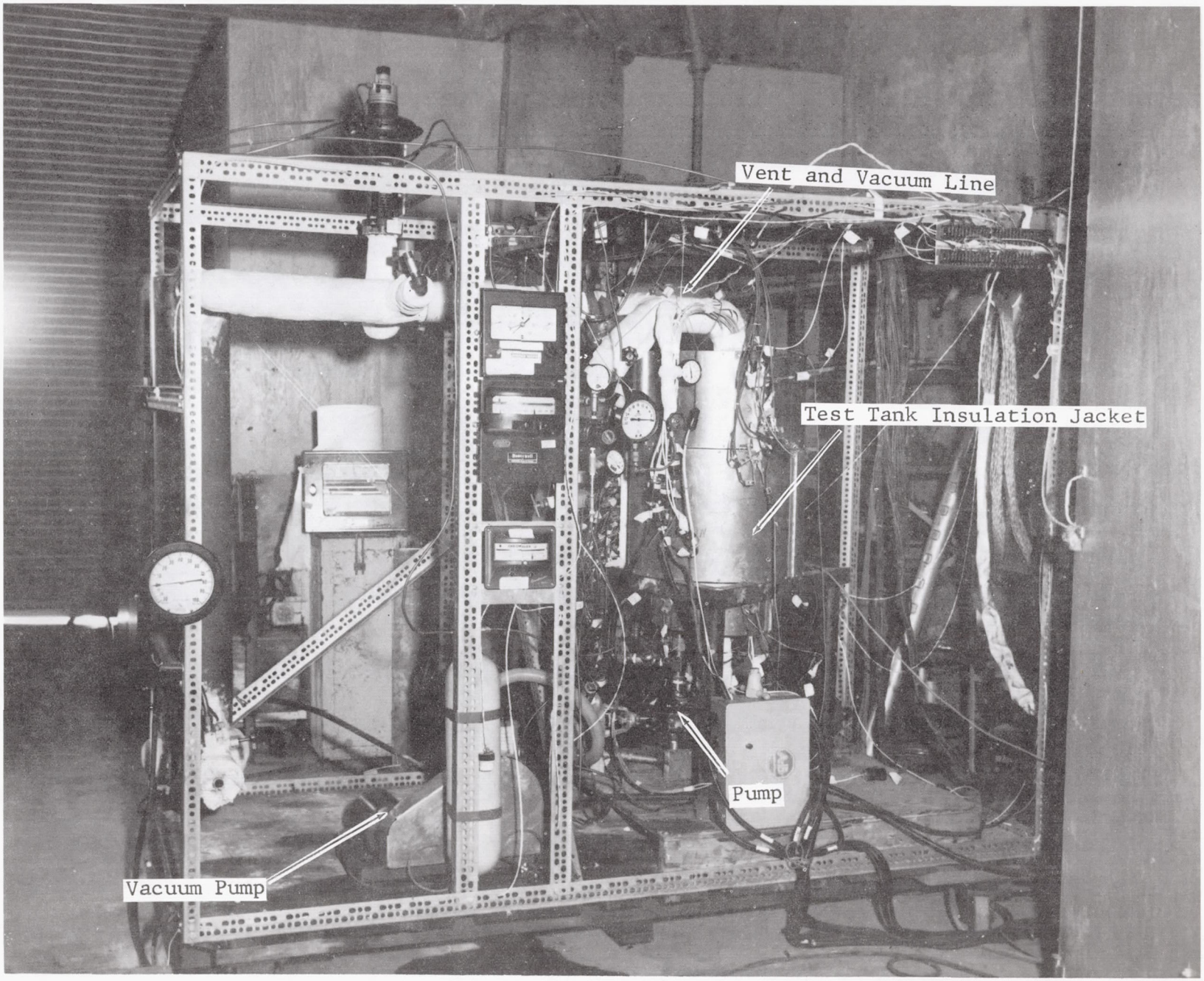

Figure 4-8 Photograph of the Closed Tank Test System

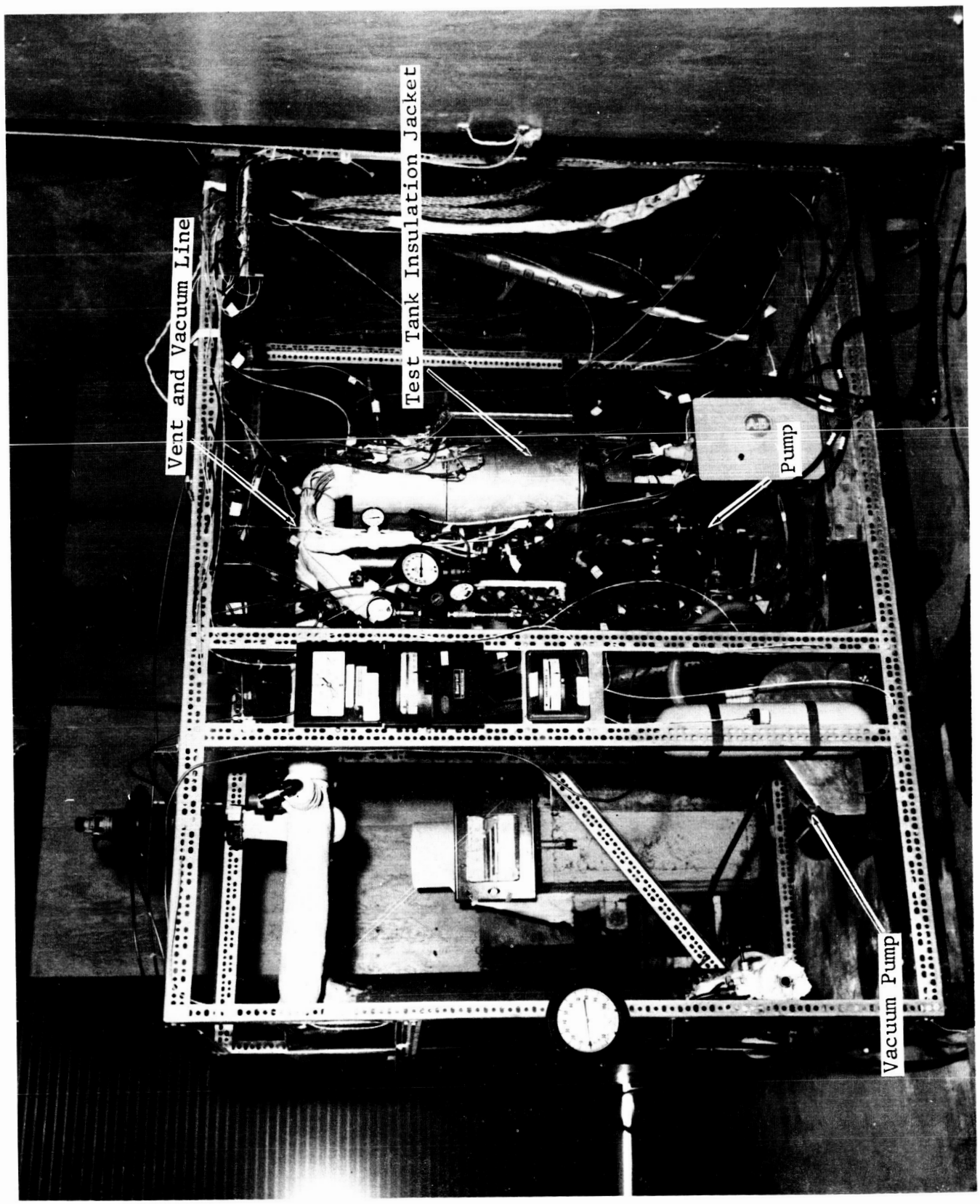

Figure 4-8 Photograph of the Closed Tank Test System

Tank Heaters and Insulation Modifications

The top bulkhead internal and external heaters were modified. The top inside heater was formed from two metal sheathed, flexible heater coils wound around the outside of a stainless steel shell which had been shaped to the contours of the inside surface of the top bulkhead. Each heater was a Chromalox model TR-10012, 100 inches in length, 0.246 inches in diameter and rated at 2100 W. Ceramic felt insulation (Carborundum Co. Fiberfrax) was placed between heater elements and the outer shell. The heater was clamped to the shell. Electrical connections to the heater were made through feed-throughs in the tank top. The steel shell was then spot welded to the inside of the tank head. Figure 4-9 shows a schematic of the arrangement.

The top outside heater consisted of three of the same Chromalox heater elements wound around the outside of the top bulkhead. Figure 4-10 shows a photograph of the installed outside heater.

The entire tank was insulated with 4-1/8 inch layers of Fiberfrax. The tank was then enclosed in a 3 inch urethane foam insulation jacket which was removable. This appears in Figure 4-8 as the large shiny cylinder in the middle of the test rig.

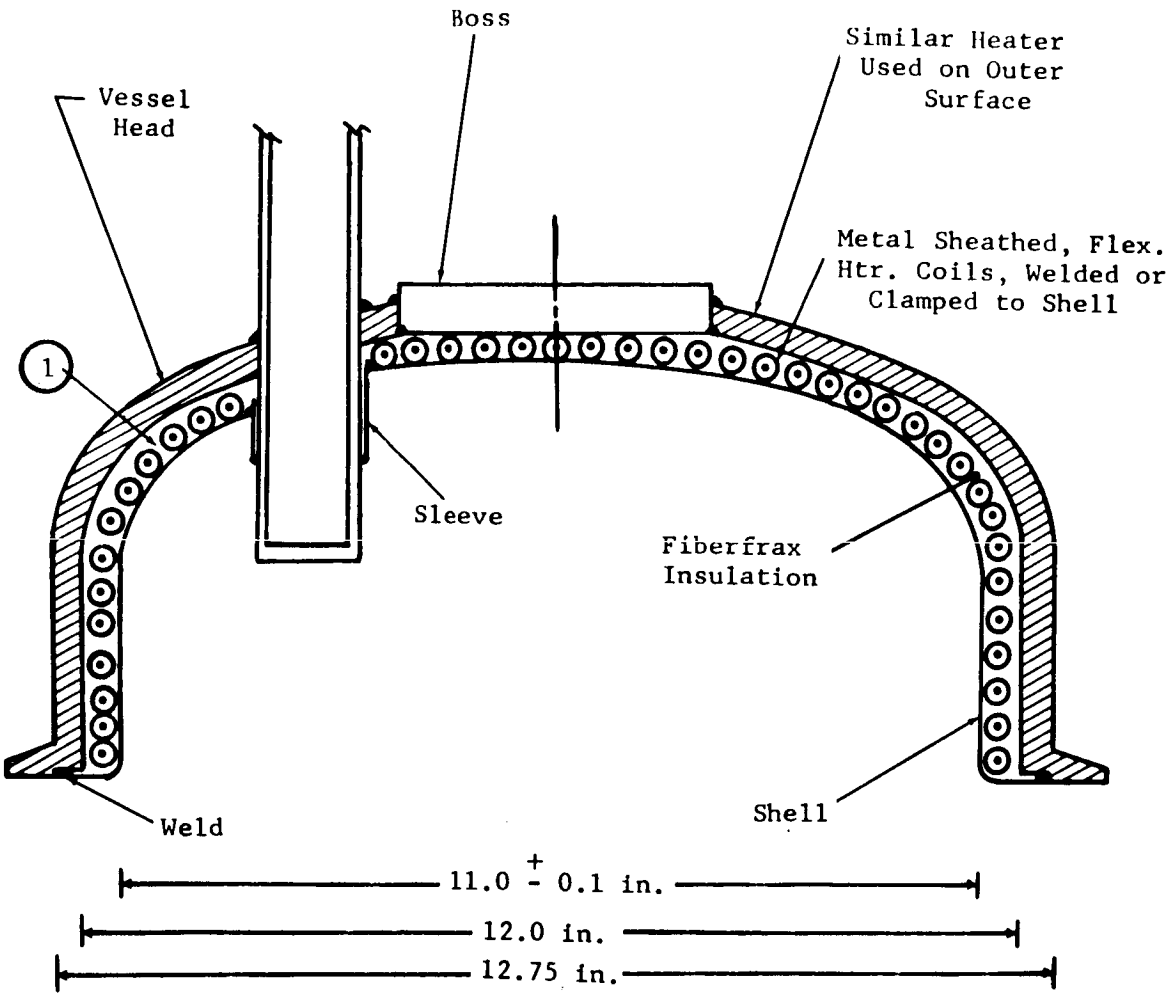

① Annulus vented to outside

Figure 4-9 Top Inside Heater and Shell Design

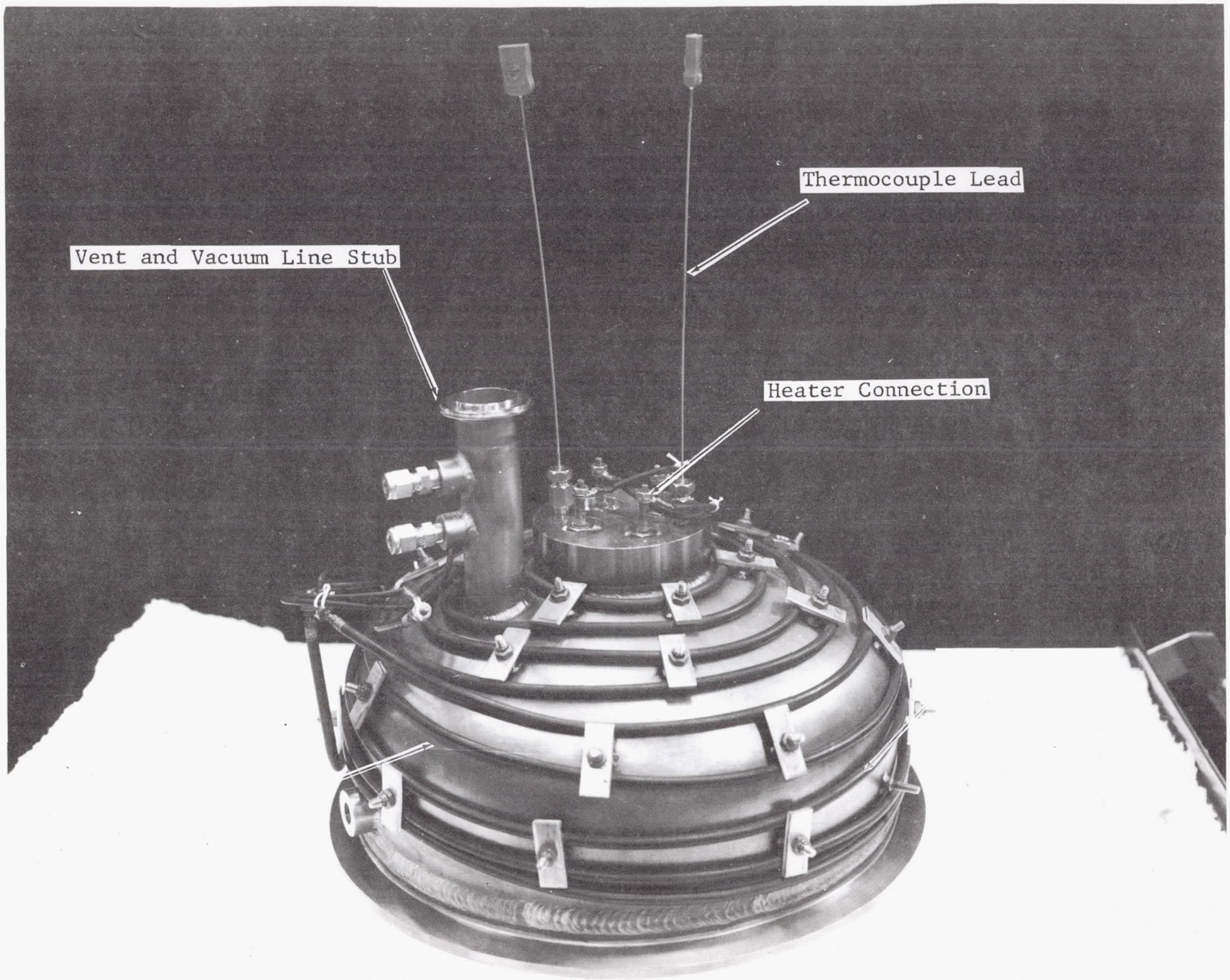

Figure 4-10 Photograph of Closed Tank Top Bulkhead and Outside Heater

Pump and Pump Flow Loop Modifications

The pump and pump flow loop were changed from the previous configuration and corresponded to the system described for the open tank in Subsection 4.3.2.1. The only nozzle used was 0.032 inches in diameter.

Vacuum System

A vacuum pump was connected to the test tank in order to pump the system down to the saturation pressure of the water prior to testing.

4.3.3.2 Control Systems and Components

Three additions were made to the control system. These were (1) a remote control unit for the pump motor speed (2) vacuum pump switches and (3) steam and pump loop remote temperature controls. The remaining controls and components are described in Reference 1.

4.3.3.3 Instrumentation System and Components

Primary modifications made in the instrumentation system involved rearrangement of the temperature sensors and pressure and flow measurement components. These changes are described below. The data recording and processing

methods are the same as used in the open tank tests. These methods are described in Subsection 4.3.2.3.

Temperature Measurements

The temperature sensors in the liquid and ullage of the closed test tank were the same as those used in the open tank tests. The rake arrangement is shown in Figure 4-11.

Flow Rate Measurement

Except for the jet flow rate measurements, the flow measurement methods are the same as described in Subsection 4.3.2.3.

Pressure Measurement

Measurements of the tank ullage pressure were made using two redundant pressure transducers. The low range transducer was a Statham Instruments, Model PA822-50 with a range of 0-50 psia. The high range transducer was a Statham Instruments, Model PA822-100 with a range of 0-100 psig. Both transducer readings were recorded by the digital data recording system. In addition, the high range transducer was recorded on a single point continuous strip-chart recorder. The use of the two redundant transducers provided improved data reliability and sensitivity.

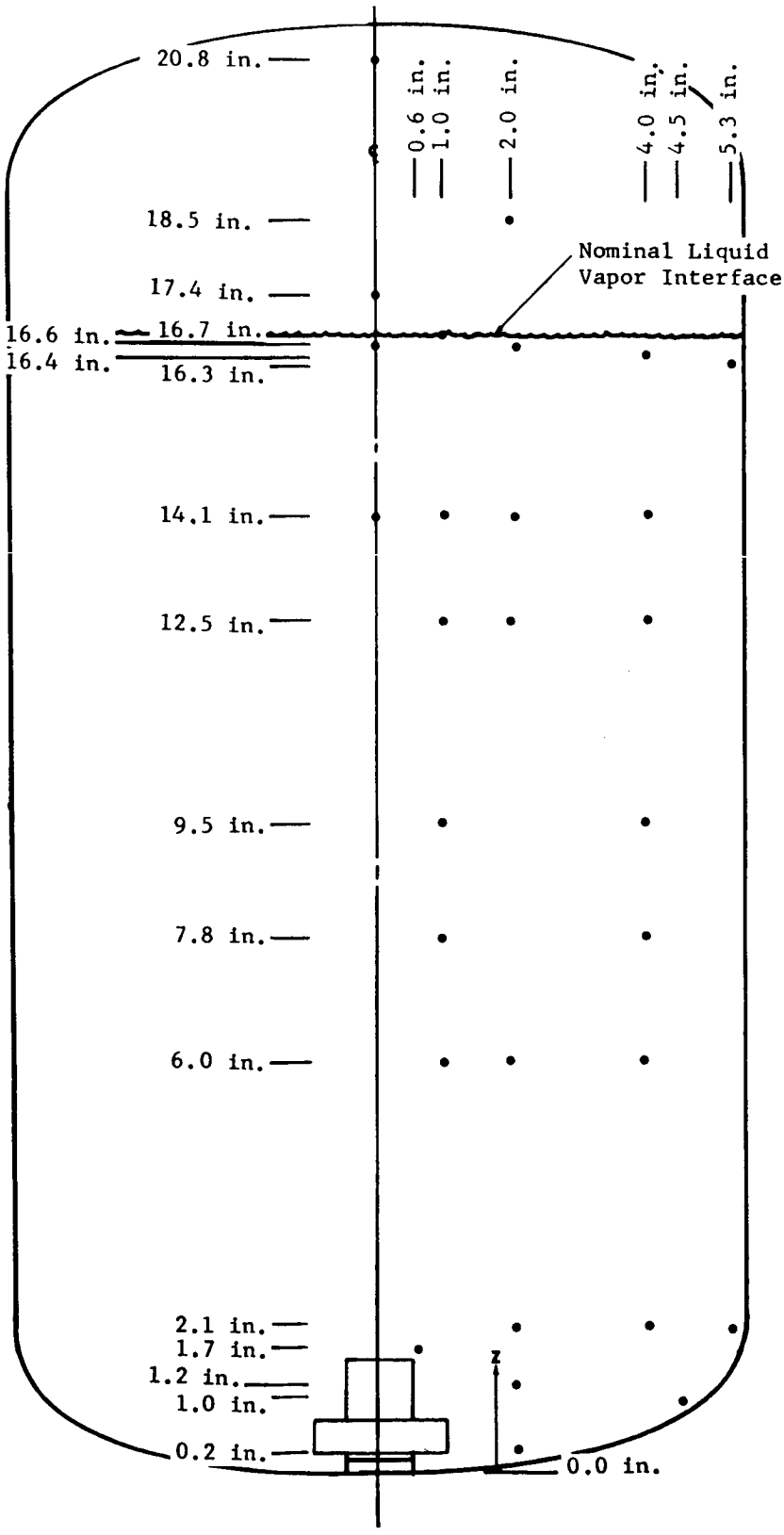

Figure 4-11 Schematic of Thermocouple Rake Assembly For Closed Tank Tests

4.4 TEST PROCEDURES

4.4.1 Open Tank Test Procedures

The open tank tests were planned primarily to study axial jet stratification reduction. In addition, a 60° jet was used to evaluate the concept of using a system intermediate between an axial jet and a radial jet. No stratification or draining tests were planned except as incidental phases of the destratification tests. The data taken were intended to supplement and expand data taken during previous open tank tests and hence the test procedure was similar to that reported in Reference 1.

The data taken during the tests consisted of temperature measurements as a function of time and tank position. In addition, 16 mm color movies were made of dye movements during mixing and flow penetration of the stratified layer. Test variables included flow rate, nozzle size, heating rate, type of heating, type of tank bottom, and liquid height above the nozzle.

Four axial jet nozzle diameters were used in the tests: 0.032, 0.082, 0.127 and 0.25 inch. The 60° jet tests considered only one outlet area corresponding to the area

of the 0.25 inch axial jet nozzle. This required an opening of 0.008 inches in width.

The test tank was heated using various combinations of top, bottom, and side heating in order to provide a range of data. These heater combinations were as follows: top, bottom, side, top and bottom, and side and bottom. Top heating rates were a nominal 940 and 94 watts. The nominal sidewall heating rate was 6900 watts. Bottom heating rates were nominal values of 82, 820, 1280 and 1640 watts. There were variations in these rates due to variations in power settings. Initial stratification was produced either by heating a top layer of the fluid with the top heater or by injecting hot dye near the liquid surface.

Two bottom bulkheads were used in these tests; a convex and a concave bulkhead. The tests performed on the concave bulkhead were extensions of the earlier open tank tests. The convex bulkhead tests were an entirely new test series.

Two water levels were used in the tests with the concave bottom bulkhead; 17.7 and 8.7 inches above the nozzle.

Three water levels were used with the convex bottom bulkhead; 23.8, 14.8 and 6.7 inches above the nozzle. The differences between the concave and convex water levels was due to the lower nozzle position in the convex tests. The actual water levels above the flange joining the bottom bulkhead and the cylindrical section were the same as shown in the following sketch.

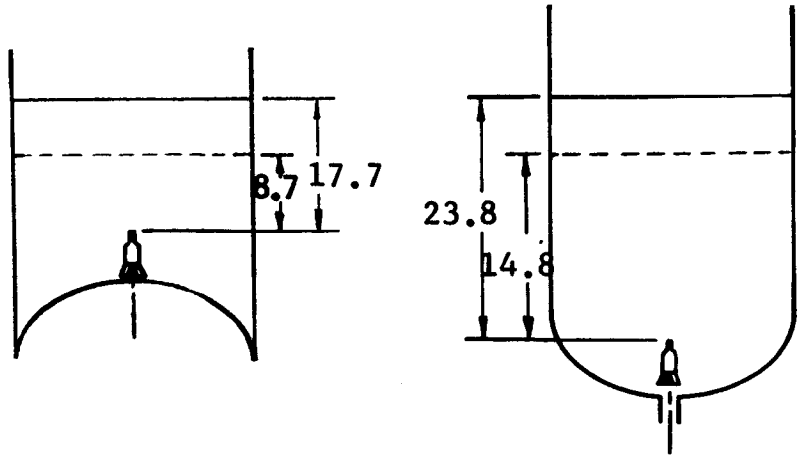

Concave Tank Bottom

Convex Tank Bottom

Flow rates were set prior to each test run. The flow rates were based on experience gained in earlier tests and were chosen to mix the tank to a desired condition. On occasion, the preset flow rates were not sufficient to reduce stratification to required levels, and the flow

was increased during the tests. In some tests, the effect of bottom heating free convection on the stratified layer was observed. In general, mixing was accomplished in the following steps:

1. Flow from the jet (in some cases bottom heating free convection) was started with the desired heating rates turned on.

2. The temperature distribution was observed during the test until the residual temperature stratification appeared to reach a quasi-steady state.

3. If the observed residual temperature stratification was equal to or less than the desired level, the test was terminated. If the residual stratification was larger than desired, the flow was increased and the procedure repeated.

The mixing of the stratified layer by the jet or by free convection was observed by dying the stratified layer. In the case of free convection due to bottom heating, cold dye was occasionally placed on the tank bottom. The jet flow was observed by injecting dye into the nozzle prior to testing. Penetration of the stratified layer by the jet was also observed by placing dye immediately under the stratified layer.

Dye movements in the tank were recorded on 16 mm color film. Filming was begun at the time the jet was

turned on (or in the case of free convection, when the bottom heater was turned on). The filming continued until the entire tank was filled with dye. These films were then viewed to obtain measurements of dye movement as a function of time.

Figure 4-12 summarizes the desired open tank operating conditions. Figure 4-13 shows a flow diagram of the general test procedure for open tank tests. The actual operating conditions are shown in Table 2.0-1 of Volume II.

4.4.2 Closed Tank Test Procedures

The closed tank water tests were intended to amplify the open tank water tests and to provide data on mixing in a pressurized tank with a condensable ullage. The test procedure was somewhat different since no movies were made and the development of the stratified layer was accomplished in a slightly different manner. Also, ullage pressure data was taken during these tests. As in the open tank tests no stratification or draining tests were conducted except as incidental parts of the mixing test procedure.

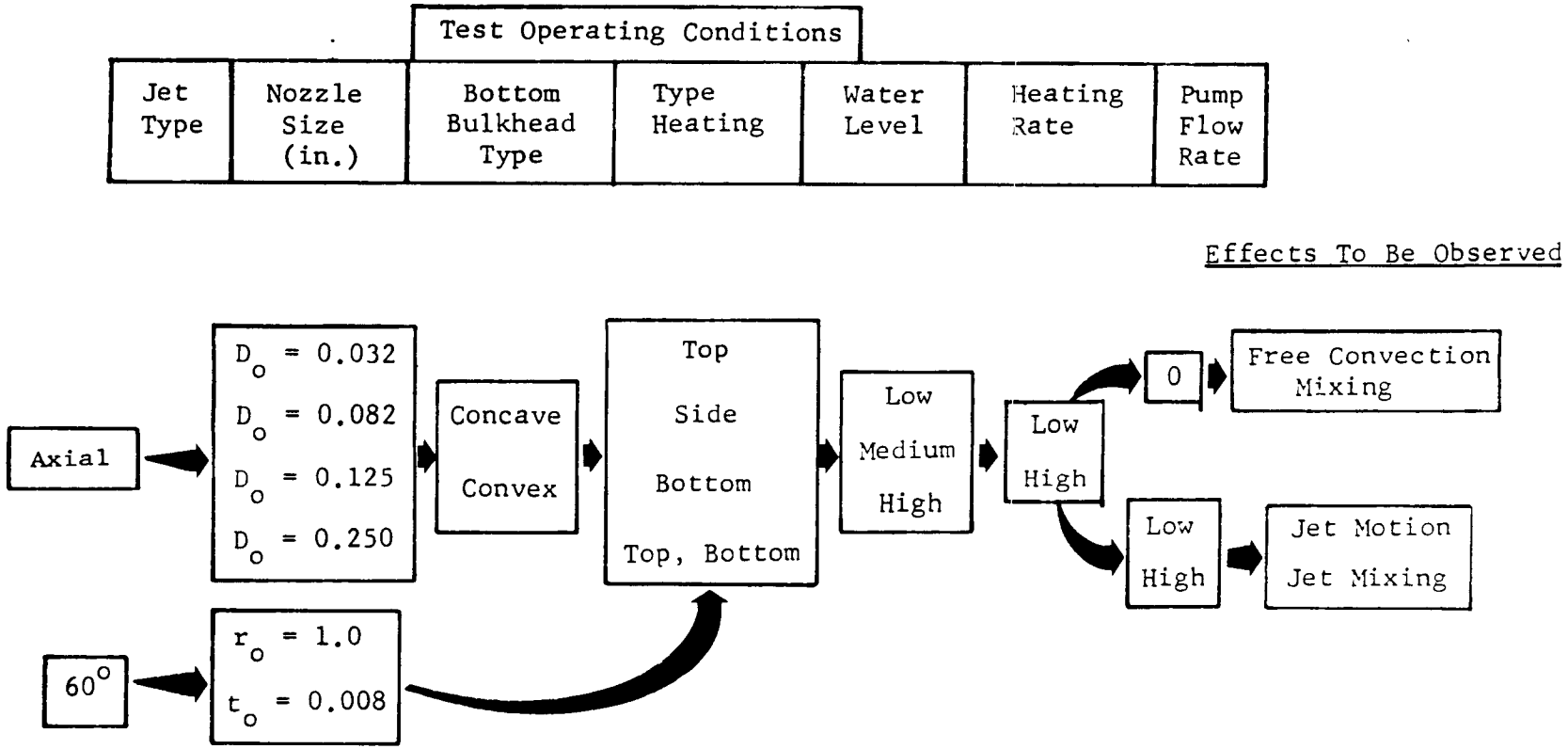

Figure 4-12 Open Tank Experimental Test Operating Conditions

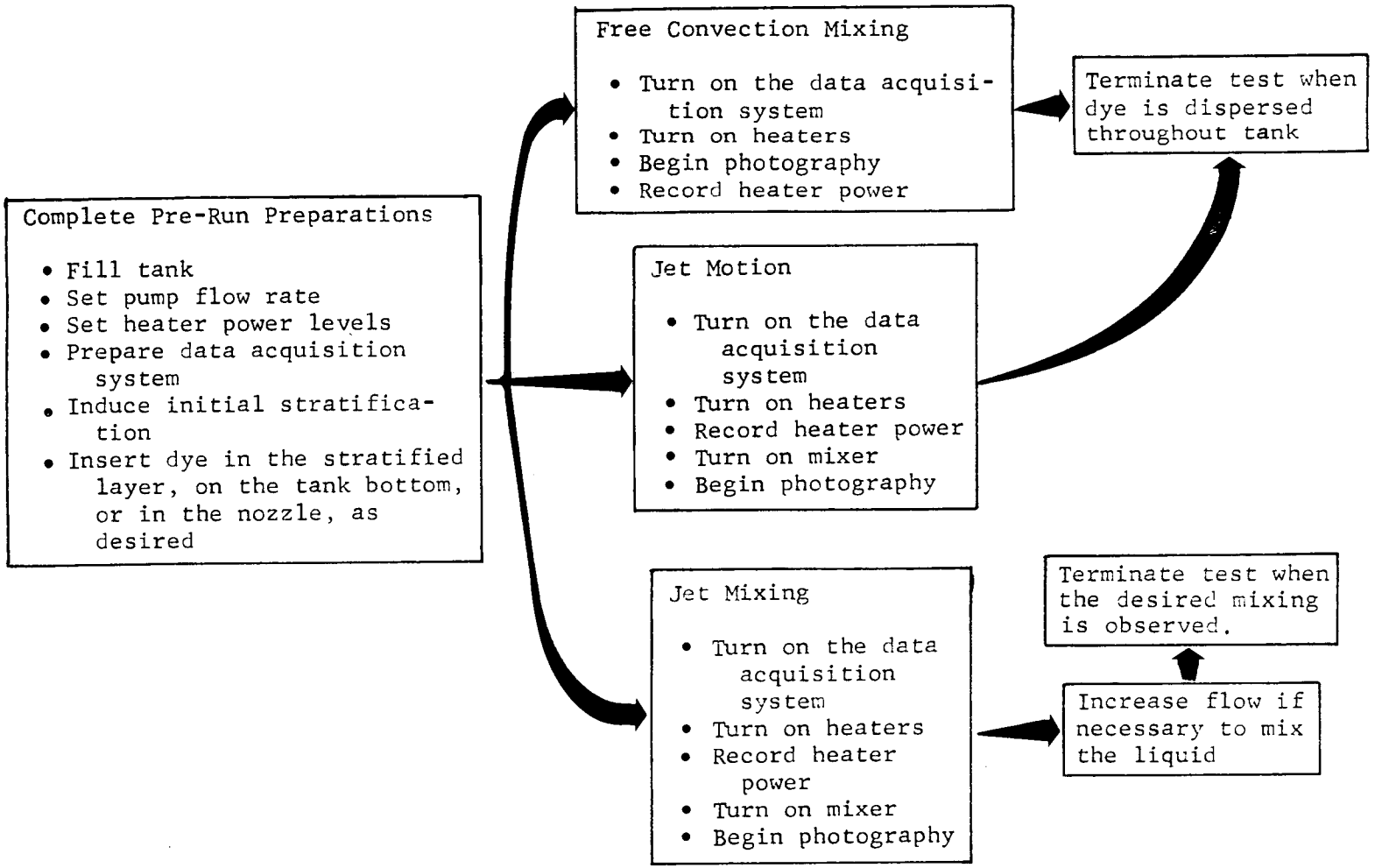

Figure 4-13 Test Procedure for Open Tank Tests

The data taken during the tests consisted of temperature and ullage pressure histories during mixing. The test variables included heating rates, flow rates, and liquid level above the nozzle. Only the convex bottom bulkhead and 0.032 inch nozzles were used in these tests.

The test tank was heated using various combinations of top, bottom, and sidewall heating. The primary heating combinations were either top or bottom heating. The top heating rate had a nominal value of 1280 watts. The nominal bottom heating rate was 1500 watts.

Three liquid levels were considered during the tests. These levels were 12.36, 14.7, and 15.2 inches above the nozzle. The values are the initial water levels and do not reflect changes due to evaporation, condensation, or density changes of the water.

The initial flow rates were based on previous results from the open tank tests. These were changed where necessary to reflect the thinner stratification layer and lower stratification levels in the closed tank tests. The stratified layer was relatively thin since a ullage heater rather than an immersion top heater was used to induce initial stratification.

The initial pressure in the tank prior to inducing stratification was either atmospheric or the saturation pressure of the water in the tank. Tests in which the initial pressure was atmospheric were run mainly to check out the test system, compare closed system data with open tank data, and to determine operating procedures. The tests of primary interest were run with the closed tank pressure initially pumped down to the saturation pressure of the water. This was done in order to substantially reduce the amount of non-condensable gases (air) in the tank and to better simulate actual conditions in a liquid hydrogen tank. After the initial tank evacuation the ullage heaters were usually used to increase the tank pressure prior to stratification reduction.

The basic test steps were as follows:

1. Fill the test tank to desired water level and evacuate tank to saturation pressure.
2. Induce temperature stratification using top heater in the ullage.
3. Turn on jet and attempt to reduce stratification.
4. If temperature stratification or ullage pressure are not reduced, increase the flow rate and continue mixing

Figure 4-14 summarizes the desired closed tank operating procedures. Figure 4-15 shows a flow diagram of the general test procedure for the closed tank tests. The actual operating conditions are shown in Table 3.0-1 of Volume II.

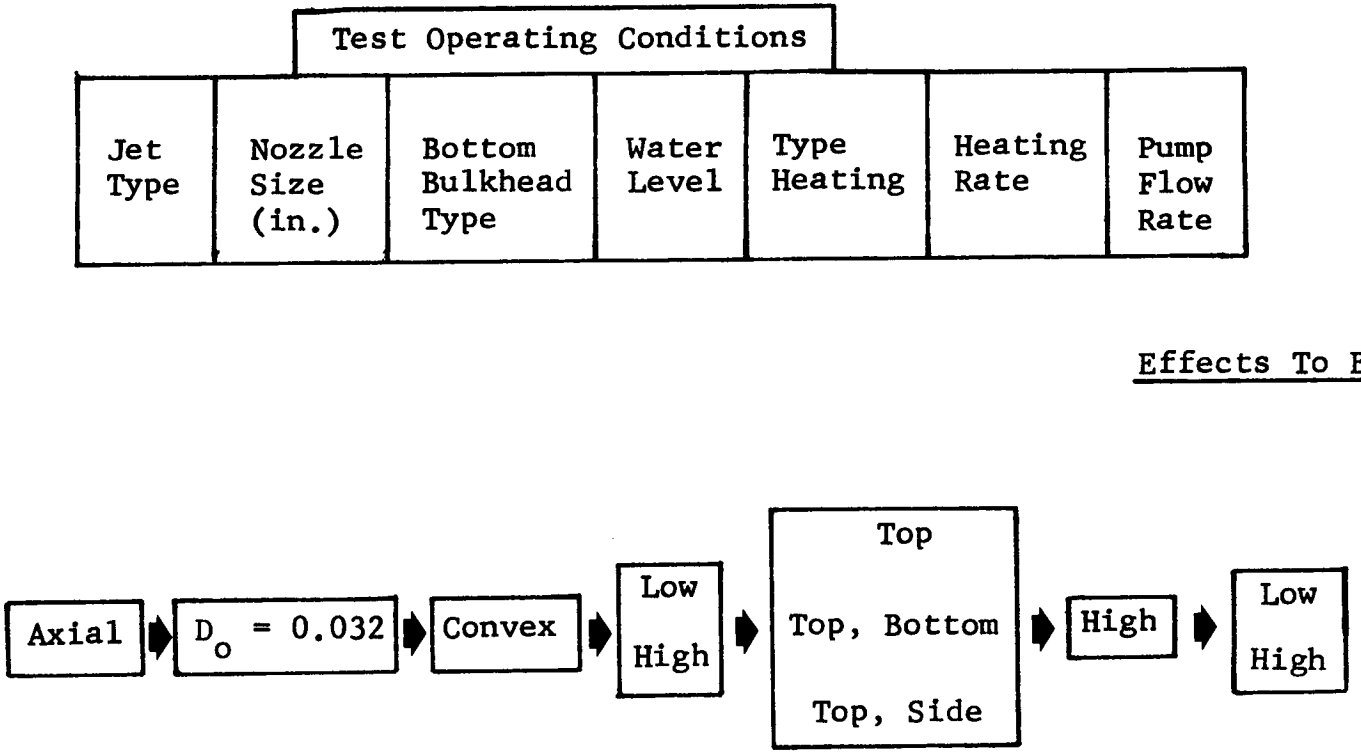

Figure 4-14 Closed Tank Experimental Operating Conditions

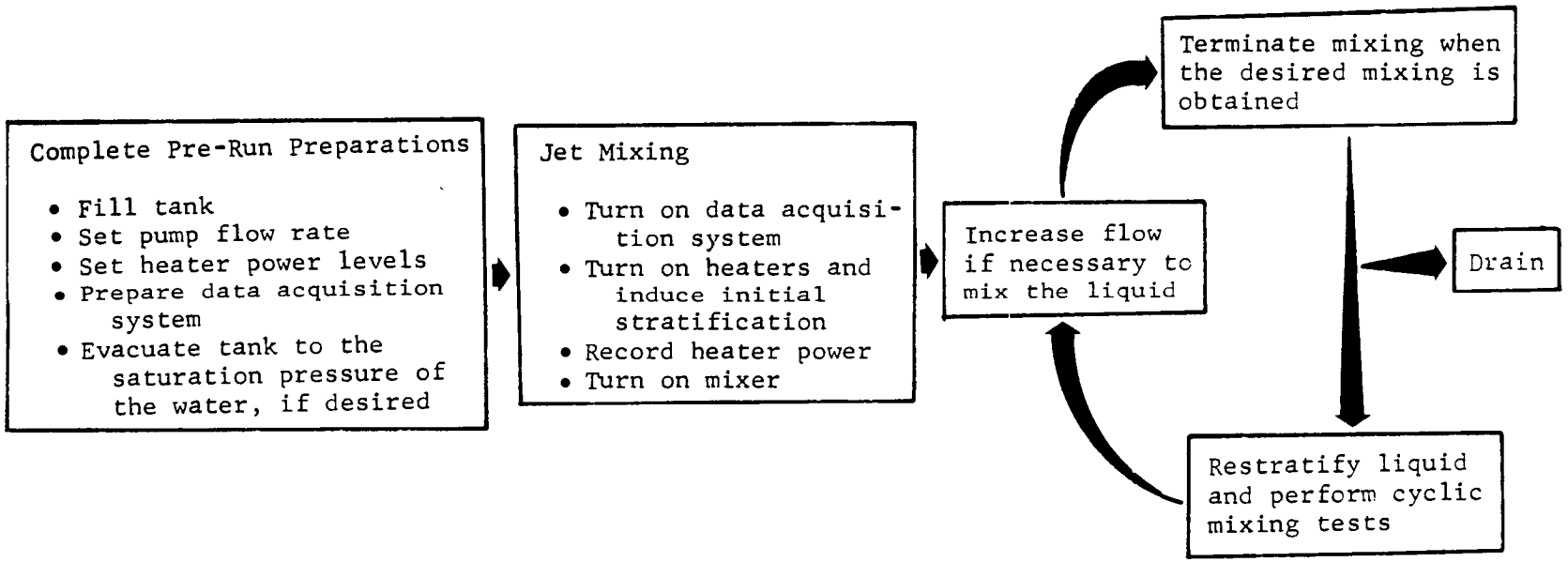

Figure 4-15 Test Procedure For Closed Tank Tests

4.5 EXPERIMENTAL DATA

The experimental data obtained in the open and closed tank tests during this study consists of temperature, pressure, and dye position data as a function of time. The data obtained is concerned mainly with mixing conditions. Results of 58 open tank tests and 20 closed tank tests are reported. Due to the large amount of data obtained and utilized, the data is shown separately in Volume II of this report. The following sections contain a discussion of the data and show only representative cases of the actual data. The experimental data correlations made from the test data are discussed in Section 5. The miniature test data obtained consisted of 8 mm movies of the ullage breakup and the liquid/vapor flow characteristics during mixing. The results of these tests, the test procedure, and test apparatus are discussed in Subsection 4.5.3.

4.5.1 Open Tank Test Data

The open tank test data are divided into four categories: (1) axial jet motion, (2) bulk fluid motion, (3) free convection, (4) free convection and mixing data for drain conditions. The open tank data are shown in Section 2 of Volume II. The various types of data are discussed in the following subsections.

The test data reflects a variety of test conditions. The effect of tank geometry are reflected by use of different water levels and tank bottoms. The open tank tests were conducted in an open lucite cylindrical-tank with convex and concave tank bottoms (the terms concave and convex with respect to the tank bottoms are defined in the following sketch.)

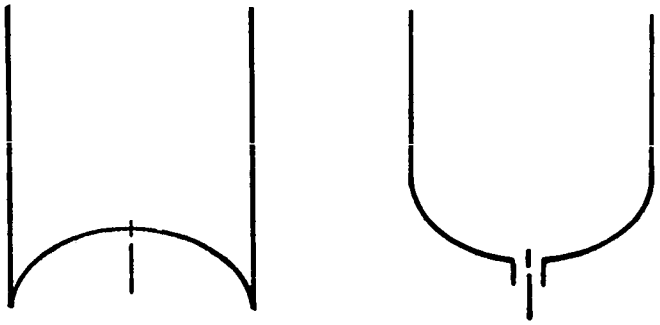

Concave Tank Bottom

Convex Tank Bottom

The water levels in these tests were 6.7, 8.7, 14.8, 17.7 and 23.8 inches above the mixer nozzle exit.

The various combinations of top, bottom and sidewall heating were used to resolve the effects of the different types of heating on mixing. In addition, a "no heating" condition was employed to simulate the low bouyancy condition which would be encountered in a low-g environment. The term "no heating" refers to a case in which there was no heat input to the fluid during mixing. Instead, the top layer was heated prior to mixing in order to induce a temperature difference between the surface of the liquid and the bulk liquid.

Nozzle diameters of 0.032, 0.083, 0.125, and 0.25 inches were used with various flow rates in order to determine the effect of various jet Reynolds numbers on mixing. The flow rates varied from 0.02 to 1.0 gpm depending on the nozzle used.

4.5.1.1 Jet Motion Data

The axial jet motion data was obtained visually from film data of the axial jet moving up to the liquid/vapor interface as shown in the following sketch

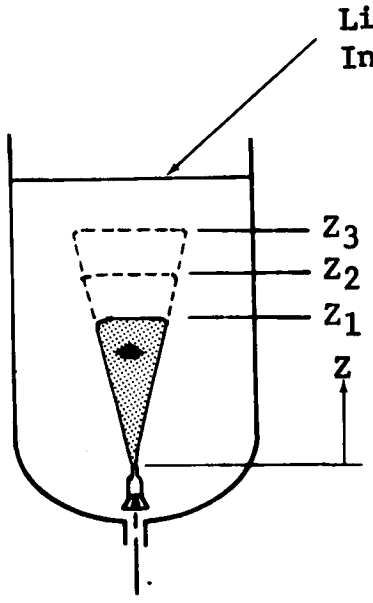

θ_j (Sec)	Z (in.)
0	0
θ_1	Z_1
θ_2	Z_2
θ_3	Z_3

A typical example of jet motion data is shown in Figure 4-16 in comparison with an analytical prediction based on jet centerline velocity. Two general characteristics were observed in the jet motion tests. The first observation was that the axial jet moved upward in a general conical shape as predicted by theory. The second observation was that the jet appeared to penetrate the stratified layer immediately except in cases with a large temperature difference and a thick stratified layer.

4.5.1.2 Bulk Fluid Motion Data

Bulk fluid motion data was obtained visually from film data and from temperature data obtained from a digital recording system. The visual bulk fluid motion data was obtained in much the same manner as the jet motion data. A sketch showing the hot dye layer moving down as a function of time is shown below.

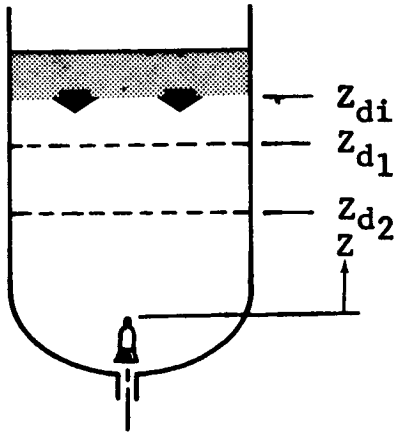

θ_1 (sec)	Dye Location (in.)
0	Z_{d_i}
θ_1	Z_{d_1}
θ_2	Z_{d_2}

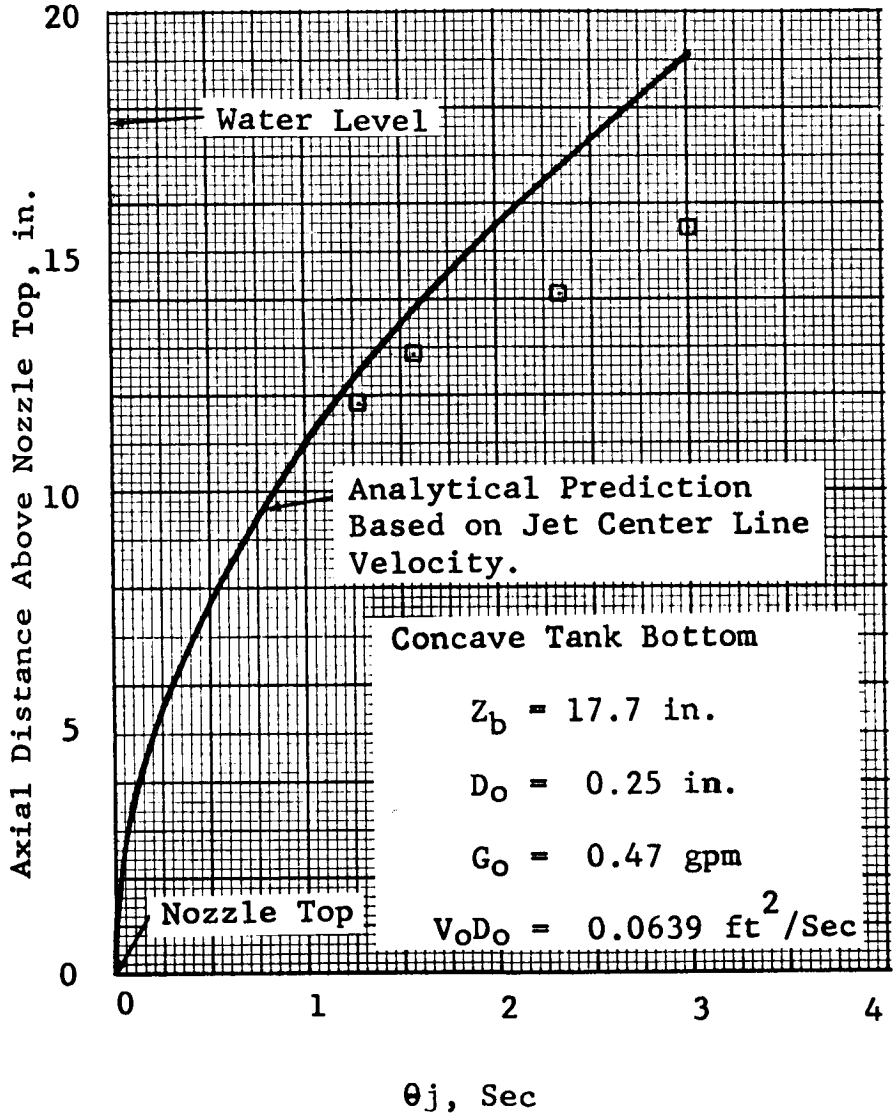

Figure 4-16 Axial Jet Motion After Pump Turned On: Test 135, Run 39

Figure 4-17 is a typical example of the visual bulk fluid motion data. The dye moves down the tank with an exponential decrease in speed.

The temperature distributions in the tank are shown parametrically with time. The surface temperature, the temperature at the nozzle, and the mean tank temperature are shown as functions of time. The sketch below shows the physical locations of the various temperature measurements.

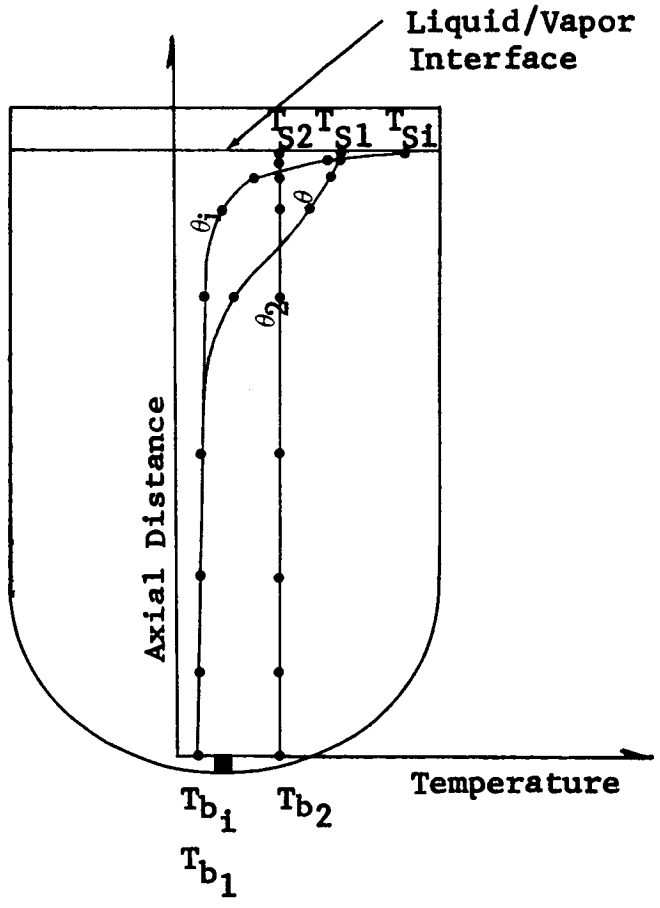

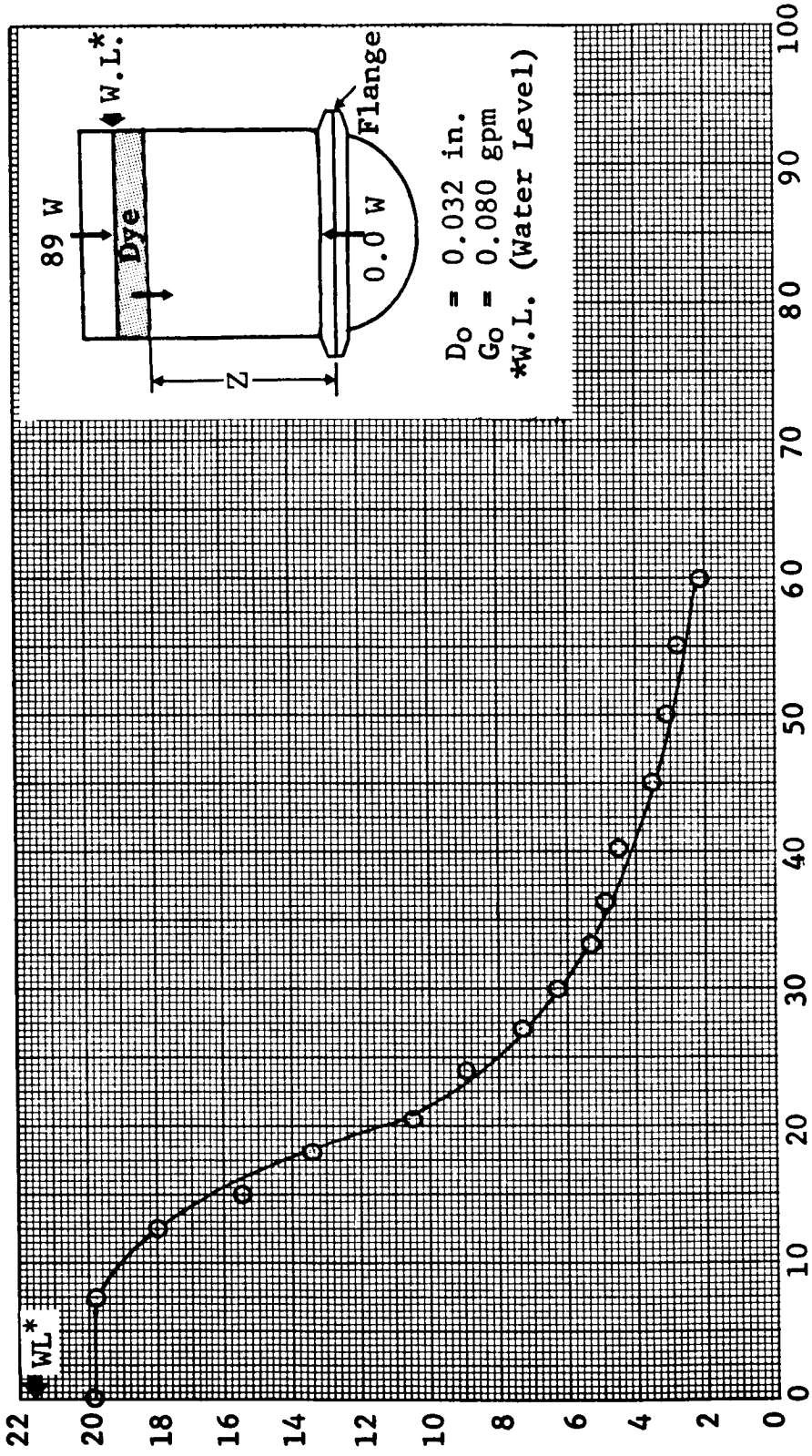

Figure 4-17 Axial Jet Dye Layer Motion: Test 5, Run 50

A typical example of temperature distributions plotted parametrically in time is shown in Figure 4-18. Figure 4-19 shows the average temperature at the nozzle exit and the average surface temperature (shown in the sketch above) as a function of time after the pump was turned on. Radial temperature variations were small except near the stratified layer at the time the layer began to mix. When there were several temperature data points at an axial level, an average value was used.

The following sketch shows a temperature distribution at a given time and the corresponding tank volume for which each thermocouple or group of thermocouples is assumed to indicate a temperature.

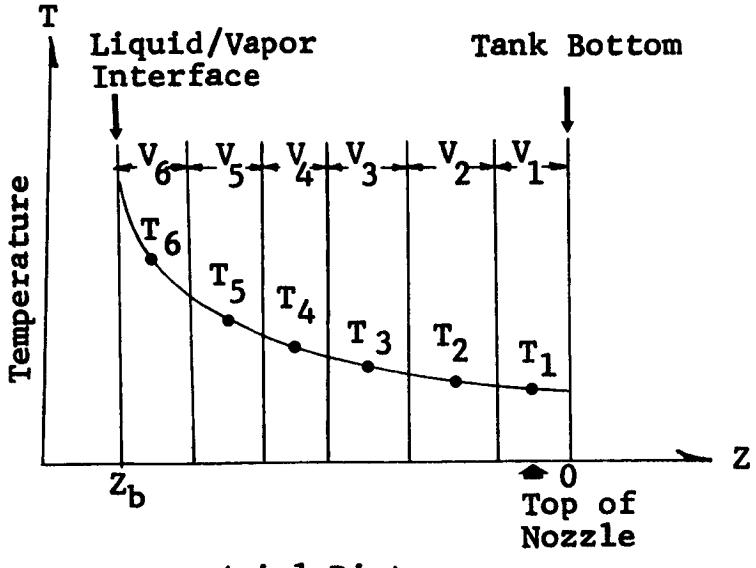

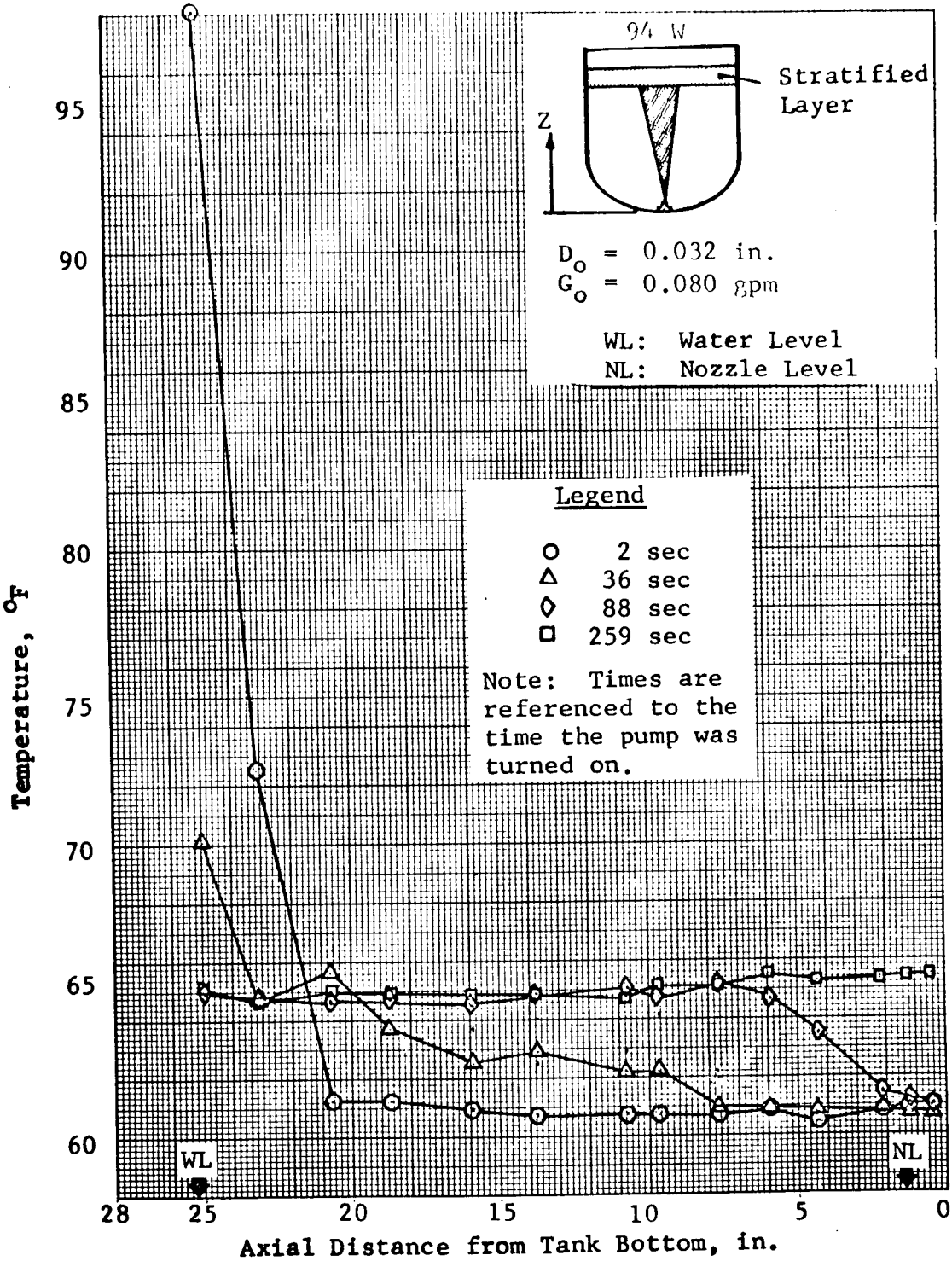

Figure 4-18 Temperature Distribution for Axial Jet Flow: Test 5, Run 50

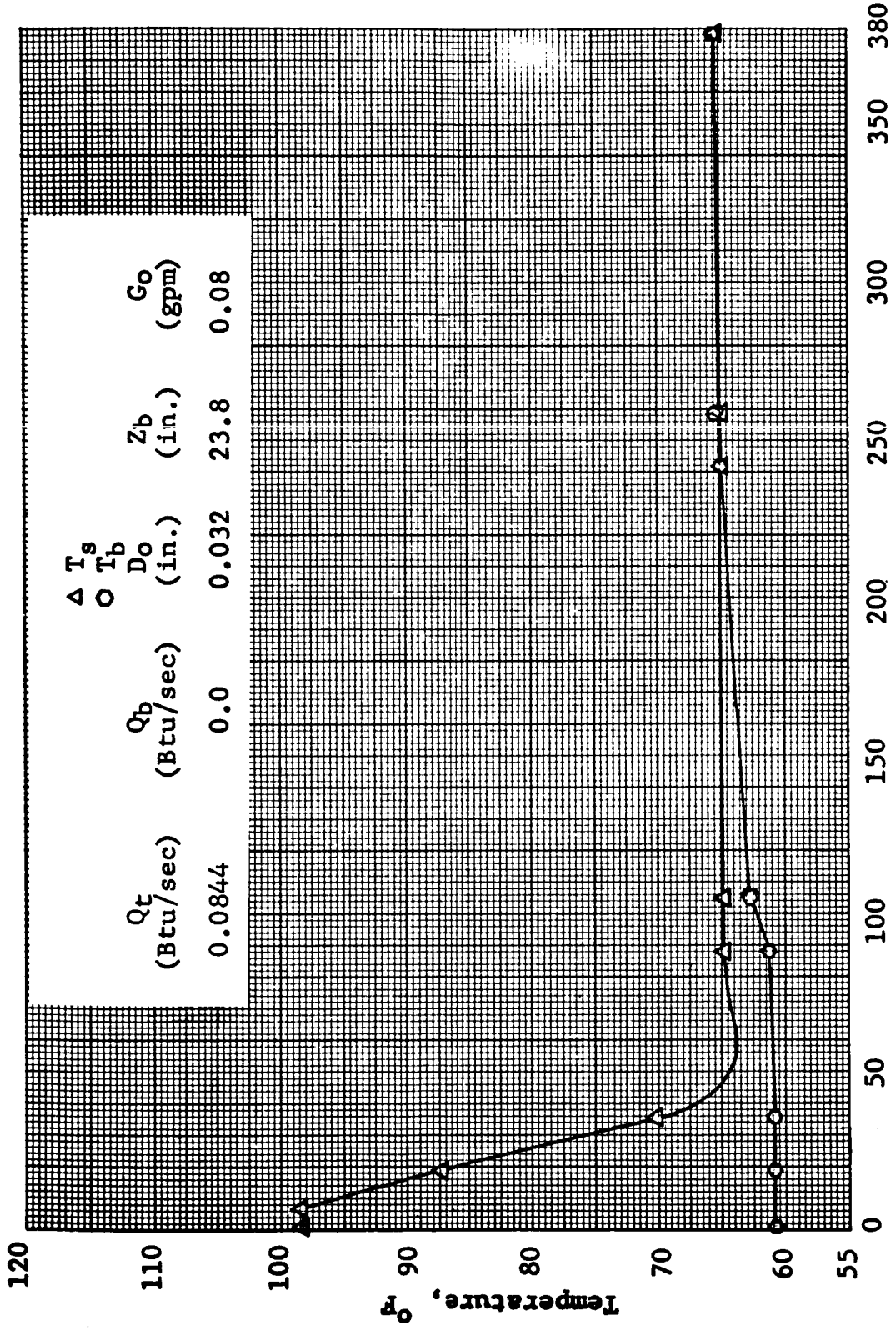

Figure 4-19 Transient Temperature Destratification: Test 5, Run 50

From a temperature distribution such as this, a mean tank temperature can be calculated from the equation

$$T_m = \frac{\sum V_i \, T_i}{V_t}$$

where

V_i = fluid volume

T_i = temperature of fluid volume

V_t = total tank volume

The mean tank temperature minus the initial mean tank temperature when the pump was turned on, $T_m - T_{mi}$, along with the surface temperature minus the mean temperature, $T_s - T_m$, is shown in Figure 4-20. When the slope of the mean temperature rise with time (in Figure 4-20) reaches a constant value, it was used to calculate the total heat input to the fluid from the equation

$$Q_m = M_\ell \, c_p \, \frac{\Delta T}{\Delta \theta}$$

where

M_ℓ = the mass of the liquid

c_p = the specific heat of the fluid at a constant pressure

The total heat input is also shown in Figure 4-20. This value differed from the heater energy input due to heating by the lights for the photography.

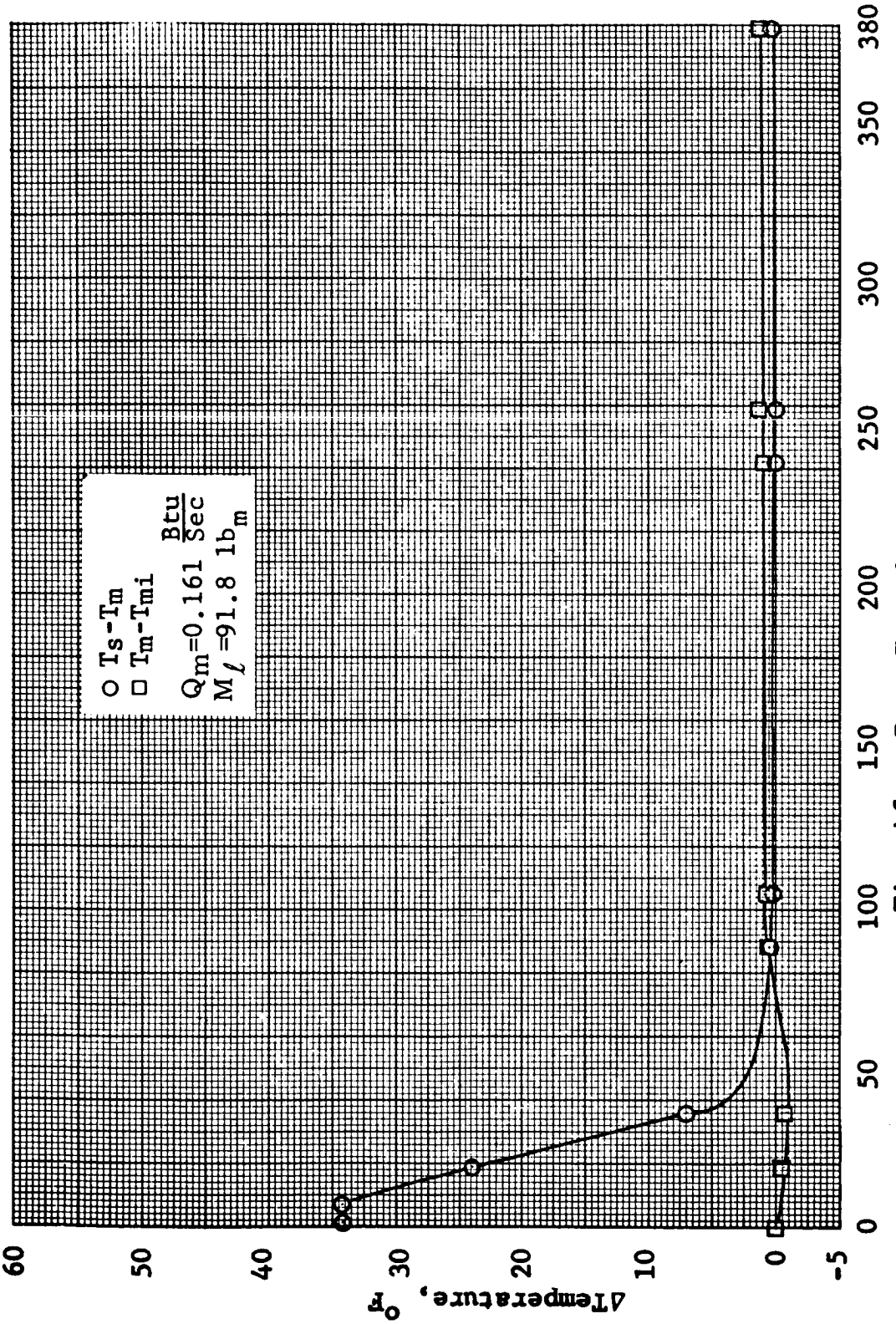

Figure 4-20 Transient ΔTemperature Destratification: Test 5, Run 50

4.5.1.3 Free Convection Data

Free convection data were obtained for bottom heating conditions. This free convection data consisted of dye motion data and temperature distributions. Figure 4-21 shows a plot of the dye position with time. In these tests, cool dye was placed in the bottom of the tank and the bottom heater turned on. The heating caused the dyed water to form free convection currents. The temperature distributions for a bottom heating free convection case is shown in Figure 4-22. The bottom heating free convection reduces the stratified layer and promotes mixing. It was noted that the initial free convection dye streamers tended to follow the curvature of the bottom bulkhead, i.e. for the convex bottom the dye began to rise near the sides of the tank and for the concave bottom, the dye began to rise near the middle of the tank. In both cases, however, the dye was soon leaving from all zones of the bottom.

4.5.1.4 Free Convection and Mixing Data for Drain Conditions

Free convection dye data during draining are shown in Figure 4-23. The dye rose due to free convection until the drain was initiated and then moved down. Figure 4-24 is a plot of the drain line temperatures with and without mixing.

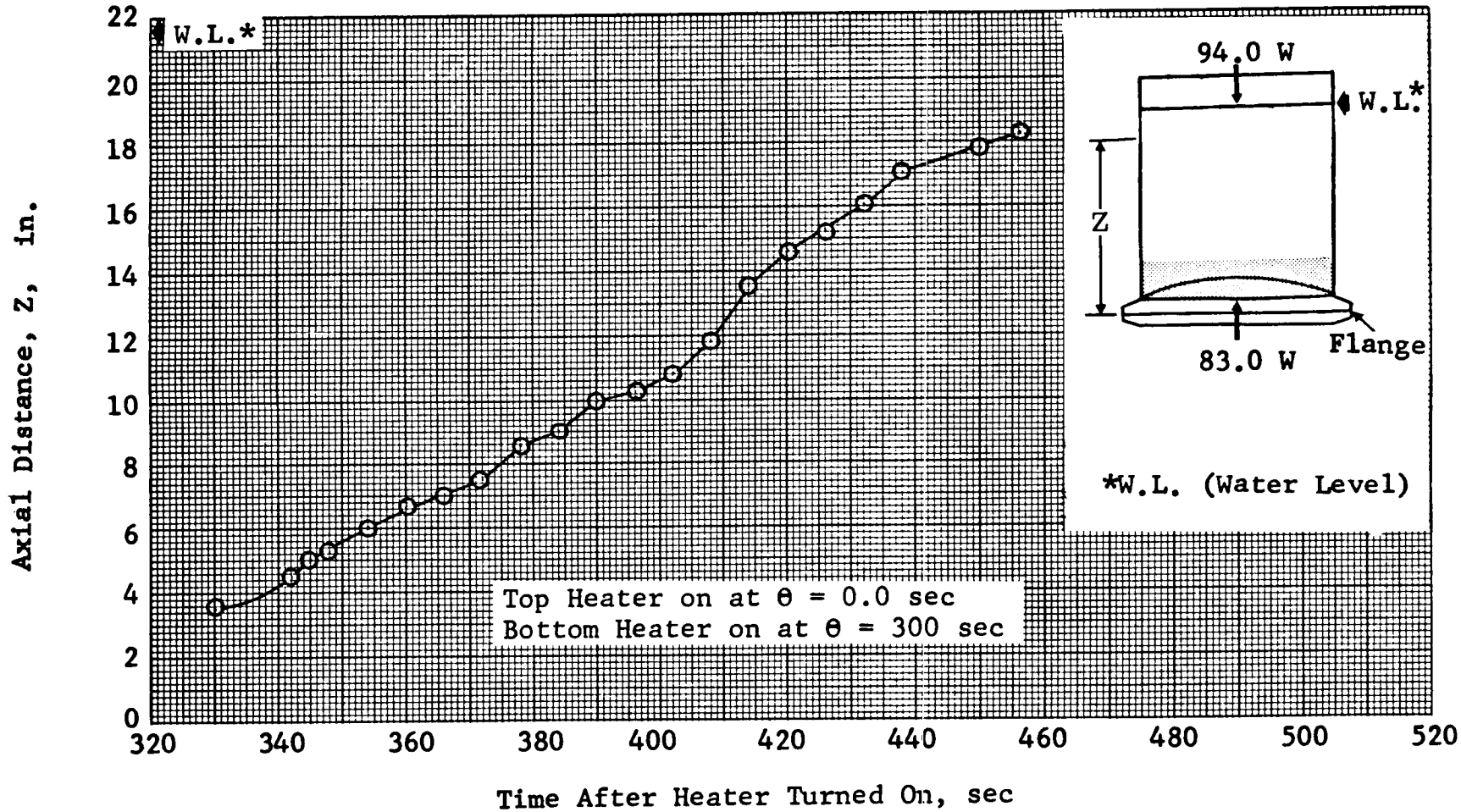

Figure 4-21 Axial Jet Dye Layer Motion: Test 163, Run 30

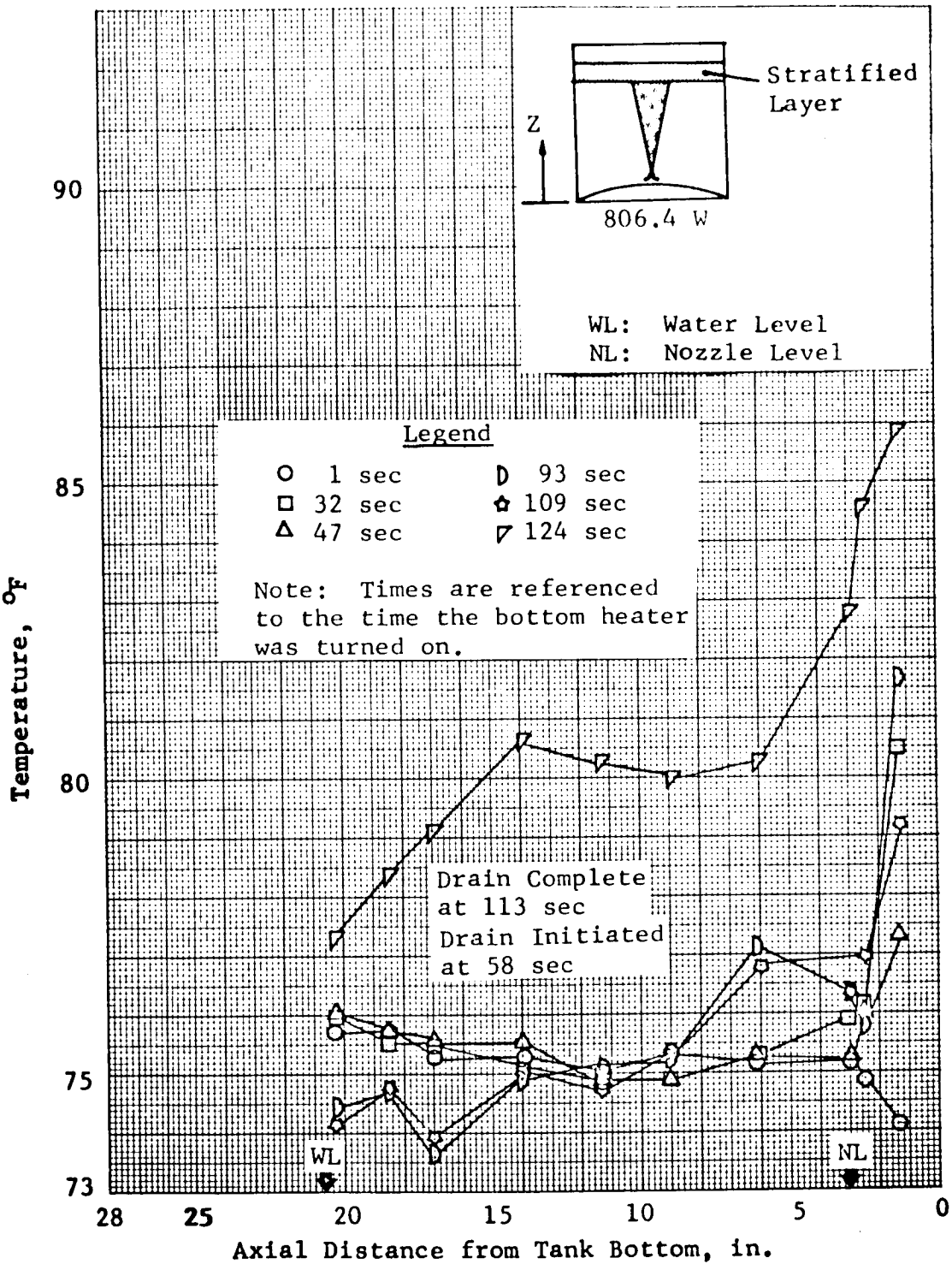

Figure 4-22 Temperature Distribution for Axial Jet Flow: Test 166, Run 33

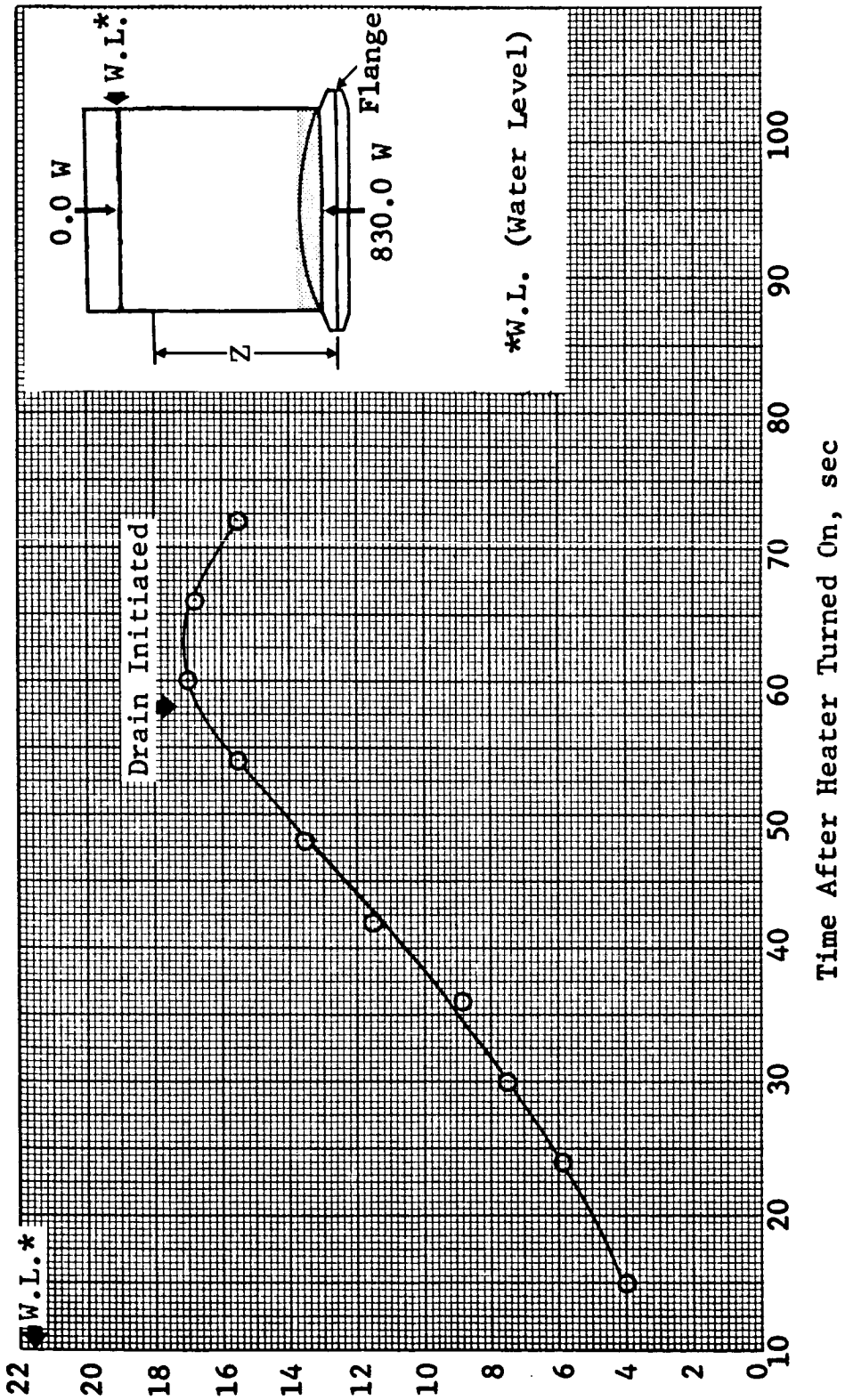

Figure 4-23 Axial Jet Dye Layer Motion: Test 166, Run 33

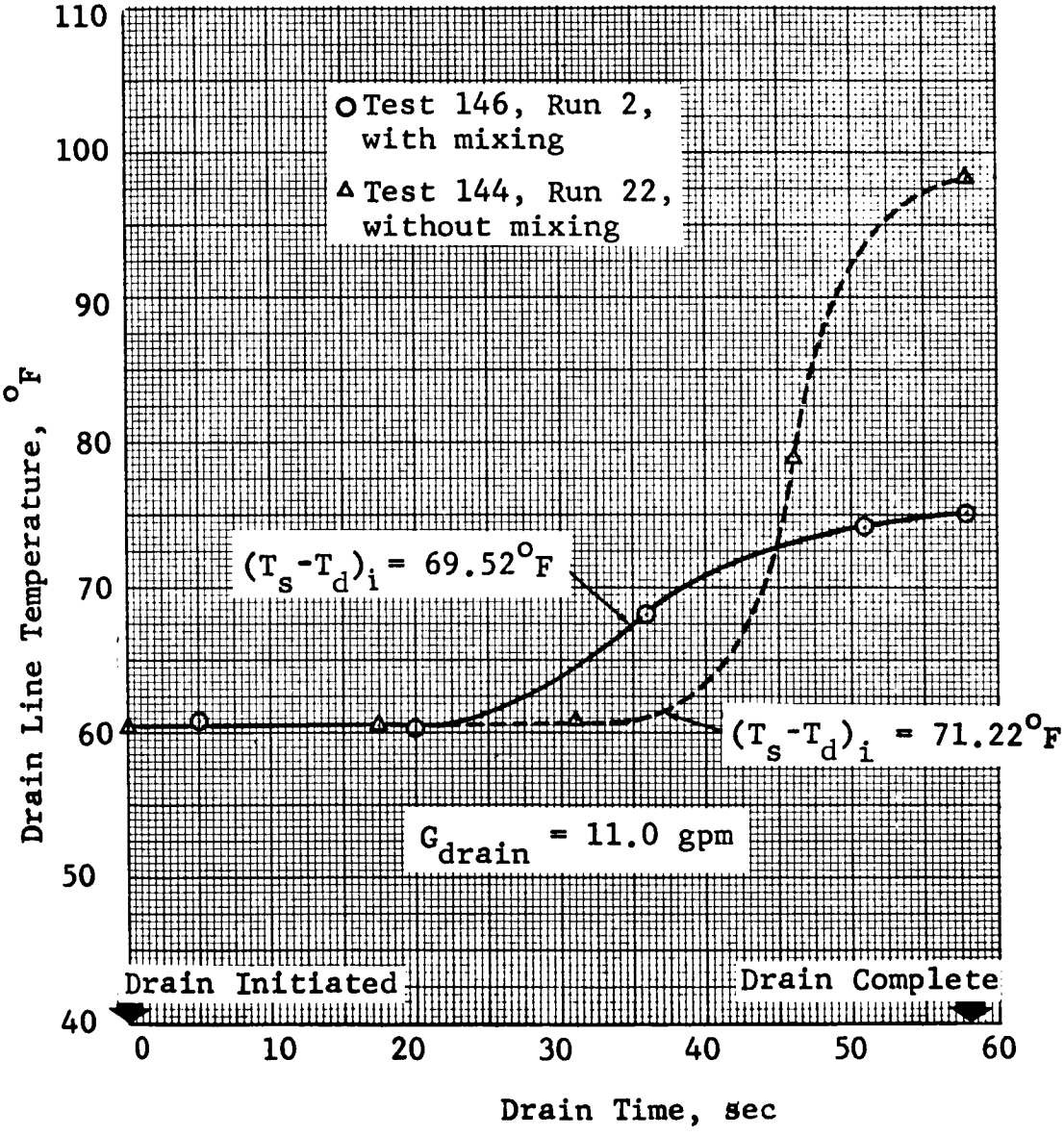

Figure 4-24 Drain Line Temperature With and Without Mixing

The sudden rise of the drain line temperatures for the non-mixing case confirms the visual evidence that the stratified layer remains essentially intact in a draining tank without a mixer operating.

4.5.2 Closed Tank Experimental Data

The closed tank experimental data consists of pressure and temperature measurements during twenty mixing tests. This data is shown in Section 3.0 of Volume II. The data considers only convex bulkhead and the 0.032 inch diameter nozzle. Water levels were set at 12.36, 14.7, and 15.2 inches above the nozzle. Heating conditions were either top or top and bottom heating. Flow rates were 0.08, 0.09, 0.1, 0.15, 0.22 and 0.234 gpm. Tank pressures at the time the mixer was turned on ranged from 1.9 to 42 psia.

Temperature data shown in Volume II consists of a surface temperature measured by a thermocouple located on the nominal liquid/vapor interface and a temperature at the nozzle exit as a function of time during mixing. Figure 4-25 shows a typical example. The surface temperature measurements are not always exactly the temperature of the liquid/vapor interface due to variations in liquid level. The liquid level in the tank varied slightly from the nominal values of 12.36, 14.7, and 15.2 inches above the nozzle due to four possible reasons as follows: minor inaccuracy in filling the tank prior to testing, evaporation to the ullage during heating prior to mixing, condensation from the ullage during mixing,

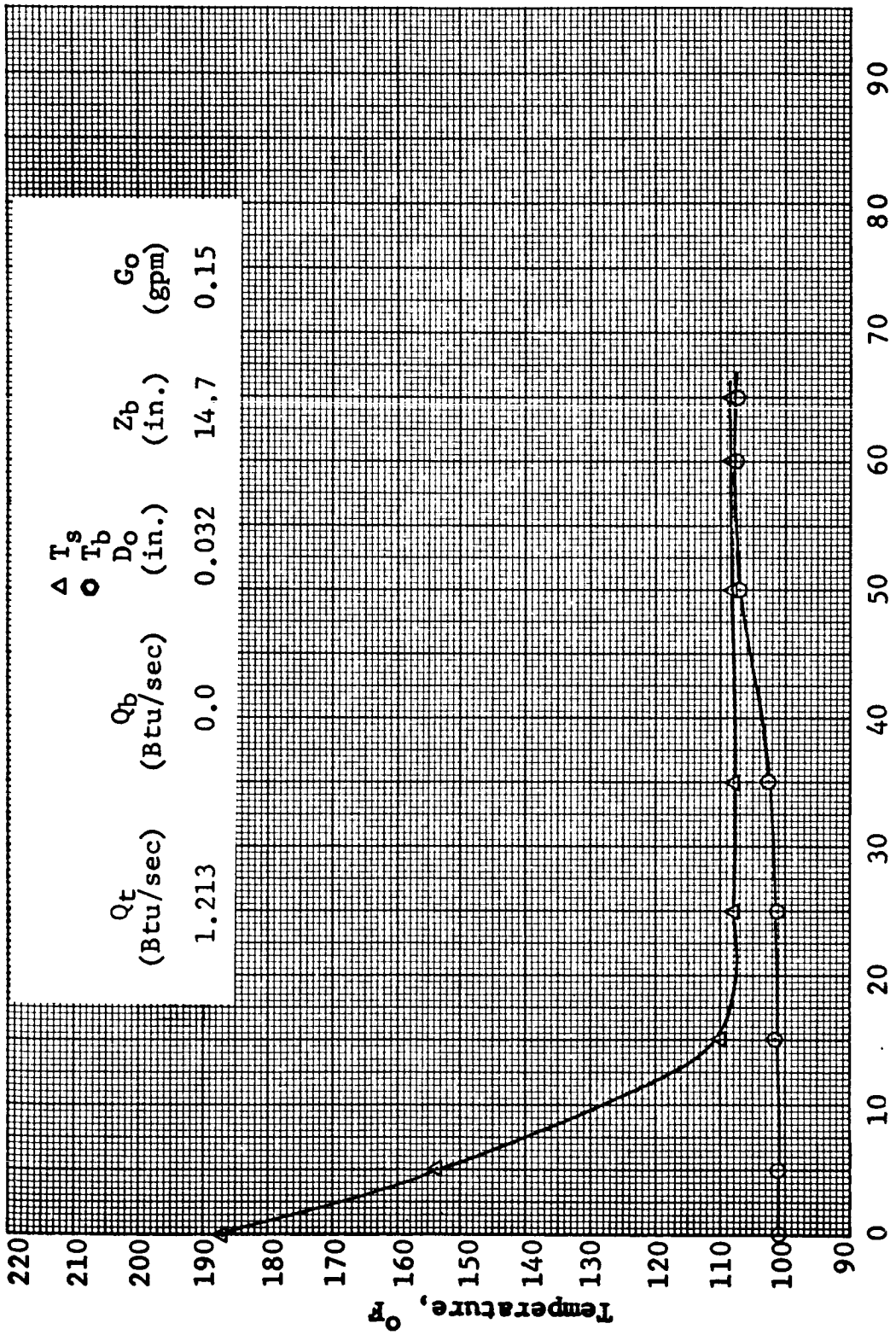

Figure 4-25 Transient Temperature Destratification: Test 13, Run 15

and density changes in the water due to heating. These variations were all apparently small, but could not be measured during a test. The temperatures measured by the thermocouples on the liquid/vapor interface were, in all cases, less than the saturation temperature of the water at the ullage pressure. Also after mixing, these temperatures were always slightly less than or equal to the mean bulk fluid temperatures. In addition, the temperatures recorded from these thermocouples were always less than temperatures obtained from thermocouples which were definitely in the ullage. All of this indicates that the temperatures from these thermocouples provide a reasonable indication of the surface temperature. The transient change of the surface temperature was extremely fast. This was apparently due to "thin" stratified layer in comparison with the open tank stratified layer. This was indicated by the large temperature difference between the surface temperature and temperatures indicated from the next layer of thermocouples. The thinner stratified layer was due to the heating of the top fluid layer by an ullage heater rather than a heater immersed in the liquid. The rapid change in the surface temperature coupled with the time required to make a complete scan of the 25 data channels of the Dymec recorder and the 12 points on the strip chart

resulted in significant temperature changes between successive surface temperature data points at the beginning of mixing. In order to obtain temperatures between these points, a linear interpolation was made. This linear interpolation in many cases does not predict temperature changes as rapidly as they occur and ignors any constant temperature condition between two data points. The following sketch illustrates this condition.

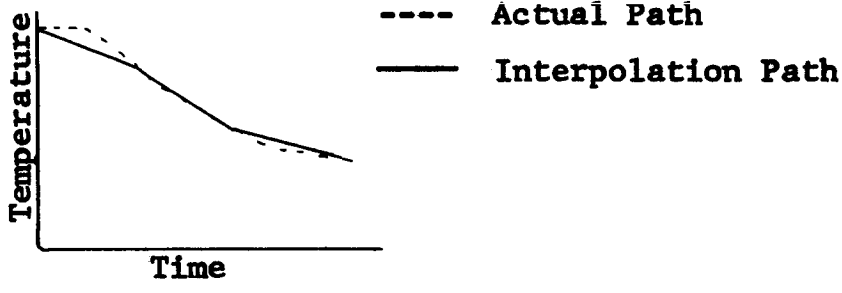

The condition often seen in the open tank tests of a constant or rising surface temperature immediately after the mixer began operation was not seen in any of the closed tank tests. This was apparently due to the data acquition systems scan time being too long to record the rapid penetration of the thin stratified layer by the jet.

Temperature differences between the surface temperature and the mean temperature of the fluid are shown as in Figure 4-26. These figures also show the temperature difference between the mean initial temperature and the mean temperature at various time after the mixer began operation. These

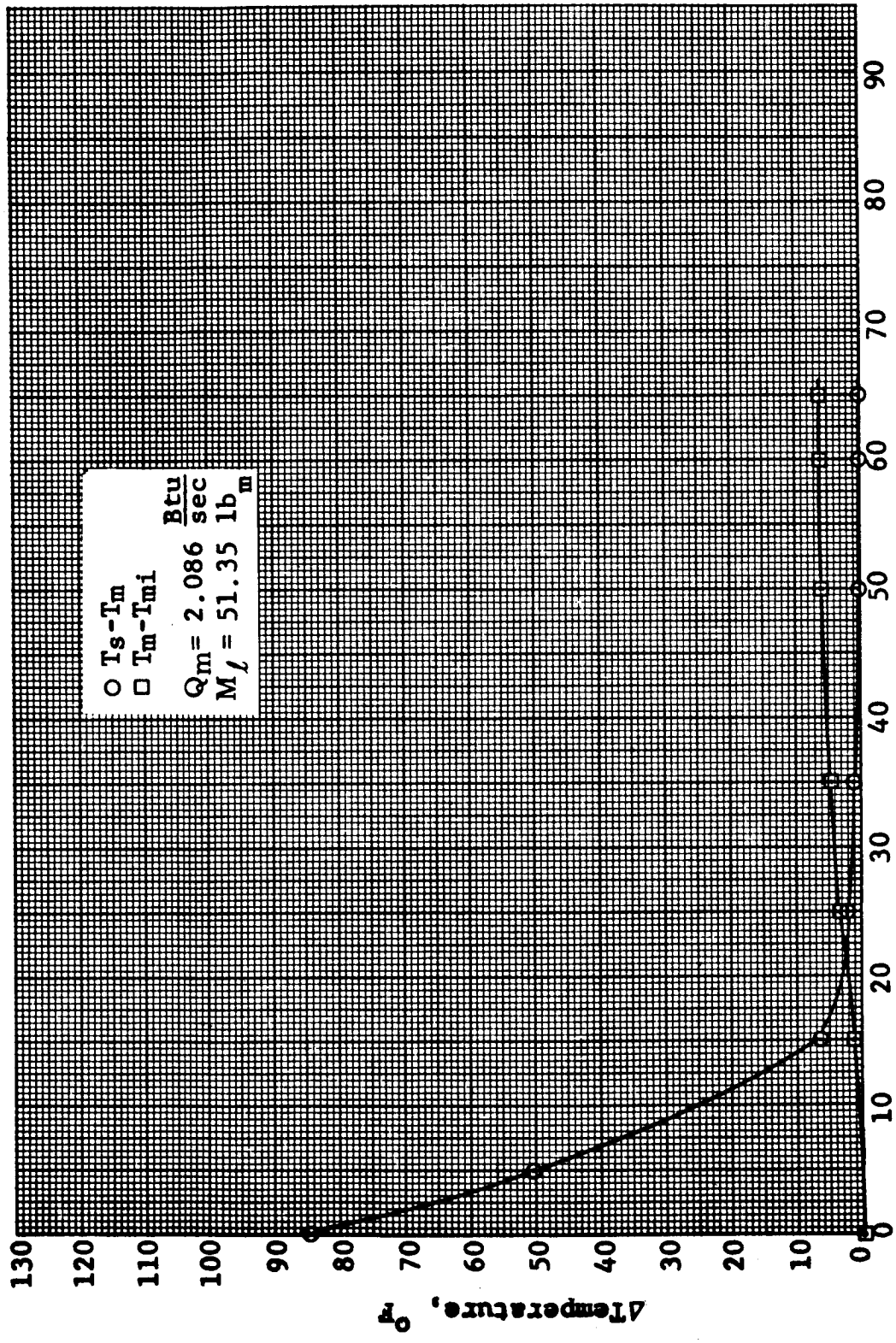

Figure 4-26 Transient ΔTemperature Destratification: Test 13, Run 15

figures also show the mass of liquid in the tank and the total heat absorbed during a mixing cycle. The total heat absorbed, calculated from

$$Q_{Absorbed} = M_{\ell} \; C_p \; (T_{mean_{initial}} - T_{mean_{final}})$$

was always greater than the actual heating of the tank during mixing operation. An energy balance was made for each test for the entire period of heating as a check of computation accuracy. This energy balance showed, as would be expected, that the total heat absorbed by the fluid was always less than the total heat input to the tank. The energy absorbed during mixing would then include energy obtained from cooling the tank mass.

The final temperature difference between the surface temperature was usually too small to be accurately measured. There was only one case in which good mixing was not obtained rapidly. This case, Test 13, Run 14, was a top heating case with a low flow rate. During mixing, the temperature difference between the mean temperature and the initial mean temperature, in general, remained fairly constant and then increased quickly as the tank pressure decayed. This indicated the condensation of vapor from the ullage as well as mixing of the stratified layer.

Pressure data shown in Volume II consists of the ullage pressure as a function of time during mixer operation. Figures 4-27 and 4-28 show representative types of data taken. Figure 4-27 shows one of seven cases in which there was a constant ullage pressure after the mixer began operation, followed by a sharp pressure drop, a partial pressure recovery, and then a gradual reduction in pressure toward a minimum value. Figure 4-28 shows one of five cases which had a constant pressure for a period after the jet was turned on and then a gradual pressure decay to a minimum value. Also, three cases exist with a pressure rise after mixing began, followed by the sharp pressure drop, recovery, and gradual pressure decay. Four cases exist with a pressure rise followed by a gradual pressure decay. One case exists in which the pressure began a sharp drop at the same time mixing was initiated. The sharp pressure drop occurred in six of the ten top and bottom heating cases and five of the the top heating cases. All sharp pressure drops occured during test with higher flow rates (0.15 and 0.22 gpm) and higher water levels (14.7 and 15.2 inches), however other tests under these conditions showed a gradual pressure decay. Since the sharp pressure drop is a transient effect, it is probably due to the jet suddenly partially penetrating the stratified layer

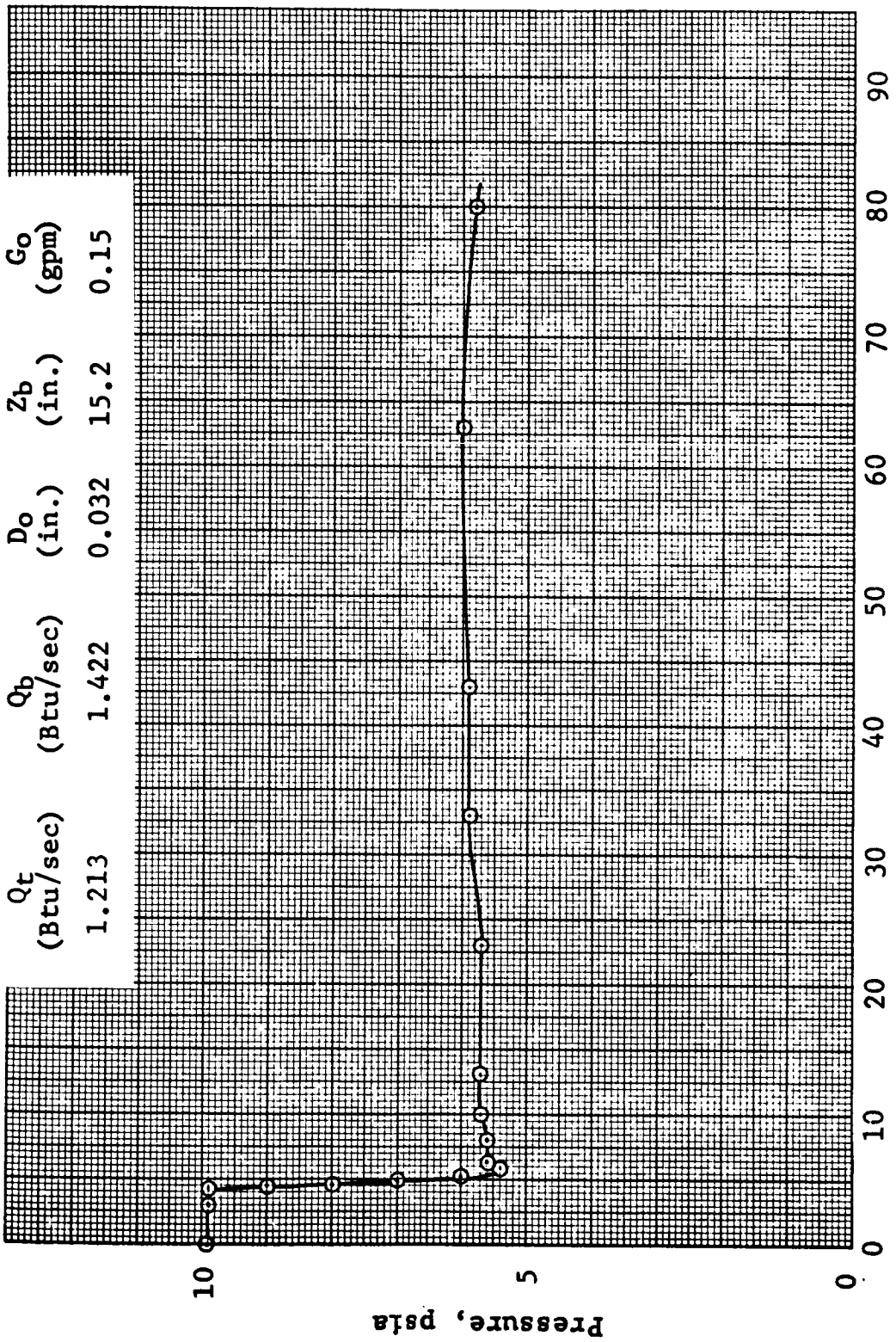

Figure 4-27 Transient Pressure Decay: Test 12, Run 8

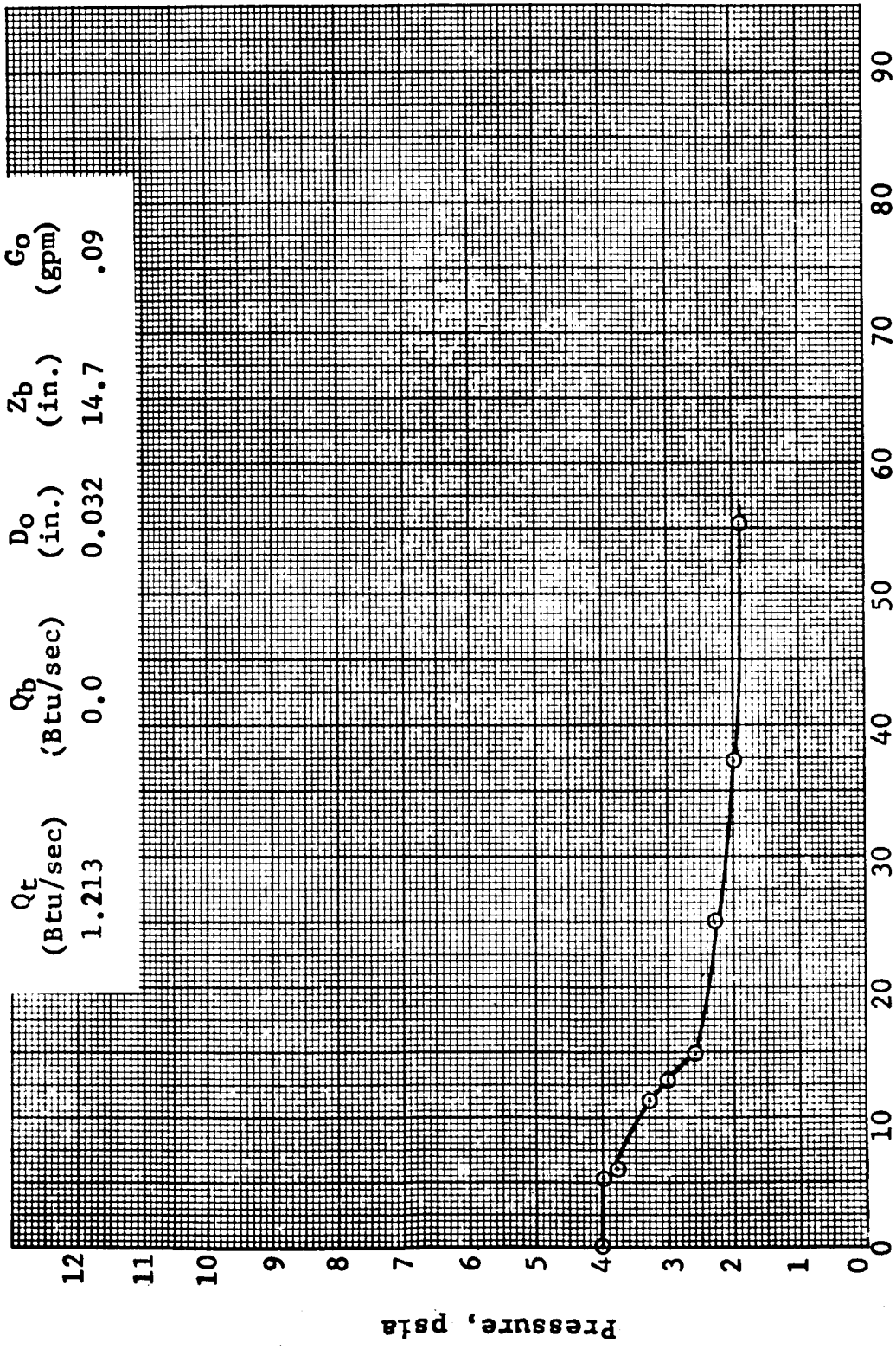

Figure 4-28 Transient Pressure Decay: Test 13, Run 14

and causing local cooling of the ullage. The pressure recovery then might be due to the hot surface fluid reforming until the jet erodes the layer. This is conjecture however.

The period of a constant pressure or pressure rise continued after the mixer began operating reflects the time required for the jet to move to the stratified layer and erode or penetrate it and begin to cool the surface and the ullage. This corresponds to temperature data from the open tank tests in which the surface temperature remained constant or continued to increase after mixing began. This erosion effect is visually shown in Reference 36 . This period of constant or rising pressure indicates that there was probably a corresponding surface temperature effect that was not seen due to the length of the data scans.

Figure 4-29 shows the pressure spike formed in the tank after draining, venting, and closing the vent. Since the tank is empty when the mixer is turned on, the jet impinges on the hot upper bulkhead. The pressure spike is due to some of the fluid evaporating as it cools the top bulkhead and heater.

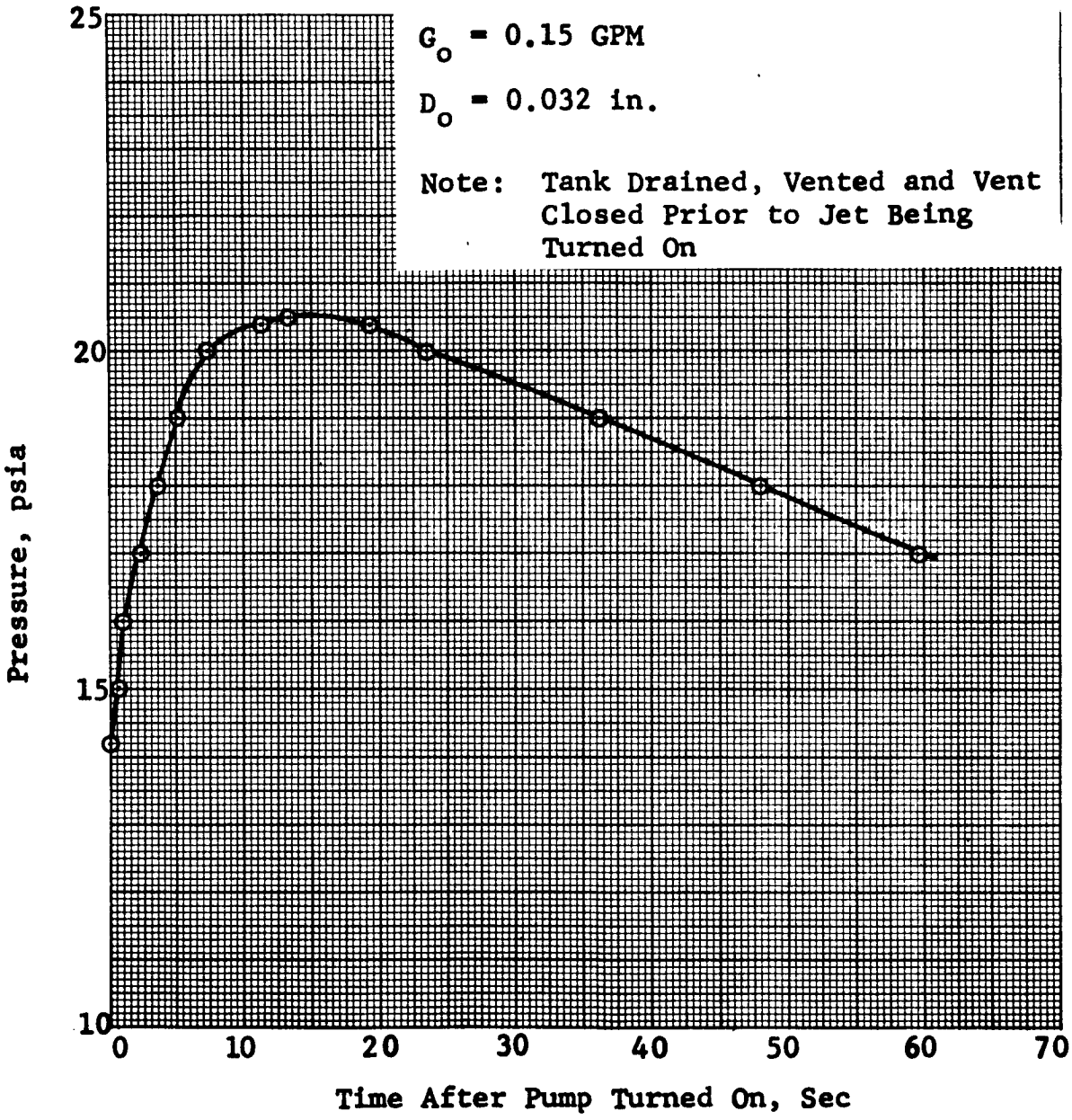

Figure 4-29 Pressure Spike Caused By Jet Impinging On Top Bulkhead After Tank Drained and Vented: Test 14, Run 21

4.5.3 Miniature Tank Low Gravity Mixing Simulation

The tests conducted in a miniature tank designed to simulate the curved liquid/vapor interface found in low gravity environments are described in this section. Due to the simplicity of the test apparatus and procedures and in order to maintain continuity in presenting this experimental work, this section describes the test apparatus and procedures in addition to presenting the test data.

The miniature tank tests were conducted to investigate ullage break-up and liquid-vapor flow characteristics due to axial jet mixing in a simulated low gravity environment. The miniature tank tests were conducted using water as the test fluid and air as the vapor to simulate liquid and vapor phases of cryogenic propellants. Figure 4-30 shows a schematic of the miniature tank low gravity mixing simulation test apparatus. As shown in the figure, the test system consisted of plumbing lines for water, pressure gage, glass test tube (test tank), nozzle, and a graduated cylinder for measuring the flow out of the system. Also, included (but not shown) was a stop watch, an 8 mm movie camera, and lights for photography.

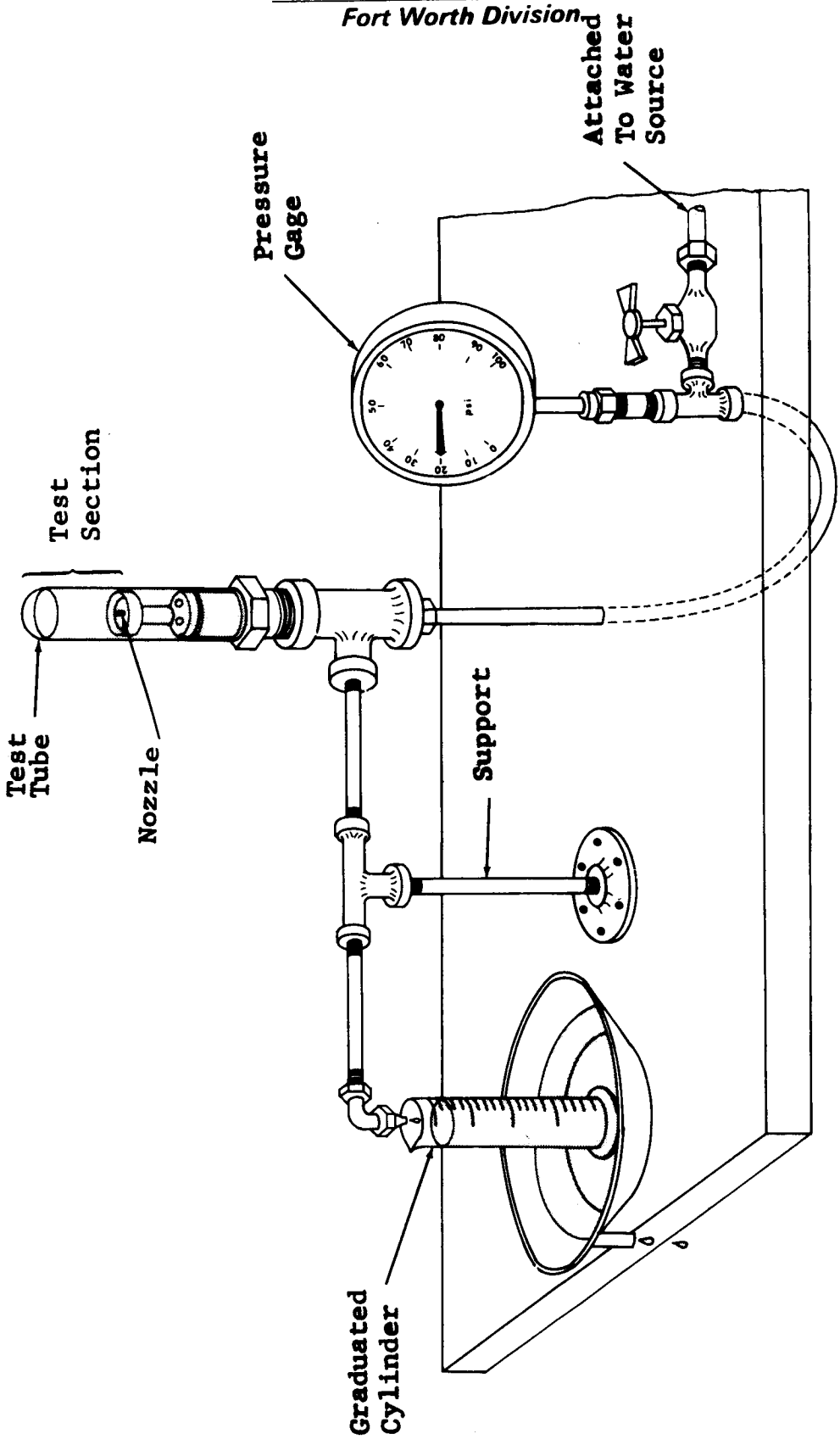

Figure 4-30 Schematic of Miniature Test Apparatus For Low-g Simulation

Two interchangeable glass tubes with approximately hemispherical tops were used as the test tank. These tubes were 13 and 6 mm in diameter, respectively. The smaller tube utilized an adapter to insert it in the test apparatus. The flow nozzle is located at the base of the tank. Two nozzles were utilized in these tests. They were 0.0356 and 0.0216 cm in diameter. The pressure drop across the jet nozzle was measured by a pressure gage upstream from the nozzle. Ordinary tap water at about 45 psi was used as the water source. The flow rate was measured by the use of graduated cylinder and a stop watch. Two graduated cylinders, 5 and 25 ml in capacity, were used to measure the water flowing out of the tank during a test. The flow rate was obtained by measuring the time required for the flow out of the system to fill the graduated cylinder.

The test procedure was to fill the test tank with water by detaching the apparatus from the bench and inverting the test tube to allow the trapped air to escape through the drain line. After the tank was filled, the selected water level was obtained by the use of an air bleed valve which allowed air to bubble back into the test tube. The tests were conducted by starting at a high water level and low flow rate. The water level was fixed and the flow rate increased from test to test. After all tests were performed at a given

water level, the water level was lowered and tests were conducted at the reduced water level.

During each test, pressure drop and flow rate readings were made. Other data obtained included the thickness of the jet rising from the liquid/vapor interface, the height the jet rose above the interface, the liquid level, and the maximum and minimum bubble diameter (when bubbles were formed).

The range of variables and the corresponding dimensionless parameters covered in this set of experiments are tabulated in Table 4-1 and 4-2. The two tube diameters selected yield Bond number conditions of 4.7 and 22, respectively (based on the tank diameter). The jet Reynolds number obtained in the tests varied from about 600 (laminar) to above 7000. The Froude number varied from 13.6 to 4100. The variation in the Froude number covered a range of conditions from the point in which the jet slightly penetrated through the liquid/vapor interface to the point at which the ullage was broken up.

The results of the tests are shown in Table 4-1 and 4-2. Approximately twenty tests were conducted using both test tanks and nozzle sizes. A large portion of the total tests were conducted with the large diameter tube and nozzle. The large nozzle diameter (0.0356 cm) was used in most of the tests because all of the observed flow conditions could not be obtained with

Table 4-1
LAMINAR FLOW TEST RESULTS

	Test Number 1	2	3	4	5	6	7
Tank length, L, cm	2.6	2.6	2.6	1.0	2.6	2.6	2.6
Tank diameter, D_t, cm	1.3	1.3	1.3	0.6	1.3	1.3	1.3
Nozzle diameter, D_o, cm	0.0356	0.0356	0.0216	0.0216	0.0356	0.0356	0.0356
Liquid level, Z_b, cm	0.03	1.1	0.8	0.5	2.1	1.7	1.1
Jet thickness, δ, cm	0.02	0.03	0.02	0.025	0.05	0.04	0.03
Liquid jet height, h_m, cm	0.4	1.5	1.8	0.5	0.5	0.9	1.5
Time to fill 25 ml flask, sec	193.0	122.5	195.0	195.0	99.5	112.0	97.0
Maximum bubble diameter, cm	-	-	-	-	-	-	-
Minimum bubble diameter, cm	-	-	-	-	-	-	-
Outlet velocity, V_o, cm/sec	130.1	205.0	349.8	349.8	252.4	224.2	258.9
Nozzle pressure drop, psi	<1.0	<1.0	5.0	5.0	<1.0	<1.0	<1.0
L/D_t	2.0	2.0	2.0	1.67	2.0	2.0	2.0
Z_b/D_o	2.53	30.9	37.0	23.1	59.0	47.8	30.9
δ/Z_b	0.065	0.027	0.025	0.05	0.024	0.0235	0.027
h_m/Z_b	1.33	1.36	2.25	1.0	0.24	0.529	1.36
D_{bmin}/D_t	-	-	-	-	-	-	-
D_{bmax}/D_t	-	-	-	-	-	-	-
Reynolds Number, V_oD_o/ν	415.5	654.1	884.0	884.0	806.0	716.1	826.8
Bond Number, $\rho g D_t^2/\sigma g_c$	22.0	22.0	22.0	4.7	22.0	22.0	22.0
Froude Number, V_o^2/gD_t	13.6	24.57	96.0	208.1	50.0	39.5	52.6
Weber Number, $\rho V_o^2 D_t/\sigma g_c$	292.3	741.3	2113.0	978.0	1100.0	869.0	1157.5
	I	II	III				

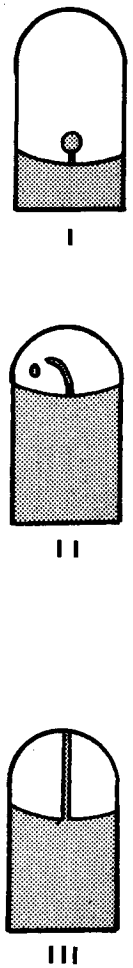

Table 4-2
TURBULENT FLOW TEST RESULTS

	Test Number												
	8	9	10	11	12	13	14	15	16	17	18	19	20
Tank length, L, cm	2.6	2.6	2.6	2.6	2.6	2.6	1.0	2.6	2.6	2.6	2.6	2.6	2.6
Tank diameter, D_t, cm	1.3	1.3	1.3	1.3	1.3	1.3	0.6	1.3	1.3	1.3	1.3	1.3	1.3
Nozzle diameter, D_o, cm	0.0216	0.0356	0.0356	0.0356	0.0356	0.0356	0.0216	0.0216	0.0356	0.0356	0.0356	0.0356	0.0356
Liquid level, Z_b, cm	0.8	1.1	1.1	1.7	1.7	2.1	0.5	2.0	1.1	1.7	2.1	1.8	2.1
Jet thickness, δ, cm	0.05	0.05	0.13	0.08	0.15	0.15	0.05	-	-	-	-	-	-
Liquid jet height, h_m, cm	1.1	1.5	1.5	1.5	0.9	0.5	0.5	0.6	1.5	0.9	-	-	-
Time to fill 25 ml flask, sec	110.0	42.0	29.9	48.6	29.0	46.4	55.0	55	15.4	18.1	15.8	11.0	11.2
Maximum bubble diameter, cm	-	-	-	-	-	0.5	0.2	0.7	0.4	0.4	0.3	0.15	0.15
Minimum bubble diameter, cm	-	-	-	-	-	0.5	0.2	0.7	0.1	0.05	0.05	0.05	0.05
Outlet velocity, V_o, cm/sec	377.0	597.9	839.9	516.7	865.9	541.2	1240.0	1240.0	1630.7	1387.4	1589.4	2282.	2243.
Nozzle pressure drop, psi	12.0	3.9	6.8	2.8	7.2	3.2	40.0	40	25.0	19.0	24.0	44.	43.5
L/D_t	2.0	2.0	2.0	2.0	2.0	2.0	1.67	2.0	2.0	2.0	2.0	2.0	2.0
Z_b/D_o	37.0	30.9	30.9	47.8	47.8	59.0	23.1	92.6	30.9	47.8	59.0	36.5	59.0
δ/Z_b	0.0625	0.045	0.118	0.047	0.088	0.071	0.1	-	-	-	-	-	-
h_m/Z_b	1.375	1.36	1.36	0.529	0.529	0.238	1.0	0.3	1.36	0.529	-	-	-
D_{bmin}/D_t	-	-	-	-	-	0.385	0.33	0.54	0.308	0.308	0.23	0.115	0.115
D_{bmax}/D_t	-	-	-	-	-	0.385	0.33	0.54	0.077	0.038	0.038	0.038	0.038
Reynolds Number, V_oD_o/ν	2391.3	1910.0	2682.0	1650.2	2765.5	1728.0	3135.0	3135.	5208.	4431.0	5076.0	7290.0	7160.0
Bond Number, $\rho g D_t^2/\sigma g_c$	22.0	22.0	22.0	22.0	22.0	22.0	4.7	22.0	22.0	22.0	22.0	22.0	22.0
Froude Number, V_o^2/gD_t	111.0	280.6	553.7	209.6	588.5	230.0	2615.0	1207.7	2087.3	1511.0	1983.0	4091.0	3947.0
Weber Number, $\rho V_o^2 D_t/\sigma g_c$	2405	6173.2	12181.7	4610.3	12947.6	5060.0	12290.0	26571.0	45920.0	33240.0	43623.0	89999.0	86839.0

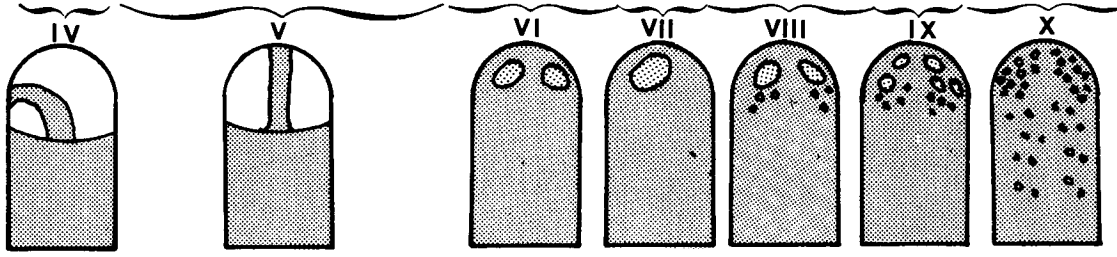

the small tube and nozzle diameter. The smaller diameter tank (6 mm) was not suited for detailed visual observation because of the small size. The variables, D, L, h_m, etc. are shown in the sketch below.

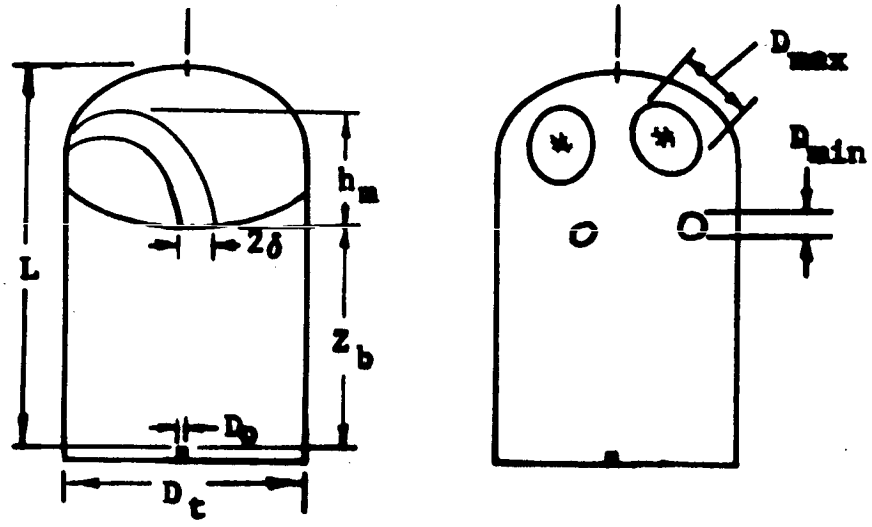

It was found that approximately ten flow regimes existed in the small tank tests. A number of the regimes categorized were in the jet laminar flow regime, as characterized by a Reynolds number less than 2000. (laminar flow jets are not expected to have application to low g large tank storage conditions.) The results presented in Tables 4-1 and 4-2 are categorized into the ten flow regimes. The range of variation of the dimensionless parameters corresponding to the flow regimes are tabulated.

Flow regimes I through III are typical of flow types

which occur in laminar flow. Regimes IV through VII are turbulent flow regimes in which the bubbles are not broken up. Bubble breakup begins in Regime VIII. Very significant bubble breakup results from flow in Regime X. In this regime, the ullage was broken into small bubbles with diameters an order of magnitude less than the tank diameter.

In these tests, jet Reynolds numbers up to 7000 were reached, while jet Reynolds numbers of 100,000 or greater are expected in large scale cryogenic propellant tanks. It was not physically possible to obtain very high Reynolds numbers in the small tank test (and still maintain the appropriate ratio of tank length to nozzle outlet diameter) because the outlet velocity would be such that the pressure drop across the nozzle would be significantly greater than 1000 psi. There was little Reynolds number effect on jet mixing above the transition region. The jet velocity distribution, jet spread angle and mass entrainment ratio is independent of the Reynolds number in turbulent flow regimes.

The principle limitation of this set of experiments was the inability to simulate the large jet Reynolds numbers that would occur in a large space vehicle and still maintain an appropriate ratio of the tank length to the nozzle diameter. The same limitation exists with other 1-g small tank tests.

In fact, it would be difficult even with a 3 or 4 foot diameter cryogenic tank to simulate both the Reynolds number and the proper ratio of the tank length to nozzle diameter for a large tank.

Page intentionally left blank

SECTION 5

EXPERIMENTAL AND ANALYTICAL DATA CORRELATIONS

This section presents the experimental data correlations and comparisons of data with analytical predictions for both open and closed tank tests. The first type of correlations shown are transient data correlations of the type shown in Volume II. Only representative data are shown in this section due to the large amount of transient data obtained from these tests. All of the transient data are documented in Volume II. The transient data consist of

1. Correlation of the bulk fluid motion data
2. Correlation of the temperature decay
3. Correlation of the energy distribution in the tank
4. Correlation of the pressure decay

The comparison of transient data with the analytical prediction indicates that the fluid mixes faster than predicted when the initial buoyancy force divided by the square of the inertial force of the axial jet ($N_i^* = N_{G_r}/N_{R_e}^2$) is less than approximately 50. When $N^* > 50$ the fluid mixes slower than predicted by a linear prediction derived (Ref. 1) from a dye data correlation.

The second type of experimental data correlation summarized the following areas of investigation:

1. Time required for an axial jet to reach the liquid/vapor interface (jet transit time).
2. Time required to penetrate a stratified layer (buoyancy effect).
3. Time required to reduce the temperature difference, $T_s - T_b$, to a given fraction of its initial value (mixing time).
4. Time required to reduce the pressure to a given fraction of its initial value (mixing time).
5. Quasi-steady mixing analysis (performance as predicted in Reference 1).

The results of the first correlation show that the time required for an axial jet to reach the liquid/vapor interface was approximately twice as fast as predicted by the analytic expression derived in Appendix A.

$$\frac{V_o D_o \theta_j}{D_t^2} = 0.076 \, (Z_b/D_t)^2$$

where

V_o is the jet velocity at the nozzle exit

D_o is the nozzle diameter

D_t is tank diameter

θ_j is the time required for the jet to traverse the tank

Z_b is the liquid level above the nozzle

The results of the second type of correlation indicate that the time required for the jet to penetrate a hot stratified layer is proportional to the following parameter (derived from work shown in Reference 1)

$$N = \frac{4N_i^{*}b^2 \quad (I_{m_i} - I_{m_i}^{\ 2})}{1 + 2\ I_{m_i}}$$

where

N_i^* is the ratio of the initial values of the Grashof number divided by the square of the Reynolds number

b is a ratio of the jet thickness to the distance from the nozzle

I_{m_i} is the initial value of the energy integral

for values of this quantity greater than 1.0. For values of this quantity less than 1.0 (which would be expected in actual low-g application) the mixing time required to penetrate the stratified layer is negligible.

Plots of $(T_s-T_b)/(T_s-T_b)_i$ versus N* indicate that the mixing time required for the difference between the surface temperature and the temperature of the nozzle exit, T_s-T_b, to reach a given fraction of its initial value is proportional to

N_i^* for values of N_i^* greater than approximately 50, if the value of N_i^* is less than 50, the mixing time required to reach this particular end condition is almost constant. Conservative values of the dimensionless mixing time ($V_o D_o \theta_1 / D_t^2$) may be obtained from these data in order to predict mixing times under a low-g environment since N_i^* for this condition would be much less than 50. The fourth type of data correlation for the closed tank pressure sustains the results obtained above for the temperature data.

The results of the quasi-steady mixing analysis indicate that the performance prediction given in Reference 1 is conservative for the final values of N^* less than 1.0. The value of N_f^* less than 1.0 would be expected in a low-g environment. The analytical prediction given in Reference 1 is

$$\lambda_{mf} = \frac{Q_m}{(T_s - T_m)\, \dot{m}_o\, C_p} = 0.456\, \frac{Z_b}{D_o}$$

where

$\lambda_{m_f^f}$ is the performance parameter based on final conditions

Q_m is the heat absorbed by the fluid

$\dot{m}_o$ is jet mass flow rate at the nozzle

C_p is the specific heat

When Z_b/D_t is included in the performance correlation, the data correlates much better since the volume of the jet was excluded in the derivation of λ_{m_f}. Now considering the performance to be given by

$$\lambda_{m_f} \quad D_o D_t / Z_b^2$$

and correlating this as a function of N_f^*, the performance increases with increasing Z_b/D_t. This performance improvement is due to the jet diameter increasing as the jet traverses the tank.

5.1 OPEN TANK TRANSIENT DATA CORRELATION

This section describes the open tank experimental transient data correlations shown in Volume II. The transient data correlations are presented in three different forms per test. The first type is the correlation of the bulk fluid motion dye data which shows fluid particle movement due to bulk fluid motion. Figure 5-1 is a typical plot of bulk fluid motion data along with an analytical prediction derived in Appendix B. In this figure the axial location of the dye above the nozzle, Z_d, divided by the initial dye location just before the dye starts to move, Z_{di}, is shown as a function of dimensionless time, $V_o D_o \theta_1 / D_t^2$. Here θ_1 is equal to zero at the time when the dye starts to move. The sketch below shows time relationships used in the dye correlations.

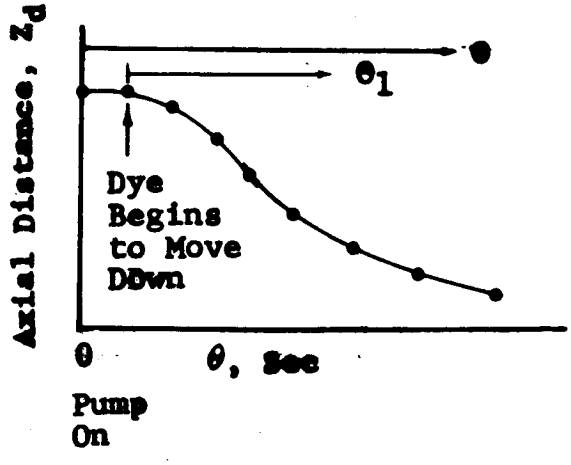

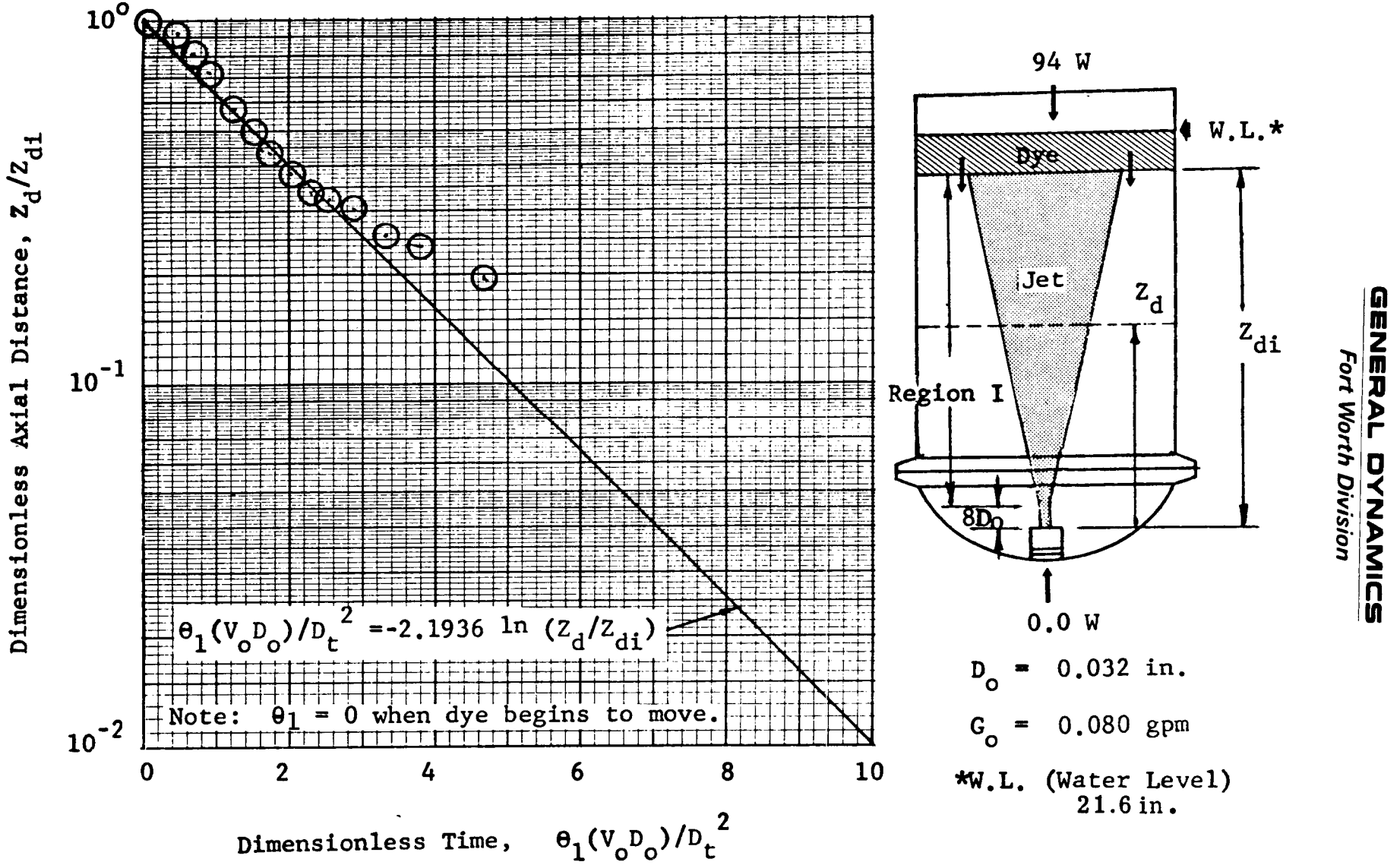

Figure 5-1 Correlation of Axial Jet Dye Layer Motion for Region I: Test 5, Run 50

Figure 5.2 is a summary plot of the axial jet bulk fluid motion dye data. In this plot the general tendency seems to be, that for $N^* \geq 50$ the data falls above the analytical prediction and for $N^* < 50$ the transient dye correlations fall below the analytical prediction. This graphically illustrates the effect of buoyancy on mixing.

The transient decay of the surface temperature is correlated in a manner similar to that of the transient dye data. A typical correlation of the transient temperature decay is shown in Figure 5-3. In this figure the temperature difference between the surface temperature, T_s, and the average temperature at the nozzle top, T_b, along with the difference between T_s, and the mean tank temperature, T_m, divided by the initial value of each term, $(T_s-T_b)_i$ or $(T_s-T_m)_i$, are shown as a function of $V_oD_o\theta_1/D_t^2$. Here θ_1 is the time after the surface temperature, T_s, begins to decrease. Time relationships are illustrated in the sketch below.

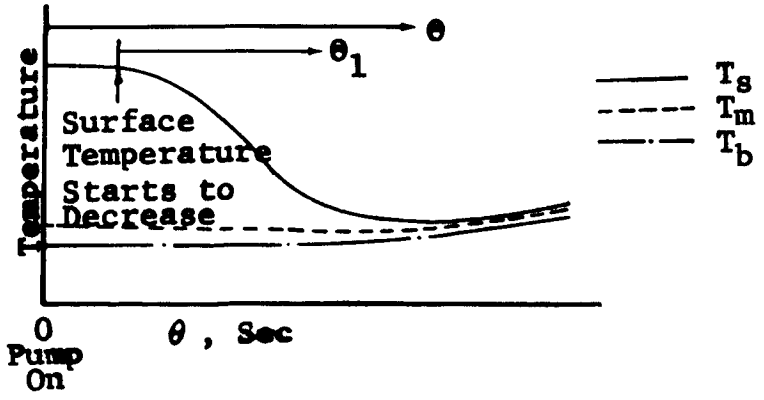

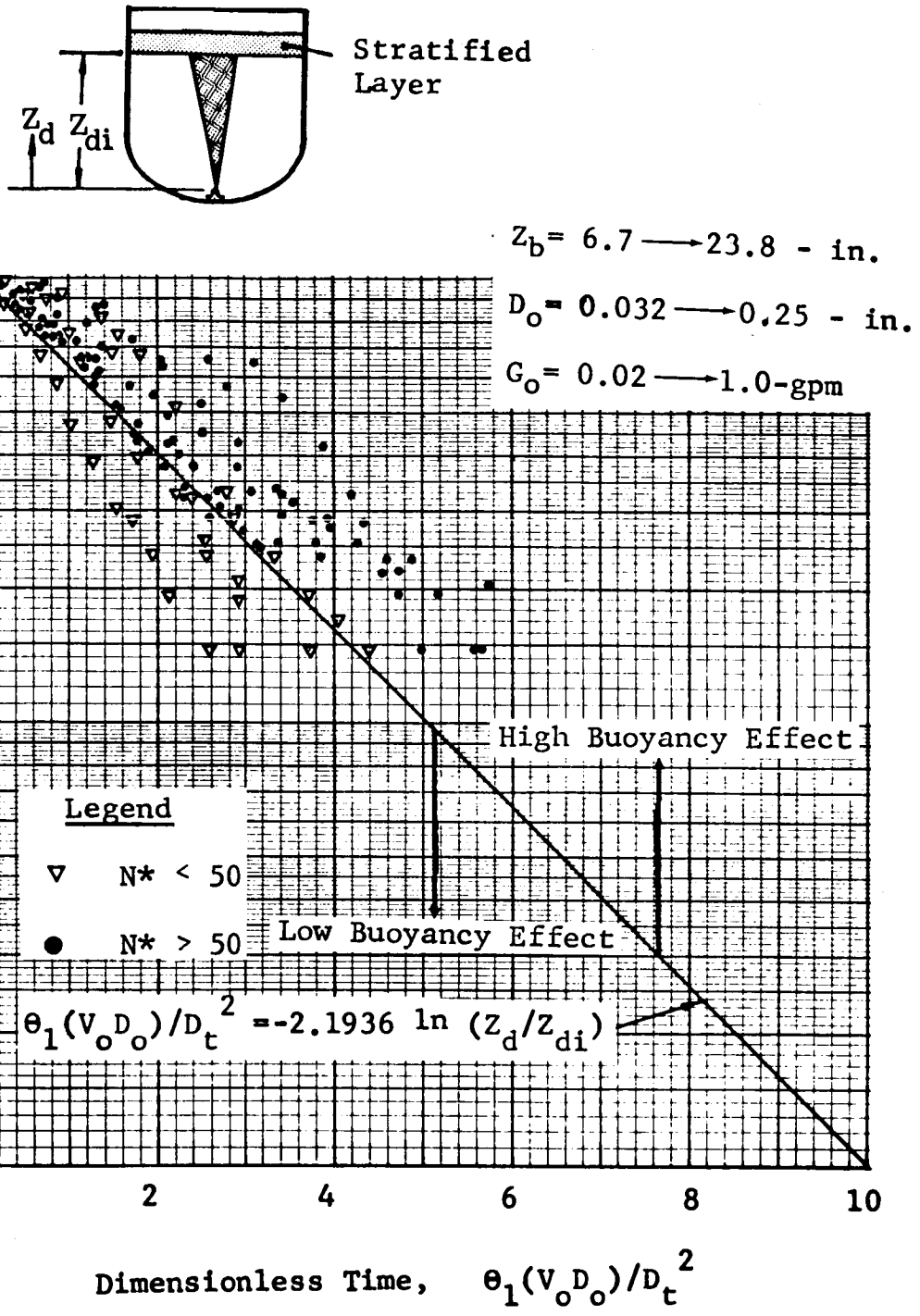

Figure 5-2 Comparison of Axial Jet Bulk Fluid Motion Dye Data Taken In Tank With Convex Bottom

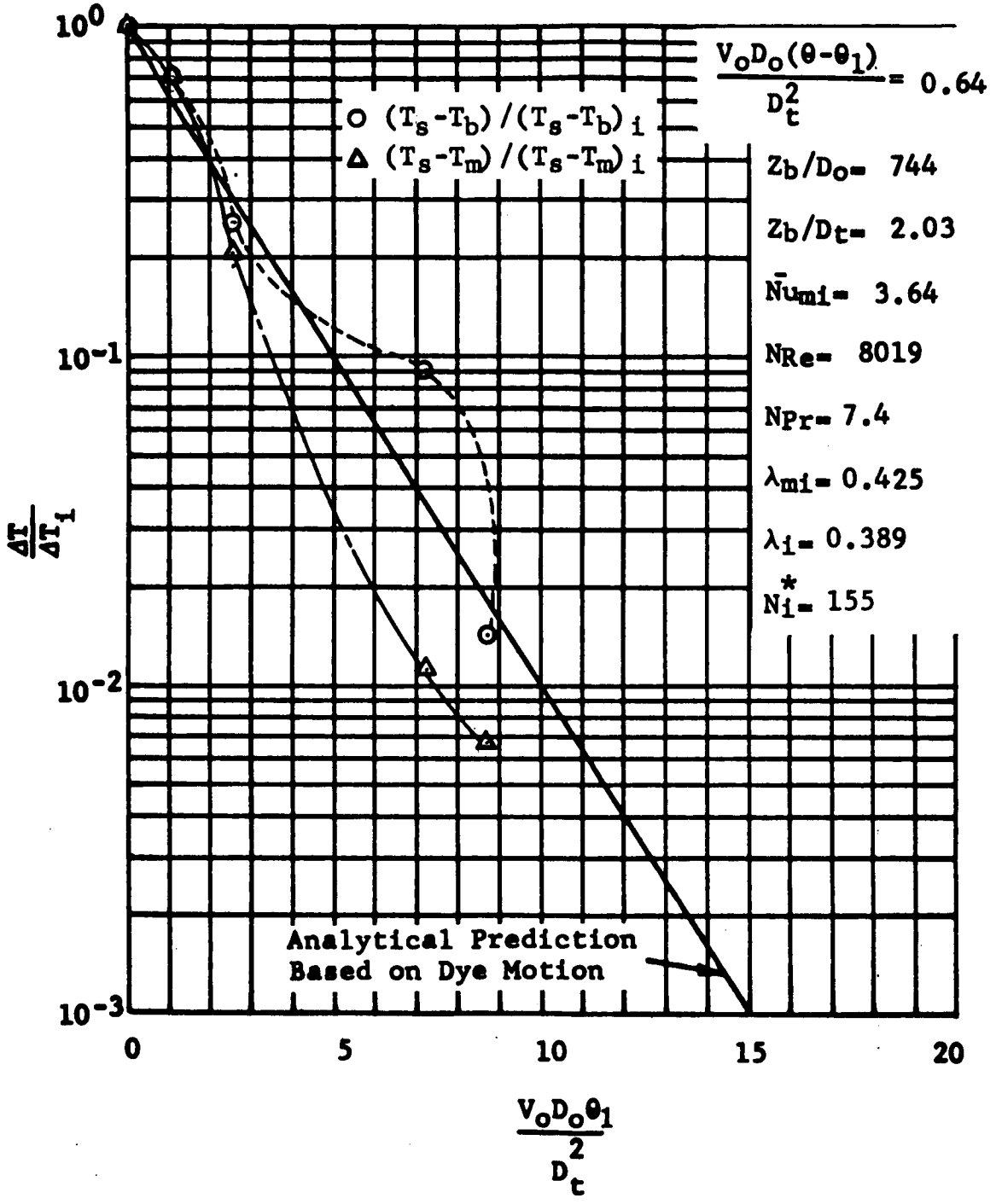

Figure 5-2 Fraction of Initial Temperature Difference After Surface Temperature Starts to Drop (Pump on at θ=0.0 sec; Surface Temp. Drops at θ_1=0.0 sec): Test 5, Run 50

An analytical prediction based on dye motion is also shown in Figure 5-3 (see Appendix E).

Various nondimensional groups are listed on the plots of the transient temperature decay. The first nondimensional group shown is

$$\frac{V_o D_o}{D_t^2} (\theta - \theta_1)$$

This represents the nondimensional time before the temperature starts to drop and indicates the mixing time due to buoyancy.

The second group, Z_b/D_o, represents the axial location of the liquid level in terms of the number of nozzle diameters above the nozzle. This parameter was varied from 70.8 to 744 to determine the effect of liquid height on mixing performance. (Mixing performance is measured in terms of the parameter, λ derived in Reference 1; λ is proportional to Z_b/D_o).

The next ratio shown in Z_b/D_t, this ratio was varied to determine the effect of geometry on mixing. The next parameter listed is the initial Nusselt number, $\bar{N}_{u_{m_i}}$, based on the initial temperature difference between T_s and T_m .

$$\bar{N}_{u_{mi}} = \frac{q\ D_t}{2\ (T_s - T_m) K}$$

where

q = the heat input to the tank calculated from the mean tank temperature rise with time divided by the heated area.

D_t = the tank diameter

T_s = surface temperature

T_m = mean tank temperature

K = thermal conductivity

The Reynolds number, N_{Re}, is shown next and is equal to

$$N_{Re} = \frac{V_o D_o}{\nu}$$

where

V_o = the nozzle outlet velocity

D_o = the nozzle diameter

ν = the kinematic viscosity of water at the mean tank temperature and 1 atm pressure.

The Prandtl number, N_{Pr}, for water at the mean tank temperature is shown next. (Values of N_{Pr} were taken from Reference 37)

The next two parameters, λ_{mi} and λ_i, are indications of the performance and are calculated from

$$\lambda = \frac{Q_m}{\Delta T_i \dot{m}_o C_p}$$

where

Q_m = the total heat input calculated from the mean temperature rise with time

$\dot{m}_o$ = the pump mass flow rate

C_p = the specific heat of the fluid at a constant pressure.

The distinction between λ_{mi} and λ_i is that the ΔT_i used in the calculation of λ_{mi} is $(T_s-T_b)_i$. When either one of these parameters is divided by the final value of the corresponding ratio of $\Delta T/\Delta T_i$, a measure of the mixing performance will be obtained. The Grashof number, N_{Gr_i}, divided by the Reynolds number squared is shown next and is denoted by N_i^*.

$$N_i^* = \frac{N_{Gr_i}}{N_{Re}^2} = \frac{g\ \beta\ (T_s-T_b)_i\ Z_b^3}{(V_oD_o)^2}$$

where

g = the acceleration due to gravity on the fluid

β = the coefficient of thermal expansion

$(T_s-T_b)_i$ = the initial temperature difference between the surface temperature and the nozzle top.

Z_b = the liquid height above the nozzle outlet

V_o = the velocity of the fluid leaving the nozzle

D_o = the nozzle diameter

N_i^* gives a measure of the initial buoyancy force due to stratification.

Figure 5-4 shows the transient energy integral, I_m, as a function of $V_o D_o \theta / D_t^2$. The energy integral is given by

$$I_m = 1 - \frac{T_s - T_m}{T_s - T_b}$$

and is a measure of the energy distribution in the tank. As I_m approaches 1.0 the tank's fluid contents become mixed. If I_m becomes greater than 1.0 there is an inverse stratification in the tank. Using the information shown on transient plots, correlations of end conditions may be made.

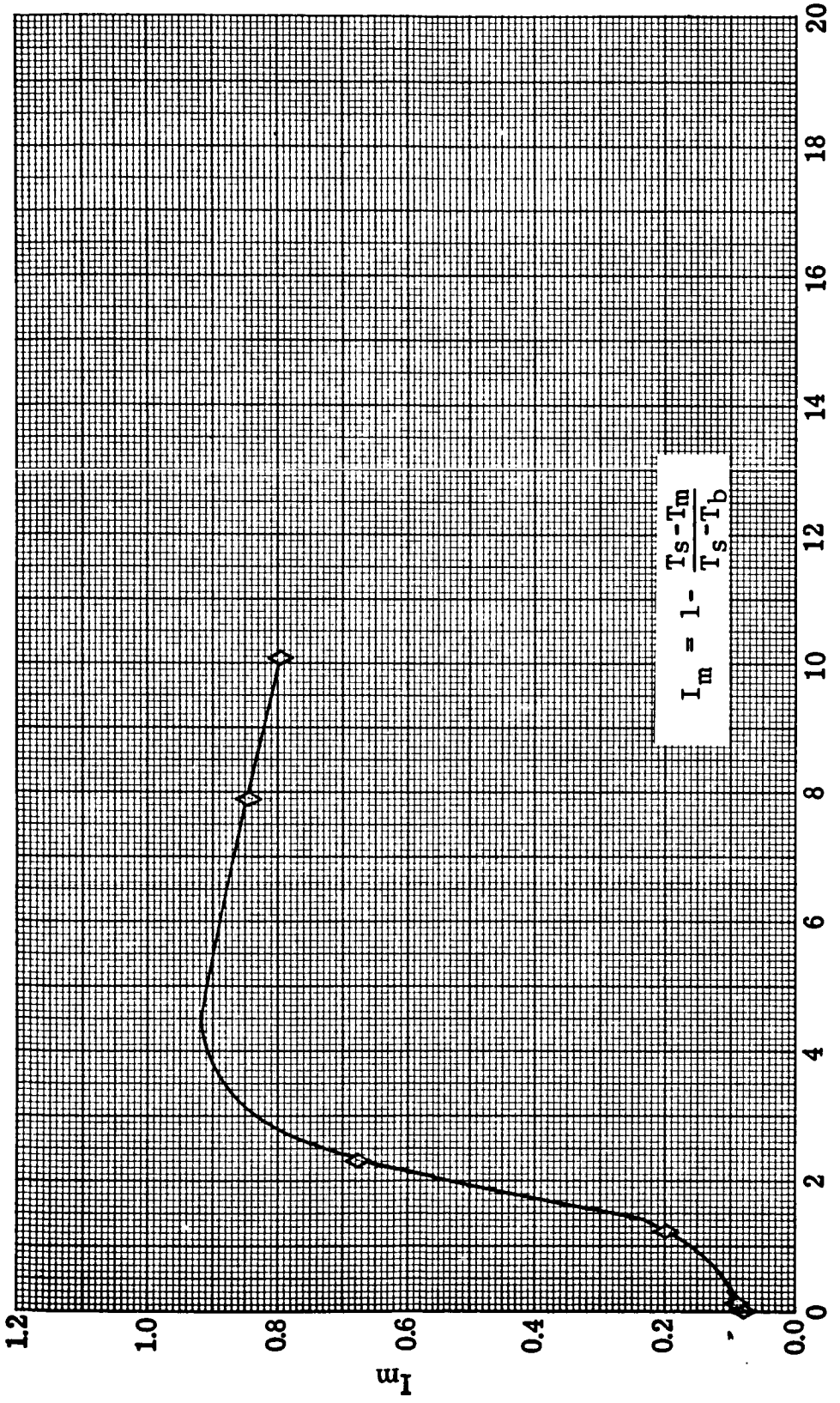

Figure 5-4 Transient Energy Integral: Test 165, Run 32

5.2 OPEN TANK DATA CORRELATIONS

This section describes some of the experimental verifications of the analytical predictions given in Reference 1 concerning the performance of an axial jet. The dimensionless parameters described in Section 5.1 were used in the correlation of experimental data after it had reached a quasi-steady state. The correlated results for various heating combinations include:

1. A correlation of the dimensionless time for the axial jet to reach the liquid vapor interface $(V_o D_o \Delta\theta_j / D_t^2)$ as a function of Z_b/D_t.
2. A correlation of the dimensionless time before the surface temperature starts to drop minus the time it takes the jet to reach the surface $V_o D_o(\theta-\theta_1-\theta_j)/D_t^2$ as a function of $N = \frac{4N_{i\,b}^{*2}(I_{mi}-I_{mi}^2)}{1+2I_{mi}}$
3. Correlations of the dimensionless time after the temperature starts to drop to the point where the temperature difference between T_s and T_b reaches a given percentage of its initial value as a function of N_i^*.

4. A correlation of $V_o D_o(\theta-\theta_1-\theta_j)/D_t^2$ as a function of Grashof number and parametric with the Reynolds number.
5. A correlation of the mixing performance as a function of N_f^*.

The results of the open tank test will now be presented as outlined above. The first figure, Figure 5-5 shows a correlation of the visual data on the axial jet moving up to the liquid vapor interface. It is apparent that this data was approximately twice that predicted by the analytical prediction based on general centerline velocity,

$$\frac{V_o D_o\ \theta_j}{D_t^2} = 0.076 \left(\frac{Z_b}{D_t}\right)^2$$

Figure 5-6 shows the dimensionless time before the temperature starts to drop minus the time for the jet to reach the surface as predicted by the equation above as function of N. It is clear from this data, that as the buoyancy force increases (N_i^* increases) the mixing time increases. Figure 5-7 shows the closed tank data based on the dimensionless time before the tank pressure began to decay presented along with the Figure 5-6 data. From this it is seen that the mixing time due to the buoyancy effect is small at low values of N ($N<1$). This shows that in an actual low-g environment where $N<1$ this

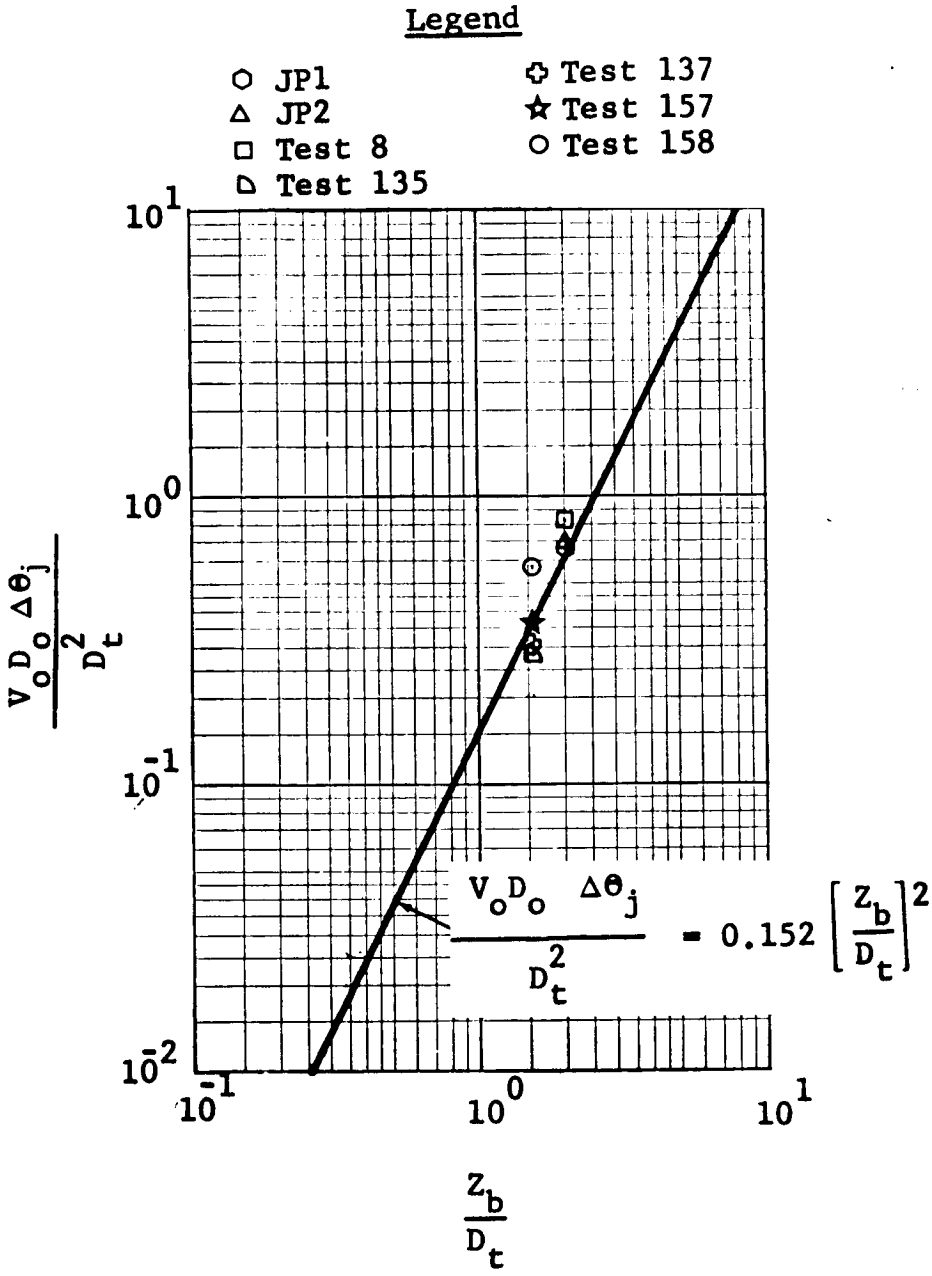

Figure 5-5 Correlation of Axial Jet Motion Data: Open Tank Test

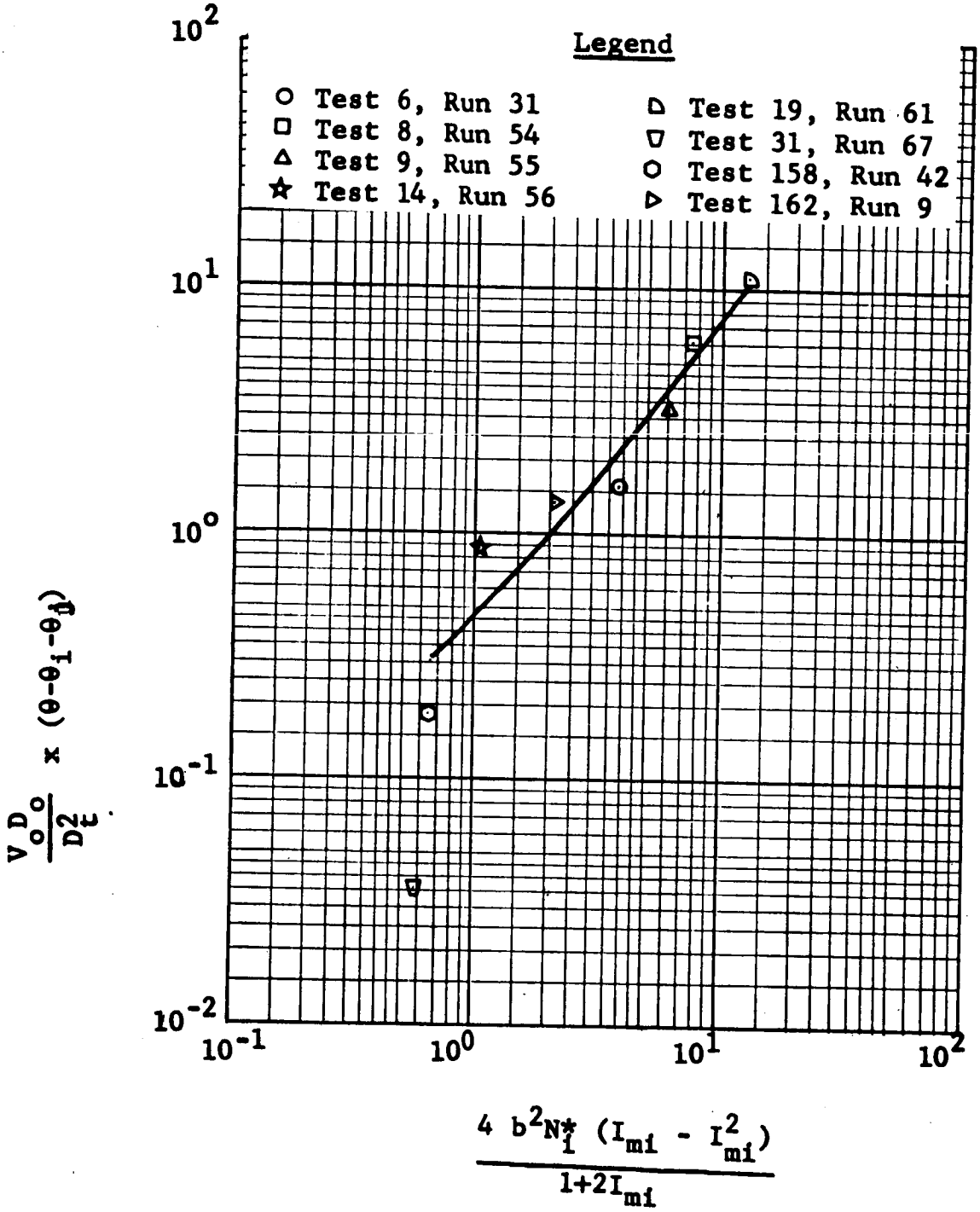

Figure 5-6 Effect of Buoyancy on Mixing Time: Closed Tank Test

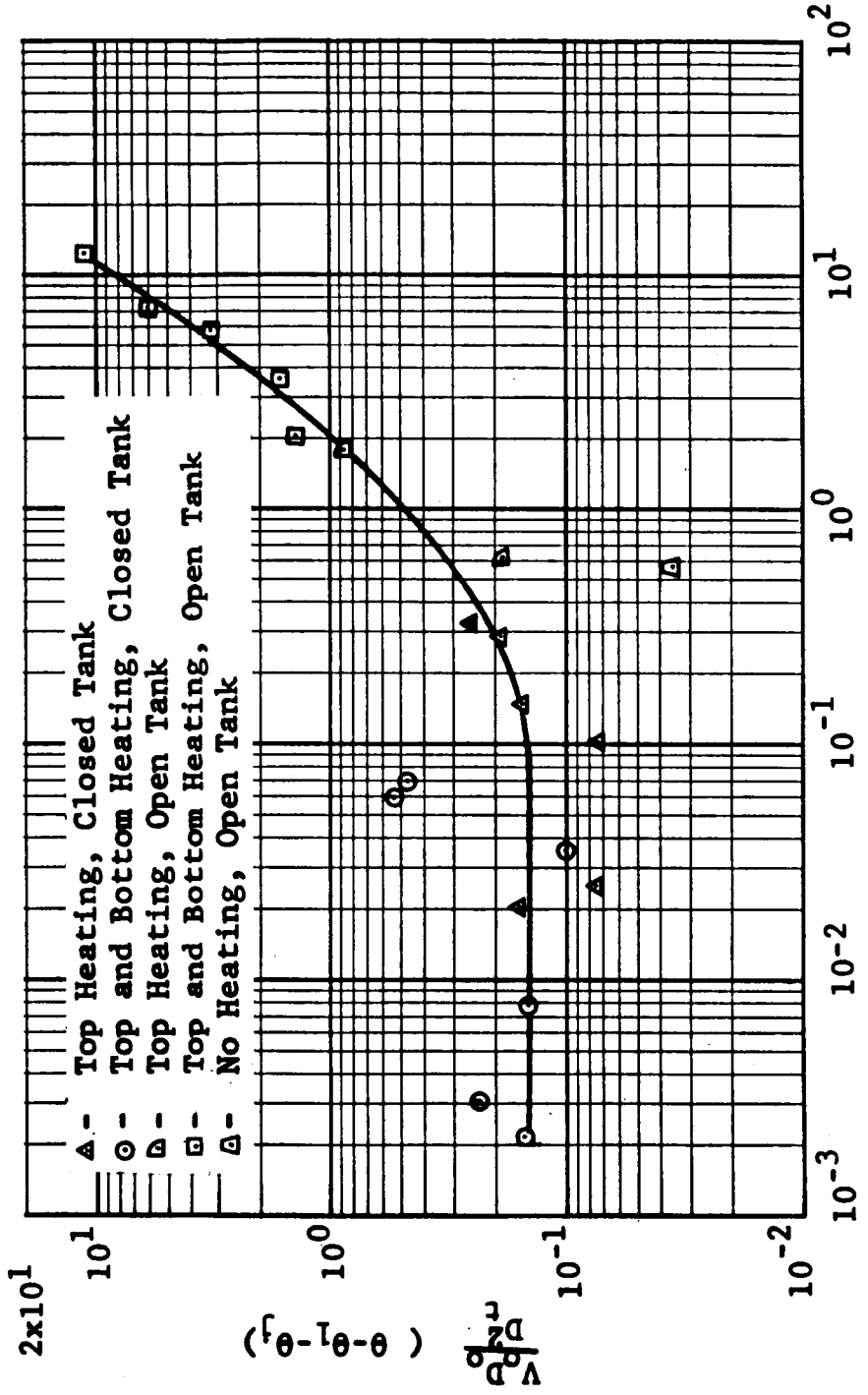

Figure 5-7 Mixing Time Due to Buoyancy Effect: Open And Closed Tank Tests

particular effect may be ignored in the prediction of a mixing time.

Figure 5-8, Figure 5-9, and Figure 5-10 show the dimensionless time taken for the temperature difference T_s-T_b to reach 0.2, 0.1, and 0.5 of its initial value, respectively, as a function of N_i^*. Here the dimensionless time taken for the temperature difference to reach a given fraction of its initial value increases with N_i^*. At a value of N_i^* of 50 in Figure 5-8 the dimensionless time taken to reach a value of $T_b^* = (T_s-T_b)(T_s-T_b)_i = 0.2$ becomes almost constant. As the desired value of $\Delta T/\Delta T_i$ decreases as shown in Figures 5-9 and 5-10, the dimensionless time increases. To show the effect of $N_{G_{ri}}$ and N_{Re} separately on $V_oD_o\theta_1/D_t^2$ Figure 5-8 was curve fitted between $50 \leq N_i^* \leq 760$. This yields

$$\left(\frac{V_oD_o\theta_1}{D_t^2}\right)_{T_b^*=0.2} = 0.034 \left(\frac{N_{G_{ri}}}{N_{Re}^2}\right)^{0.88}$$

Then plotting $V_oD_o\theta_1/D_t^2$ as a function of $N_{G_{ri}}$ and parametrically in N_{Re} Figure 5-11 is obtained. From plots such as Figure 5-8 through Figure 5-11 a conservative value of dimensionless mixing time may be chosen after the appropriate N_i^* is calculated.

From Reference 1 the analytical performance prediction is

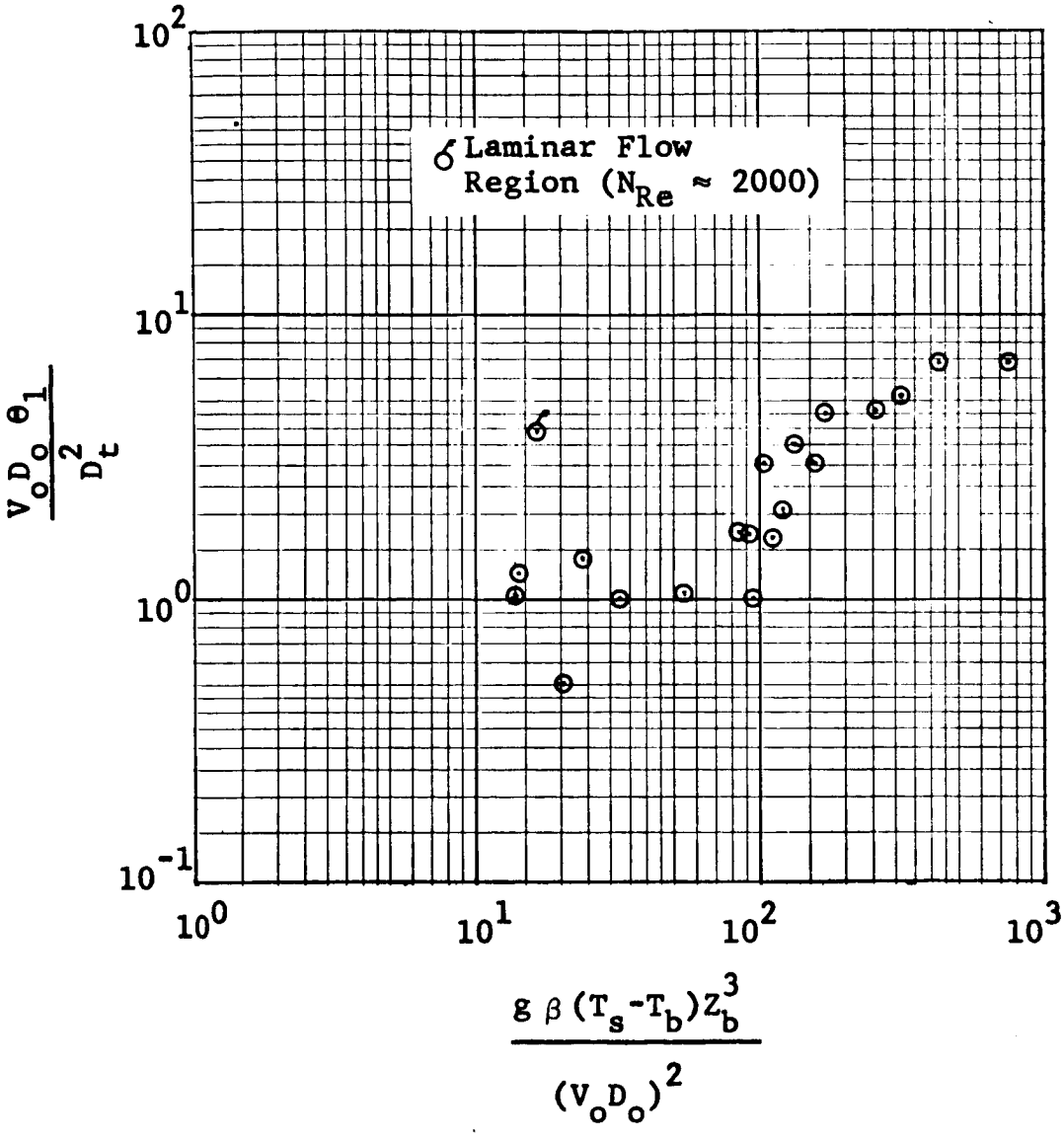

Figure 5-8 Correlation of Dimensionless Time For (T_s-T_b) To Reach 0.2 Of Its Initial Value: Open Tank Test

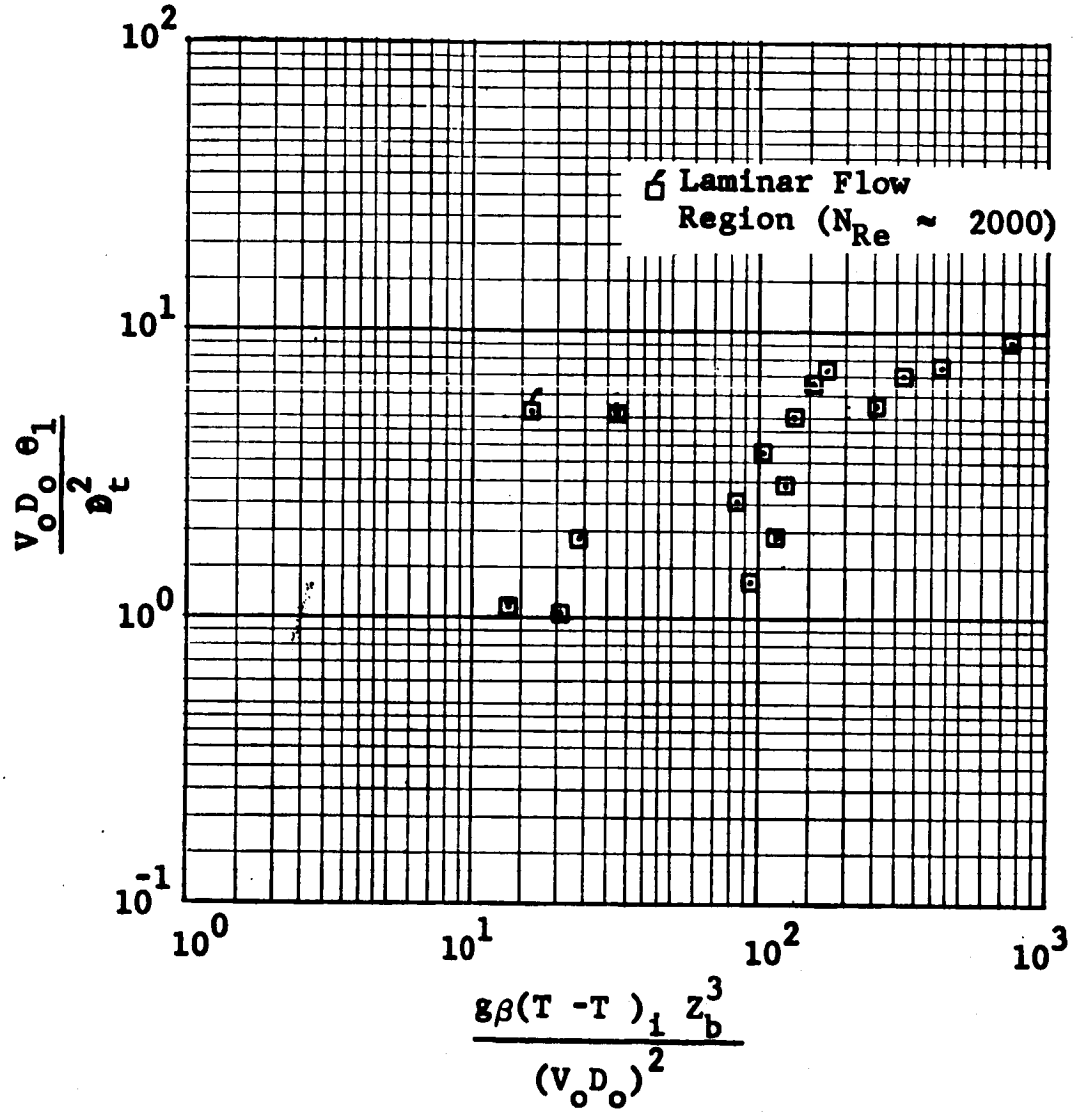

Figure 5-9 Correlation of Dimensionless Time For $(T_s - T_b)$ to Reach 0.1 Of Its Initial Value: Open Tank Test

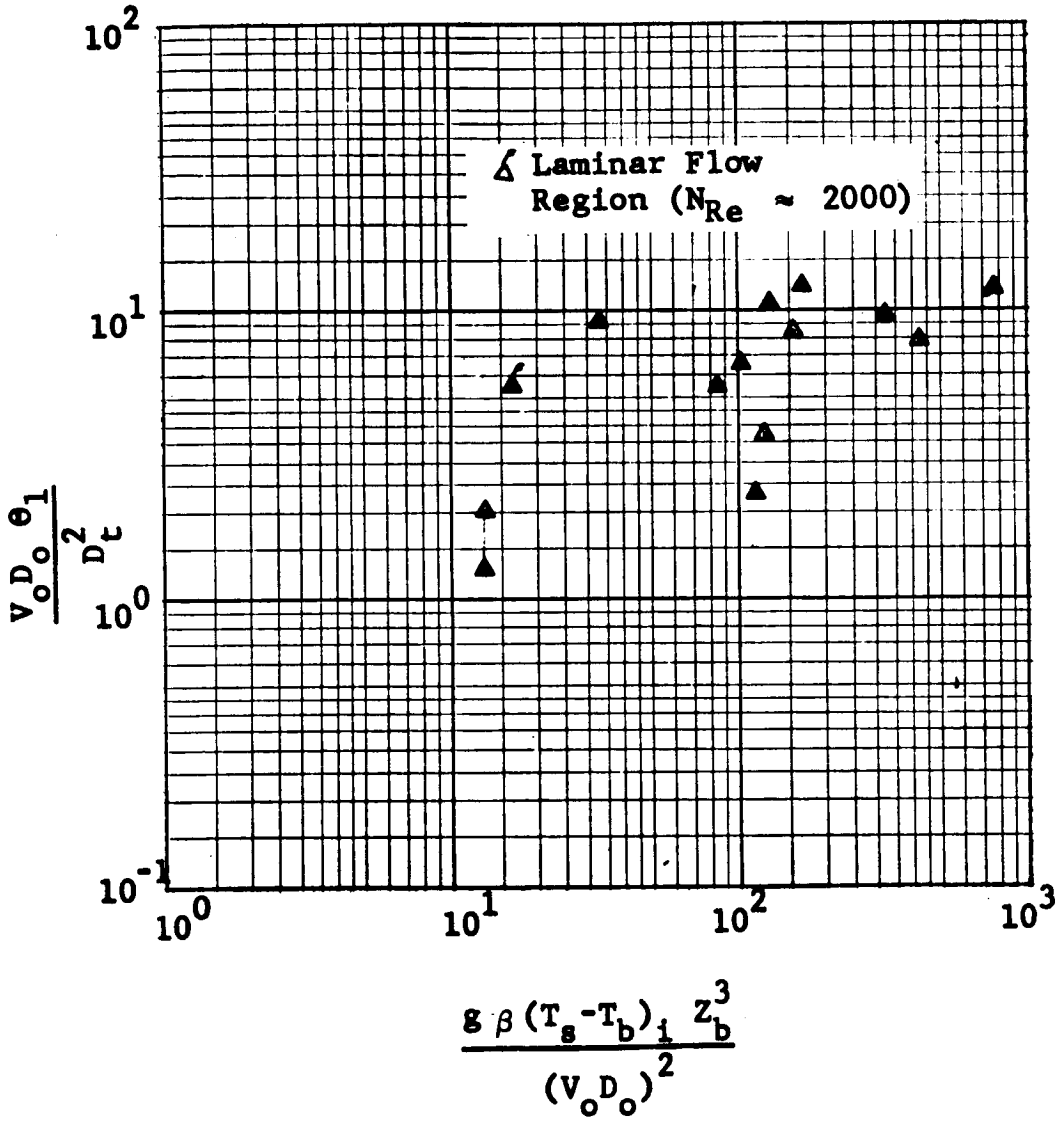

Figure 5-10 Correlation of Dimensionless Time For (T_s-T_b) To Reach 0.05 Of Its Initial Value : Open Tank Test

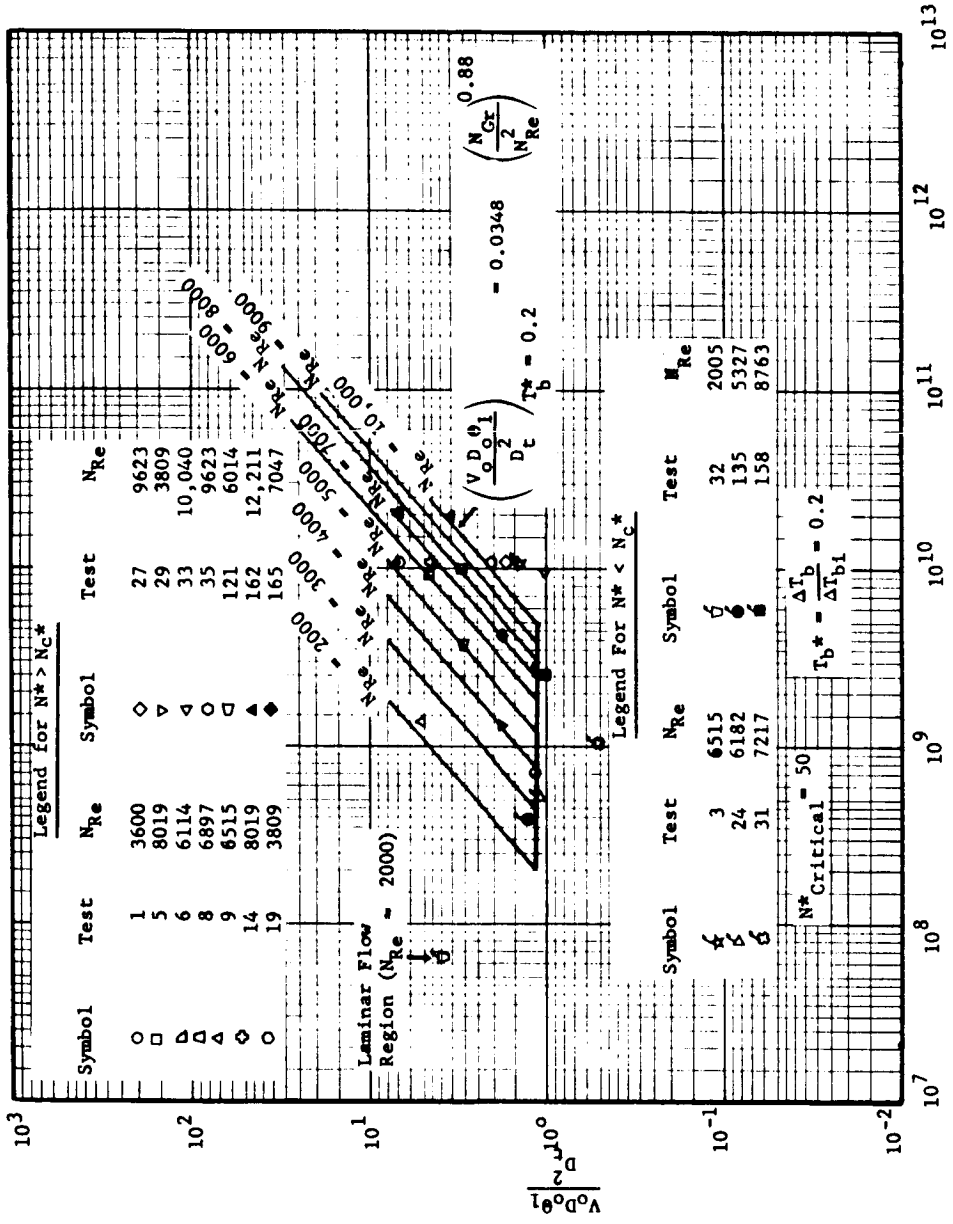

Figure 5-11 Correlation of Axial Jet Mixing Time Data for $(T_s-T_b)/(T_s-T_b)_i = 0.2$: Open Tank Test

$$\lambda_{mf} = 0.456 \frac{Z_b}{D_o}$$

Therefore, λ_{mf} (D_o/Z_b) plotted as a function of the final N_f^* should be a constant equal to 0.456. Figure 5-12 shows the above performance parameter plotted as a function of N_f^*. Here it is seen that $\lambda_{mf}(D_o/Z_b)$ is inversely proportional to N_f^*. For values of $N_f^* < 1$ the actual performance is about a factor of 4 greater than the predicted performance. Hence, in an actual low-g environment where $N_f^* < 1$ the analytical performance is conservative.

As the axial jet travels toward the liquid/vapor interface it spreads at a given slope (b = 0.25) as it entrains fluid. The further the jet travels, the greater the mass flow rate across a plane perpendicular to the jet becomes until the jet spreads to the width of the tank walls. To include this particular effect in the correlation, $\lambda_{mi}(\frac{D_o}{Z_b})$ is multiplied by D_t/Z_b and correlated as a function of N_f^*. Figures 5-13 and 5-14 show this particular performance correlation for top heating and top and bottom heating respectively.

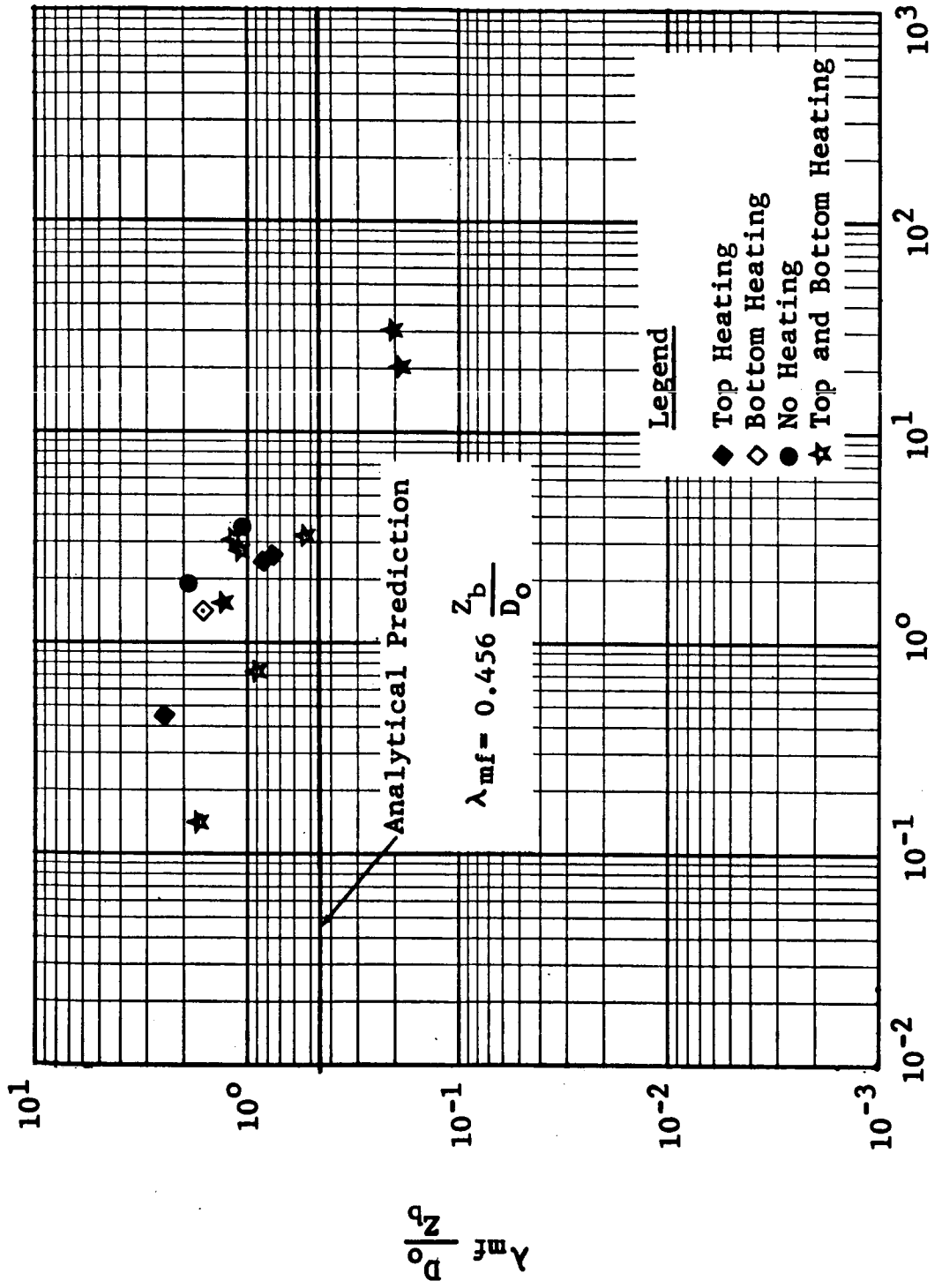

Figure 5-12 Correlation of Axial Jet Mixing Performance : Open Tank Test

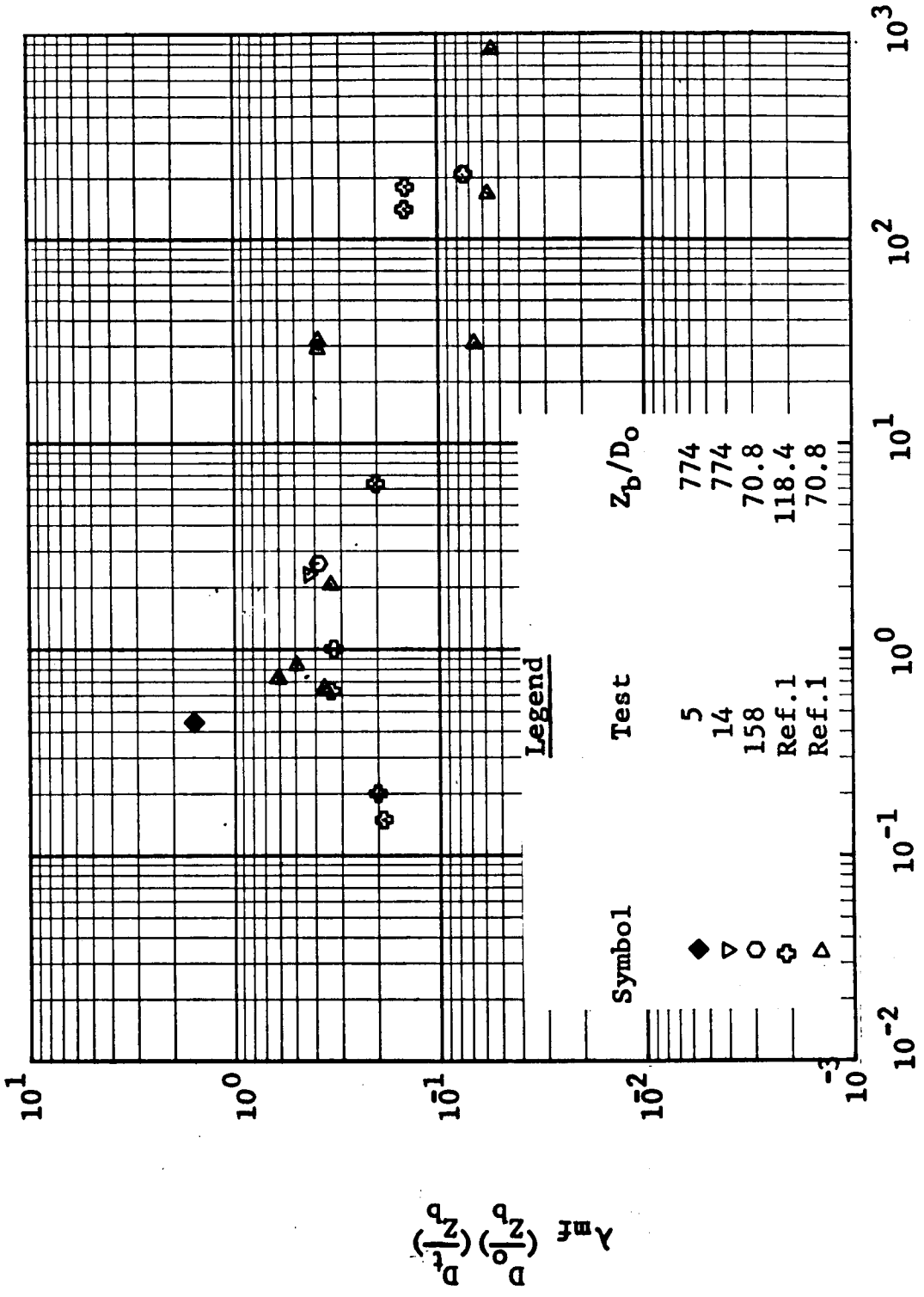

Figure 5-13 Axial Jet Performance Correlation For Top Heating Condition : Open Tank Test

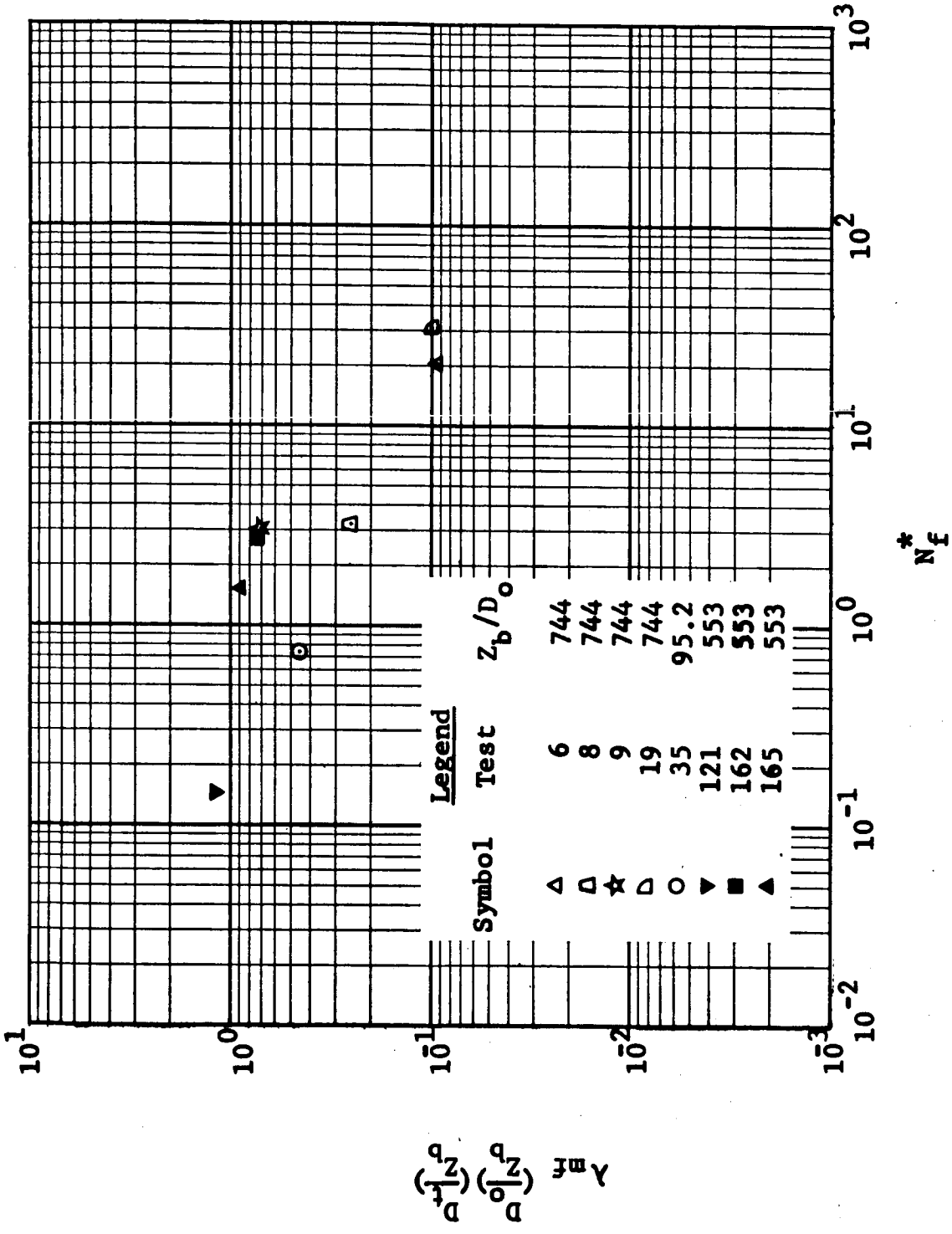

Figure 5-14 Axial Jet Performance Correlation For Top and Bottom Heating Condition : Open Tank Test

5.3 CLOSED TANK TRANSIENT DATA CORRELATIONS

The closed tank pressure and temperature data correlations shown in Section 3 of Volume II were performed in much the same manner as the open tank temperature correlations. The correlations consist of dimensionless temperatures, dimensionless pressure, and the energy integral shown as a function of dimensionless time.

Two pressure correlations were considered. The first correlation considered was

$$\frac{P - P_{min}}{P_i - P_{min}}$$

where P_{min} is the minimum tank pressure to which the initial tank pressure, P_i, decays and the term P indicates the tank pressure at any time after the jet was turned on. In all but one of the tests the minimum pressure occurred toward the end of the test. The one exception occurred during a sharp initial pressure drop after which the tank pressure partially recovered and gradually decayed. Examination of the data showed that in all cases the minimum tank pressure was greater than the saturation pressure of the water at the mean fluid temperature. Most of the closed tank tests were performed as successive cycles of stratification and mixing. Comparison of pressure

data for successive cycles showed that the pressure difference between the minimum tank pressure and the saturation pressure of the water increased during successive cycles. This is shown in Figure 5-15. Results of pressurization for leak detection before and after tests indicated that leaks were developing during the tests. It was assumed that the difference between the minimum pressure and saturation pressure of the water was due to the partial pressure of noncondensable gases (air). In addition to the leaks other possible sources of the non-condensable gases were residual air remaining after evacuation of the tank to the saturation pressure of the water prior to a test, dissolved air coming out of the water, and outgassing from the foam insulation between the heaters and the tank shell. In order to consider the effect of the non-condensable gases, a second pressure correlation was used. This correlation was

$$\frac{P - P_{NC_f} - P_{mean}}{P_i - P_{NC_f} - P_{mean_i}}$$

where P_{mean} is the saturation pressure of water at the mean temperature of the water, P_{NC_f} is the partial pressure of non-condensable gases in the tank. P_{NC_f} was taken as the difference between the final tank pressure and the final mean pressure for each mixing cycle. This value was assumed to be

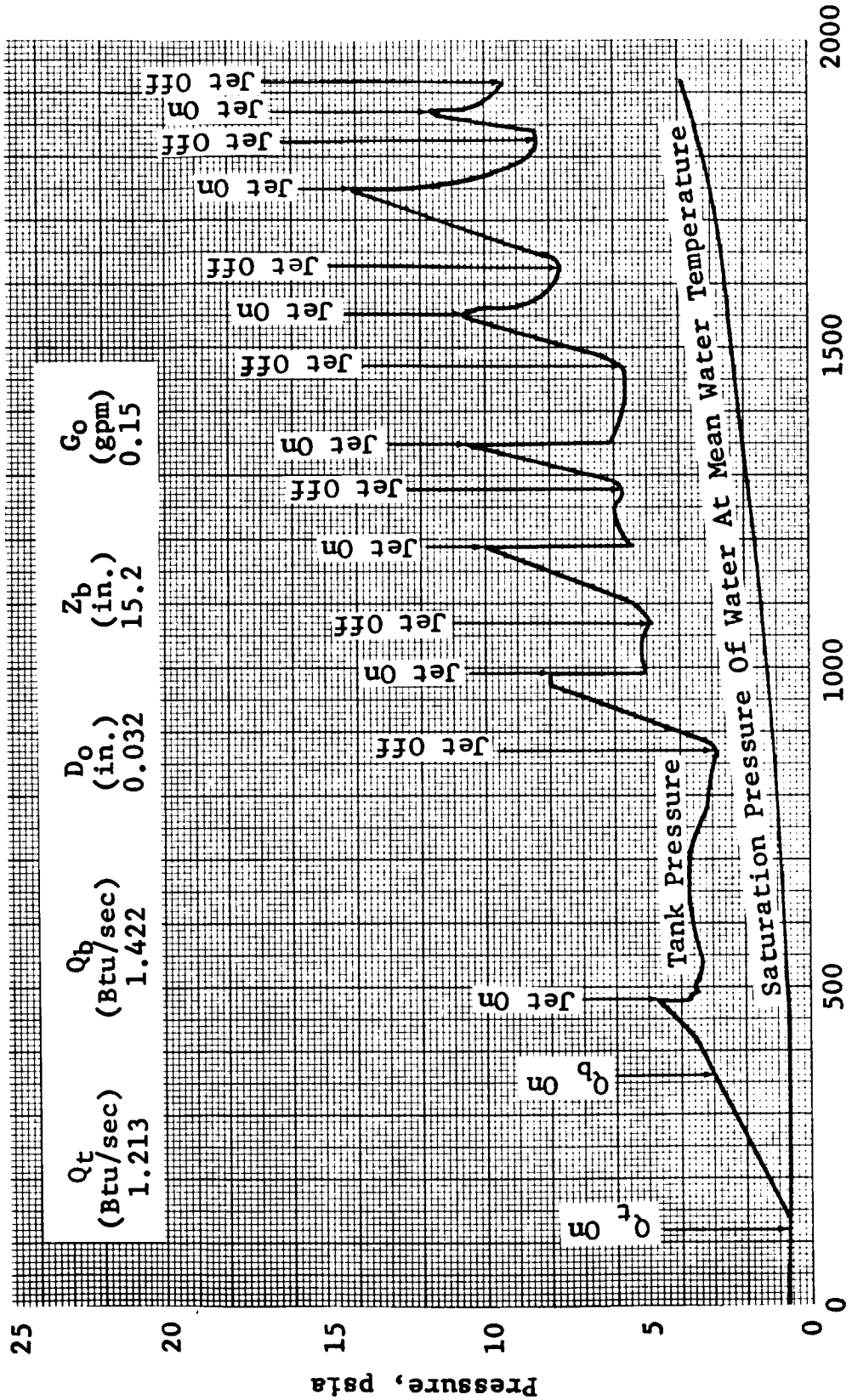

Figure 5-15 Tank Pressure History During Cycle Test: Test 12, Run 6 - 12

constant during a given run or cycle of a test. This correlation is shown in Section 3 of Volume II.

Since the mean temperature change of the water during a mixing cycle was usually small, the value of P_{mean} was essentially constant. Thus

$$P_{NC_f} + P_{mean_i} \approx P_{NC_F} + P_{mean} \approx P_{min}$$

and

$$\frac{P - P_{min}}{P_i - P_{min}} \approx \frac{P - P_{NC_f} - P_{mean}}{P_i - P_{NC_f} - P_{mean_i}}$$

Figure 5-16 shows a typical result of the dimensionless pressure correlation versus $V_o D_o \theta_1 / D_t^2$. The value of θ_1 was taken as zero when the pressure began to decay. The term θ_1 was used rather than time after the mixer began operating since the correlation of $\Delta P / \Delta P_i$ versus $\frac{V_o D_o}{D_t^2} \theta$ in most cases showed a constant pressure or a slight pressure rise for a short time period after the jet was turned on. The correlations of dimensionless temperatures for the closed tanks do not show a similar trend although this was seen in open tank temperature correlations. The discrepancy between the two data trends can be attributed to a combination of several factors.

Some delay in the pressure or temperature decay would be expected after the jet was turned on if for no other reason than the transit time required for the jet to travel from the nozzle outlet to the stratified layer; this is given in

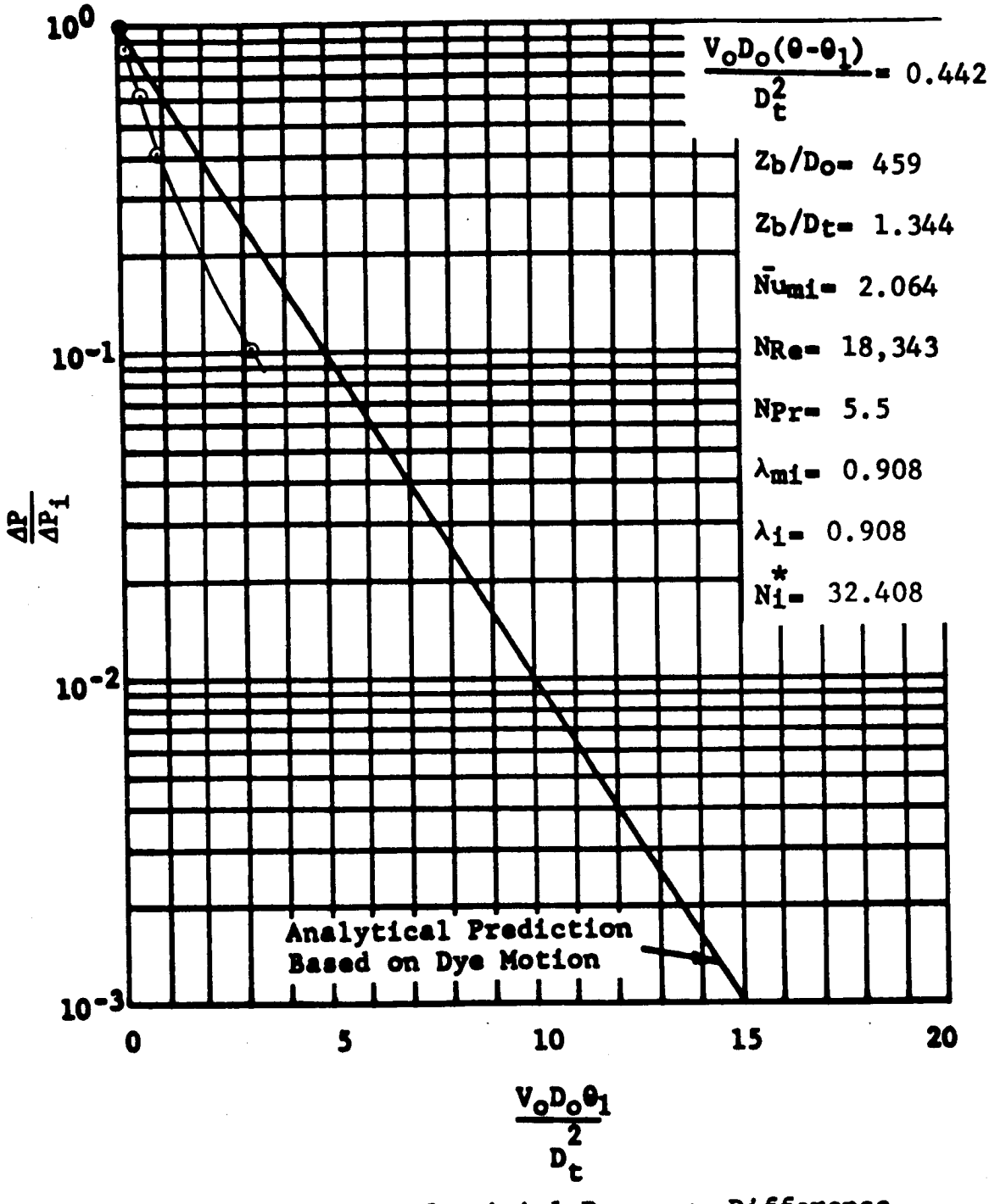

Figure 5-16 Fraction of Initial Pressure Difference After Ullage Pressure Starts to Drop (Pump on at θ=0.0 sec; Ullage Pressure Drops at θ_1=0.0 sec): Test 15, Run 22

dimensionless form as

$$\frac{V_o D_o}{D_t^2} \theta_j = 0.152 \left(\frac{Z_b}{D_t}\right)^2$$

However, subtraction of this term from the value of $V_o D_o \theta / D_t^2$ when the pressure began to decrease usually left a non-zero remainder. Additional time would be required for the jet to erode or penetrate the stratified layer and begin to cool the liquid surface and the ullage. This was a common effect in the open tank tests and is visually shown in the jet penetration section of Reference 36. However, the thickness of the stratified layer was much thinner in the closed tank and required less penetration time. This would significantly reduce the value of $\frac{V_o D_o \theta}{D_t^2}$ at which the surface temperature would begin to decrease and cause a corresponding decay in the ullage pressure.

For comparison, Figure 5-16 also shows the analytical prediction of the bulk fluid motion based on the dye data. In general the pressure decay occurs somewhat faster than this prediction, indicating that the analytical prediction is conservative. The dimensionless parameters shown in Figure 5-16 are the same as described in Section 5.1 except that the term $V_o D_o (\theta - \theta_1)/D_t^2$ is the dimensionless time required for the pressure decay to begin after the jet was turned on.

A representative temperature correlation is shown in Figure 5-17. This correlation is similar to those performed for the open tank tests. The parameters shown are $(T_s-T_b)/(T_s-T_b)_i$ and $(T_s-T_m)/(T_s-T_m)_i$ as a function of $V_oD_o\theta_1/D_t^2$. The term θ_1 is defined as zero when the tank pressure begins to decay. This was used since the length of the data scans precluded any recording of a constant surface temperature after the mixer began operation. This figure also shows the analytical prediction of the bulk fluid motion based on dye data. The temperature decay was, in most cases, much faster than predicted by this curve, again indicating that the analytical prediction is conservative. The rapid drop in temperature reflects the thin stratified layer present in the closed tank tests and consequently the low buoyancy effect.

Figure 5-18 shows a representative correlation of the transient energy integral, I_m, for the closed tank tests. The initial values of I_m were, in all cases, small. As mixing proceeded, the energy distribution rapidly became more uniform and the energy integral often approached a value of 1.0 indicating that the fluid was extremely well mixed. The energy integrals shown in Volume II do not necessarily cover the entire mixing period since temperature differences became too small to

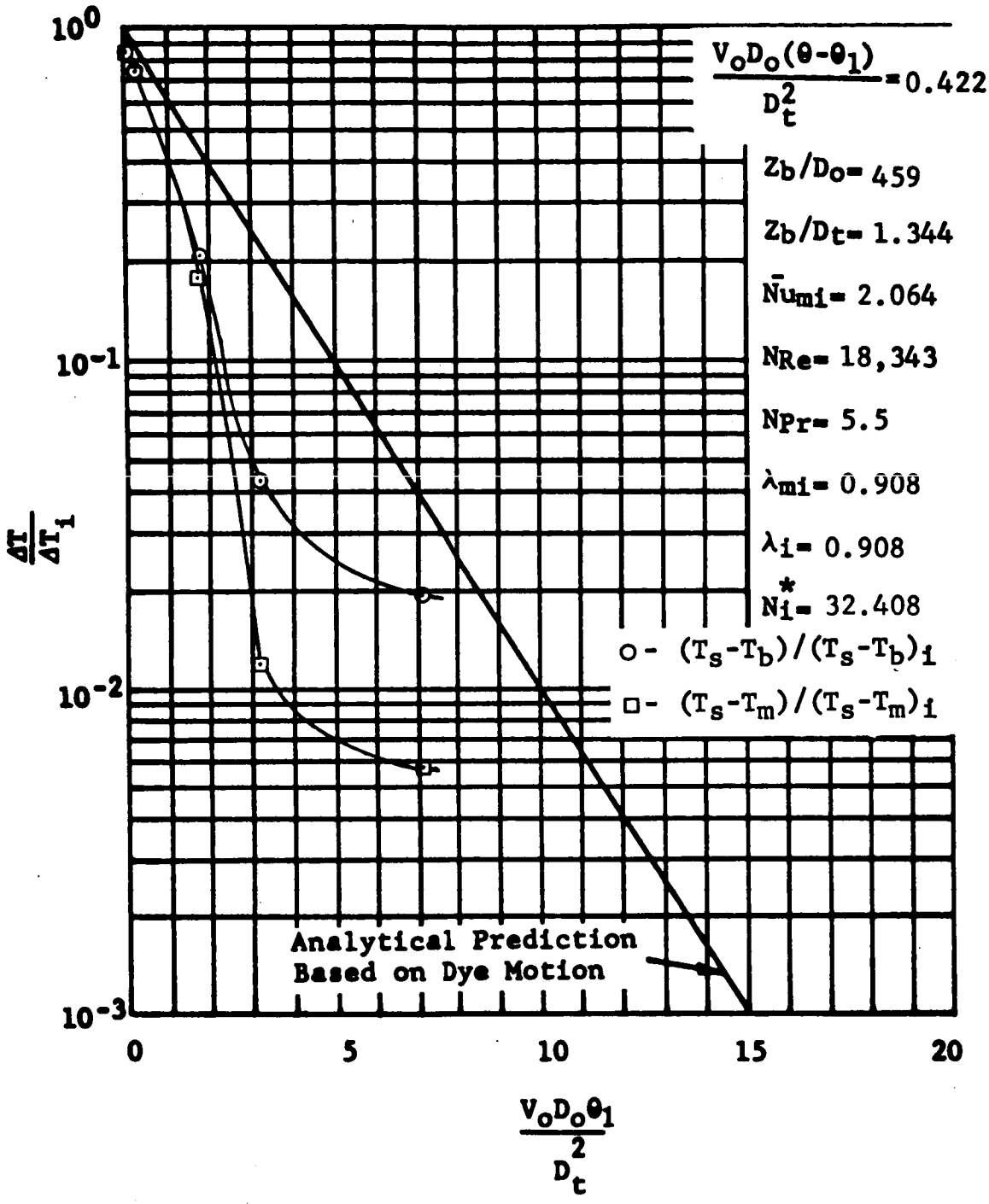

Figure 5-17 Fraction of Initial Temperature Difference After Ullage Pressure Starts to Drop (Pump on at θ=0.0 sec; Ullage Pressure Drops at θ_1=0.0 sec): Test 15, Run 22

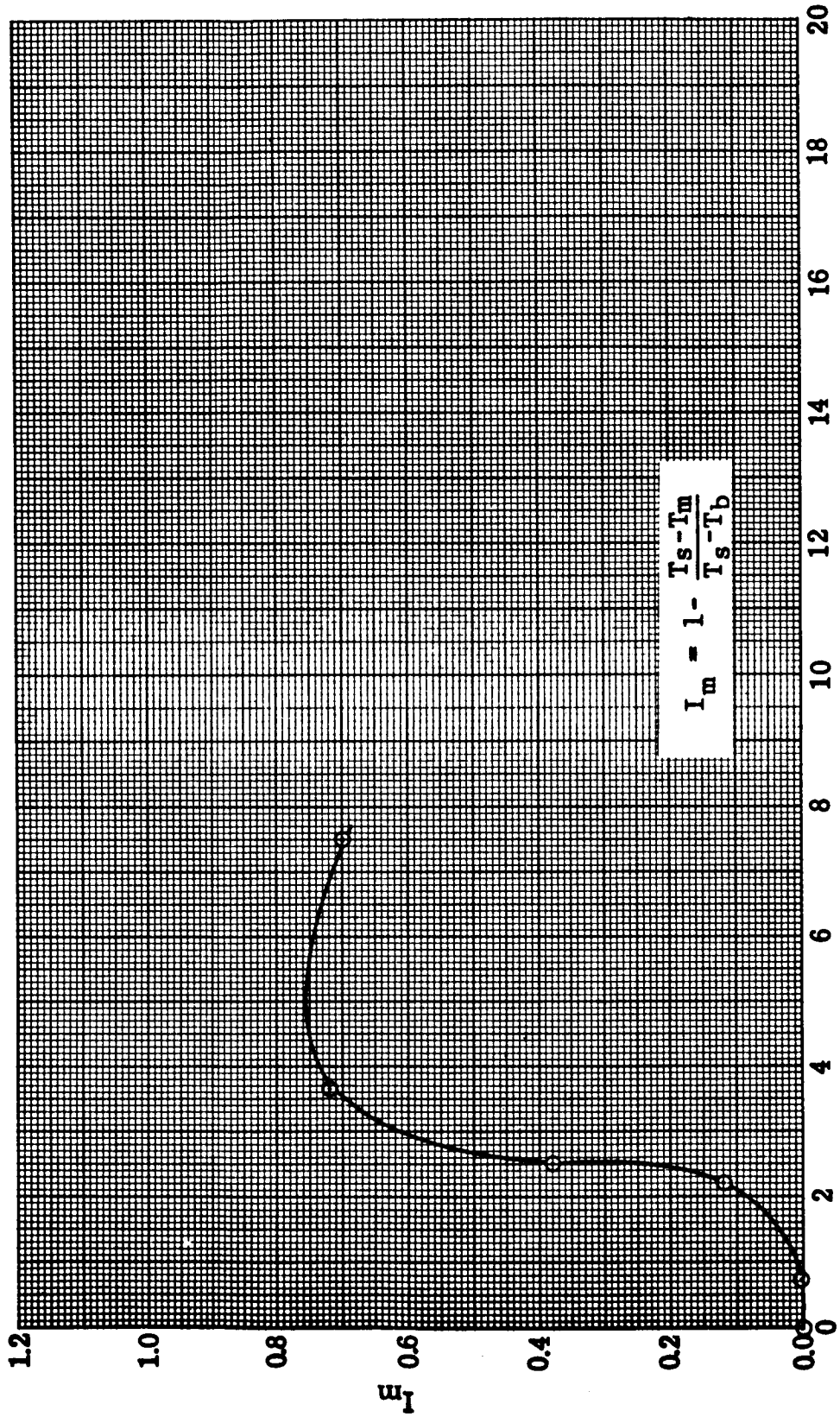

Figure 5-18 Transient Energy Integral: Test 15, Run 22

be accurately measured. Also, surface temperature measurements in some cases fluctuated toward the end of tests precluding good interpolations between data points.

5.4 CLOSED TANK DATA CORRELATIONS

This section presents correlations of the closed tank data using some of the dimensionless parameters described in Section 5-1. The correlations consist of the following:

1. A correlation of the dimensionless time before the ullage pressure begins to decay minus the time it takes the jet to reach the surface, $V_o D_o(\theta-\theta_1-\theta_j)/D_t^2$, as a function of a dimensionless parameter
$$N = \frac{4b^2 N_i^*(I_{m_i}-I_{m_i}^2)}{1 + 2\ I_{m_i}}$$
2. Correlations of the dimensionless time after the ullage pressure begins to decrease until the temperature difference, T_s-T_b, reaches 20, 10, and 5 percent of its initial value as a function of N_i^*
3. Correlations of the dimensionless time after the ullage pressure begins to decay until $\Delta P/\Delta P_i$ reaches 20, 10, and 5 percent of its initial value as a function of N_i^*
4. Correlation of the dimensionless time after the ullage pressure begins to decay until the pressure reaches a minimum value as a function of N_i^*.

Figure 5-19 shows the correlation of the dimensionless time before the ullage pressure begins to decay, less the time

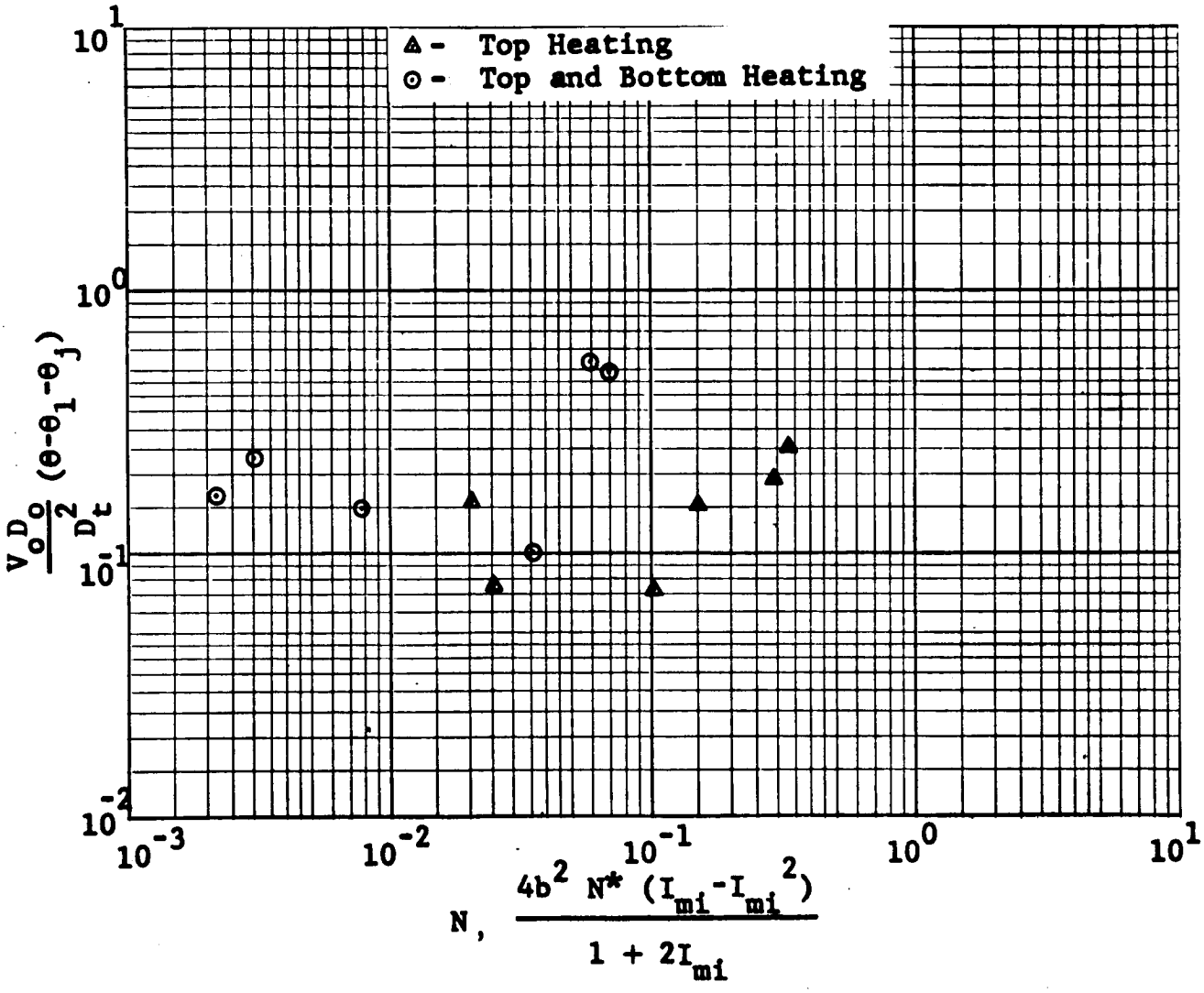

Figure 5-19 Effect of Buoyancy On Mixing Time: Closed Tank Test

it takes the jet to reach the surface, as a function of N. The point at which the ullage pressure began to decay was used as a reference rather than the surface temperature since the closed tank data scans were not short enough in duration to record the rapid initial surface temperature decay. This correlation indicates, that for the range of N_i^* considered in the closed tank tests, the delay in the mixing of the tank due to buoyancy is small. This confirms the theory that the buoyancy effect may be ignored in low-g environments. This data is also shown in combination with the open tank results in Figure 5-7.

Figure 5-20, 5-21, and 5-22 show the dimensionless time, after the closed tank ullage pressure began to decay, required for the temperature difference, T_s-T_b, to decrease to 20, 10 and 5 per cent of its initial value. The data grouping indicates that the dimensionless time required for each fraction of the initial temperature to be obtained is essentially constant for values of $N_i^* < 50$. As the fraction of the initial temperature decreases, the dimensionless time required increases. The data points shown on these figures which are grouped separately from the majority of the data points are for tests with a very sharp initial pressure drop and small pressure recovery. As the fraction of initial temperature

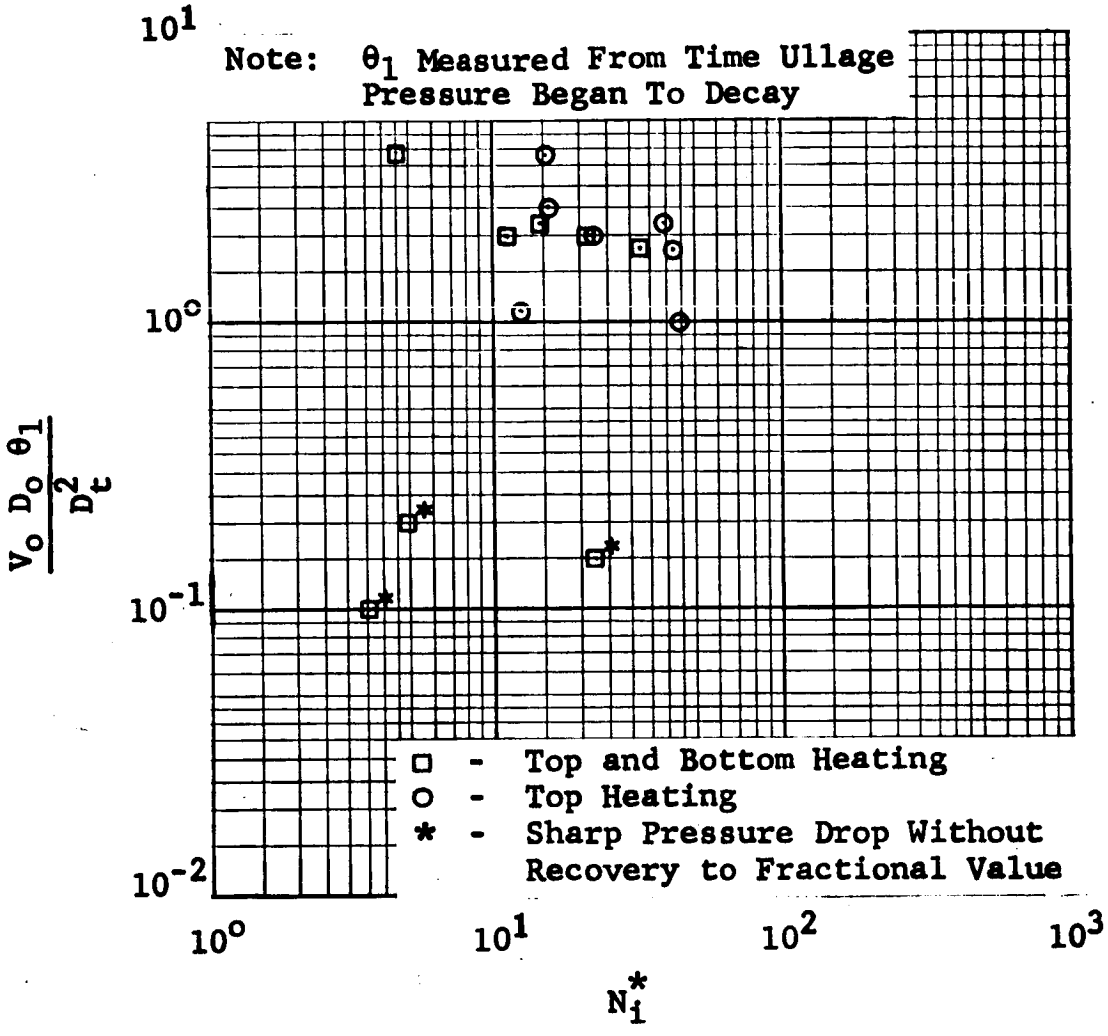

Figure 5-20 Correlation of Dimensionless Time For T_s-T_b To Reach 0.2 of Its Initial Value; Closed Tank Tests

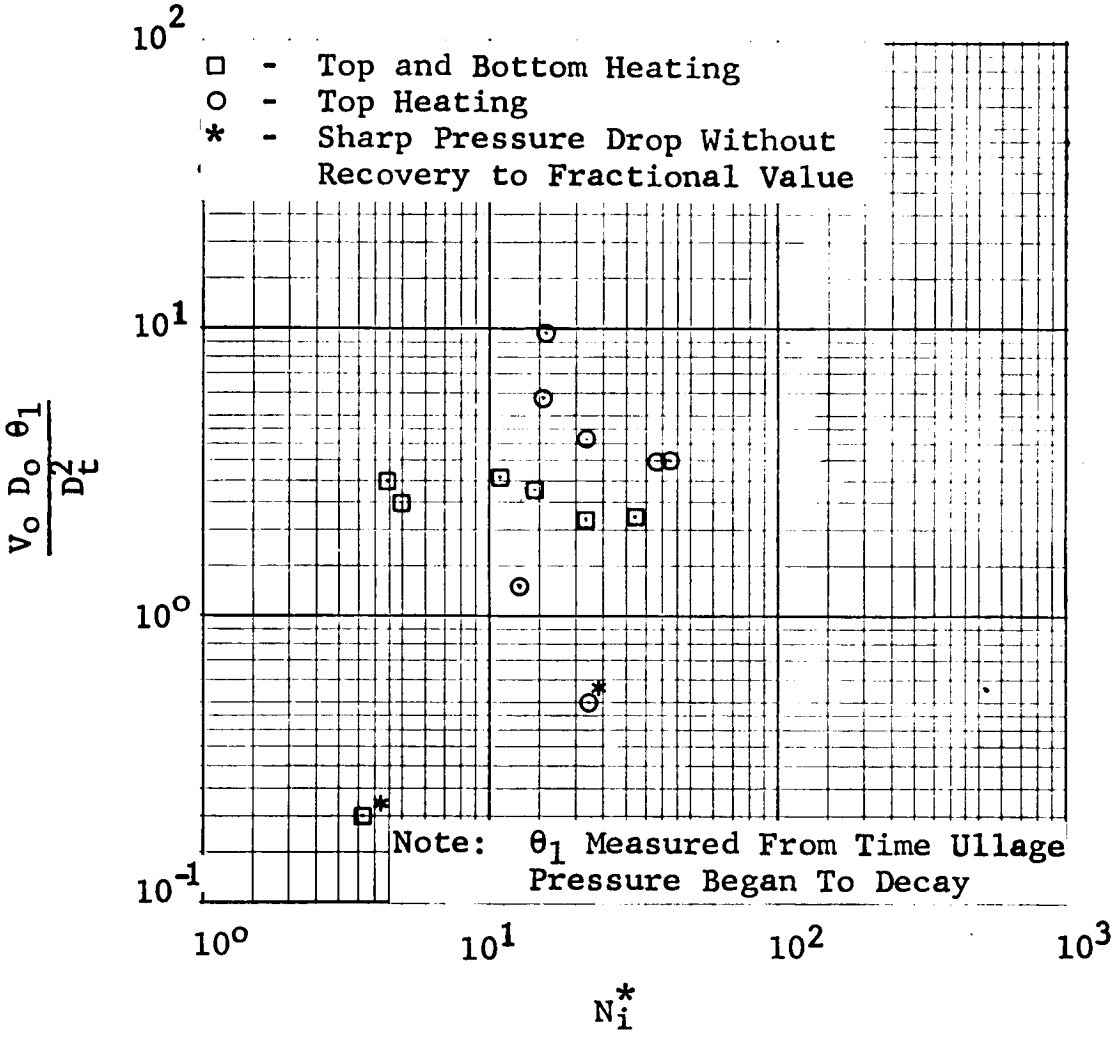

Figure 5-21 Correlation of Dimensionless Time For T_s-T_b To Reach 0.1 of Its Initial Value: Closed Tank Test

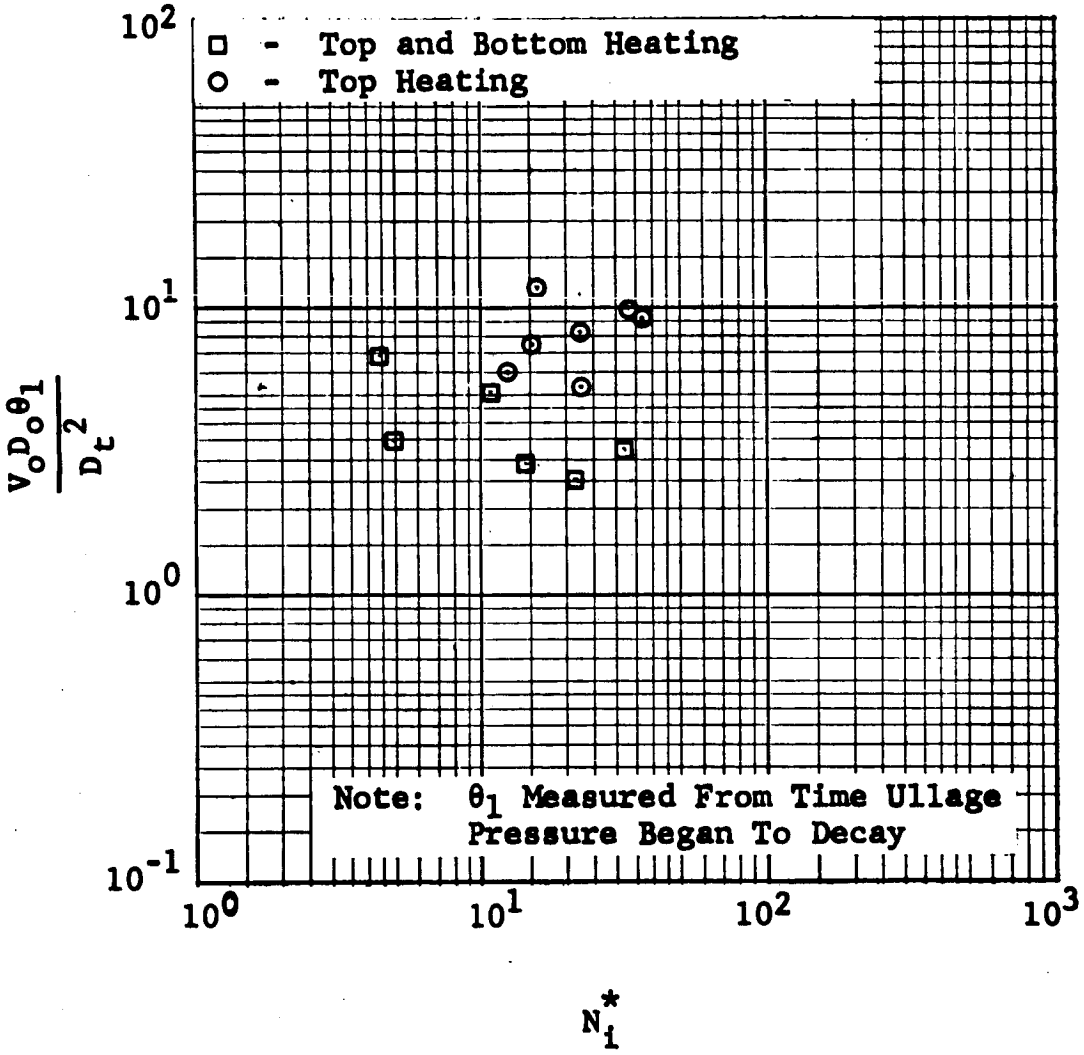

Figure 5-22 Correlation of Dimensionless Time For T_s-T_b To Reach 0.05 of Its Initial Value: Closed Tank Test

difference decreases, these data points begin to follow the general trend. This data expands and has agreement with the open tank data.

Figures 5-23, 5-24, and 5-25 show a correlation of the dimensionless time before the ullage pressure begins to decay, until the pressure drop reaches values of 20, 10, and 5 per cent of the initial pressure difference defined in Section 5.2 as a function of N_i^*. These correlations show that the dimensionless time for the pressure decay to reach each fraction of the initial pressure is essentially constant. As with the temperature correlation, the dimensionless time increases as the pressure fraction decreases. Data points outside the primary groupings are for tests in which the initial sharp pressure drop fell below the pressure fraction for each group and did not recover. This data also indicates that buoyancy effects may be ignored in low-g environments.

Figure 5-26 shows a correlation of the dimensionless time after the ullage pressure begins to decay until the ullage pressure reaches a minimum value. This correlation indicates that the dimensionless time is independent of N_i^*.

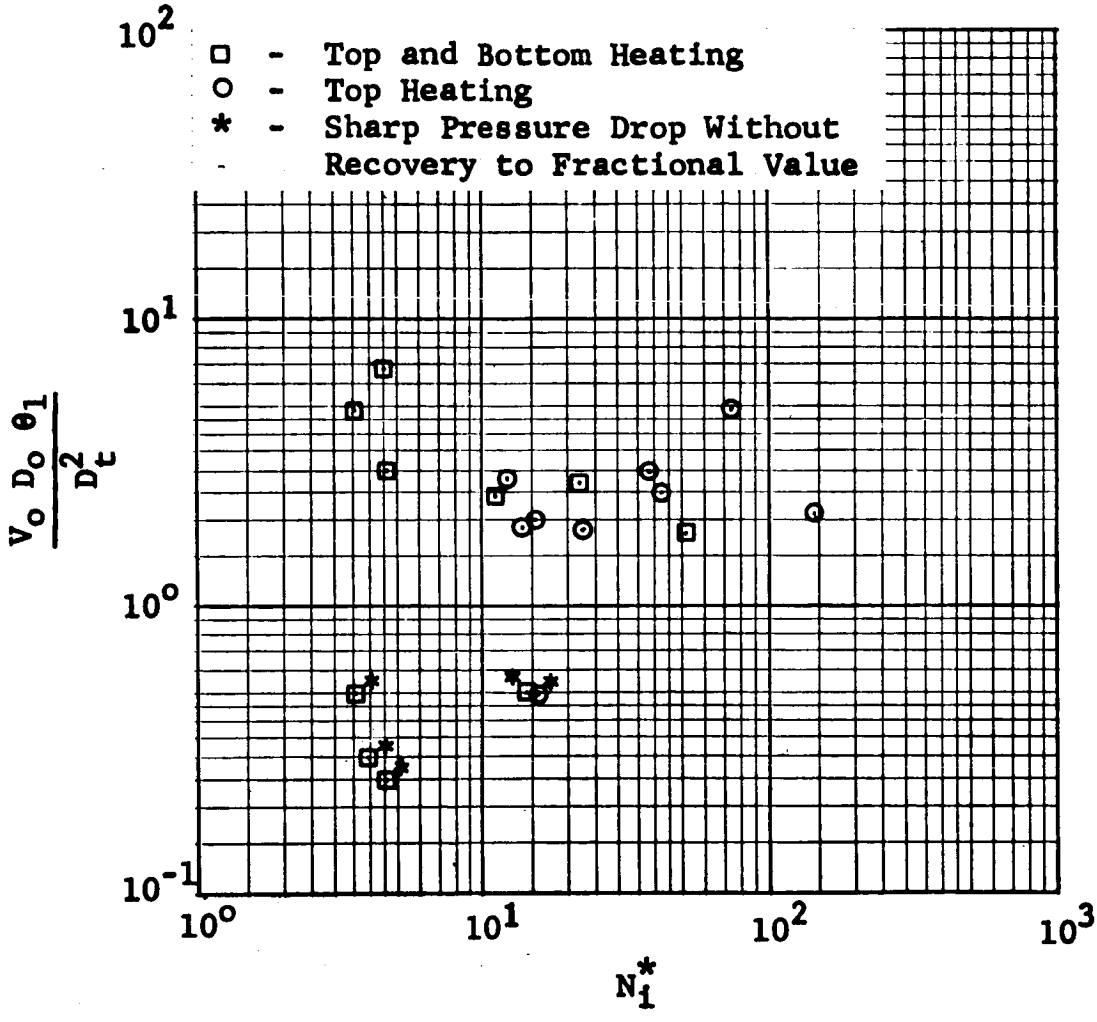

Figure 5-23 Correlation of Dimensionless Time For Ullage Pressure To Reach 0.2 of Its Initial Value: Closed Tank Tests

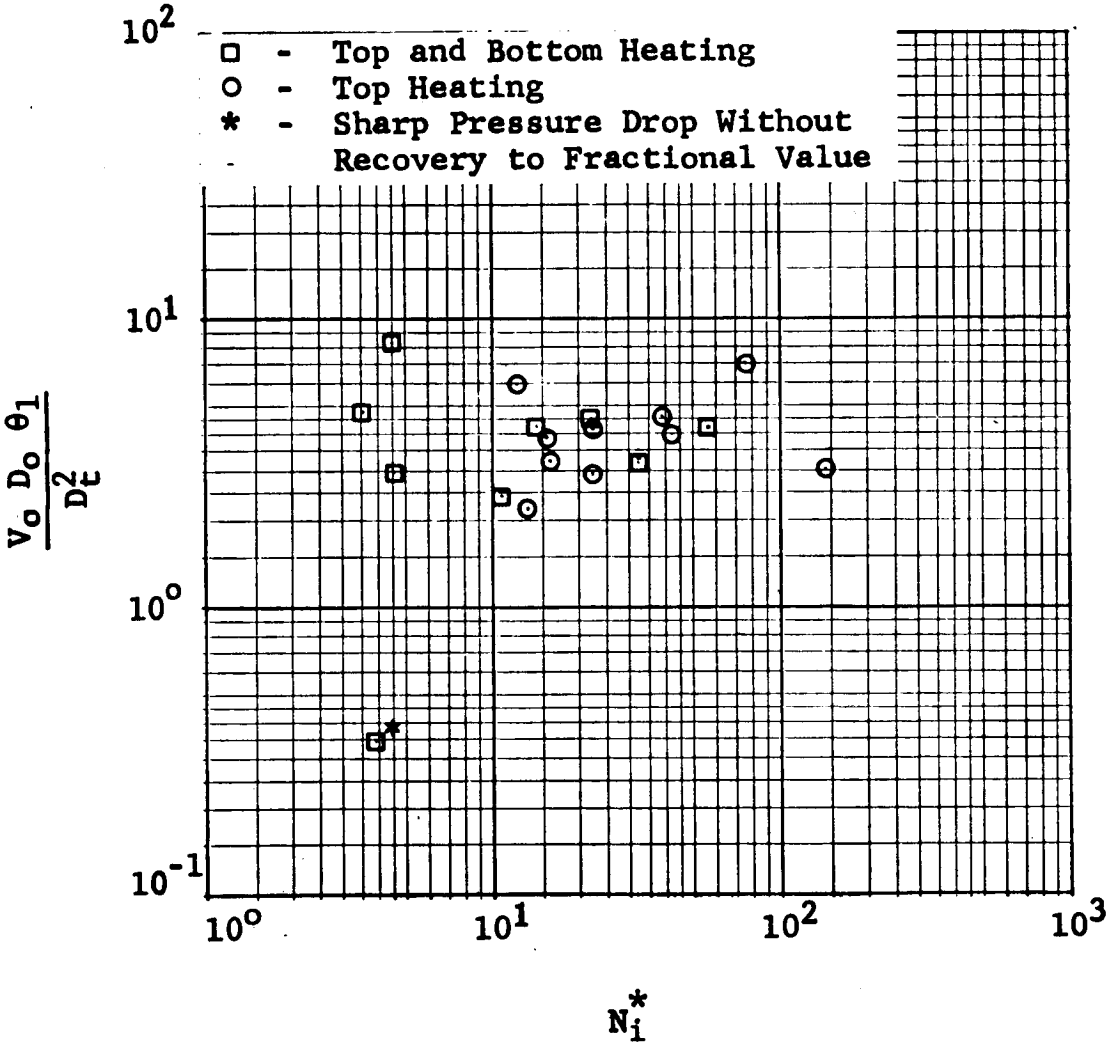

Figure 5-24 Correlation of Dimensionless Time For Ullage Pressure To Reach 0.1 of Its Initial Value: Closed Tank Tests

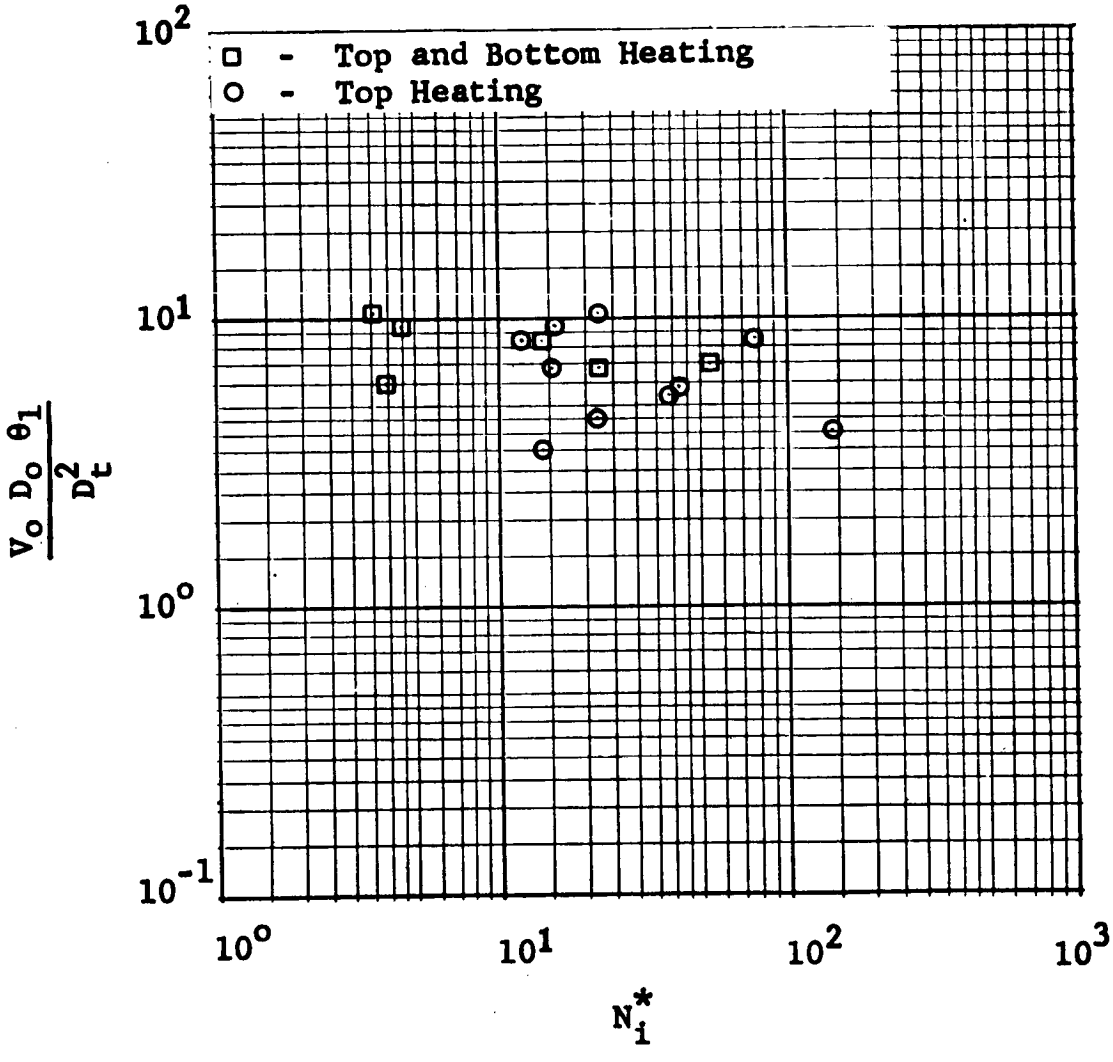

Figure 5-25 Correlation of Dimensionless Time For Ullage Pressure To Reach 0.05 of Its Initial Value: Closed Tank Tests

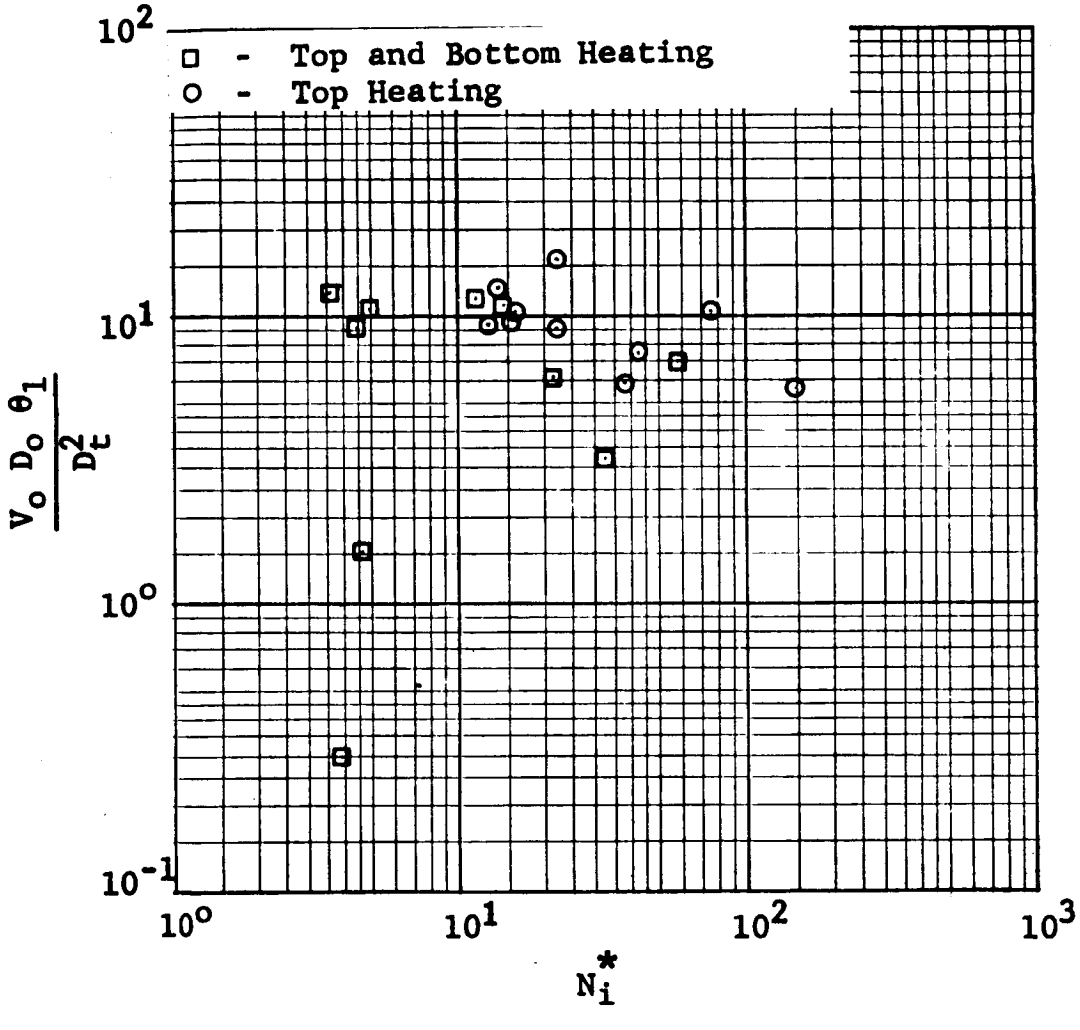

Figure 5-26 Correlation of Dimensionless Time For Ullage Pressure To Reach Its Minimum Value: Closed Tank Tests

SECTION 6

CONCLUSIONS

Principal conclusions derived from the analytical and experimental investigations during this study are as follows:

1. For typical space environments, the cryogenic propellant thermodynamic conditions will depart sufficiently from equilibrium to warrant the use of a mixer for typical modes of storage because of the resulting tank and boiloff weight savings.
2. The use of mechanical mixers (specifically, jet concepts) is feasible. This conclusion is based primarily on weight considerations, since all of the essential factors that determine feasibility are taken into account by the evaluation of the overall weight of the concept.
3. The jet mixing concepts are superior to other mechanical mixing concepts for typical spacecraft conditions primarily because of weight and simplicity.
4. The mixer concept is required for all modes of low-g storage.
5. Because of the discrepancies in mixing time correlations (see Ref. 1), the mixing time should be defined as the time required for

the temperature (or pressure) difference to decay to a specified fraction (e.g., 0.1) of the initial differences. It was found that the fractional difference in temperature is an exponential function of the dimensionless time, $V_o D_o \theta / D_t^2$, and the mixing time varies over a wide range of values depending upon the selected fraction of the initial difference.

6. Mixers should be located at each end of the tank for nonvented storage modes.
7. For the space vehicle mission conditions examined, the stratification process is initially controlled by boiling at the heat shorts (a heat transfer mechanism which typically results from a combination of thermal conduction and evaporation/condensation processes.
8. Ullage de-encapsulation of the mixers requires a more stringent mixer performance criterion than do ullage break-up considerations.
9. The effect of bouyancy on jet-mixing may be neglected under low gravity conditions, whereas under one-g conditions bouyancy effects will establish mixer design criteria for large cryogenic propellant tanks.

10. Mixing, as demonstrated by the test results, was adequately acheived with a tank diameter to mixer outlet diameter ratio as high as 370 (approximately the same ratio as a one inch diameter nozzle in a 32 foot diameter tank).

11. For the vehicle mission case studied, the minimum weight vane-axial pump systems occur at minimum power levels, and minimum power level pumps should be selected for mixing. In addition to weight savings, low flow rates in the tank minimize jet induced sloshing and resulting altitude control weights.

12. Experimental mixing in a pressurized tank indicated that the temperature decay occurred, in general, slightly faster than the pressure decay.

Page intentionally left blank

SECTION 7

RECOMMENDATIONS

The recommendations of this study concerning analytical and experimental investigations and mixer design are given below.

In the case of analytical investigations, the following analyses are recommended:

1. Perform an analysis to investigate the relation between temperature and pressure response (decay) during mixing.
2. Perform a more detailed analysis of boiling at the heat shorts.
3. Perform a detailed analysis of pressure spike during the initial phase of mixing.
4. Perform an analysis of jet induced sloshing, investigate means by which it can be minimized and evaluate the associated weight penalties (due to attitude control reactions).
5. Perform a further ullage breakup analysis which includes the breakup of a bubble moving relative to liquid flow.
6. Perform a detailed analysis of thermal conduction in the tank supports and in the propellant in the

vicinity of the tank supports.

7. Evaluate the heat transfer coefficient in the vicinity of the liquid-vapor interface during mixing.
8. For one-g demonstration tests either with a non-cryogenic or cryogenic fluid, conduct a detailed application of the analysis of the effect of buoyancy on mixing (developed in this study).

In the case of mixer design studies:

1. The mixer operational control system should be refined. For "early" applications, a two-pressure level activation and deactivation method is recommended due to its simplicity and reliability.
2. The required number of duty cycles and stratification development time for two pressure level mixer control should be evaluated. For nonvented storage, the tank contents are not completely mixed when this control technique is utilized since the mixer is always cut off at the final equilibrium pressure (which can be significantly higher than the equilibrium pressure at any time during the mission).
3. In "early" applications of a mixer for propellant thermodynamic condition control, conventional mixers

are recommended since the differential weight penalty for conventional design is slight if the total operating time is not excessive (e.g. less than 500 hours).

4. In addition, consideration should be given to the development of oversized (for desired power-level) vane-axial pumps which typically produce a few watts fluid power and are 4 to 6 inches in diameter. The electric motor would have an operating speed of a few hundred rpm.

5. A cursory investigation should be conducted in order to determine the feasibility of developing an A.C. motor with variable speed control (the pump increases in speed when vapor is ingested), or use of a conventional D.C. motor as an alternative to the yet unproven (to the knowledge of the authors) brushless D.C. motor.

6. An investigation of the mixing requirements during a boost phase of a mission should be conducted. Because of the anticipated large influence of buoyancy effects on mixing, a separate and larger vane-axial mixer is tentatively recommended for such applications.

7. The hydraulic efficiency of vane-axial (or tube axial) mixer with a characteristic high specific speed (e.g. 30,000) should be investigated. It was concluded as part of this study, that the specific speed of a pump used solely for mixing should have a high (as feasible) specific speed within the limitation of reasonably high hydraulic efficiencies.

Recommended further experimental investigations:

1. In addition to drop tower tests of ullage breakup presently being conducted by NASA, drop tower tests of ullage de-encapsulation of a mixer should be conducted.
2. A study of jet induced sloshing should be conducted in small scale low-g simulation tests (limited applicability due to viscous damping) and drop tower tests.
3. Larger scale one-g cryogenic or noncryogenic tank tests (e.g. from 4 to 10 ft in diameter) should be conducted to extend jet mixing performance data. Extreme care should be taken to account for the buoyancy effects (free convection flow currents and jet flow retardation).
4. Initial transients in temperature stratification and initiation of boiling at heat shorts in a simulated

tank should be investigated in drop tower tests.

5. Condensing heat transfer coefficients should be experimentally evaluated for axial jet impingement in the vicinity of the liquid vapor interface.
6. Bubble removal from a heated surface and the resulting bubble motion should be experimentally investigated in small scale bench and/or drop tower tests.
7. An investigation should be conducted to define orbital experiments of stratification and mixing. It is recommended that emphasis be placed on mixing tests by the use of an experiment design philosophy in which mixer performance is tested under severe simulated mission conditions.

REFERENCES

1. Poth, L. J., et al., A Study of Cryogenic Propellant Stratification Reduction Techniques, Annual Report General Dynamics Fort Worth Division Report FZA-419, 15 September 1967.

2. Poth, L. J., et al., A Study of Cryogenic Propellant Stratification Reduction Techniques, Sixth Quarterly Progress Report, FPR-027-17, 15 October 1967.

3. Poth, L. J., et al., A Study of Cryogenic Propellant Stratification Reduction Techniques, Sixth Quarterly Progress Report, FPR-027-20, 15 January 1968.

4. Poth, L. J., et al., A Study of Cryogenic Propellant Stratification Reduction Techniques, Seventh Quarterly Progress Report, FPR-027-23, 15 April 1968.

5. Vliet, G. C., and Brogan, J. T., "Experimental Investigation of the Effects of Baffles on Natural Convection Flow and on Stratification", Proceedings of the Conference on Propellant Tank Pressurization and Stratification, NASA/MSFC, 20-21 January 1965.

6. Neff, B. D., "Investigation of Stratification Reduction Techniques", Proceedings of the Conference on Propellant Tank Pressurization and Stratification, NASA/MSFC, 20-21 January 1965.

7. Pedreyra, D. C., "Stratification Reduction by Means of Bubble Pumps", Propellant Tank Pressurization and Stratification Conference, NASA/MSFC, 20-21 January 1965.

8. Mitchell, R. C., et al., Study of Zero-Gravity Vapor/Liquid Separation, General Dynamics Convair Division Report GDC-DDB65-009, January 1966.

9. Sterbentz, W. H., Liquid Propellant Thermal Conditioning System, Lockheed Missiles and Space Company Report, LMSC-A839783, 20 April 1967.

R E F E R E N C E S (Cont'd)

10. Bradshaw, R. D., et al., Propellant Thermodynamic Behavior, General Dynamics Convair Division Report GDC-ERR-4N-1039, December 1966.

11. Harper, E. Y., et al., "Analytical and Experimental Study of Stratification in Standard and Reduced Gravity Fields", Proceedings of the Conference of Propellant Tank Pressurization and Stratification, NASA/MSFC, 20-21 January 1965.

12. Sterbacek, Z., and Taush, P., Mixing in the Chemical Industry, Pergamon Press, London, 1965.

13. Hyman, D. J., Advances in Chemical Engineering, March, 1962.

14. Van De Vusse, J. G., "Mixing by Agitation of Miscible Liquids", Chemical Engineering Science, 4, 1955, 178-200, 209-220.

15. Weber, A. P., "Selecting Propeller Mixers", Chemical Engineering, September 1963.

16. Fossett, H., Prosser, L. E., Proc. Instn. Mech. Engrs., Vol. 160, 224, 1944.

17. Fox, E. A., and Gex, V. E., AIChE Journal, 2, (1956), 539.

18. Uhl, V. W., and Gray, J. B., Mixing Theory and Practice, Academic Press, New York.

19. Harper, E. Y., et al., "Theoretical and Experimental Studies of Zero-G Heat Transfer Modes", Lockheed Missiles and Space Company Quarterly Progress Report, 7 September 1965.

20. Holmes, L. A., and Schwartz, S. H., "The Thermodynamics of Space Storage of Liquid Propellants", Proceedings of Institute of Environmental Sciences, Volume II, April 1967.

R E F E R E N C E S (Cont'd)

21. Evaluation of AS-203 Low-Gravity Orbital Experiment, Chrysler Corporation Technical Report HSM-R421-67, 13 January 1967.

22. Vliet, G. C., et al., "Stratified Layer Flow Model -- A Numerical Approach to Temperature Stratification in Liquids Contained in Heated Vessels", AIAA Preprint No. 64-37, Aerospace Sciences Meeting, New York, 20-22 January 1964.

23. Barnett, D. O., Winstead, T. W., and McReynolds, L. S., "An Investigation of LH_2 Stratification in a Large Cylindrical Tank of Saturn Configuration", Paper U-12, 1964 Cryogenic Engineering Conference, Philadelphia, August 1964.

24. Tatom, J. W., et al., "Analysis of Thermal Stratification in Rocket Propellant Tanks", Advances in Cryogenic Engineering, Vol. 9, Plenum Press, New York, 1964.

25. Barakat, H. Z., "Transient Laminar Free Convection Heat and Mass Transfer in Two-Dimensional Closed Containers Containing Distributed Heat Source", Proceedings of the Conference on Propellant Tank Pressurization and Stratification, Vol. II, NASA/MSFC, 20 January 1965.

26. Barakat, H. Z., and Clark, J. A., "Analytical and Experimental Study of the Transient Laminar Natural Convection Flow in Partially Filled Liquid Containers", Proceedings of the Third International Heat Transfer Conference, Volume II, Chicago, Illinois, 9 August 1966.

27. Neff, R., "A Survey of Stratification in Cryogenic Liquid", Advances in Cryogenic Engineering, Vol. 5, Plenum Press, New York, 1959.

28. Tatum, J. W., and Carlson, W. O., "Transient Turbulent Free Convection in Closed Containers", Proceedings of the Third International Heat Transfer Conference, Vol. II, Chicago, Illinois, 7-12 August 1966.

R E F E R E N C E S (Cont'd)

29. Liebenberg, D. H., and Edeskuty, F. J., "Pressurization Analysis of a Large Scale Liquid-Hydrogen Dewar", International Advances in Cryogenic Engineering, Vol. 10, University of California, Los Alamos Scientific Laboratory, Los Alamos, New Mexico, 1964.

30. Robbins, J. H., and Rogers, A. C., "An Analysis on Predicting Thermal Stratification in Liquid Hydrogen", Paper 64-426, AIAA Meeting, Washington, D. C., 29 June 1964.

31. Goodwin, D. W., et al., Thermal Protection Systems for Cryogenic Propellant on Interplanetary Space Vehicles, General Dynamics Fort Worth Division Report FZA-416, 21 September 1966.

32. Barry, D. G., et al., Parametric Study of Optimized Liquid-Hydrogen Thermal Protection Systems For Nuclear Interplanetary Spacecraft, General Dynamics Fort Worth Division Report FZA-434, 31 August 1968.

33. Modular Nuclear Vehicle Study Phase II, Vol. III, Nuclear Propulsion Module-Vehicle Design, Lockheed Missiles and Space Company, LMSC-A830246, 1 March 1967.

34. Extraterrestrial Reliquefaction of Cryogenic Propellant, Marquardt Corporation Report No. 6099, 11 December 1965.

35. Satterlee, H. M. and Hollister, M. P., Engineers Handbook Low-G Propellant Behavior, Lockheed Missiles and Space Company Report LMSC-A874831, 15 May 1967.

36. Documentary Film, A Study of Cryogenic Propellant Stratification Reduction Techniques, General Dynamics Fort Worth Division, October 1968.

37. Kreith, Frank, Principles of Heat Transfer, International Textbook Company, Scranton, Pennsylvania, 1961.

38. Schlichting, Herman, Boundary Layer Theory, McGraw-Hill Book Company, Inc., New York, 1960.

R E F E R E N C E S (Cont'd)

39. Hyman, D. J. Advances in Chemical Engineering, 3, 1962

40. Personal Communication from G. H. Caine, Pesco Products, to L. J. Poth, General Dynamics Fort Worth Division, 1968.

41. Stark, J. A. et al., Study of Zero-Gravity Vapor-Liquid Separator, Second Monthly Progress Report, General Dynamics Convair Division Report 584-4-4, 9 September 1966.

42. Caine, G. H., and Pradhan, A. V., Pumps or Fans For Destratification of Liquid and Gas, Pesco Products Report 0-5, 28 July 1967.

A P P E N D I X

APPENDIX A

JET MOTION EQUATIONS

The time required for the jet to reach the liquid/vapor (as shown in the sketch below) and the initial bulk fluid flow to begin are given in dimensionless form below

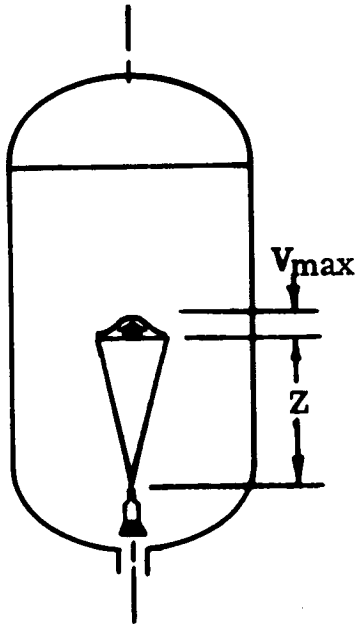

The maximum velocity of the jet is (Ref. 38)

$$V_{max} = 6.57 \frac{V_o D_o}{Z}$$

Assuming

$$\frac{dZ}{d\theta} = V_{max}$$

Hence

$$\frac{V_o D_o \theta_j}{D_t^2} = 0.076 \left(\frac{Z_b}{D_t}\right)^2$$

The experimental data in Section 5 indicated that the actual dimensionless time is twice that predicted, or

$$\frac{V_o D_o \theta_j}{D_t^2} = 0.152 \left(\frac{Z_b}{D_t}\right)^2$$

SYMBOLS AND ABBREVIATIONS

D_o	Nozzle diameter, ft
D_t	Tank diameter, ft
V_o	Velocity of the fluid at the nozzle, ft/sec
V_{max}	Jet Centerline velocity, ft/sec
Z	Axial distance, ft
Z_b	Distance from the nozzle to the liquid/vapor interface, ft
θ_j	Time for an axial jet to reach the liquid/vapor interface, sec

APPENDIX B

SUMMARY OF EQUATIONS FOR BULK FLUID MOTION IN TANK

The equations for bulk fluid motion are given for both the convex and concave bulkheads for various tank regions. The convex bulkhead is shown below

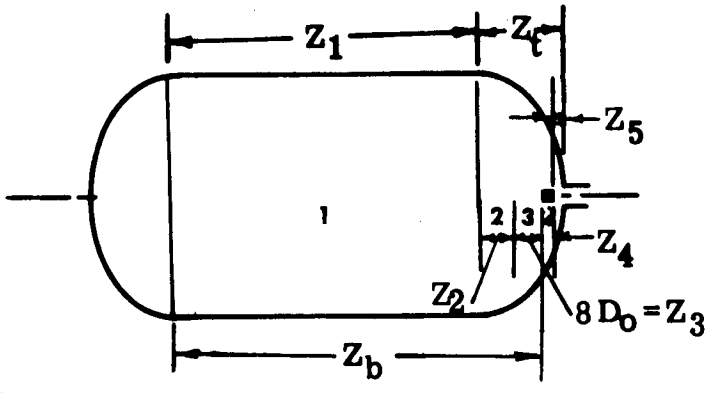

The dimensionless time required for a fluid particle to move from Z_1 to Z_t, neglecting jet area, is

$$\frac{V_o D_o \theta_1}{D_t^2} = 2.193 \ln \frac{Z_1+Z_t-Z_4-Z_5}{Z_t-Z_4-Z_5}$$

The dimensionless time required for a fluid particle to move from Z_1 to Z_t Region 1, including jet area, is

$$\frac{V_o D_o \theta_1}{D_t^2} = 2.193 \left\{ \ln \left[\frac{Z_1+Z_t-Z_4-Z_5}{Z_t-Z_4-Z_5} \right] - 2b^2 \left(\frac{Z_1+Z_t-Z_4-Z_5}{D_t} \right)^2 \left[1-\left(\frac{Z_1+Z_t-Z_4-Z_5}{Z_t-Z_4-Z_5} \right)^2 \right] \right\}.$$

The dimensionless time in Region 2 (from Z_t to $8D_o$) is

$$\frac{V_o D_o \theta_2}{D_t^2} = 2.193 \left[1-(1-Z_4^*-Z_5^*)^2\right] \ln\left[\frac{Z_t(1-Z_4^*-Z_5^*)}{8D_o}\right] + 1.5\,(1-Z_4^*-Z_5^*)^2 + \frac{1}{2}\left(\frac{8D_o}{Z_t}\right)^2 - 16\,\frac{D_o}{Z_t}\,(1-Z_4^*-Z_5^*)$$

where

$$Z^* = \frac{Z}{Z_t}$$

In Region 3, assuming a mass flow rate ratio of $\dot{m}/\dot{m}_o = 1 + 0.331\ Z/D_o$ in region between $Z/D_o = 0$ to $Z/D_o = 8$, the dimensionless time is

$$\frac{V_o D_o \theta_3}{D_t^2} = 3.9099 - 169.7\left(\frac{D_o}{Z_t}\right)^2 + 146.04\left[\left(\frac{D_o}{Z_t}\right)^2 + 0.331\,(1-Z_4^*-Z_5^*)\frac{D_o}{Z_t}\right] - 35.687\left[\frac{D_o}{Z_t} + 0.331\,(1-Z_4^*-Z_5^*)\right]^2$$

In Region 4, below the nozzle, the dimensionless time is

$$\frac{V_o D_o \theta_4}{D_t^2} = \frac{Z_t}{D_o}\left[Z_4^* + \frac{1}{3}\,(1-Z_4^*-Z_5^*)^3 - \frac{1}{3}\,(1-Z_5^*)^3\right]$$

For a concave bulkhead

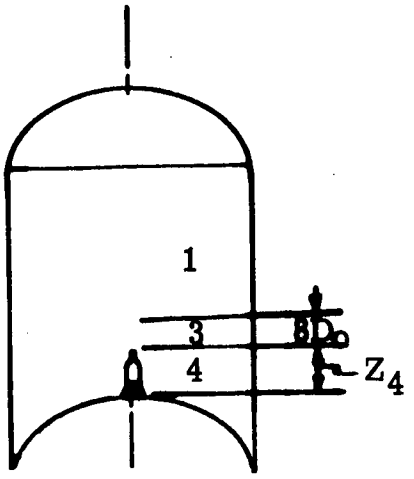

Region 1 is the same as for the convex bulkhead.

Region 2 does not exist for the concave bulkhead.

In Region 3 for a straight tank section, the dimensionless time is

$$\frac{V_o D_o \theta_3}{D_t^2} = 3.91$$

and in Region 4, below the nozzle

$$\frac{V_o D_o \theta_4}{D_t^2} = \frac{Z_4}{D_o}$$

SYMBOLS AND ABBREVIATIONS

b	Slope at which an axial turbulent jet spreads
D_o	Nozzle diameter, ft
D_t	Tank diameter, ft
$\dot{m}$	Mass flow rate, lbm/sec

$\dot{m}_o$ Nozzle mass flow rate

V_o Velocity of the fluid at the nozzle, ft/sec

Z Axial distance

Z_b Distance from the nozzle top to the liquid/vapor interface, ft

Z_t Distance from the bottom of the ellipsoidal tank bottom to the junction of the ellipsoidal tank bottom and the cylindrical tank wall, ft

Z_1 For a convex tank bottom, distance from the liquid/vapor interface to the junction of the cylindrical tank wall and the convex ellipsoidal tank bottom; or for a concave tank bottom, the distance from the liquid/vapor interface to 8 D_o above the nozzle, ft

Z_2 Distance from the junction of the cylindrical tank wall and the ellipsoidal tank bottom to 8 D_o above the nozzle, ft

Z_3 Distance from 8 D_o above the nozzle to the nozzle top, ft

Z_4 Distance from the nozzle top to the bottom of the mixer, ft

Z_5 Distance from the bottom of the mixer to the tank bottom, ft

Z^* Dimensionless axial distance, Z/Z_t

Z_1^* Dimensionless axial distance, Z_1/Z_t

Z_2^* Dimensionless axial distance, Z_2/Z_t

Z_3^* Dimensionless axial distance, Z_3/Z_t

Z_4^* Dimensionless axial distance, Z_4/Z_t

Z_5^* Dimensionless axial distance, Z_5/Z_t

θ_1 Time for a fluid particle to traverse Z_1, sec

θ_2 Time for a fluid particle to traverse Z_2, sec

θ_3 Time for a fluid particle to traverse Z_3, sec

θ_4 Time for a fluid particle to traverse Z_4, sec

APPENDIX C

FLOW IN THE VICINITY OF THE LIQUID/VAPOR INTERFACE

Under a high Bond number condition the jet flow decelerates as it approaches the liquid/vapor interface. It is assumed that the thickness of this region is on the order of the jet thickness, δ. The jet thickness increases with the distance from the nozzle exit as shown below:

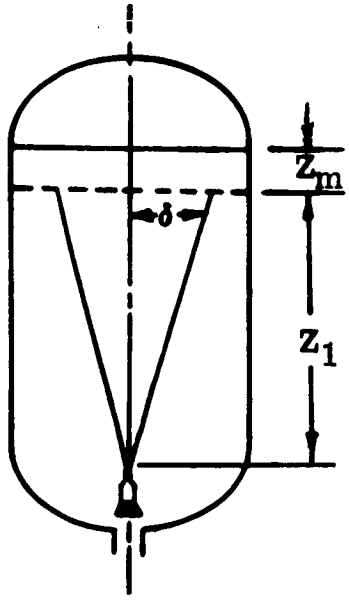

The equation for the jet thickness is

$$\delta = bZ = bZ_1 = Z_m$$

where b is usually around 0.25.

The region of interest, in dimensionless form, is within the axial distance below the interface of

$$0 < Z_m^* < 0.25$$

where

$$Z_m^* = Z_m/Z_1$$

When the jet is turned on, a transient flow occurs which causes a particle, a distance of Z_m from the interface, to move toward the interface as shown below:

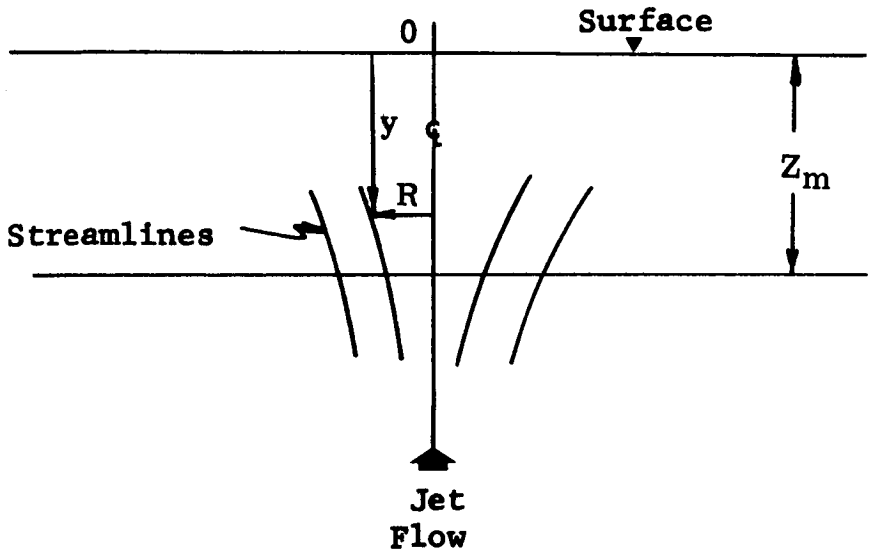

In a potential flow region the flow velocities of the particle are given as

$$V_R = C_1 R$$

and

$$V_Y = -2C_1 y$$

where C_1 is a constant determined by the flow entering this region. In addition, the velocities, V_R and V_Y, are related to the stream function, ψ , by

$$V_Y = \frac{1}{R} \frac{\partial \psi}{\partial R}$$

and

$$V_R = -\frac{1}{R}\frac{\partial \psi}{\partial Y}$$

Integrating the above equations yields

$$\psi = -C_1 R^2 y$$

this confirms the expressions for the velocities.

The mass flow rate across the section in the first sketch bounded by the dashed line is

$$\dot{m} = \rho V_y \pi R^2$$

The jet mass flow rate from Reference 1 can be equated to this mass flow rate and the value of the constant C_1 determined

$$\dot{m} = \rho V_y \pi R^2 = 0.456Z\ \dot{m}_o/D_o$$

$$2C_1 y \rho \pi R^2 = 0.456Z\, \pi D_o^2 V_o \rho / 4D_o$$

$$C_1 = 0.456Z\ V_o D_o / 8yR^2$$

The expression for the movement of a particle initially entering the region and moving to very near the liquid/vapor interface can now be found. Choosing the expression for the axial velocity

$$V_y = dy/d\theta = -2yC_1$$

and integrating yields

$$\frac{y}{y_o} = e^{-2C_1\theta}$$

where y_o can be assumed to be equal to δ .

The streamline selected for integration (the path the particle follows) is determined by the selection of y. The selection of $y = y_o = \delta = R$ and $R = bZ$ yields

$$C_1 = \frac{0.456\ V_o D_o}{8b^3\ D_t^2}\left(\frac{D_t}{Z_1}\right)^2$$

Substitution of the expression for C_1 into the expression for y/y_o and $b = 0.25$ yields

$$\frac{y}{y_o} = e^{-16\ \theta^*(D_t/Z_1)^2}$$

where θ^* is a dimensionless time

$$\theta^* = 0.456\ V_o D_o \theta / D_t^2$$

With the above assumptions, the particle movement in the vicinity of the interface is given by

$$\frac{y}{\delta} = e^{-16\ \theta^*(D_t/Z_1)^2}$$

For the value of $D_t/Z_1 = 0.5$, this expression reduces to

$$\frac{y}{\delta} = e^{-4\theta^*}$$

For typical open tank water tests performed in this study, the stratification layer thickness was about 10 per cent of the axial distance above the nozzle. Consequently, the use of $b = 0.1$ and $D_t/Z_1 = 0.5$ are appropriate for these tests. Hence for $V_o D_o \theta / D_t^2 = 0.1$

$$y = 0.058\delta$$

As an example, when $\delta = 2.4$ inches, the particle has moved to within 0.13 inches of the interface.

SYMBOLS AND ABBREVIATIONS

b	Slope at which an axial turbulent jet spreads
C_1	Flow constant, $0.456ZV_oD_o/8yR^2$, 1/sec
D_o	Nozzle diameter, ft
D_t	Tank diameter, ft
$\dot{m}$	Mass flow rate into stratified layer, lbm/sec
$\dot{m}_o$	Jet mass flow rate at the nozzle, lbm/sec
R	Radial distance from the centerline of the axial jet, ft
V_R	Radial velocity of a fluid particle, ft/sec
V_y	Axial velocity of a fluid particle, ft/sec
y	Axial distance from the liquid/vapor interface, ft
y_o	Axial diatance from the liquid/vapor interface to the bottom of the mixing region, ft
Z	Axial distance, ft
Z_m	Axial distance from the liquid/vapor interface to the bottom of the mixing region, ft
Z_1	Distance from the bottom of the mixing region to the nozzle, ft
Z_m^*	Dimensionless axial distance, Z_m/Z_1
δ	Radius of the turbulent jet, ft
θ	Time after the mixer is turned on, sec

θ^* Dimensionless mixing time, $0.456\ V_o D_o \theta / D_t^2$

ρ Fluid density, lbm/ft^3

ψ Stream function, ft^2/sec

APPENDIX D

MEAN JET TEMPERATURE

An important phenomena associated with axial jet mixing is the relation between the mean jet temperature and the mean bulk temperature. It will be shown that the mean jet temperature and the bulk temperature at any level above the nozzle are identical if the following conditions are present:

1. The jet region considered is not in the immediate vicinity of an interface or tank wall.
2. The tank environment is such that buoyancy forces do not affect jet motion.
3. The jet outlet is located very near the tank bottom.
4. The dominate stratification takes place in the axial direction.

As a result of the assumption that the mean temperature of the jet and the bulk fluid at any section are identical, the jet fluid reaching the interface region is very near the mixed or mean temperature. In fact, it is possible that the mean jet temperature reaching the interface will be below the mean bulk temperature due to the lack of fluid

entrainment near the interface. The sketch shown below illustrates the jet and bulk fluid motion regions

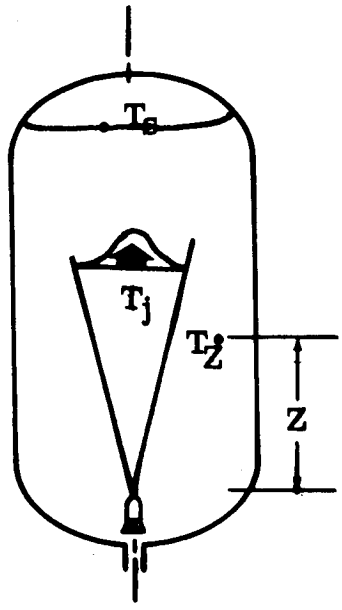

From page 161, Reference 1, the mean jet temperature is

$$T_j = T_b + \frac{T_s - T_b}{P+1} \left(\frac{Z}{Z_b}\right)^P$$

When the bulk temperature is

$$T_Z = T_b + (T_s - T_b) \left(\frac{Z}{Z_b}\right)^P$$

eliminating $(T_s - T_b)(Z/Z_b)^P$ from the equation for T_j yields

$$T_j = T_b + \frac{(T_Z - T_b)}{P+1}$$

The energy integral is

$$I = \frac{1}{P+1}$$

The mean bulk temperature from Z = 0 to any point Z is

$$T_m = T_b + \frac{(T_Z - T_b)}{P+1}$$

or

$$T_m = T_b + I\,(T_Z - T_b)$$

By comparison of the equation for the mean bulk temperature with that of the jet it can be seen that the mean bulk temperature is the same as the mean jet temperature.

SYMBOLS AND ABBREVIATIONS

I	Energy integral, 1/P+1
P	Exponent related to the energy distribution in the tank
T_b	Temperature at the nozzle, ^oR
T_j	Temperature of the jet, ^oR
T_m	Mean bulk fluid temperature, ^oR
T_Z	Temperature of the fluid outside the jet at an axial distance Z, ^oR
Z	Axial distance, ft

APPENDIX E

SUMMARY OF THE EQUATIONS FOR TRANSIENT TEMPERATURE DECAY DURING MIXING

The results are given for the case of a thin initial stratified layer whose thickness is less than or equal to that of a mixing region in the neighborhood of the interface. Four tank regions are defined as shown below

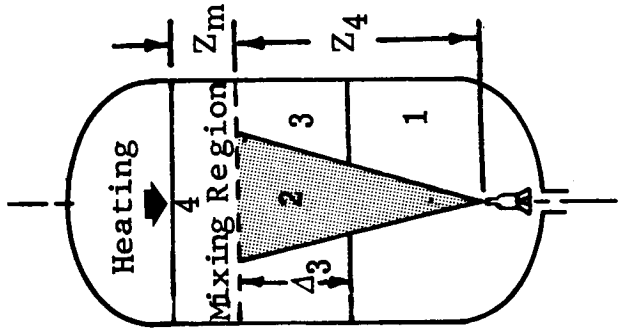

Region 1 is of uniform bulk temperature, T_{bi}. Region 2 consists of the axial jet. The mean temperature of the jet below Region 3 is uniform and equal to that of the surrounding bulk temperature T_{bi}. Region 3 does not exist initially. Region 3 grows according to a mass balance at the lower interface between Region 1 and 3. As Region 3 grows with time the mean jet temperature increases such that the jet temperature entering Region 4 is equal to the mean bulk fluid temperature below the mixing region.

Initially the stratified layer thickness is assumed to be of depth, Z_m. In actuality, if the stratified layer is less than Z_m, an initial energy integral, I_{4i}, can be appropriately defined such that

$$I_{4i} = \frac{T_{m4i} - T_{bi}}{T_{si} - T_{bi}}$$

Heating of the liquid is assumed to occur during mixing either as a result of external heat inputs or due to vapor condensation at the interface. An overall energy balance in Region 4 and 3 yields

$$\Delta_1 (T_s - T_{bi}) I_3 + Z_m (T_s - T_{bi}) I_4 = Z_m (T_s - T_{bi}) I_{4i} + \frac{\dot{Q}\,\theta}{\rho C_p A}$$

An energy balance in Region 4 yields

$$Z_m \frac{d\left[I_4 (T_s - T_{bi})\right]}{d\theta} = \left[(T_s - T_{bi}) I_3 \Delta_1 - Z_4 (T_s - T_{bi})\right] C^* + \frac{\dot{Q}}{\rho C_p A}$$

where

$$C^* = 0.456 \frac{V_o D_o}{D_t^2}$$

The two energy equations can be non-dimensionalezed such that

$$\Delta_1^* = \Delta_1/Z_4$$

$$T_s^* = (T_s-T_{bi})/(T_s-T_b)_i$$

$$\theta^* = C^*\theta = 0.456\,\frac{V_o D_o \theta}{D_t^2}$$

$$\dot{Q}^* = \frac{\dot{Q}}{(Z_4)(T_s - T_b)_i\, C_P\, A\, C^*}$$

The results are

$$\Delta_1^*\, T_s^*\, I_3 + Z_m^*\, T_s^*\, I_4 = Z_m^*\, I_{4i} + \dot{Q}^*\theta^* \qquad (1)$$

and

$$Z_m^*\,\frac{d(I_4 T_s^*)}{d\theta^*} = T_s^*\, I_3\, \Delta_1^* - T_s^* + \dot{Q}^* \qquad (2)$$

Also the mean temperature is

$$T_m = T_{bi} + \frac{(T_s-T_b)_i\, I_4 Z_m^*}{1 + Z_m^*} + \frac{(T_s-T_b)_i\, \dot{Q}^*\, \theta^*}{1 + Z_m^*}$$

or in dimensionless form

$$\frac{T_m-T_{bi}}{(T_s-T_b)_i} = \frac{I_4\, Z_m^*}{1 + Z_m^*} + \frac{\dot{Q}^*\theta}{1 + Z_m^*}$$

Using Equation 1 to solve for T_s^* yields

$$T_s^* = \frac{Z_m^* I_{4i}}{\Delta_1^* I_3 + Z_m^* I_4} + \frac{\dot{Q}^* \theta^*}{\Delta_1^* I_3 + Z_m^* I_4}$$

From the bulk fluid motion

$$\Delta_1^* = 1 - e^{-\theta^*}$$

For no heating, $\dot{Q}^* = 0$

$$T_s^* = \frac{Z_m^* I_{4i}}{\Delta_1^* I_3 + Z_m^* I_4}$$

As $\theta^* \longrightarrow \infty$, $\Delta_1^* \longrightarrow 1.0$

$$T_s^* = \frac{Z_m^* I_{4i}}{I_3 + Z_m^* I_4}$$

A significant parameter is the dimensionless temperature difference between the surface temperature, T_s, and the mean temperature T_m. This represents the amount of temperature drop (related directly to pressure drop) than can still be achieved by further mixing or more vigorous mixing. The dimensionless mean temperature difference is

$$\frac{T_s - T_m}{(T_s - T_b)_i} = \frac{Z_m^* I_{4i}}{\Delta_1^* I_3 + Z_m^* I_4} + \frac{\dot{Q}^* \theta^*}{\Delta_1^* I_3 + Z_m^* I_4} - \frac{I_{4i} Z_m^*}{1 + Z_m^*} - \frac{\dot{Q}^* \theta^*}{1 + Z_m^*}$$

or for initial conditions when $\theta^* = 0$ and $\Delta_1^* = 0$,

$$\frac{(T_s - T_m)_i}{(T_s - T_b)_i} = \left[\frac{1 + Z_m^* (1-I_4)}{1 + Z_m^*}\right] \frac{I_{4i}}{I_4}$$

or

$$\frac{T_s - T_m}{(T_s - T_m)_i} = \frac{I_4}{1 + Z_m^* (1-I_4)} \left[\frac{1 - \Delta_1^* I_3 + Z_m^* (1-I_4)}{\Delta_1^* I_3 + Z_m^* I_4}\right] \left[Z_m^* - \frac{\dot{Q}^* \theta^*}{I_{4i}}\right]$$

The above equation holds for I_3 and I_4 when they are either constant or functions of time. If I_3 and I_4 are assumed to be constant during mixing, the dimensionless temperature decay can be obtained from the above equation. For I_3, I_4 and I_{4i} approaching 1.0, the above equation yields

$$\frac{T_s - T_m}{(T_s - T_m)_i} = \frac{(1-\Delta_1^*)}{\Delta_1^* + Z_m^*} \left(Z_m^* - \dot{Q}^* \theta^*\right)$$

Since $\Delta_1^* = 1 - e^{-\theta^*}$

$$\frac{T_s - T_m}{(T_s - T_m)_i} = \frac{e^{-\theta^*}}{(1 + Z_m^* - e^{-\theta^*})} \left(Z_m^* - \dot{Q}^* \theta^*\right)$$

If I_3 and I_4 are not assumed to be constant, two more independent equations are required. Equation 2 is the only one readily available. The simultaneous solution of Equations 1 and 2 yields (assuming $I_4 = I_{4i}$)

$$T_s^* = \frac{Z_m^* I_4}{1 + Z_m^* I_4} + \left[\frac{1}{1 + Z_m^* I_4} - \frac{\dot{Q}^*}{(1 + Z_m^* I_4)^2}\right] e^{-\theta^*\left(1+\frac{1}{I_4 Z_m^*}\right)}$$

$$+ \frac{\dot{Q}^*}{1 + Z_m^* I_4}\left(\frac{1}{1 + Z_m^* I_4} + \theta^*\right)$$

and

$$\frac{(T_s - T_m)_i}{(T_s - T_b)_i} = \frac{Z_m^* I_4 (1 + Z_m^* - 1 - Z_m^* I_4) + (1 + Z_m^* I_4)}{(1 + Z_m^* I_4)(1 + Z_m^*)}$$

and the dimensionless difference between the surface and mean temperature is

$$\frac{T_s - T_m}{(T_s - T_m)_i} = \frac{1}{(Z_m^* I_4 Z_m^* (1-I_4) + 1 + Z_m^* I_4)}\left\{(Z_m^* I_4 + \dot{Q}^*\theta^*)(Z_m^*(1-I_4))\right.$$

$$\left. + (1+Z_m^*)\left[\left(1 + \frac{\dot{Q}^*}{1 + Z_m^* I_4}\right)\exp\left(-\theta^*\left(1 + \frac{1}{Z_m^*} I_4\right)\right) + \frac{\dot{Q}^*}{1+Z_m^* I_4}\right]\right\}$$

SYMBOLS AND ABBREVIATIONS

A	Area, ft^2
C*	Mixing constant, $0.456\ V_oD_o/D_t^2$, 1/sec
C_p	Specific heat at a constant pressure, Btu/lbm ^oF
D_o	Nozzle diameter, ft
D_t	Tank diameter, ft
I_3	Energy integral for mixing region 3
I_4	Energy integral for mixing region 4
I_{4i}	Initial energy integral for mixing region 4
$\dot{Q}$	Heat input to the tank, Btu/hr
$\dot{Q}^*$	Dimensionless heat input, $Q/Z_4C_pAC^*(T_s-T_b)_i$
T_b	Bulk fluid temperature, ^oR
T_{bi}	Initial bulk fluid temperature, ^oR
T_m	Mean fluid temperature, ^oR
T_{m4i}	Initial mean fluid temperature of mixing region 4, ^oR
T_s	Surface temperature, ^oR
T_{si}	Initial surface temperature, ^oR
T_s^*	Dimensionless surface temperature, $(T_s-T_{bi})/(T_s-T_b)_i$
V_o	Nozzle exit velocity, ft/sec
Z_m	Mixing region thickness, ft
Z_m^*	Dimensionless mixing region thickness, Z_m/Z_4

Z_4 Axial distance between mixing region and nozzle exit, ft

Δ_1 Thickness of region 1, ft

Δ_3 Thickness of region 3, ft

Δ_1^* Dimensionless thickness of region 1, Δ_1/Z_4

θ Time, sec

θ^* Dimensionless mixing time, $0.456\ V_o D_o \theta / D_t^2$

ρ Density, lbm/ft^3

Subscripts

i Initial

APPENDIX F

EFFECT OF BUOYANCY ON MIXING

Three equations are given which describe the effect of buoyancy on the penetration of a stratified fluid by an axial jet. Reference 39 gives the outlet diameter required to produce mixing as

$$V_o > \left(40 g \beta (T_s - T_b) Z\right)^{1/2}$$

An analytical expression is derived in Reference 1/ for the jet penetration of a stratified layer in terms of the centerline jet velocity without stratification

$$\frac{V_{max}}{V'_{max}} = \left[1 - \frac{4b^2 P N^*}{(P+1)(P+3)}\right]^{1/2}$$

where

$$N^* = g\beta \frac{(T_s - T_b) Z^3}{(V_o D_o)^2}$$

Substituting $I_m = 1/P+1$ in the above equation yields

$$\frac{V_{max}}{V'_{max}} = \left(1 - N\right)^{1/2}$$

where

$$N = \frac{4b^2 N^* (I_m - I_m^2)}{1+2I_m}$$

It can be seen that as N⟶1, the centerline velocity⟶0.

A third expression has been derived to estimate the distance, h_m, that the jet will initially penetrate a stratified layer. The sketch below illustrates the physical situation:

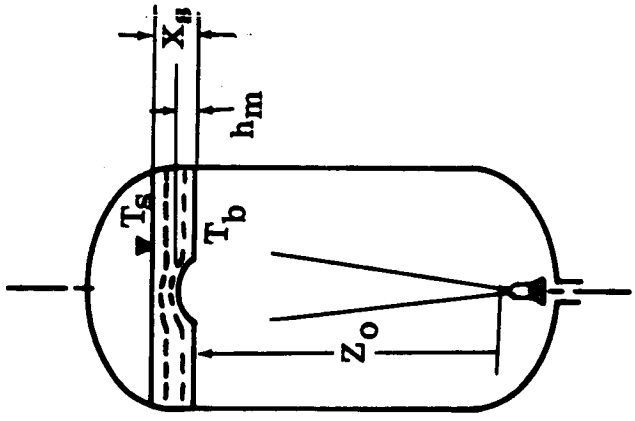

The resulting equation is

$$h_m/X_s = \frac{(P+1)(P+2)}{4b^2 N_o^*} (Z_o/X_s)^{1/P+1}$$

where

$$N_o^* = g\beta \frac{(T_e - T_b) Z_o^3}{(V_o D_o)^2}$$

The required depth of penetration can be selected as the stratified layer depth and the jet outlet momentum in terms of $V_o D_o$ can be calculated.

SYMBOLS AND ABBREVIATIONS

b	Slope at which axial turbulent jet spreads
D_o	Nozzle diameter, ft
g	Acceleration, ft/sec^2
h_m	Initial penetration of a stratified layer by the jet, ft
I_m	Energy integral, $1/P+1 = 1 - \frac{T_s - T_m}{T_s - T_b}$
N	$4b^2 N^* (I_m - I_m^2) / 1+2I_m$
N^*	$g \beta (T_s - T_b) Z_o^3 / (V_o D_o)^2$
P	Exponent related to the energy distribution in the tank
T_b	Temperature of the bulk fluid, ^oR
T_s	Surface temperature, ^oR
V_{max}	Centerline velocity, ft/sec
V'_{max}	Centerline velocity of the jet without heating, ft/sec
V_o	Nozzle exit velocity, ft/sec
X_s	Thickness of stratified region, ft
Z	Axial distance, ft
Z_o	Distance from the nozzle top to the bottom of the stratified region, ft
β	Thermal coefficient of expansion, $1/^oF$

APPENDIX G

SUMMARY OF ULLAGE ENCAPSULATION EQUATIONS

Mixer design criteria associated with ullage encapsulation has been divided into three categories (See Reference 4). The three criteria developed for de-encapsulation of the mixer by a vapor jet are

1. Liquid/vapor interface breakup
2. Bubble motion induced
3. Bubble detachment from the tank wall

These three conditions are illustrated below

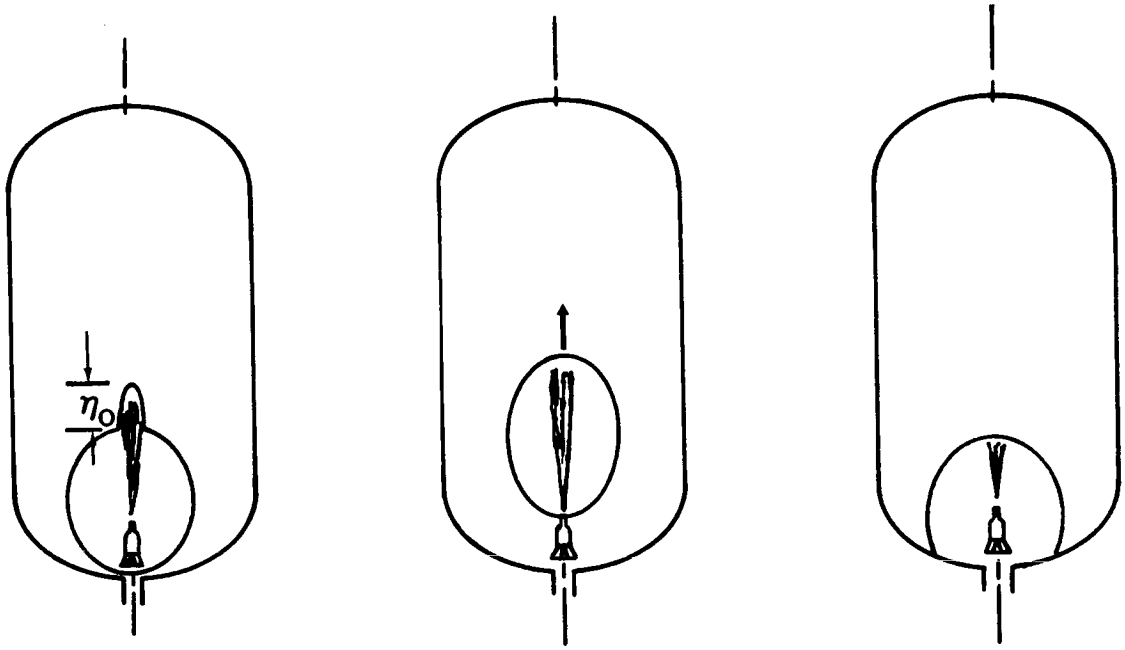

Vapor Jet Penetration of Interface

Bubble Motion After Jet is Turned On

Bubble Detachment

The following equation describes the criterion for vapor penetration of the liquid/vapor interface:

$$\frac{\eta_o}{D_b}\left[1+\frac{4B_* g_c\ \sigma}{(\rho_\ell-\rho_v)gD_b^{\,2}}\right]^{1/2}\left(\frac{\pi}{2K_2^{\,2}}\right)^{1/2}=\left[\frac{\rho_v(V_oD_o)^2}{4(\rho_\ell-\rho_v)g\eta_o^{\,3}}\right]^{1/2}$$

for $\eta_o = D_b$, $K_2 = 6.5$, $B_* = 125$.

The mixer fluid power-outlet diameter product is

$$P_oD_o = 1.7\text{x}10^{-4}\ \rho_i\left[\frac{\rho_\ell}{\rho_v}\ gD_b^{\,3}\left(1+\frac{500\sigma g_c}{\rho_\ell\, gD_b^{\,2}}\right)\right]^{3/2}$$

where $\rho_i = \rho_\ell$ if the pump does not speed up when vapor is ingested. The vapor power requirement is given by setting $\rho_i = \rho_v$.

The above equation can be simplified for

$$\frac{\rho_\ell\ gD_b^{\,2}}{\sigma\, g_c} = N_{Bo_b} < 5.0$$

and results in the following expression for the mixer fluid power-outlet diameter product.

$$P_oD_o = 1.9\ \rho_i\left(\frac{D_b}{\rho_v}\ g_c\sigma\right)^{3/2}$$

The differential equation for bubble motion (derived in Reference 4) is

$$\frac{d^2x}{d\theta^2} = \frac{\rho_v}{\rho_\ell}\left(\frac{V_o D_o}{D_b^3}\right)^2 - 2g$$

No motion occurs when

$$\frac{2g\rho_\ell D_b^3}{3\rho_v (V_o D_o)^2} < 1.0$$

The dimensionless time based on liquid flow conditions required to move the bubble one bubble diameter from the mixer is

$$\frac{V_o D_o \theta_e}{D_t^2} = \left[\frac{\frac{2}{3}\frac{\rho_\ell}{\rho_v}\left(\frac{D_b}{D_t}\right)^4}{1 - \frac{1.394\rho_\ell^{5/3} D_b^3 g}{\rho_v (P_{o\ell} D_o)^{2/3} g_o}}\right]^{1/2}$$

If the pump cannot speed up when vapor is injected, bubble motion takes place only if

$$P_{o\ell} D_o > \left(\frac{1.394\rho_\ell^{5/3} D_b^3 g}{\rho_v g_o}\right)^{3/2}$$

The dimensionless time based on $V_o D_o$ of the liquid and in terms of both liquid flow power and vapor fluid power is

$$\frac{V_o D_o \theta_e}{D_t^2} = \frac{\left(\frac{\rho_\ell P_{o\ell}}{\rho_v P_{ov}}\right)^{1/3} \left[\frac{2}{3} \frac{\rho_\ell}{\rho_v} \left(\frac{D_b}{D_t}\right)^4\right]^{1/2}}{\left[1 - \frac{1.394\ \rho_\ell D_b^3\ g}{\rho_v^{1/3} (P_{ov} D_o)^{2/3} g_o}\right]^{1/2}}$$

Motion takes place only if

$$P_{ov} D_o > \left(\frac{1.394 \rho_\ell D_b^3\ g}{\rho_v^{1/3}\ g_o}\right)^{3/2}$$

The derivation of the bubble detachment from the tank wall is given in Reference 4. The mixer fluid power-outlet diameter product based on liquid power is

$$P_{o\ell} D_o > 0.132\ \rho_\ell \left(\frac{g_c D_t \sigma}{\rho_v}\right)^{3/2}$$

The vapor power-outlet diameter product is

$$P_{ov} D_o > 0.132\ \rho_v \left(\frac{g_c D_t \sigma}{\rho_v}\right)^{3/2}$$

SYMBOLS AND ABBREVIATIONS

B_* Constant = 125

D_b Bubble diameter, ft

D_o Nozzle diameter, ft

g Acceleration, ft/sec^2

g_c Constant = 32.2 lbm-ft/lb$_f$-sec^2

g_o Acceleration of gravity, ft/sec^2

K_2 Constant = 6.5

N_{Bo_b} Bubble Bond number, $\rho R_b^2 \bar{g}/\bar{g}_c \sigma$

P_o Fluid power, watts

P_{o_ℓ} Fluid power for pumping liquid, watts

P_{ov} Fluid power for pumping vapor, watts

q_w Heat flux at the tank wall, Btu/hr-ft^2

R_b Bubble radius, ft

r_t Tank radius, ft

T_w Wall temperature, ^oR

V_o Velocity of the fluid at the nozzle, ft/sec

ρ_i Density, lbm/ft^3

ρ_ℓ Density of the liquid, lbm/ft^3

ρ_v Density of the vapor, lbm/ft^3

σ Surface tension, lb$_f$/ft

η_o Height of jet penetration above bubble, ft

θ Time, sec

θ_e Time required to move a bubble a distance of one bubble diameter from the mixer, sec

APPENDIX H

TANK WALL HEAT TRANSFER DURING MIXING

The dimensionless temperature difference between the tank wall (T_w) and the bulk fluid (T_b) is shown in Figure A-1 as a function of the dimensionless distance above the nozzle and the fluid power-outlet diameter product for liquid hydrogen. The predictions are based on the heating of a flat plate under turbulent flow conditions. The temperature difference in the vicinity of the mixer ($Z/Z_b < 0.04$) is greater than one degree Rankine. For this reason mixers are placed in each end of the tank.

SYMBOLS AND ABBREVIATIONS

T_b	Bulk fluid temperature, ^oR
T_w	Tank wall temperature, ^oR
Z	Axial distance above nozzle, ft
Z_b	Axial distance between nozzle and liquid/vapor interface, ft

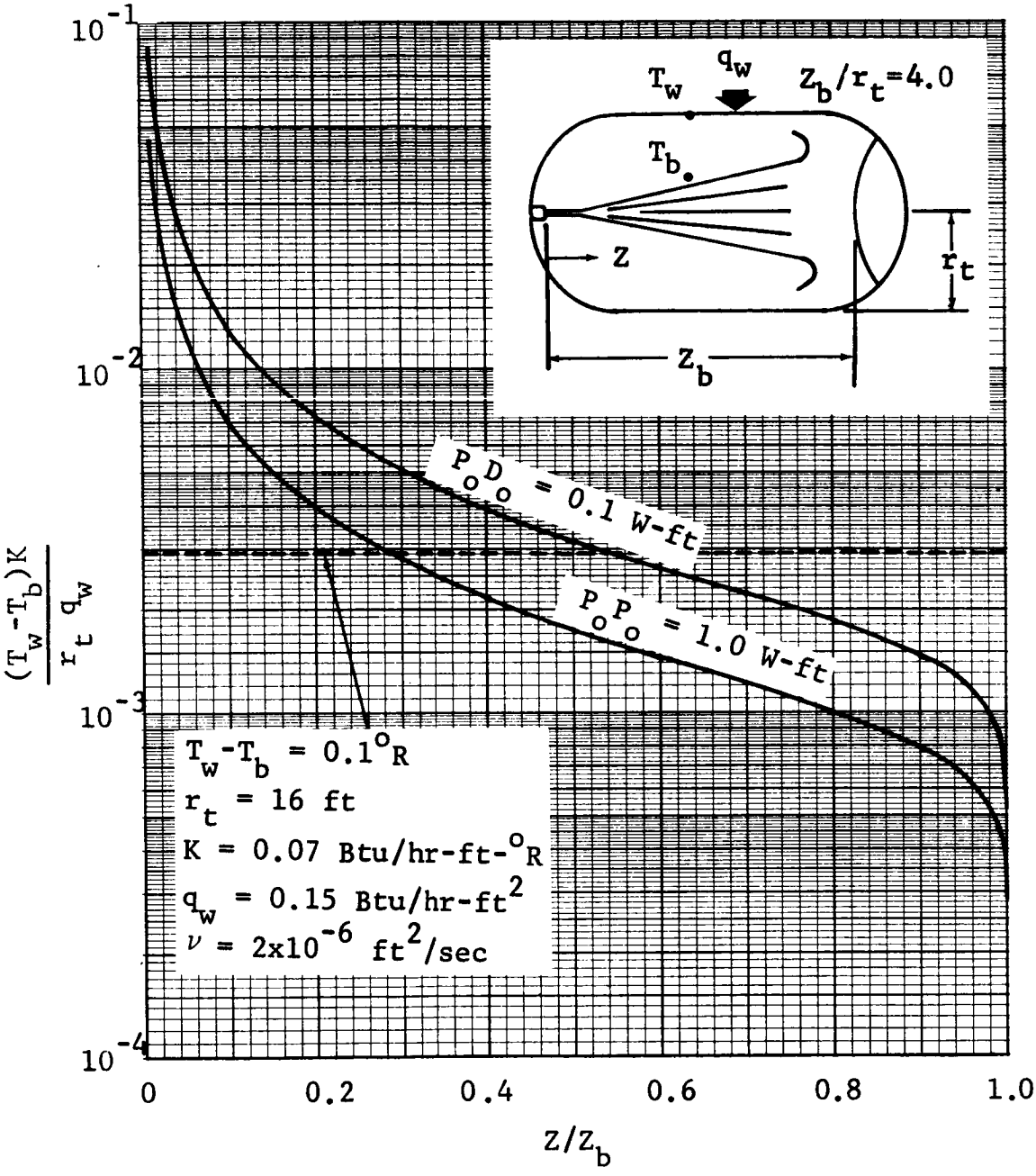

Figure A-1 Dimensionless Temperature Difference at LH_2 Tank Wall During Mixing

APPENDIX I

AXIAL FLOW PUMP CHARACTERISTICS

One of the basic characteristic parameters associated with pump design and applications is the specific speed. The specific speed, N_s, is defined in this study as

$$N_s = \frac{(n,\ \text{rpm})\ (G,\ \text{gpm})^{1/2}}{(H,\ \text{feet})^{3/4}}$$

The specific speed as defined is dimensionless but an inconsistent set of units are used.

A constant to account for unit conversion yields a consistent definition of the specific speed, N_s, the specific speed thus defined is

$$N_s' = N_s/2815$$

where

$$N_s' = \frac{(\Omega,\ \text{rad/sec})\ (G,\ \text{ft}^3/\text{sec})^{1/2}}{(gH,\ \text{ft}^2/\text{sec}^2)^{3/4}}$$

N_s' is used when analytical derivations were required. The results are presented in terms of N_s by the use of the appropriate conversion constant, 2815.

The specific speed characterizes the type of pump required. A gear pump, for example, has a specific speed less than 1.0, whereas an axial flow pump (large flow rate, low pressure rise) has a specific speed greater than 8000. For applications with a large pressure rise and a low flow rate, the corresponding specific speed is low.

The head coefficient, ψ , is a dimensionless pressure (head) rise of the pump. The head coefficient, ψ , is defined as

$$\psi = \frac{gH}{\Omega^2 r_B^2}$$

where r_B is either the blade radius (used in this study) or the mean blade radius (used by pump designers). There is no difficulty in converting the results of this study to correspond with design parameters used by pump manufacturers since the head coefficient differs only by a constant.

The pump pressure rise as a function of flow rate is a convenient way to present pump output performance. In nondimensionless form the pressure rise across the pump as a function of flow rate can be represented in terms of the head coefficient ψ and the flow coefficient, ϕ . The flow

coefficient, ϕ , can be defined in terms of the specific speed, the head coefficient and the geometry coefficient, ξ as

$$\phi = (N_s/2815)^2 \psi^{3/2}/\pi\xi_2$$

where

$$\xi_2 = A_2/\pi r_B^2$$

and A_2 is the axial flow cross-sectional area of the pump. A vane-axial pump usually has a single rotor stage with a deswirl-stationary stage. The flow into the pump is usually assumed to have no prerotation. As a result, an approximate relation exists between the head coefficient and the flow coefficient.

$$\psi = 1.0 - \phi \cot \beta_2$$

where β_2 is the rotor stage exit flow angle. Eliminating ϕ from the above equation, a relation between N_s and ψ is obtained such that

$$N_s = 2815\ (\pi/\cot \beta_2)^{1/2} \left[1 - (r_h/r_B)^2\right]^{1/2} \left(\frac{1-\psi}{\psi^{3/2}}\right)^{1/2}$$

where r_h is the hub radius.

A typical rotor exit flow angle is 21^{o}. The results of ψ versus N_s are shown in Figure A-2 for $\beta_2 = 21^{o}$ and $r_h/r_b = 0.625$. The pump performance prediction is shown in Figure A-2 along with data for a small vane axial fan operating in air.

The predicted result conforms quite well with other vane axial and shrouded fans (tube-axial) shown in Figure A-3 and A-4. An operating point for a liquid hydrogen pump manufactured by Pesco Products is also shown on the curves. The knowledge of an approximate relationship between N_s and ψ is required to size the nozzle outlet, D_o.

SYMBOLS AND ABBREVIATIONS

D_o	Nozzle outlet diameter, ft
G	Pump flow rate, gpm
g	Acceleration, ft/sec^2
H	Pressure head, ft
n	Pump speed, rpm
N_s	Specific speed
N_s'	$N_s/2815$
r_B	Blade radius, ft
r_h	Hub radius, ft
β	Rotor stage exit flow angle, deg

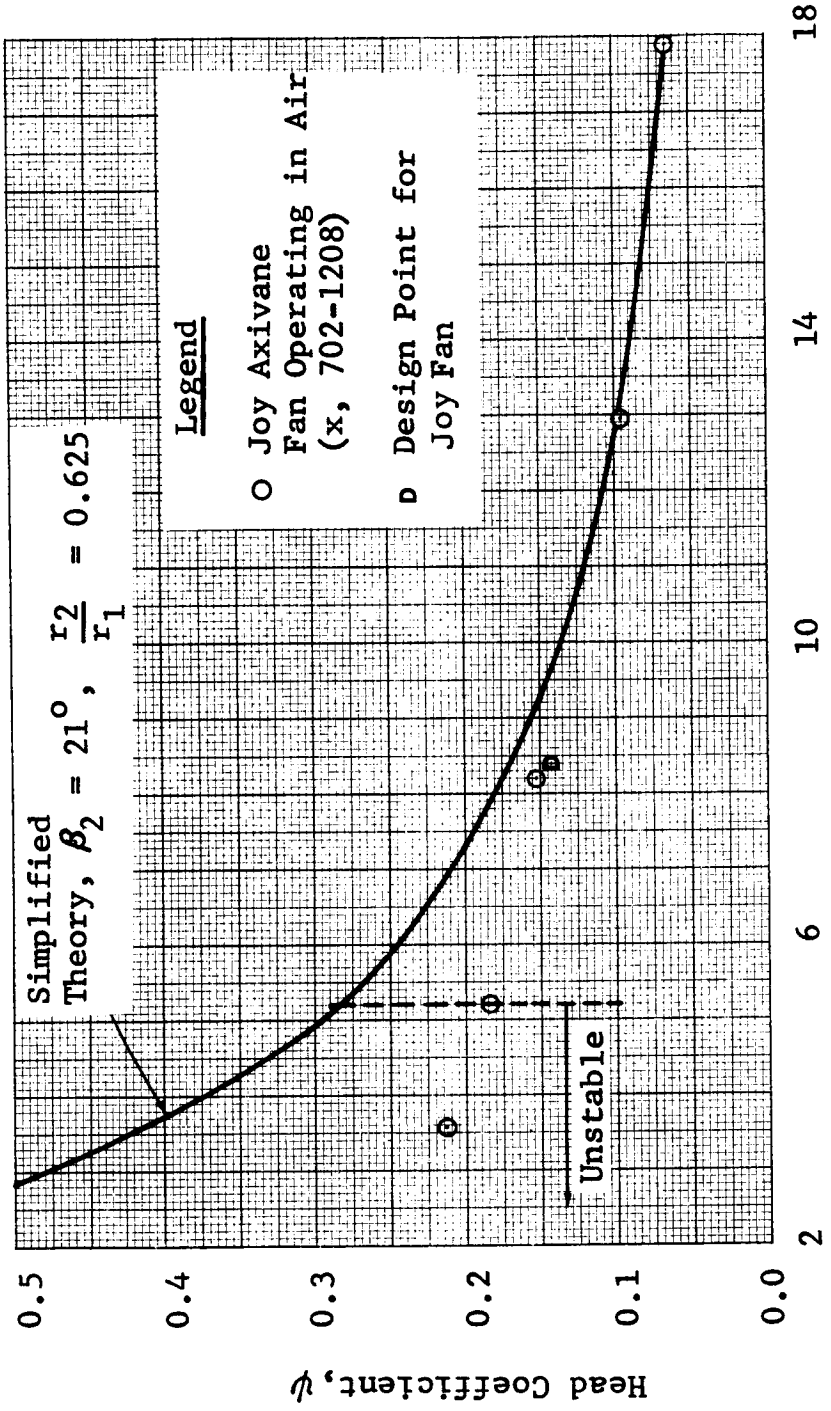

Figure A-2 Simplified Performance Prediction for Vane-Axial Fans

Vaneaxial Fans

○- Rotron Aximax 3
Impeller Diameter: 2.8 in.
Speed: 3600 rpm

□- Rotron Aximax 3
Impeller Diameter: 2.8 in.
Speed: 2400 rpm

△- Joy Axivane Model AVR20-12D802
Impeller Diameter: 2.0 in.
Speed: 10,500 rpm

▽- AiResearch Class MDF8
Impeller Diameter: 1.95 to 1.99 in.
Speed: 22,200 rpm

◇- Globe VAX - 2-MC
Impeller Diameter: 2.0 in.
Speed: 19,500 rpm

▷- Globe VAX - 3-FC
Impeller Diameter: 2.0 in.
Speed: 20,00 rpm

△- Globe Type GR
Impeller Diameter: 4.767
Speed: 8000 rpm

◦-Pesco Products LH_2 Pump
Impeller Diameter: 1.9 in.
Speed: 3200 rpm

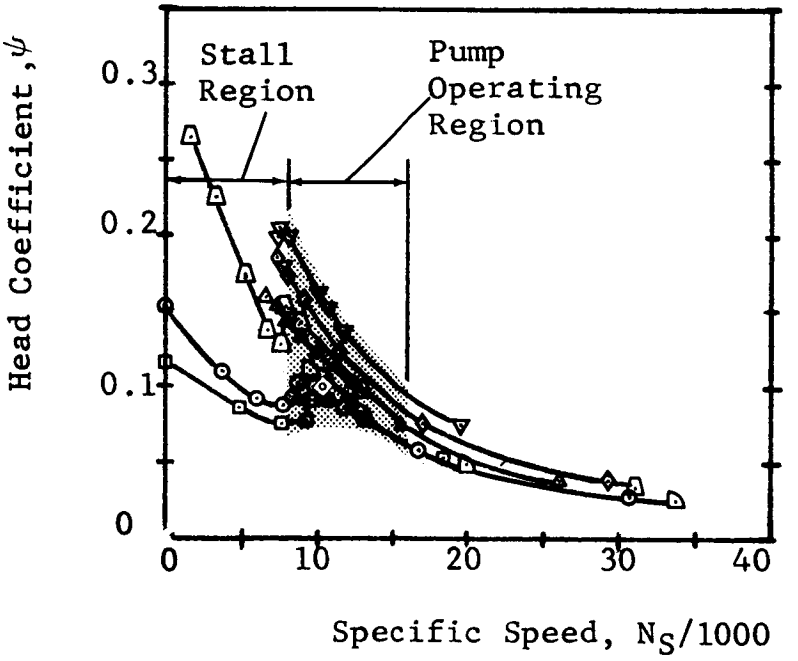

Figure A-3 Performance Data For Typical Vaneaxial Fans Operating in Air

Globe Industries, Inc. Bulletins
C-3246 and C-3456 respectively

△ Propeller Diameter: 3 in.
Speed: 3,500 rpm @ Free Air
□ Propeller Diameter: 6.5 in.
Speed: 3,150 rpm @ Free Air

Data for Air Research Class MDF44 Fan
○ Propeller Diameter: 10.93 in.
Speed: 4850 rpm

Data for Rotron Model DF Fan Type 301
▽ Propeller Diameter: 3.0 in.
Speed: 2400 rpm

Pesco Products LH_2 Pump
● Impeller Diameter: 1.9in.
Speed: 3200 rpm

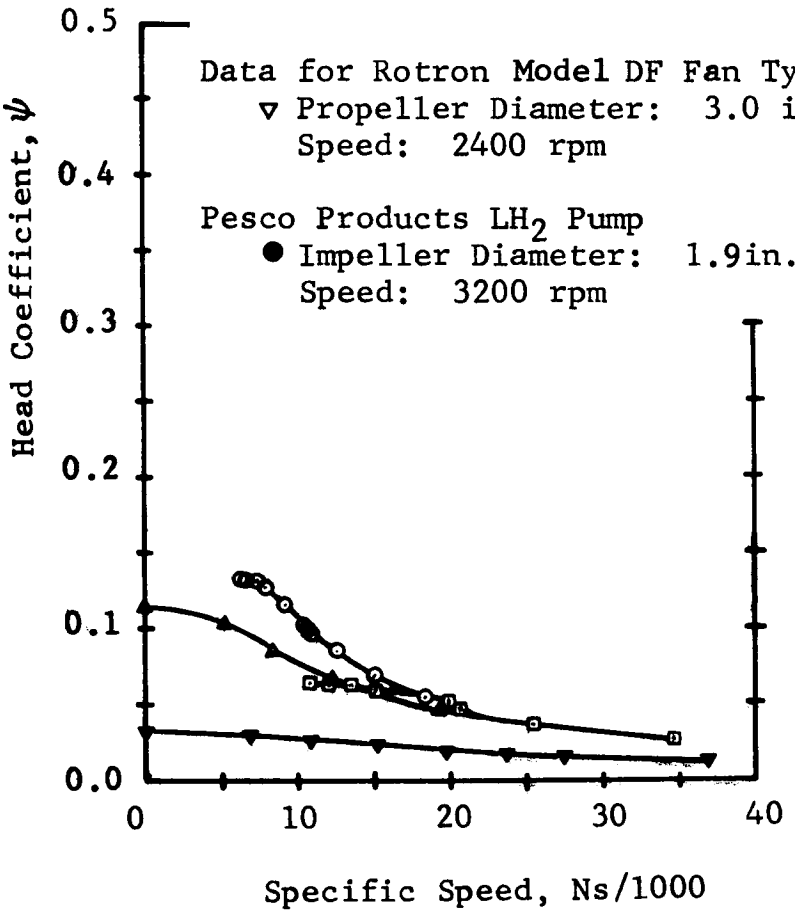

Figure A-4 Performance Data For Typical Shrouded Fans Operating in Air.

ξ Geometry coefficient

ϕ Flow coefficient

ψ Head coefficient

Ω Impeller angular velocity, rad/sec

APPENDIX J

SUMMARY OF PUMP-NOZZLE MATCHING EQUATIONS

The outlet nozzle diameter should be selected such that the pump operates at or near the pump design point. When a mixer is used solely for mixing, a nozzle should be attached to the pump to provide the design "pressure drop" of the pump. In cases in which the sole purpose of the mixer is to circulate fluid, the pressure drop should be as small as feasible (N_s as high as possible). There is some difficulty in obtaining high fan efficiencies when the specific speed is exceedingly high. This point has not been investigated in the study. In this study, it is assumed that reasonable hydraulic efficiencies can be obtained (60% for small vane axial pumps).

The pressure drop due to the nozzle is the velocity head

$$\Delta P = \frac{K\rho V_o^2}{2g_c}$$

Where K is a loss coefficient and is usually assumed to be 1.0 and V_o is the outlet velocity.

The above expression combined with equations defining the specific speed, head coefficient and the volume flow

equation yields an expression between the nozzle and blade diameter

$$D_o = D_B \, (1.6853 \times 10^{-4}) \, K^{1/4} \, \psi^{1/2} \, N_s$$

In addition to the relationship between the pump blade and nozzle diameter, the required pump speed is given by

$$n = \frac{3.144 \times 10^5}{\psi N_s \, D_B^2 \, K^{1/12}} \left(\frac{P_o D_o}{\rho} \right)^{1/3}, \text{ rpm}$$

Also the electric motor output torque is

$$T = \frac{25.5 \, \psi^{1/2}}{\eta_p} \, D_B \, \rho^{1/3} \, (D_o P_o)^{2/3}, \text{ oz-in}$$

where η_p is the pump hydraulic efficiency.

From the definition of specific speed and fluid power the following relationship is obtained between the vapor and liquid pump speed.

$$\frac{n_v}{n_\ell} = \left(\frac{\rho_\ell}{\rho_v} \right)^{1/3} \left(\frac{\psi_\ell}{\psi_v} \right)^{3/6} \left(\frac{P_{o\ell}}{P_{ov}} \right)^{1/3} \left(\frac{N_{s\ell}}{N_{sv}} \right)^{2/3}$$

for $\psi_\ell = \psi_v$ and $N_{s_\ell} = N_{sv}$

$$n_v / n_\ell = (P_{ov} / P_{o\ell})^{1/3} \, (\rho_\ell / \rho_v)^{1/3}$$

SYMBOLS AND ABBREVIATIONS

D_B	Blade diameter, ft
D_o	Nozzle diameter, ft
g_c	Constant = 32.2 lbm-ft/lb_f-sec^2
K	Thermal conductivity, Btu/hr-ft-^oR
n	Pump speed, rpm
n_ℓ	Pump speed for pumping liquid, rpm
n_v	Pump speed for pumping vapor, rpm
N_s	Specific speed
N_{s_ℓ}	Specific speed for pumping liquid
N_{s_v}	Specific speed for pumping vapor
P_o	Fluid power, watts
P_{o_ℓ}	Liquid fluid power, watts
P_{o_v}	Vapor fluid power, watts
T	Motor output torque, in-oz
V_o	Nozzle outlet velocity, ft/sec
ΔP	Nozzle pressure drop, psi
ρ	Density, lbm/ft^3
ρ_ℓ	Liquid density, lbm/ft^3
ρ_v	Vapor density, lbm/ft^3
η_p	Pump hydraulic efficiency
ψ	Head coefficient

ψ_ℓ Head coefficient for pumping liquid

ψ_ℓ Head coefficient for pumping vapor

APPENDIX K

ELECTRIC MOTOR EFFICIENCY

A.C. electric motors have the following typical efficiencies as a function of input power (Reference 40).

Input power, watts	Efficiency
1.0	10%
10.0	35%
100.0	75%

A curve fit in the region between 1 and 20 watt power input yields

$$\eta_e = 0.1(P_i)^{0.524}$$

or since

$$\eta_t = 0.155(P_o)^{1/3}$$

$$\eta_e = 0.2656(P_o)^{0.349}$$

also

$$\frac{\eta_e}{\eta_t} = 1.71\ P_o^{0.016}$$

or for all practical purposes

$$\frac{\eta_e}{\eta_t} = 1.71$$

in the input power range between 1 and 20 watts.

SYMBOLS AND ABBREVIATIONS

P_i Input power, watts

P_o Fluid power, watts

η_e A. C. electric motor efficiency

η_t Overall efficiency

APPENDIX L

OVERALL MOTOR PUMP EFFICIENCY

Estimates of the overall electric pump motor efficiency as a function of fluid power are required to determine the weight attributable to a mixing subsystem. Estimates have been obtained by personal communication with Gerald Caine of Pesco Products. In addition, data is given by Stark (Reference 41) and Sterbentz (Reference 9) in previous studies conducted in this area. The results are shown in Figure A-5 for both AC and brushless DC motors.

Based on the data available, the DC brushless motor driven pumps have a higher overall efficiency, especially at low fluid power. No actual data on the brushless DC motor operating liquid hydrogen were available, whereas the data for AC pump/motor efficiency were obtained from actual pumps. As a result, the AC pump/motor data were used in the weight estimates. A curve fit of the AC pump/motor data results in the following equation.

$$\eta_t = 0.155(P_o)^{0.333}$$

where η_t is the overall efficiency divided by 100 and P_o is the fluid power.

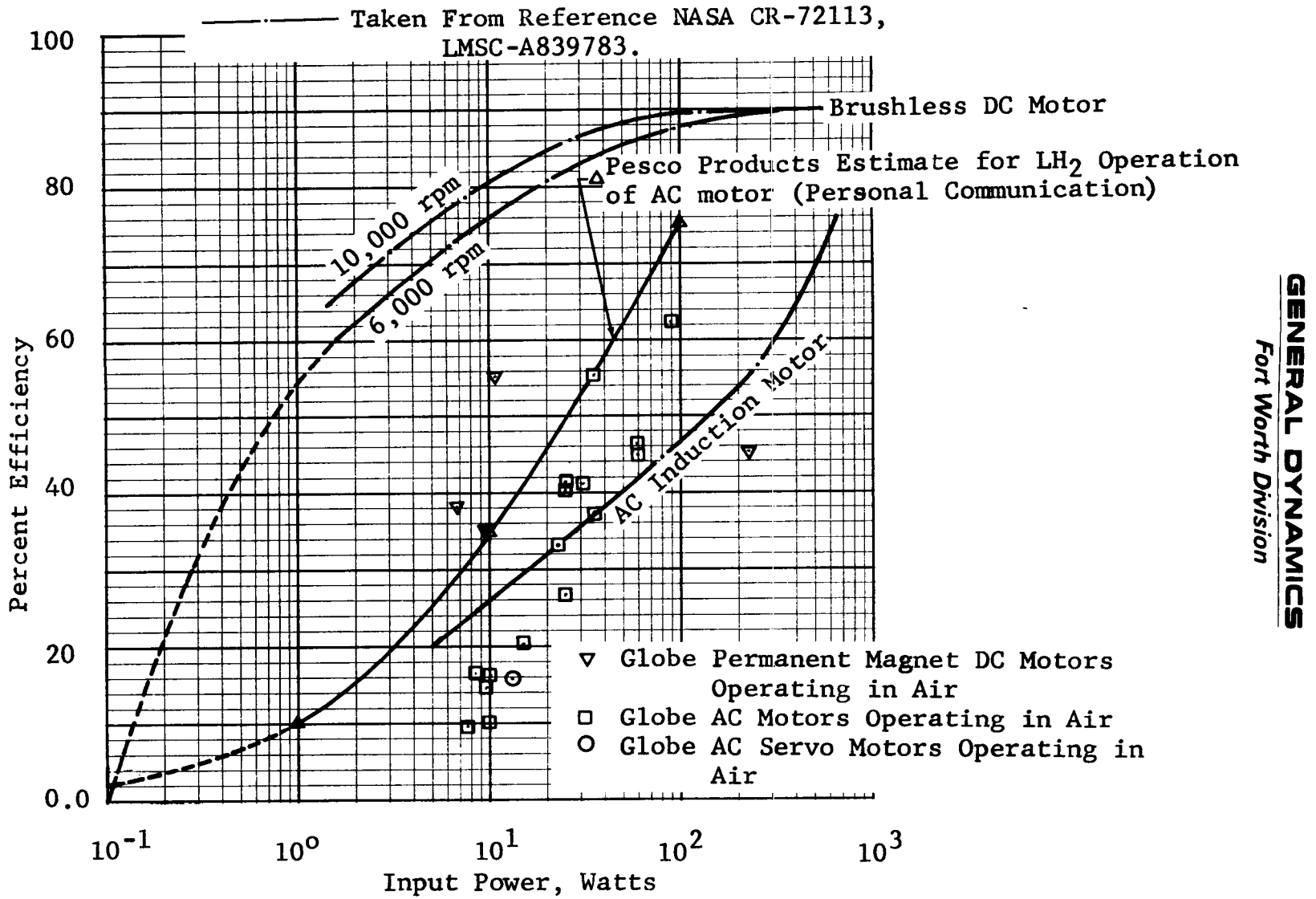

Figure A-5 Comparison of Electric Motor Efficiencies

APPENDIX M

PUMP IMPELLER WEIGHT

Typical pump impeller weights are obtained from Figure 6 (Reference 42). A curve fit of the maximum weight yields

$$W_f = 20\ D_b^{2.34},\ \text{pounds}$$

where D_b is the impeller diameter in feet. In addition to the fan weight, the support weight and nozzle weight may double the above number. Hence

$$W_f = 20\ C_{sn}\ D_b^{2.34}$$

where $C_{sn} \approx 2.0$.

SYMBOLS AND ABBREVIATIONS

C_{sn} Support and nozzle weight coefficient, $C_{sn} \approx 20$

D_b Impeller blade diameter, ft

W_f Fan weight, lb_m

APPENDIX N

WEIGHT OF ELECTRIC MOTORS

For a parametric study such as the one conducted herein, an algebraic expression for a cryogenic electric motor as a function of size, power, torque and/or speed is highly desirable. Crane and Pradhan (Reference 42) indicate that the principle factors affecting electric motor weight is the electric motor torque. A curve fit of Figure 7 of Reference 42 for the case of total weight of separate motor including typical motor housing yields

$$W_e = 0.194\ T^{0.6497},\ \text{pounds}$$

where T is the torque in ounce inches.

The electric motor weight becomes

$$W_e = 21.0 \left(\frac{\eta_e\ P_o}{\eta_t\ n} \right)^{0.65},\ \text{pounds}$$

where η_e is the electric motor efficiency (divided by 100), η_t is the overall efficiency, n is the speed in rpm and P_o is the fluid power in watts.

Since

$$\frac{\eta_e}{\eta_t} \approx 1.7$$

$$W_e = 29.6 \left(\frac{P_o}{n}\right)^{0.65}, \text{ pounds}$$

SYMBOLS AND ABBREVIATIONS

n	Motor speed, rpm
P_o	Fluid power, watts
T	Motor torque, in - oz
W_e	Electric motor weight, lb_m
η_e	A. C. electric motor efficiency
η_t	Overall efficiency